

ALASKA LNG PROJECT	DOCKET No. CP17-___-000 RESOURCE REPORT No. 13 LNG APPENDICES PART 2 OF 19	Doc No: USAKE-PT-SRREG-00- 000006-000 APRIL 14, 2017 REVISION: 0
	PUBLIC	

Part 2 of 19 of Appendices for Resource Report No. 13 LNG

	RR13 APPENDIX TABLE OF CONTENTS	USAI-PE-SRREG-00-000013-000-B 14 APRIL 2017 REVISION: 1
	PUBLIC	APPENDIX COVERSHEET

APPENDIX 13I – NATURAL HAZARD DESIGN INVESTIGATIONS AND FORCES

I.1 - Seismic Hazard Evaluation

Document Number:	Description:	Revision:	Appendix:
USAL-FG-GRHAZ-00-002015-001	LNG Facilities Probabilistic Seismic Hazard Analysis (PSHA) Report	Rev 0	Public

Alaska LNG



LNG FACILITIES PROBABILISTIC SEISMIC HAZARD ANALYSIS (PSHA) REPORT

USAL-FG-GRHAZ-00-002015-001

Rev	Date	Revision Description	Originator	Reviewer / Endorser	Response Code	Approver			
A	4-Mar-16	Issued for Review	S. Giannakos / J. Goodman	A. Younan	2	M. Ilankatharan / J. Sowers / O. El Menchawi			
0	5-May-16	Issued for Use	S. Giannakos / J. Goodman			M. Ilankatharan / J. Sowers / O. El Menchawi			
Document Control No.	Country	Facility	Originator	Discipline	Type	Sub-Type	Location	Sequence	Identifier
	US	AL	FG	G	R	HAZ	00	002015	001



FUGRO CONSULTANTS, INC.

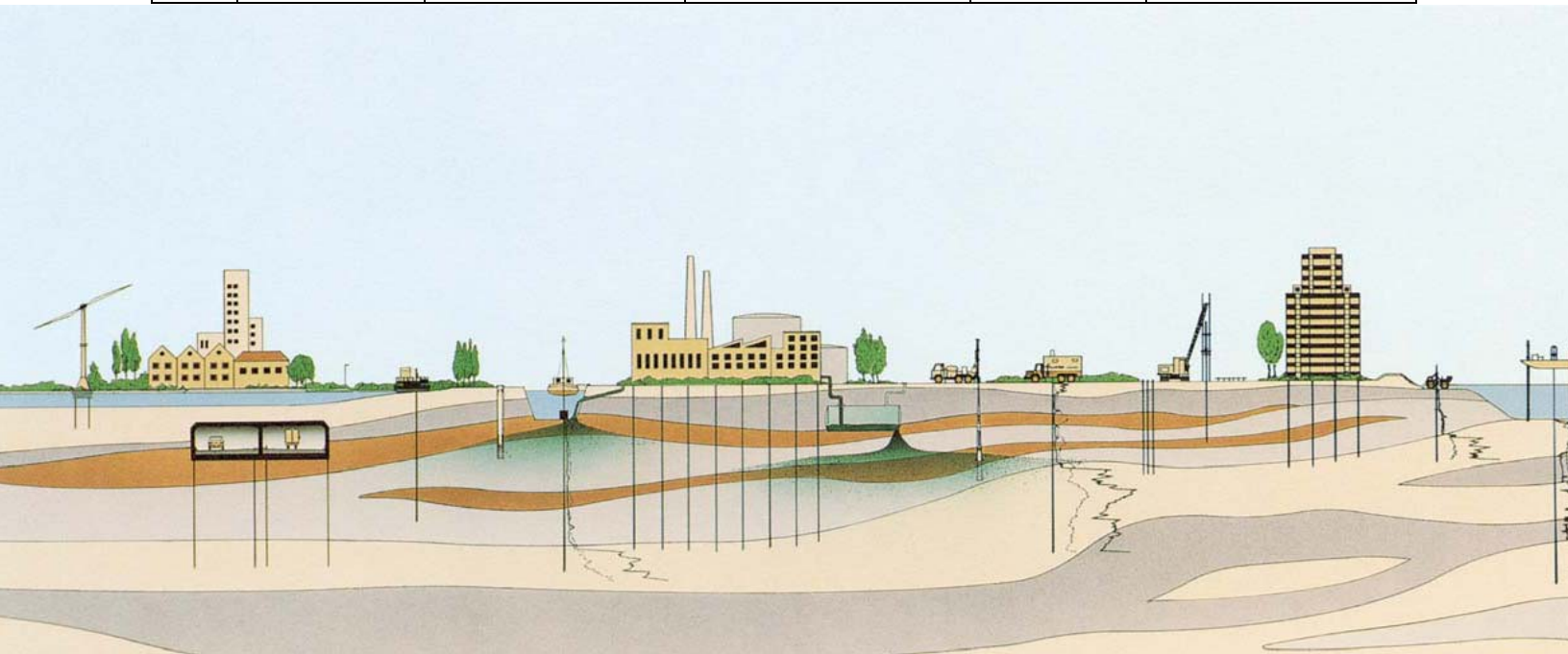
Alaska LNG

PRE-FEED LNG FACILITIES PROBABILISTIC SEISMIC HAZARD ANALYSIS (PSHA) REPORT ALASKA LNG PROJECT NIKISKI, ALASKA

AKLNG DOCUMENT NO. USAL-FG-GRHAZ-00-002015-001

REPORT NO. 04.10140334-6
EXXONMOBIL ALASKA LNG LLC (EMALL)
HOUSTON, TEXAS

Rev	Date	Revision Description	Originator	Reviewer	Approver
A	4-Mar-16	Issued for Review	S. Giannakos / J. Goodman		M. Ilankatharan / J. Sowers / O. El Menchawi
0	5-May-16	Issued for Use	S. Giannakos / J. Goodman		M. Ilankatharan / J. Sowers / O. El Menchawi



6100 Hillcroft (77081)
Houston, Texas 77274
Tel: (713) 369-5400
P.O Box 740010
Fax: (713) 369-5518

AKLNG Document No. USAL-FG-GRHAZ-00-002015-001
Fugro Report No. 04.101400334-6
May 5, 2016

ExxonMobil Alaska LNG LLC (EMALL)
10613 W. Sam Houston Pkwy N, Suite 500
Houston, TX, 77064

Attention: Patrick Wong
Geotechnical Engineer/Technical POC

**Pre-FEED
LNG Facilities Probabilistic Seismic Hazard Analysis (PSHA) Report
Alaska LNG Project
Nikiski, Alaska**

Fugro Consultants, Inc. (Fugro) is pleased to present this final report of our Probabilistic Seismic Hazard Analysis (PSHA) for the Pre-FEED investigations at the Alaska LNG facilities located in Nikiski, Alaska. Our services were authorized under Service Work Order No. AKLNG-FUG-US-003 Rev 0, dated February 5, 2015 in accordance with the Service Agreement No. A2275592 between Fugro and ExxonMobil Global Services Company, dated October 29, 2012. Fugro is performing the pre front-end engineering and design (Pre-FEED) level geophysical and geotechnical site investigation (G&G) for the proposed AKLNG Project since August 2014.

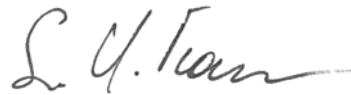
This report presents a characterization of seismic sources relevant to the proposed site, followed by the results of the PSHA calculations and development of design time histories for onshore and nearshore locations within the project area.

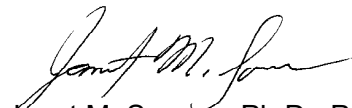
FUGRO CONSULTANTS, INC.

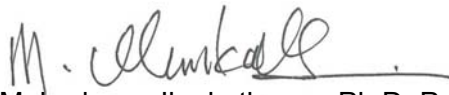
We appreciate the opportunity to be of service to EMALL. Please call us at (713) 369-5400 if you have any questions or comments concerning this report, or when we may be of further assistance.

Sincerely,
FUGRO CONSULTANTS, INC.
TBPE Firm Registration No. 299


Joshua Goodman, P.G, C.E.G.
Senior Project Geologist


Spyros Giannakos, Ph.D., P.E.
Project Engineer


Janet M. Sowers, Ph.D., P.G.
Associate Geologist


Mahadevan Ilankatharan, Ph.D. P.E.
Senior Engineer


Osman El Menchawi, Ph.D., P.E, G.E.
Principal Geotechnical Engineer

Copies Submitted: E-mail

TABLE OF CONTENTS

	<u>Page</u>
1.0 INTRODUCTION.....	1-1
1.1 Project Description	1-1
1.2 Work Authorization	1-1
1.3 Scope and Organization.....	1-1
1.4 Limitations of this Study	1-2
1.5 Summary and Findings.....	1-3
1.5.1 Probabilistic Seismic Hazard Analyses.....	1-3
1.5.2 Development of Ground Acceleration Time Histories.....	1-5
2.0 SEISMOTECTONIC SETTING	2-1
2.1 Introduction.....	2-1
2.2 Regional Tectonic Framework, and Tectonic and Physiographic Elements.....	2-1
2.2.1 Cook Inlet Basin.....	2-2
2.2.2 Kenai Mountains and Chugach Mountains	2-4
2.2.3 Talkeetna Mountains	2-6
2.2.4 Western Alaska Range	2-6
2.3 Historical Seismicity	2-6
2.3.1 1899 M 7.2 Kenai Earthquake	2-8
2.3.2 1912 M 7.1 Alaska Peninsula Earthquake.....	2-8
2.3.3 1928 M 7.3 Gulf of Alaska Earthquake	2-8
2.3.4 1933 M 7.1 Anchorage Earthquake	2-8
2.3.5 1934 M 7.1 Southern Alaska Earthquake	2-8
2.3.6 1946 M 7.2 Unimak Earthquake	2-9
2.3.7 1949 M 7.0 Gulf of Alaska Earthquake	2-9
2.3.8 1964 M 9.2 Great Alaskan Earthquake.....	2-9
2.3.9 2002 M 7.9 Denali Earthquake	2-9
2.3.10 2014 M 7.9 Rat Islands Earthquake	2-10
2.4 Potential Seismic Sources in Southern Alaska	2-10
2.4.1 Aleutian Subduction Zone.....	2-10
2.4.2 Yakutat Microplate	2-11
2.4.3 Intraslab	2-11
2.4.4 Southern Alaska Block.....	2-12
3.0 SEISMIC SOURCE CHARACTERIZATION.....	3-1
3.1 Introduction.....	3-1
3.2 Aleutian Subduction Zone Interface	3-2
3.2.1 Interface Geometry	3-2

	3.2.2	Interface Activity Rate Scenarios, Recurrence, and Magnitudes.....	3-3
3.3		Intraslab Source	3-4
3.4		Shallow Crustal Fault Sources	3-4
	3.4.1	Cook Inlet fault-cored folds	3-5
	3.4.2	Castle Mountain-Lake Clark fault system	3-12
	3.4.3	Excluded Faults	3-20
3.5		Upper Crustal Areal Source	3-20
3.6		Earthquake Recurrence and Activity Rates.....	3-21
	3.6.1	Introduction	3-21
	3.6.2	Seismicity Catalog and Grid Source Models	3-21
4.0		PSHA METHODOLOGY	4-1
	4.1	PSHA Framework.....	4-1
	4.1.1	PSHA Calculations	4-2
	4.2	Treatment of Uncertainty.....	4-2
	4.3	Implementation.....	4-3
	4.4	Near Source and Directivity Effects.....	4-4
5.0		SEISMIC HAZARD ANALYSES.....	5-1
	5.1	Project Location.....	5-1
	5.2	Site Classification	5-3
	5.3	Magnitude Probability Density Functions	5-4
	5.4	Horizontal Ground Motion Prediction Equations	5-5
	5.5	Definition of Design Level Events.....	5-6
	5.6	Extending the Design Spectra to Long Periods.....	5-7
	5.7	Probabilistic Seismic Hazard Analyses Results	5-8
	5.7.1	Seismic Hazard Curves	5-8
	5.7.2	Horizontal Uniform Hazard Response Spectra (UHRS)	5-8
	5.7.3	Seismic Hazard Deaggregation by Seismic Source	5-13
	5.7.4	Seismic Hazard Deaggregation by Earthquake Magnitude, Distance and Epsilon.....	5-14
	5.8	Comparison with Regional Studies	5-15
	5.9	Horizontal Ground Motions per NFPA 59A 2006 / ASCE 7-05.....	5-16
	5.9.1	Operational Basis Earthquake (OBE).....	5-16
	5.9.2	Maximum Considered Earthquake (MCE) / Safe Shutdown Earthquake (SSE)	5-17
	5.9.3	Design Earthquake (DE) Spectrum	5-21
5.10		Vertical Ground Motions per NFPA 59A 2006 / ASCE 7-05.....	5-24
6.0		DEVELOPMENT OF GROUND ACCELERATION TIME HISTORIES	6-1
	6.1	Ground Motion Selection.....	6-1
	6.2	Approach.....	6-2

6.2.1	Modification of Selected Seed Motions.....	6-2
6.2.2	Rotation of Original Motions to FN and FP Components.....	6-3
6.2.3	Time-Domain Spectral Matching	6-3
6.2.4	Baseline Correction	6-3
6.2.5	Validation per the ASCE 4-98 Requirements	6-4
6.3	Spectrally Matched Motions Per NFPA 59A 2006.....	6-4
7.0	REFERENCES.....	7-1
	APPENDIX A	A-1
	APPENDIX B	B-1
	APPENDIX C	C-1
	APPENDIX D	D-1
	APPENDIX E	E-1

TABLES

	<u>Page</u>
1.1 Peak Ground Acceleration Values of Horizontal Component at the Ground Surface ($V_{s30} = 885$ ft/s) per NFPA 59A 2006 and ASCE 7-05 for Nearshore Facilities	1-4
1.2 Peak Ground Acceleration Values of Horizontal Component at the Ground Surface ($V_{s30} = 885$ ft/s) per NFPA 59A 2006 and ASCE 7-05 for Onshore Facilities	1-4
1.3 Peak Ground Acceleration Values of Vertical Component at the Ground Surface ($V_{s30} = 885$ ft/s) per NFPA 59A 2006 and ASCE 7-05 for Onshore Facilities	1-5
1.4 Peak Ground Acceleration Values of Vertical Component at the Ground Surface ($V_{s30} = 885$ ft/s) per NFPA 59A 2006 and ASCE 7-05 for Nearshore Facilities	1-5
3.1 Subduction Zone Seismic Sources	3-15
3.2 Cook Inlet Basin Upper Plate Fault Sources	3-16
3.3 Non-Cook Inlet Basin Upper Plate Fault Sources	3-19
5.1 Coordinates of Representative Locations	5-1
5.2 Closest Distance to Seismic Sources	5-2
5.3 Empirical Correlations for Shear Wave Velocity	5-4
5.4 Selected Ground Motion Prediction Equations	5-6
5.5 Horizontal Response Spectra (5% damping) for 475 and 2475-year Events for the Onshore and Nearshore Sites with No Directivity, for Site Class D ($V_{s30} = 885$ ft/s).....	5-10
5.6 Horizontal Response Spectra (5% damping) for 475 and 2475-year Events for the Onshore and Nearshore Sites with Fault Normal Directivity, for Site Class D ($V_{s30} = 885$ ft/s)	5-11
5.7 Horizontal Response Spectra (5% damping) for 475 and 2475-year Events for the Onshore and Nearshore Sites with Fault Parallel Directivity, for Site Class D ($V_{s30} = 885$ ft/s)	5-12
5.8 Horizontal Response Spectra (5% damping) for 475 and 2475-year Events for the Onshore and Nearshore Sites with Average Directivity, for Site Class D ($V_{s30} = 885$ ft/s)	5-13
5.9 5-percent Damped Horizontal Acceleration Response Spectrum at Ground	

	Surface for OBE per NFPA -59A 2006, $V_{s30} = 885$ ft/s.....	5-17
5.10	5-percent Damped Horizontal Acceleration Response Spectrum for the Onshore Location for SSE/MCE at the Ground Surface per NFPA 59A 2006 / ASCE 7-05, $V_{s30} = 885$ ft/s	5-20
5.11	5-percent Damped Smoothed Horizontal Acceleration Response Spectrum for the Nearshore Location for SSE/MCE at the Ground Surface per NFPA 59A 2006 / ASCE 7-05, $V_{s30} = 885$ ft/s	5-21
5.12	5-percent Damped Horizontal Acceleration Response Spectrum for the Onshore Location for Design Earthquake (DE) at the Ground Surface per ASCE 7-05, $V_{s30} = 885$ ft/s	5-23
5.13	5-percent Damped Horizontal Acceleration Response Spectrum for the Nearshore Location for Design Earthquake (DE) at the Ground Surface per ASCE 7-05, $V_{s30} = 885$ ft/s	5-24
5.14	List of Acceleration Records in Alaska for Site Class D and Rupture Distance up to 31 mi / 50 km from the Delaney Park Downhole Array Station	5-25
5.15	List of Acceleration Records in Alaska for Site Class D and Rupture Distance up to 31 mi / 50 km from the Pacific Earthquake Engineering Research (PEER) Center NGA Motion Database	5-26
5.16	Recommended V/H Ratios for the Development of Vertical Spectra for Site Class D at the Project Site	5-27
5.17	5%-damped Vertical Spectra at Ground Surface per NFPA-59A 2006.....	5-28
5.18	5%-damped Vertical Spectra at Ground Surface per ASCE 7-05.....	5-29
6.1	Summary of Selected Seed Motion Characteristics.....	6-2

ILLUSTRATIONS

	<u>Plate</u>
Site Location Map	1
Tectonic Framework of Southern Alaska	2
Regional Fault Map	3
Seismicity Map	4
Top Mesozoic Unconformity Depth Map of the Cook Inlet Basin	5
Stratigraphic Column of Cook Inlet Basin	6
Megathrust Interface Model	7
Wesson et al (2007) Model of Intraslab Seismicity M6.0 Earthquakes With Depths of 31 to 50 Mi (50 to 80 Km)	8
Wesson et al (2007) Model of Intraslab Seismicity M6.0 Earthquakes With Depths of 50 to 75 Mi (80 to 120 Km)	9
Cook Inlet Fault-Cored Fold Source Model	10
Non-Cook Inlet Basin Upper Plate Fault Source Model	11
Folds and Faults Mapped From Seismic Reflection Data	12
Conceptual Fault-Propagation Fold Model	13
Seismic Reflection Line 203_290, Showing Middle Ground Shoal Fault-Fold System	14
Cross-Section of the Northern Cook Inlet	15
Diagrammatic Cross Section of the Granite Point Anticline Area	16
Conceptual Cross Section of Upper Cook Inlet Basin at the Latitude of the Site	17
Wesson et al (2007) Model M6.0 Earthquake Events Not Associated with Megathrust Events (0 to 31 Mi / 0 to 50 Km Depth)	18
Probabilistic Seismic Hazard Analyses Components	19
Generic Logic Tree for Treatment of Epistemic Uncertainties	20
PSHA Locations	21
Development of Shear Wave Velocity Profiles for the Onshore LNG Facilities	22
Development of Shear Wave Velocity Profiles for the Nearshore LNG Facilities	23
Summary of Shear Wave Velocity Data Obtained from Downhole Seismic Shear Wave Velocity Tests in the Onshore and Nearshore Project Area During Phases 1 and 2	24
Example Magnitude Probability Density Functions	25

Example Annual Recurrence Predicted by Different Magnitude PDF Models 26

475-Year Return Period Horizontal Acceleration Response Spectra Estimated
 for the Representative Onshore Locations ($V_{s30} = 885$ ft/s) 27

2475-Year Return Period Horizontal Acceleration Response Spectra Estimated
 for the Representative Onshore Locations ($V_{s30} = 885$ ft/s) 28

475-Year Return Period Horizontal Acceleration Response Spectra Estimated
 for the Representative Nearshore Locations ($V_{s30} = 885$ ft/s) 29

2475-Year Return Period Horizontal Acceleration Response Spectra Estimated
 for the Representative Nearshore Locations ($V_{s30} = 885$ ft/s) 30

Comparison of 475- and 2475-Year Return Period Horizontal Acceleration Response
 Spectra Estimated for the Representative Onshore and Nearshore Locations
 ($V_{s30} = 885$ ft/s)..... 31

Comparison of 475- and 2475-Year Return Period Horizontal Acceleration Response
 Spectra Estimated for the Representative Onshore Location ($V_{s30} = 885$ ft/s)
 to the Phase 1 PSHA Results ($V_{s30} = 900$ ft/s)..... 32

Mean Annual Hazard Curves at Different Structural Periods for the Onshore
 Location - No Directivity ($V_{s30} = 885$ ft/s)..... 33

Mean Annual Hazard Curves at Different Structural Periods for the Nearshore
 Location - No Directivity ($V_{s30} = 885$ ft/s)..... 34

5-Percent Damped Horizontal Acceleration Response Spectra for the Onshore Location
 for 475 and 2475-Year Return Period Events - No Directivity ($V_{s30} = 885$ ft/s) 35

5-Percent Damped Horizontal Acceleration Response Spectra for the Nearshore
 Location for 475 and 2475-Year Return Period Events - No Directivity
 ($V_{s30} = 885$ ft/s)..... 36

5-Percent Damped Horizontal Acceleration Response Spectra for the Onshore Location
 for 475 and 2475-Year Return Period Events - No Directivity (ND), Fault Normal
 (FN) and Fault Parallel (FP) Directivity Effects ($V_{s30} = 885$ ft/s) 37

5-Percent Damped Horizontal Acceleration Response Spectra for the Nearshore Location
 for 475 and 2475-Year Return Period Events - No Directivity (ND), Fault Normal
 (FN) and Fault Parallel (FP) Directivity Effects ($V_{s30} = 885$ ft/s) 38

FN/ND and FP/ND ratios for 475 and 2475 Years 39

Annual Hazard Curves per Seismic Source at PGA - Onshore Location ($V_{s30} = 885$ ft/s) 40

Annual Hazard Curves per Seismic Source at 1 Sec - Onshore Location ($V_{s30} = 885$ ft/s) 41

Annual Hazard Curves per Seismic Source at 3 Sec - Onshore Location ($V_{s30} = 885$ ft/s) 42

Annual Hazard Curves per Seismic Source at PGA - Nearshore Location ($V_{s30} = 885$ ft/s) 43

Annual Hazard Curves per Seismic Source at 1 Sec - Nearshore Location ($V_{s30} = 885$ ft/s) 44

Annual Hazard Curves per Seismic Source at 3 Sec - Nearshore Location ($V_{s30} = 885$ ft/s) 45

Deaggregation of the Hazard by Seismic Sources for PGA, S_a ($T=1.0$ Sec) and
 S_a ($T=3.0$ Sec), for 475-Year Return Period - Onshore Location ($V_{s30} = 885$ ft/s)..... 46

Deaggregation of the Hazard by Seismic Sources for PGA, S_a ($T=1.0$ Sec) and
 S_a ($T=3.0$ Sec), for 2475-Year Return Period - Onshore Location ($V_{s30} = 885$ ft/s)..... 47

Deaggregation of the Hazard by Seismic Sources for PGA, S_a ($T=1.0$ Sec) and
 S_a ($T=3.0$ Sec), for 475-Year Return Period - Nearshore Location ($V_{s30} = 885$ ft/s)..... 48

Deaggregation of the Hazard by Seismic Sources for PGA, S_a ($T=1.0$ Sec) and
 S_a ($T=3.0$ Sec), for 2475-Year Return Period - Nearshore Location ($V_{s30} = 885$ ft/s).... 49

Deaggregation of the Hazard by Magnitude and Distance - Onshore Location
 ($V_{s30} = 885$ ft/s)..... 50

Deaggregation of the Hazard by Magnitude and Distance - Nearshore Location
 ($V_{s30} = 885$ ft/s)..... 51

Uniform Hazard Spectra, Comparison of the Onshore Location with USGS Studies
 (USGS UHS for $V_{s30} = 760$ m/s (2493 ft/s) Amplified Using ASCE Amplification
 Factors)..... 52

5-percent Damped Horizontal Acceleration Response Spectrum at Ground
 Surface ($V_{s30} = 885$ ft/s) for OBE per NFPA-59A (2006) - Fault Normal (FN) and
 Fault Parallel (FP) 53

Development of the 150% Median Onshore Deterministic Response Spectrum - No
 Directivity ($V_{s30} = 885$ ft/s) 54

Development of the 150% Median Nearshore Deterministic Response Spectrum - No
 Directivity ($V_{s30} = 885$ ft/s) 55

Development of Maximum Considered Earthquake (MCE) Spectrum at Ground
 Surface ($V_{s30} = 885$ ft/s) per ASCE 7-05 - Onshore Location, Fault Normal 56

Development of Maximum Considered Earthquake (MCE) Spectrum at Ground
 Surface ($V_{s30} = 885$ ft/s) per ASCE 7-05 - Onshore Location, Fault Parallel..... 57

Development of Maximum Considered Earthquake (MCE) Spectrum at Ground

Surface ($V_{s30} = 885$ ft/s) per ASCE 7-05 - Nearshore Location, Fault Normal	58
Development of Maximum Considered Earthquake (MCE) Spectrum at Ground	
Surface ($V_{s30} = 885$ ft/s) per ASCE 7-05 - Nearshore Location, Fault Parallel.....	59
5-percent Damped Smoothed Horizontal Acceleration Response Spectra at Ground	
Surface ($V_{s30} = 885$ ft/s) per ASCE 7-05 Guidelines - Nearshore Location, Fault	
Normal and Fault Parallel.....	60
Comparison of Maximum Considered Earthquake (MCE) Spectra at Ground Surface	
($V_{s30} = 885$ ft/s) per ASCE 7-05 Estimated for the Representative Onshore	
and Nearshore Locations ($V_{s30} = 885$ ft/s))	61
Comparison of Maximum Considered Earthquake (MCE) Spectra (FN and FP) at	
Ground Surface ($V_{s30} = 885$ ft/s) per ASCE 7-05 Estimated for the	
Representative Onshore Location to the Phase 1 PSHA Results ($V_{s30} = 900$ ft/s)	62
Development of Design Earthquake (DE) Spectrum at Ground Surface ($V_{s30} = 885$ ft/s)	
per ASCE 7-05 - Onshore Location, Fault Normal	63
Development of Design Earthquake (DE) Spectrum at Ground Surface ($V_{s30} = 885$ ft/s)	
per ASCE 7-05 - Onshore Location, Fault Parallel	64
Development of Design Earthquake (DE) Spectrum at Ground Surface ($V_{s30} = 885$ ft/s)	
per ASCE 7-05 - Nearshore Location, Fault Normal	65
Development of Design Earthquake (DE) Spectrum at Ground Surface ($V_{s30} = 885$ ft/s)	
per ASCE 7-05 - Onshore Location, Fault Parallel	66
5-percent Damped Horizontal Acceleration Response Spectra at Ground Surface	
($V_{s30} = 885$ ft/s) per NFPA-59A 2006 Guidelines - Onshore Location	67
5-percent Damped Horizontal Acceleration Response Spectra at Ground Surface	
($V_{s30} = 885$ ft/s) per ASCE 7-05 Guidelines - Onshore Location	68
5-percent Damped Horizontal Acceleration Response Spectra at Ground Surface	
($V_{s30} = 885$ ft/s) per NFPA-59A 2006 Guidelines - Nearshore Location	69
5-percent Damped Horizontal Acceleration Response Spectra at Ground Surface	
($V_{s30} = 885$ ft/s) per ASCE 7-05 Guidelines - Nearshore Location	70
Vertical to Horizontal Spectral Acceleration Ratios (V/H) of Alaska Records for Site	
Class D and R = 0 - 31 mi (0 - 50 km).....	71
5-percent Damped Vertical Acceleration Response Spectra at Ground Surface	
($V_{s30} = 885$ ft/s) per NFPA-59A 2006 Guidelines	72

5-percent Damped Vertical Acceleration Response Spectra at Ground Surface
 ($V_{s30} = 885$ ft/s) per ASCE 7-05 Guidelines..... 73

Spectrally Matched MEP Motion, EW Component, 2010 Chile EQ, OBE Level per
 NFPA 59A 2006 – Onshore and Nearshore, Fault Normal 74

Spectrally Matched MEP Motion, NS Component, 2010 Chile EQ, OBE Level per
 NFPA 59A 2006 – Onshore and Nearshore, Fault Parallel..... 75

Spectrally Matched MEP Motion, V Component, 2010 Chile EQ, OBE Level per
 NFPA 59A 2006 – Onshore and Nearshore..... 76

Spectrally Matched CTO Motion, 180 Component, 2001 El Salvador EQ, OBE Level per
 NFPA 59A 2006 – Onshore and Nearshore, Fault Normal 77

Spectrally Matched CTO Motion, 270 Component, 2001 El Salvador EQ, OBE Level per
 NFPA 59A 2006 – Onshore and Nearshore, Fault Parallel..... 78

Spectrally Matched CTO Motion, UP Component, 2001 El Salvador EQ, OBE Level per
 NFPA 59A 2006 – Onshore and Nearshore..... 79

Spectrally Matched Carlo Motion, 090 Component, 2002 Denali EQ, Alaska, OBE Level per
 NFPA 59A 2006 – Onshore and Nearshore, Fault Normal 80

Spectrally Matched Carlo Motion, 360 Component, 2002 Denali EQ, Alaska, OBE Level per
 NFPA 59A 2006 – Onshore and Nearshore, Fault Parallel..... 81

Spectrally Matched Carlo Motion, UP Component, 2002 Denali EQ, Alaska, OBE Level per
 NFPA 59A 2006 – Onshore and Nearshore..... 82

Spectrally Matched DZC Motion, 180 Component, 1999 Duzce EQ, Turkey, OBE Level per
 NFPA 59A 2006 – Onshore and Nearshore, Fault Normal 83

Spectrally Matched DZC Motion, 270 Component, 1999 Duzce EQ, Turkey, OBE Level per
 NFPA 59A 2006 – Onshore and Nearshore, Fault Parallel..... 84

Spectrally Matched DZC Motion, UP Component, 1999 Duzce EQ, Turkey, OBE Level per
 NFPA 59A 2006 – Onshore and Nearshore..... 85

Spectrally Matched Unio Motion, N00W Component, 1985 Mexico EQ, OBE Level per
 NFPA 59A 2006 – Onshore and Nearshore, Fault Normal 86

Spectrally Matched Unio Motion, N90W Component, 1985 Mexico EQ, OBE Level per
 NFPA 59A 2006 – Onshore and Nearshore, Fault Parallel..... 87

Spectrally Matched Unio Motion, UP Component, 1985 Mexico EQ, OBE Level per
 NFPA 59A 2006 – Onshore and Nearshore..... 88

Spectrally Matched MEP Motion, EW Component, 2010 Chile EQ, SSE Level per NFPA 59A 2006 – Onshore, Fault Normal	89
Spectrally Matched MEP Motion, NS Component, 2010 Chile EQ, SSE Level per NFPA 59A 2006 – Onshore, Fault Parallel	90
Spectrally Matched MEP Motion, V Component, 2010 Chile EQ, SSE Level per NFPA 59A 2006 – Onshore	91
Spectrally Matched CTO Motion, 180 Component, 2001 El Salvador EQ, SSE Level per NFPA 59A 2006 – Onshore, Fault Normal	92
Spectrally Matched CTO Motion, 270 Component, 2001 El Salvador EQ, SSE Level per NFPA 59A 2006 – Onshore, Fault Parallel	93
Spectrally Matched CTO Motion, UP Component, 2001 El Salvador EQ, SSE Level per NFPA 59A 2006 – Onshore	94
Spectrally Matched Carlo Motion, 090 Component, 2002 Denali EQ, Alaska, SSE Level per NFPA 59A 2006 – Onshore, Fault Normal	95
Spectrally Matched Carlo Motion, 360 Component, 2002 Denali EQ, Alaska, SSE Level per NFPA 59A 2006 – Onshore, Fault Parallel	96
Spectrally Matched Carlo Motion, UP Component, 2002 Denali EQ, Alaska, SSE Level per NFPA 59A 2006 – Onshore	97
Spectrally Matched DZC Motion, 180 Component, 1999 Duzce EQ, Turkey, SSE Level per NFPA 59A 2006 – Onshore, Fault Normal	98
Spectrally Matched DZC Motion, 270 Component, 1999 Duzce EQ, Turkey, SSE Level per NFPA 59A 2006 – Onshore, Fault Parallel	99
Spectrally Matched DZC Motion, UP Component, 1999 Duzce EQ, Turkey, SSE Level per NFPA 59A 2006 – Onshore	100
Spectrally Matched Unio Motion, N00W Component, 1985 Mexico EQ, SSE Level per NFPA 59A 2006 – Onshore, Fault Normal	101
Spectrally Matched Unio Motion, N90W Component, 1985 Mexico EQ, SSE Level per NFPA 59A 2006 – Onshore, Fault Parallel	102
Spectrally Matched Unio Motion, UP Component, 1985 Mexico EQ, SSE Level per NFPA 59A 2006 – Onshore	103
Spectrally Matched MEP Motion, EW Component, 2010 Chile EQ, SSE Level per NFPA 59A 2006 – Nearshore, Fault Normal	104

Spectrally Matched MEP Motion, NS Component, 2010 Chile EQ, SSE Level per NFPA 59A 2006 – Nearshore, Fault Parallel	105
Spectrally Matched MEP Motion, V Component, 2010 Chile EQ, SSE Level per NFPA 59A 2006 – Nearshore	106
Spectrally Matched CTO Motion, 180 Component, 2001 El Salvador EQ, SSE Level per NFPA 59A 2006 – Nearshore, Fault Normal	107
Spectrally Matched CTO Motion, 270 Component, 2001 El Salvador EQ, SSE Level per NFPA 59A 2006 – Nearshore, Fault Parallel	108
Spectrally Matched CTO Motion, UP Component, 2001 El Salvador EQ, SSE Level per NFPA 59A 2006 – Nearshore	109
Spectrally Matched Carlo Motion, 090 Component, 2002 Denali EQ, Alaska, SSE Level per NFPA 59A 2006 – Nearshore, Fault Normal	110
Spectrally Matched Carlo Motion, 360 Component, 2002 Denali EQ, Alaska, SSE Level per NFPA 59A 2006 – Nearshore, Fault Parallel	111
Spectrally Matched Carlo Motion, UP Component, 2002 Denali EQ, Alaska, SSE Level per NFPA 59A 2006 – Nearshore	112
Spectrally Matched DZC Motion, 180 Component, 1999 Duzce EQ, Turkey, SSE Level per NFPA 59A 2006 – Nearshore, Fault Normal	113
Spectrally Matched DZC Motion, 270 Component, 1999 Duzce EQ, Turkey, SSE Level per NFPA 59A 2006 – Nearshore, Fault Parallel	114
Spectrally Matched DZC Motion, UP Component, 1999 Duzce EQ, Turkey, SSE Level per NFPA 59A 2006 – Nearshore	115
Spectrally Matched Unio Motion, N00W Component, 1985 Mexico EQ, SSE Level per NFPA 59A 2006 – Nearshore, Fault Normal	116
Spectrally Matched Unio Motion, N90W Component, 1985 Mexico EQ, SSE Level per NFPA 59A 2006 – Nearshore, Fault Parallel	117
Spectrally Matched Unio Motion, UP Component, 1985 Mexico EQ, SSE Level per NFPA 59A 2006 – Nearshore	118
Comparison of Significant Duration $D_{(5-95)}$ of Spectrally Matched Horizontal Ground Motions for OBE Level per NFPA 59A 2006 with the Deterministic Estimates using Empirical Relationships	119
Comparison of Significant Duration $D_{(5-95)}$ of Spectrally Matched Horizontal Ground	

Motions for SSE Level for Onshore Location per NFPA 59A 2006 with the
Deterministic Estimates using Empirical Relationships..... 120

Comparison of Significant Duration $D_{(5-95)}$ of Spectrally Matched Horizontal Ground
Motions for SSE Level for Nearshore Location per NFPA 59A 2006 with the
Deterministic Estimates using Empirical Relationships..... 121

APPENDICES

Appendix A. Time-Dependent Calculations for the Alaska Megathrust Seismic Source	A1
Appendix B. Sensitivity Analysis for the Denali Fault Planar Source	B1
Appendix C. Design Spectra Per NFPA-59A 2013 and IBC (2012).....	C1
Appendix D. Development of Ground Acceleration Time Histories Per NFPA-59A 2013.....	D1
Appendix E. Characteristics of Spectrally Matched Ground Motions.....	E1

1.0 INTRODUCTION

1.1 Project Description

ExxonMobil Alaska LNG LLC (EMALL) is developing the onshore and nearshore LNG facilities in Nikiski, Alaska ([Plate 1](#)). Fugro Consultants Inc. (Fugro) is currently providing geotechnical site exploration, geohazard assessment, and earthquake engineering services for this project. Fugro performed Probabilistic Seismic Hazard Analyses (PSHA) to develop ground motion criteria for the planned facilities per the requirements of National Fire Protection Agency (NFPA 59A 2006) and ASCE 7-05. PSHA was conducted using a time-weighted average shear velocity in the upper 30 meters (V_{s30}) of 885 ft/s (270 m/s) to develop ground motions at the ground surface in the onshore and nearshore locations. The PSHA ground motions estimated at the ground surface are used to conduct liquefaction potential evaluations for the onshore and nearshore facilities in the companion Seismic Engineering report (Fugro Report No. 04.10140334-13).

In Phase 1, Fugro had performed PSHA (Fugro Report No. 04.10140094-6) using a V_{s30} of 900 ft/s (275 m/s) to develop ground motions at the ground surface for the onshore areas, per the requirements of NFPA 59A 2006 / ASCE 7-05 and NFPA 59A 2013 / ASCE 7-10. Since then, additional geotechnical explorations and geophysical investigation have been performed at the location of the onshore and nearshore facilities for Phase 2. In addition, the seismotectonic model used in the Phase 1 PSHA has been refined based primarily on additional geophysical data collected and industry data reviewed during Phase 2 of this project. Based on the review of data obtained from Phase 2 geophysical investigation and other available data sources, the refined site-specific seismotectonic model has included an updated characterization of local faults within a five-mile radius of project facilities. Therefore, this report presents updated design ground motion criteria and supersedes all previous ground motion evaluation reports.

Finally, additional analyses were also performed to develop ground motion criteria per the requirements of NFPA 59A 2013 and ASCE 7-10. The ground motion results per the requirements of NFPA 59A 2006 and ASCE 7-05 are presented in the main text of the report and the results for NFPA 59A 2013 and ASCE 7-10 are presented in [Appendices C and D](#), per the request of EMALL.

1.2 Work Authorization

The work was authorized under contract to ExxonMobil Alaska LNG LLC (EMALL), under work Order No. AKLNG-FUG-US-003 Rev 0, Agreement number A2275592, effective February 5, 2015.

1.3 Scope and Organization

Fugro conducted Probabilistic Seismic Hazard Analyses (PSHA) to estimate the severity of ground motions at the ground surface that may affect the future onshore and nearshore structures which will be developed as a part of the LNG project.

Fugro's scope of work for the seismic hazard analyses included the following tasks:

- Task 1 – Refinement of Seismotectonic Model;
- Task 2 – Probabilistic Seismic Hazard Assessment (PSHA);
- Task 3 – Development of Time Histories; and
- Task 4 – Reporting.

[Section 2.0](#) describes the regional tectonic setting of the project area, and includes discussions of regional historical seismicity and seismotectonic elements. [Section 3.0](#) provides detailed descriptions of the seismic source characterization parameters of the seismotectonic model, to be used in the seismic hazard analyses. [Section 4.0](#) describes the methodology used for PSHA, while [Section 5.0](#) presents the analysis and the PSHA results in the form of acceleration response spectra at the ground surface. [Section 6.0](#) presents the development of ground acceleration time histories. [Section 7.0](#) lists the references cited in this study. The approved scope of work for seismic hazard analyses also includes liquefaction potential evaluations and seismic slope stability evaluations. These evaluations will be presented in the forthcoming Seismic Engineering Report for the project (Fugro Report No. 04.10140334-13) and the Onshore Integrated Site Characterization and Geotechnical Engineering Report (Fugro Report No. 04.10140334-14), respectively.

1.4 Limitations of this Study

This report has been prepared solely to assist ExxonMobil Alaska LNG LLC (EMALL), and the engineering team members in the Pre-FEED design of the Nikiski terminal facility. The results herein apply to the specific locations mentioned and are not applicable to other locations.

Seismic hazard analysis is a dynamic, rapidly evolving field of earthquake engineering. It is likely that the standard of practice in the project region for these services will evolve over the next few years. In addition, new information regarding fault extent, geometry, and activity may also become available. Consequently, the results presented in this study should be reviewed if new data become available during the design of the project.

This report has been prepared for the exclusive use of ExxonMobil Alaska LNG LLC (EMALL), and its agents for the specific application to the proposed LNG terminal in Nikiski, Alaska. In our opinion, the findings, conclusions, professional opinions, and recommendations presented herein were prepared in accordance with generally accepted current seismic hazard geotechnical engineering practice.

Although information contained in this report may be of some use for other purposes, it may not contain sufficient information for other parties or uses. If any changes are made to the project as described in this report, the conclusions and recommendations in this report shall not be considered valid unless the changes are reviewed and the conclusions and recommendations of this report are modified or validated in writing by Fugro.

1.5 Summary and Findings

1.5.1 Probabilistic Seismic Hazard Analyses

Probabilistic seismic hazard analyses (PSHA) were conducted to develop ground surface level acceleration response spectra for the planned LNG facilities of the Alaska LNG project located in Nikiski, Alaska. The study involved the following:

- Developing a detailed seismotectonic model that characterizes the various sources of seismicity that impact the project area located in Nikiski, Alaska. This process involved delineating the geometry and seismicity characteristics of potential seismogenic sources within about 124 miles (200 kilometers) of the project area.
- Conducting PSHA to compute acceleration response spectra in accordance with the requirements of National Fire Protection Agency (NFPA) 59A 2006 and ASCE 7-05 guidelines for project facilities. According to NFPA, two levels of ground motions are developed for: Operational Basis Earthquake (OBE) corresponding to 475-year return period, and a more severe Safe Shutdown Earthquake (SSE) which is same as Maximum Considered Earthquake (MCE) per ASCE 7-05. According to ASCE 7-05 two levels of design ground motions are developed for: Maximum Considered Earthquake (MCE) and for Design Earthquake (DE).
- Conducting PSHA to compute acceleration response spectra in accordance with the requirements of National Fire Protection Agency (NFPA) 59A 2013 and International Building Code (IBC, 2012) guidelines for project facilities. According to NFPA, three levels of ground motions are developed for: Operational Basis Earthquake (OBE) corresponding to 475-year return period, which is the same as the Operational Basis Earthquake (OBE) per NFPA 59A 2006, a more severe Safe Shutdown Earthquake (SSE) which is same as “Risk-adjusted” Maximum Considered Earthquake (MCE_R) per ASCE 7-10, and a third level for Aftershock Level Event (ALE), equal to $\frac{1}{2}$ of SSE. According to IBC (2012) two levels of design ground motions are developed for: “Risk-adjusted” Maximum Considered Earthquake (MCE_R) per ASCE 7-10 and for Design Earthquake (DE). These results are presented in [Appendix C](#).
- Deaggregating the seismic hazard results to identify the key contributors to the hazard in each zone in terms of earthquake magnitude, distances to the seismogenic sources, and types of seismogenic sources.

The primary results from the seismic hazard analyses were as follows:

- Review of the seismotectonic setting and historical seismicity identified interplate, intraplate and shallow crustal fault sources in the site region. Based on the information gathered from available geotechnical data for project facilities (including the in-situ shear wave velocity measurements, Interferometric Multichannel Analysis of Surface Waves and Standard

Penetration Tests), PSHA was conducted at ground surface with a time-weighted average shear wave velocity (V_s) in the top 100 feet (approximately 30 meters) (i.e., 100 ft/integral from 0 to 100 ft of $dz/V_s(z)$) of 885 ft/s (270 m/s). The V_{s30} parameter is one of the main parameters used by the Ground Motion Prediction Equations (GMPEs) especially the most recent developed GMPEs. Tables 1.1 and 1.2 summarize the horizontal PGA values at the ground surface ($V_{s30} = 885$ ft/s) for planned onshore and nearshore facility locations, respectively.

Table 1.1: Peak Ground Acceleration Values of Horizontal Component at the Ground Surface ($V_{s30} = 885$ ft/s) per NFPA 59A 2006 and ASCE 7-05 for Onshore Facilities

NFPA 59A (2006)		ASCE 7-05	
Operating Basis Earthquake (OBE) (g)	Safe Shutdown Earthquake (SSE) (g)	Maximum Considered Earthquake (MCE) (g)	Design Earthquake (DE) (g)
0.528	0.897	0.897	0.598

Table 1.2: Peak Ground Acceleration Values of Horizontal Component at the Ground Surface ($V_{s30} = 885$ ft/s) per NFPA 59A 2006 and ASCE 7-05 for Nearshore Facilities

NFPA 59A (2006)		ASCE 7-05	
Operating Basis Earthquake (OBE) (g)	Safe Shutdown Earthquake (SSE) (g)	Maximum Considered Earthquake (MCE) (g)	Design Earthquake (DE) (g)
0.528	0.901	0.901	0.601

- The deaggregation of the hazard reveals that the majority of the hazard for short structural periods (i.e. PGA) is dominated by intraslab sources for both 475- and 2475-year return periods for both onshore and nearshore locations. At longer structural periods (i.e. 1 and 3 seconds) contribution from the subduction interface, is also significant. Only one local fault, F7 - Middle Ground Shoal Anticline and Granite Point Anticline, is seen to contribute significantly (up to 32%) for the longer structural periods for 2,475-year event.
- Based on deaggregation by magnitude and distance, for both short and longer structural periods the seismic hazard at the project site is controlled by mainly three scenarios for both onshore and nearshore locations: (a) larger magnitude earthquakes, between 9 to 9.2, at distances between about 31 to 62 mi (50 km to 100 km) attributed to the megathrust

events on S2 interface (Prince William Sound), (b) intermediate to large magnitude events (i.e., 7.0 to 8.0) at distances between about 31 to 93 mi (50 km to 150 km) associated with the intermediate depth and deep intraslab subduction earthquakes, and (c) and intermediate to large magnitude shallow earthquakes (i.e., 7 to 7.5) at distances about 3.1 to 6.2 mi (5 to 10 km) from the project site.

- The vertical response spectra were developed by applying vertical to horizontal (V/H) spectral ratios to the ground surface horizontal response spectra. The estimated vertical peak ground acceleration values at surface for different shaking levels per NFPA 59A 2006 and ASCE 7-05 are reported in [Tables 1.3 and 1.4](#). The vertical response spectra at surface for OBE, SSE, ALE, MCE_R and DE in accordance with the requirements of NFPA 59A 2013 and ASCE 7-10 are presented in [Appendix C](#).

Table 1.3 Peak Ground Acceleration Values of Vertical Component at the Ground Surface ($V_{s30} = 885$ ft/s) per NFPA 59A 2006 and ASCE 7-05 for Onshore Facilities

NFPA 59A (2006)		ASCE 7-05	
Operating Basis Earthquake (OBE) (g)	Safe Shutdown Earthquake (SSE) (g)	Maximum Considered Earthquake (MCE) (g)	Design Earthquake (DE) (g)
0.407	0.691	0.691	0.461

Table 1.4 Peak Ground Acceleration Values of Vertical Component at the Ground Surface ($V_{s30} = 885$ ft/s) per NFPA 59A 2006 and ASCE 7-05 for Nearshore Facilities

NFPA 59A (2006)		ASCE 7-05	
Operating Basis Earthquake (OBE) (g)	Safe Shutdown Earthquake (SSE) (g)	Maximum Considered Earthquake (MCE) (g)	Design Earthquake (DE) (g)
0.407	0.694	0.694	0.463

1.5.2 Development of Ground Acceleration Time Histories

Five sets of accelerograms were selected to represent the shaking corresponding to Safe Shutdown Earthquake (SSE) / Maximum Considered Earthquake (MCE), and Operation Basis Earthquake (OBE) per the NFPA 59A 2006 guidelines. The ground motions were selected from

high-quality recordings with emphasis given to the overall shape of the response spectra of the recorded motion relative to the target spectrum, as well as the magnitude, distance, significant duration (D_{5-95}) and PGA of the recorded time-histories. The design data are applicable at ground surface with V_{s30} of 885 ft/s. The ground motions matched to Safe Shutdown Earthquake (SSE) / “Risk-adjusted” Maximum Considered Earthquake (MCE_R) per the NFPA 59A 2013 code are presented in [Appendix D](#).

2.0 SEISMOTECTONIC SETTING

2.1 Introduction

Geological, geophysical, tectonic, and seismological data and analyses from coastal and inland southern Alaska were used to develop a seismic source model for estimating the strong ground motion hazard at the proposed Nikiski LNG terminal site, located on the Kenai Peninsula in the Cook Inlet (referred to herein as the site, [Plate 1](#)). The study region is defined by a 124 mi (200 km) radius around the site. The study region includes all known structures and seismic sources relevant to ground motion estimations at the proposed site.

[Sections 2.1](#) and [2.2](#) provide an introduction to the regional tectonic setting and historical seismicity of the study region. [Section 2.3](#) provides a detailed discussion of potential seismic sources evaluated. [Section 3.0](#) then characterizes those seismic sources that were used as inputs to the PSHA.

2.2 Regional Tectonic Framework, and Tectonic and Physiographic Elements

The study region, centered in the upper Cook Inlet Basin, is located along the active convergent margin between the North American and Pacific plates ([Plate 2](#)). This region is characterized by high rates of seismicity and relatively frequent moderate to great earthquakes. The 1964 moment magnitude (M_w , or **M**) 9.2 Good Friday Earthquake was the largest recorded event in Alaska. Active tectonism and associated earthquake activity in the region are driven by interactions between four principal tectonic domains: (1) the Pacific Plate, (2) North American Plate, (3) Yakutat Terrane, and (4) Southern Alaska Block. The locations of these domains are shown schematically on [Plate 2](#). In summary, the Yakutat Terrane is a microplate that is partially coupled to the Pacific Plate, although it is moving north at a slower rate and along a more westerly azimuth. The Southern Alaska Block is part of the western edge of the North American Plate, but is moving differentially with respect to the rest of the plate — it is rotating in a counterclockwise fashion. The Pacific Plate is subducting below the edge of the North American Plate/Southern Alaska Block as well as below the southwestern edge of the Yakutat Terrane. The North American Plate/Southern Alaska Block is being obducted, or emplaced, onto the northern edge of the Yakutat Terrane, but without accompanying plate subduction.

At the longitude of the site region, motion of the Pacific Plate relative to the North American Plate is directed along an azimuth of approximately 349 degrees (Freymueller et al., 2013). The rate of convergence is 2.0 in/yr (52 mm/yr) to 2.7 in/yr (55 mm/yr) (Perry et al., 2009; Bruhn and Haeussler, 2006). Plate convergence is being accommodated largely by the Aleutian megathrust ([Plate 2](#)). North of the Aleutian megathrust, in the interior of south-central Alaska, north-directed motion of the plate is accommodated primarily by dextral slip along the Denali fault ([Plates 2 and](#)

3), and reverse faulting along the Castle Mountain fault (Plate 3) and Foothills fold-and-thrust belt (not shown due to its distance from the Site).

Deformation within the site region is intimately linked to northwest-directed motion of the allochthonous Yakutat microplate (Plate 2). As mentioned above, this microplate lies between the North America Plate to the north and the Pacific Plate to the south, and is being actively underthrust below the southern edge of the North American Plate at a rate of 1.7 in/yr (44 mm/yr) (Perry et al., 2009). The collision drives counterclockwise rotation in the interior of south-central Alaska (vis a vis the Southern Alaska Block, Plate 2) as well as contraction within Cook Inlet and lateral escape to the southwest (Haeussler et al., 2000; Haeussler, 2008).

Based on this tectonic framework, the site region lies within the Southern Alaska Block (which is part of the North American Plate). In the following subsections, descriptions are provided for tectonic and physiographic elements within the site region. These include: (1) the Cook Inlet Basin—a forearc basin in the upper plate of the subduction zone, (2) the Kenai and Chugach Mountains—the accretionary complex above the Aleutian megathrust, (3) the Talkeetna Mountains, and (4) the Alaska Range-Aleutian volcanic arc (Plates 3 and 4).

2.2.1 Cook Inlet Basin

The Cook Inlet basin (Plate 3) is a Tertiary forearc basin (Haeussler et al., 2000) bounded to the west-northwest by the Alaska Range and Aleutian volcanic arc, and to the east-southeast by the Chugach and Kenai Mountains. The depth to the top of the subducting Pacific slab beneath Cook Inlet rapidly increases from 22 mi (35 km) near Anchorage to 31-38 mi (50-60 km) beneath the basin's center (Page et al., 1991; Wesson et al., 2007). Four fault zones define the basin margins: the Border Range fault and Bruin Bay fault, both of which are inactive, and the Quaternary-active Castle Mountain fault and Lake Clark fault (e.g., Koehler et al., 2012a; Plate 3).

Cook Inlet Tertiary basin fill unconformably overlies the Mesozoic basement terranes bounding the inlet (Hartman et al., 1972; Haeussler et al., 2000). The Tertiary basin fill and overlying Quaternary deposits, known as the Kenai Group, have a combined thickness of over 20,000 ft (6100 m) (Hartman et al., 1972; Shellenbaum et al., 2010) (Plate 5). Formations include, from oldest to youngest, the West Foreland Formation, Hemlock Conglomerate, Tyonek Formation, Beluga Formation, and Sterling Formation (Hartman et al., 1972; Plate 6). The Pliocene and younger Sterling Formation and the overlying early Quaternary sediments constitute up to 10,000 ft (3000 m) of sediment in the central and eastern Cook Inlet Basin. They are glacial and alluvial materials sourced from the Alaska and Chugach ranges and consist of massive sandstones, conglomeratic sandstones, and interbedded claystones (Hartman et al., 1974; Calderwood and Fackler, 1972). Cook Inlet basin sediments exhibit multiple northeast-trending folds, subparallel to the basin margins (Kirschner and Lyon, 1973; Fisher et al., 1987; Magoon et al., 1976; Alaska Oil and Gas Conservation Commission, 1994; Haeussler et al., 2000; Koehler et al., 2012a). Near the Castle

Mountain fault the fold axes have a more easterly trend (Plates 3 and 4), which has been interpreted as drag from right-lateral shear along the Castle Mountain fault (Haeussler et al., 2000).

Folding of Cook Inlet forearc basin materials provides the structural traps for the inlet's numerous oil and gas fields, and these folds have been described in the geologic literature from the early 1960s (Kelly, 1961, 1963; Kirschner and Lyon, 1973; Boss et al., 1976). Since that time, understanding of the structural relationships between folds, buried faults, and earthquakes has grown substantially. Events such as the 1995 Kobe M_w 6.9 earthquake, sourced in a transpressional forearc setting, have provided valuable understanding of the seismic hazard potential in forearc settings above Benioff zones (Sugiyama, 1995; Wesnousky and Scholz, 1982). Additionally, Bucknam et al. (1992) and Johnson et al. (1996) show that events with magnitudes larger than 8.0 have likely occurred as a result of transpression within the Cascadia forearc basin overlying the subduction zone (Haeussler et al., 2000). The Alaska Quaternary Fault and Fold database (QFF) (Koehler et al., 2012a) identifies 19 potential Quaternary active tectonic structures in the Cook Inlet basin based on the correlation of magnetic and gravity lineaments with available oil and gas industry seismic reflection data.

Mapped structures in Cook Inlet are described as fault-cored anticlines (Fisher and Magoon, 1978; Haeussler et al., 2000; Bruhn and Haeussler, 2006; Haeussler and Saltus, 2011). Steeply dipping master faults accommodate predominantly reverse motion, with faults extending through the Tertiary basin fill into the Mesozoic basement (Bruhn and Haeussler, 2006). Cross-sections generated from industry seismic data indicate variable directions of structural vergence: some faults dip to the northwest while others dip to the southeast (Bruhn and Haeussler, 2006).

Haeussler et al. (2000) used existing public- and private-sector data to evaluate Quaternary activity, timing of onset, and rates of deformation of these structures. While the data permit deformation initiating as early as late Miocene time, most of it likely occurred in the late Pliocene and Quaternary, and many structures are likely still active (Haeussler et al., 2000). For example, depositional patterns within the Miocene Beluga Formation suggest that Cook Inlet deformation may have begun post-late Miocene time (Hartman et al., 1974). In contrast, the thickness of the Beluga Formation is uniform across the mapped fold axes, which indicates that folding initiated after the strata formed (Haeussler et al., 2000). In terms of assessing the Quaternary activity on the Cook Inlet folds, Haeussler et al. (2000) list the following observations and/or lines of reasoning:

- The Castle Mountain fault that bounds the basin is active. Assuming the anticlines are structurally linked with this fold, they, too, must be active;
- Virtually all strata above the base of the Pliocene Sterling Formation show uniform thicknesses across the crests of folds, indicating most of the deformation is post-Pliocene;

- Growth wedges, such as those adjacent to the Beluga and Castle Mountain fault folds, are shallow, suggesting Quaternary fold growth;
- Growth wedge margins are folded, indicating present-day deformation;
- The seafloor above the North Cook Inlet fold axis is uplifted and folded concordantly with the deeper strata;
- Diamicts at Granite Point, of possible Quaternary age, are tilted within the Granite Point anticline;
- The Ivan and Lewis River channels suggest active response to the Lewis River, Ivan River, and Stump Lake anticlines.

Historical seismicity patterns in the Cook Inlet region bolster the case for ongoing forearc basin deformation. Frequent $M \leq 3.0$ earthquakes with depths of 10 to 22 mi (15 to 35 km), clustered at 12 to 18 mi (20 to 30 km) depth (Stephens et al., 1995), occur above the Benioff zone of the subducting Pacific slab (Page et al., 1991; Stephens et al., 1995; Ratchkovski et al., 1998). An examination of focal mechanisms for 21 of these earthquakes by Ratchkovski et al. (1998) determined that two-thirds of these events were consistent with thrust motion on northeast-striking nodal planes, and the remaining one-third of events were consistent with strike-slip motion on northeast- and northwest-striking nodal planes. Haeussler et al. (2000) do not correlate any $M \leq 3.0$ earthquakes to a known structure within the Cook Inlet basin, but the depths and focal mechanisms of these earthquakes are consistent with structures resulting from Upper Cook Inlet forearc basin deformation.

A Ms 6.9 earthquake in 1933 with an epicenter location 10 ± 31 mi (16 ± 50 km) south of the Castle Mountain fault was widely felt in southern Alaska (Abe, 1984). Modified Mercalli intensity (MMI) maxima of the 1933 event were greatest on the northwest margin of Upper Cook Inlet. Haeussler et al. (2000) indicate that this intensity pattern is inconsistent with a subduction zone earthquake at this epicenter location, which would produce MMI maxima on the southeast side of Cook Inlet (Anchorage area). Instead, Haeussler et al. (2000) interpret the observed MMI from the 1933 event, with maximum intensities on the northwest side of the Cook Inlet, to indicate a seismic source within the Cook Inlet forearc basin.

2.2.2 Kenai Mountains and Chugach Mountains

Located adjacent to the Aleutian megathrust and subduction zone, the Prince William Sound area, Kenai Mountains and Chugach Mountains (Plate 3) constitute one of the world's largest accretionary complexes (Plafker et al., 1994a). In map view, this suite of features defines an arcuate, concave-to-the-south fabric, which reflects the deformational history of the accretionary prism within an evolving convergent plate margin.

The Kenai Peninsula encompasses two markedly different geomorphic domains: the Kenai Lowlands to the west and the Kenai Mountains to the east (Plate 3). The geomorphic domains are separated by the Border Ranges fault, a buried crustal suture separating the younger Mesozoic-Cenozoic Southern Margin Composite terrane to the south and east, from the older Late Jurassic-Early Cretaceous Wrangellia Composite terrane to the west and north. Extensive Late Wisconsin and earlier glacial deposits cover the Kenai Lowlands (Karlstrom, 1964), as reflected by the low relief and abundance of poorly drained bogs, ponds, and lake.

The uplifted Chugach Terrane east of the Kenai Lowlands and north of Prince William Sound forms the Kenai and Chugach Mountains, which reach elevations up to 7,000 ft (2100 m) in the Kenai and up to 13,000 ft (4000 m) in the Chugach. The Chugach Mountains continue to the north and east, bounded to the north by the Border Ranges fault and to the south by Prince William Sound. The Chugach Mountains receive abundant annual precipitation and are the source of some of Alaska's largest glaciers.

The Chugach Terrane, as described by Plafker et al. (1994a), comprises the following three assemblages: (1) Late Triassic to Early Jurassic greenschist and blueschist; (2) Mississippian to Cretaceous melange of the McHugh Complex; and (3) Upper Cretaceous flysch of the Valdez Group. The geologic make up of these terranes is described in more detail below. In the Port Graham vicinity at the southwestern tip of the Kenai Peninsula, a small area of Upper Triassic to Jurassic rocks and minor outcrops of Tertiary Tyonek Formation have been assigned to the Hidden terrane of Wilson et al. (1999). The Chugach and Hidden terranes are separated by the Border Ranges fault.

The Upper Cretaceous Valdez Group consists primarily of deformed metasedimentary greywacke, siltstone and shale, and is thought to have originated as turbidity current deposits along an oceanic trench (Tysdal and Case, 1979; Nelson et al., 1985; Winkler and Plafker, 1981; 1993). This assemblage also includes a variety of tholeiitic meta-volcanic and meta-intrusive rocks and locally a melange facies (Wilson et al., 2008). Metamorphic grade of the Valdez Group ranges from laumontite- to mid-greenschist-facies, with local amphibolite facies east of the Copper River (Nelson et al., 1985; Winkler and Plafker, 1981).

The McHugh Complex consists of diverse and variably-aged (Mississippian to Cretaceous) materials (i.e., mélangé) that represent multiple stratigraphic sequences, which were consolidated into a contiguous lithologic complex by underthrusting of the subducting Pacific plate. Melange materials include fault-bounded sequences of weakly metamorphosed clastic rocks (greywacke, arkose, siltstone, and conglomeratic sandstone); basaltic greenstone with associated radiolarian metachert, metasiltstone, and argillite; and bodies of gabbro and ultramafic plutonic rocks such as serpentized dunite with chromite, pyroxenite (Bradley et al., 1999; Wilson et al., 2008).

At the southeastern tip of the Kenai Peninsula, there are minor exposures of the Tustumena pluton, a Paleocene to Eocene granite and granodiorite body that may be part of a larger batholith exposed intermittently throughout the area (Wilson et al., 2008).

2.2.3 Talkeetna Mountains

The Talkeetna Mountains ([Plate 3](#)) are an elevated block that lies between the Copper River and Susitna basins, and contain glaciated peaks between 6,560 and 9,840 ft (2000 to 3000 m) in elevation. The Talkeetna Mountains consist of an assemblage of northeast-trending lithotectonic terranes, or fault-bounded packages of rocks with a geologic history distinct from that of adjacent bodies, including the North Talkeetna Flysch basin (not shown on accompanying figures because it is located in the northern Talkeetna Mountains, well beyond the site radius) and Wrangellia Composite Terrane (Glen et al., 2007b). The Wrangellia Composite Terrane is composed of largely late Paleozoic to early Mesozoic metavolcanic and metasedimentary rocks that originated well south of their current (~30° latitude) position, and likely were sutured together in the Late Jurassic (Csejtey et al., 1982). The terrane was then accreted onto the North America craton in the mid to late Cretaceous, and translated northward to its current location via the Fairweather-Queen Charlotte fault ([Plate 2](#); Ridgeway et al., 2002). Late Cretaceous through Tertiary volcanic and hypabyssal intrusions are also found throughout the Talkeetna Mountains and often intrude or overlie the Cretaceous accretionary structures.

2.2.4 Western Alaska Range

The Alaska Range ([Plates 1 and 3](#)) extends in a 406-mi-long (650-km-long) arc that roughly parallels the Aleutian subduction zone. It encompasses some of North America's tallest peaks, including Mt. Mickinley, the tallest at 20,320 ft (6195 m). For much of its length, the Alaska Range is bisected by the Denali fault. Superimposed onto the eastern edge of the Alaska Range is the eastern Aleutian volcanic arc. Within the site region, this includes (from north to south) the Hayes, Spurr, Redoubt, Iliamna, and Augustine volcanoes ([Plate 3](#)). Augustine volcano is the most active volcano in the eastern Aleutian arc and has had multiple eruptions in historical times. In 1883, an eruption generated a tsunami in Cook Inlet from a debris avalanche.

Upper crustal seismicity in the Alaska Range occurs primarily in the central and eastern portions, and is associated largely with the Denali fault. Seismicity in the western Alaska Range occurs at depths primarily below 37 mi (60 km), and is likely occurring within the deep subducting Pacific slab.

2.3 Historical Seismicity

The study region is characterized by moderate to high rates of seismicity, and the historical record contains several major earthquakes (defined as M_w greater than ~7), including the great Alaska earthquake of 1964, an M_w 9.2 event that is the second largest earthquake of the past 150 years

(Plate 4). The historical record of major earthquakes in most of greater southeast Alaska is robust and extends back in time to approximately 1918 (Page et al., 1991). The following paragraph describes the history of earthquake recordings in Alaska and paraphrases “Seismicity of Continental Alaska,” which was written by Page et al. (1991) and updated against Wesson et al (2007).

Written accounts of seismicity in Alaska date back to at least 1786, with distal seismograph records of seismicity in Alaska beginning with a series of major earthquakes near Yakutat Bay in 1899. The first local seismograph was sited in Sitka in 1904, with a second added in 1935 at the University of Alaska near Fairbanks. Seismograph instrumentation greatly increased after the great Alaskan earthquake of 1964, with a four-station telemetered regional network installed by the University of Alaska at Fairbanks in south and south central Alaska in 1966, and a six-station telemetered network, the Alaska Tsunami Warning Center, installed in continental Alaska and the Aleutian Islands by the US Coast and Geodetic Survey (now NOAA) in 1967. By 1973, these two networks totaled nearly 40 stations. Regional seismograph networks increased to a peak in the early 1980s, including the operation of over 50 stations by the (United States Geological Survey) USGS in the Cook Inlet and Valdez area, now operated by the Alaska Earthquake Information Center (AEIC). In 1983, university networks in western Alaska and the Kodiak Island region were discontinued, and by 1986 the number of stations operated by the USGS had dropped to 42. In 1986, the AEIC was established by Alaska statute with the mandate to collect, analyze, and archive seismic event data for the state. Currently, the AEIC records data from more than 400 stations across the state and reports on approximately 20,000 earthquakes a year (AEIC, 2013).

Plate 4 shows a catalog of seismicity within the study region with epicenter symbols scaled by size and color-coded by depth (AEIC, 2013). The earthquake catalog (Wesson et al., 2007) used in this project was assembled from a number of sources, including local networks and regional networks (US Geological Survey, and Harvard University). In discussions below, **M** can be considered equivalent to moment magnitude (M_w) unless otherwise noted.

Significant major and great earthquakes within the study region include:

- 1899 **M** 7.2 Kenai earthquake
- 1912 **M** 7.1 Alaska Peninsula earthquake
- 1928 **M** 7.3 Gulf of Alaska earthquake
- 1933 **M** 7.1 Anchorage earthquake
- 1934 **M** 7.1 Southern Alaska earthquake
- 1946 **M** 7.2 Unimak earthquake
- 1949 **M** 7.0 Gulf of Alaska earthquake

- 1964 **M 9.2** Great Alaskan earthquake
- 2002 **M 7.9** Denali earthquake
- 2014 **M 7.9** Rat Islands earthquake

Brief descriptions of all these major and great earthquakes are provided in [Sections 2.2.1 through 2.2.10](#) below. Locations of these events are shown on [Plate 4](#), where they can be identified by year and magnitude. Note that the 1964 **M9.2** Great Alaskan earthquake occurred beyond the eastern edge of the site region.

2.3.1 1899 M 7.2 Kenai Earthquake

The 1899 **M 7.2** was reported at Tyonek, AK as a “severe” (original source language) earthquake, but does not describe associated damage or deformation. The epicentral location is placed at 60.0N, 150.0W beneath the Kenai Peninsula, approximately 25 mi (40 km) west of Seward (Stover and Coffman, 1993).

2.3.2 1912 M 7.1 Alaska Peninsula Earthquake

This earthquake has an epicentral location of 61.0N, 147.5W. Estimated focal depth of this event is 56 mi (90 km), with an assigned maximum MMI of 5. No reports of injuries, damage, or surficial deformation are found (NGDC, 2012).

2.3.3 1928 M 7.3 Gulf of Alaska Earthquake

This earthquake has an epicentral location of 60.0N, 146.5W; estimated focal depth is unknown. In the Cordova area, the second of three distinct felt shocks was reported as the strongest, with men thrown from their bunks 30 mi (48 km) north of Cordova, cracking of plaster in Cordova, and numerous landslides in the mountains. Shaking in Valdez was described as “heavy,” and the felt area extended to Anchorage, Chickaloon, Matanuska, and Seward (Stover and Coffman, 1993).

2.3.4 1933 M 7.1 Anchorage Earthquake

This earthquake has an epicentral location of 61.25N, 150.75W, with an estimated focal depth of 16 mi (25 km). Houses were shaken off of foundations at Old Tyonek, plate-glass storefront windows were broken, merchandise was knocked off shelves, and telegraph lines were down 50 mi (80 km) from Anchorage. The felt area included Kodiak Island and along the Aleutian Islands, and aftershocks were numerous (Stover and Coffman, 1993).

2.3.5 1934 M 7.1 Southern Alaska Earthquake

This earthquake has an epicentral location of 61.25N, 147.5W, with an estimated focal depth of 50 mi (80 km). Windows were broken, items thrown from shelves, and telephone lines were downed in Anchorage. The felt area extended to several towns in the region (Stover and Coffman, 1993).

2.3.6 1946 M 7.2 Unimak Earthquake

This earthquake has an epicentral location of 59.11N, 148.94W, with an estimated focal depth of 35 mi (56 km). Only minor seismic damage occurred to buildings on Unimak Island. The earthquake generated a tsunami with an estimated height of 115 feet (35 meters) which destroyed the Unimak lighthouse, caused damage at Dutch Harbor and the Aleutian Island of Ikatan, the west coasts of North and South America, and produced devastating losses at Hilo, Hawaii, of 159 lives and \$26 million to property (Stover and Coffman, 1993).

2.3.7 1949 M 7.0 Gulf of Alaska Earthquake

This earthquake has an epicentral location of 59.75N, 149.0W, with an estimated focal depth of 31 mi (50 km). There are no reports of damage associated with this event.

2.3.8 1964 M 9.2 Great Alaskan Earthquake

The M 9.2, March 28, 1964 Great Alaskan earthquake had an epicenter approximately 47 mi (75 km) west of Valdez, in the north Prince William Sound. The subsurface rupture area encompasses the entire study region. The isoseismal map of the event shows the study region experienced ground shaking with Modified Mercalli scale intensities of VII in the Cook Inlet region, and VIII to X in Prince William Sound, eastern Kenai Peninsula south to Seward, and west to Anchorage and Turnagin Arm (Stover and Coffman, 1993). The earthquake is one of the largest events ever recorded since global instrumental recordings began in the late 1800s.

The 1964 earthquake ruptured approximately 497 mi (800 km) of the Aleutian megathrust with left-lateral reverse-slip motion, and produced approximately 66 ft (20 m) of maximum displacement (Christensen and Beck, 1994). The earthquake was felt over 700,000 square miles (1.8 million square kilometers) in Alaska and Canada. Coseismic vertical displacements affected an area of about 200,100 square miles (520,000 square kilometers). Prince William Sound experienced up to 38 ft (11.5 meters) of uplift, and 7.5 ft (2.3 meters) of inland subsidence (relative to sea level) occurred (Plafker, 1967). A total of 15 fatalities were attributed to the earthquake and 113 from the ensuing tsunami. In Anchorage the earthquake destroyed structures up to 6-stories-high and triggered numerous destructive landslides. On the Kenai Peninsula published literature documented extensive ground breakage which included ground cracking, and ground cracking with associated eruptions of sand and water.

2.3.9 2002 M 7.9 Denali Earthquake

The M_w 7.9 2002 Denali fault earthquake is the largest onshore strike-slip earthquake in North America in the past 150 years (Eberhart-Phillips et al., 2003). The earthquake initiated on the previously unrecognized Susitna Glacier thrust fault with a 30 mi (48 km) surface rupture and up to 36 ft (11 m) of displacement (Crone et al., 2004). The earthquake then propagated eastward, rupturing 140 mi (226 km) of the central Denali fault and 41 mi (66 km) of the Totschunda fault.

Average slip along the Denali fault was approximately 16 ft (5 m) with a maximum slip of 29 ft (8.8 m) west of the junction with the Totschunda fault (Haeussler et al., 2004). The earthquake caused no fatalities and minimal damage to infrastructure, likely because of the sparse population density near the fault. Maximum estimated intensities of the earthquake in the Study Region are Modified Mercalli scale IV in Prince William Sound and the Kenai Peninsula, and V to VI in the Susitna Basin at the northern Cook Inlet shoreline and in the Chugach Mountains northwest of Anchorage and Prince William Sound (USGS, 2011).

2.3.10 2014 M 7.9 Rat Islands Earthquake

The June 23, 2014 Rat Islands occurred about 1,200 miles (2,000 km) west of the site in the central part of the Aleutian arc at a depth of about 62 mi (100 km). Although it occurred a significant distance from the site, it is important because it is the largest intraslab earthquake to be included in the historic catalog for the Alaska-Aleutian arc. The occurrence of this event caused the M_{\max} of intraslab events to be raised to **M 8.0**, from the **M 7.5** of previous studies (e.g., Wesson et al., 2007).

The focal mechanism for the mainshock is consistent with a normal faulting event on either a northwest-striking plane that dips steeply to the northeast, or northeast-striking plane that dips at a shallow angle to the southeast. While the USGS rupture inversion prefers the northeast-striking plane, similar analysis by Cedric et al. (2014) prefers the northwest-striking, steeply dipping plane. If this is confirmed, the earthquake would be similar in tectonic character to intraslab events in the Puget Sound region.

2.4 Potential Seismic Sources in Southern Alaska

Potential seismic sources in the study region originate within one of four tectonic environments, which are described in the sections below. Any one of these environments may include multiple types of fault sources. The four tectonic environments include: (1) the Aleutian subduction zone, (2) the Yakutat microplate, (3) the deep Pacific Plate intraslab, and (4) the Southern Alaska Block. The extents of these features, except for the Pacific Plate intraslab, are shown on [Plate 2](#).

2.4.1 Aleutian Subduction Zone

The Aleutian subduction zone ([Plate 2](#)) is one of the longest and most tectonically active plate boundaries in the world. It extends for nearly 2,485 mi (4000 km) from south central Alaska to the Kamchatka peninsula in eastern Russia, and has produced one of the world's largest earthquakes—the 1964 **M 9.2** Great Alaskan earthquake. The subduction zone is comprised of three distinct tectonic environments: (1) A continental subduction zone in the east; (2) an island arc, which is defined by the central Aleutian volcanic chain; and (3) a zone of oblique subduction and transform tectonics in the west (Nishenko and Jacob, 1990). The eastern section is the most

significant portion of the subduction zone with respect to the evaluation of the seismic hazards in the Cook Inlet basin because of its proximity.

The geometry of the down-going Pacific Plate within a few hundred kilometers of the site is fairly well-known because of studies of the 1964 **M** 9.2 earthquake, seismic refraction/reflection surveys (e.g., Brocher et al., 1994), and research results from a regional seismograph network operated by the Alaska Earthquake Information Center (AEIC) (Ratchkovski and Hansen, 2002). Beneath Prince William Sound and the Kenai Mountains ([Plate 3](#)), the plate interface has an extremely low dip down to a depth of approximately 19 to 25 mi (30 to 40 km). Below this depth it descends into the upper mantle. Further to the northwest, the slab dip increases rapidly.

Historical seismicity demonstrates that the length of seismic rupture of the Aleutian interface may be controlled by segmentation boundaries. Studies of subsided peats and sediments in the Cook Inlet (Hamilton and Shennan, 2005; Hamilton et al., 2005; Shennan and Hamilton, 2006) provide additional constraints on recurrence intervals and the segmentation of the Aleutian subduction interface zone.

2.4.2 Yakutat Microplate

The Yakutat terrane, or microplate, is a 373-mi-long, 124-mi-wide (600-km-long, 200-km-wide) allochthon, which is bounded on the southwest by the Transition fault ([Plate 2](#), Haeussler, 2008). A 140-mi-long (225-km-long) portion of the microplate is being underthrust below the Chugach terrane, forming the present-day Chugach/St. Elias Range (Plafker, 1987; Meigs and Sauber, 2000; Montgomery, 2002; Spotila et al., 2004; Berger and Spotila, 2008; Berger et al., 2008; Perry et al., 2009). Geophysical, seismic and structural studies indicate that the Yakutat terrane arrived at its present location sometime after the early Pliocene (Bruns, 1983; Fletcher and Freymueller, 1999, 2003; Perry et al., 2009).

GPS measurements of contemporary regional strain show that the Yakutat microplate is moving northwest at ~ 1.7 in/yr (44 mm/yr) relative to the Southern Alaska Block (Elliott et al., 2010; [Plate 2](#)). The velocity is similar in magnitude, albeit slower, to the Pacific Plate, which introduces substantial coupling between the two plates.

The overall north-directed motion of the Yakutat microplate is well documented; however, details regarding the number, location and style(s) of faulting within the microplate itself are poorly understood (Wesson et al., 2007). Current tectonic models infer the presence of several east-striking, north-dipping thrust faults beneath the heavily glaciated region along the onshore portion of the southern Alaska coast (Wesson et al., 2007).

2.4.3 Intraslab

Intraslab earthquakes occur within the down-going Pacific Plate where the slab dip increases as it descends into the upper mantle, below the megathrust interface with the North America Plate.

These intraslab earthquakes, considered capable of reaching magnitudes of **M** 8.0, are due to factors such as ridge-push, gravitational pull of the down-going slab plate, and metamorphic reactions due to increasing temperature and pressure within the down-going plate. Notable analog earthquakes within similar tectonic settings include the 1965 **M**6.5 and 2001 **M**6.8 Nisqually, Washington earthquakes associated with the Cascadia subduction zone. In the study region, the intraslab earthquake zone consists of two parts: an intermediate zone that dips east at about 25° and located at depths between 31 and 50 mi (50 and 80 km), and a deeper zone that dips more steeply and is located at depths between 50 and 93 mi (80 to 150 km; Wesson et al., 2007). The June 23, 2014 **M** 7.9 Rat Islands earthquake ([Section 2.2.10](#)) is highly relevant to our estimation of maximum magnitudes of this seismic source.

2.4.4 Southern Alaska Block

The Southern Alaska block, a portion of the North American Plate that underlies the site and overrides the subducting Pacific Plate, includes a number of seismogenic faults. Individual faults considered in the source model are described below, and are based on documented or assumed activity levels described in the published literature. These faults are included in the source model either because of their ability to generate large earthquakes, or their close proximity to the site.

2.4.4.1 *Castle Mountain fault*

The Castle Mountain fault ([Plate 3](#)) is an active, reverse or oblique-reverse fault that can be divided into eastern and western sections. The eastern section is combined with the Caribou fault of Plafker et al. (1994b) based on parallel surface traces and evidence that both faults have Quaternary displacement. The eastern section of the fault is primarily recognized in bedrock and has no evidence for Holocene surface rupture; however, it does have documented historical seismicity of M_b 5.7 (1984 EQ documented in Lahr et al. 1980). The western section is defined by a 39-mi-long (62-km-long) Holocene fault scarp (north side up), but no known large historical seismicity (Flores and Doser, 2005). The fault trace was mapped in detail by Detterman et al. (1974) and again by Haeussler (1998) and Koehler et al., (2012b). The fault has a reported dip of 75° to the northwest (Koehler et al., 2012b).

Trenching by Haeussler et al. (2002) on the western section identified four paleo-earthquakes on the fault (including one event on an adjacent fault strand) in the past 2,800 years, yielding a recurrence interval of approximately 700 years. The most recent rupture occurred 795-675 years ago, which Haeussler et al. (2000) used to determine a shortening rate of 0.003 to 0.006 in/yr (0.07 to 0.14 mm/yr). No evidence for lateral offset was observed in the trenches. In contrast, Willis et al. (2007) used an interpreted offset post-glacial outwash channel on the western section to constrain a lateral slip rate of 0.11 to 0.14 in/yr (2.8 to 3.6 mm/yr), with a preferred rate of 0.12 to 0.13 in/yr (3.0 to 3.2 mm/yr). Koehler and Reger (2011) propose that a lateral slip rate of 0.018 to

0.025 in/yr (0.45 to 0.63 mm/yr) may be more appropriate for the western section. Fuchs (1980) proposed a post-Eocene slip rate of 0.020 to 0.024 in/yr (0.5 to 0.6 mm/yr) for the eastern section.

The Castle Mountain fault has traditionally been classified as a strike-slip fault (e.g., Bruhn and Haeussler, 2006; Haeussler and Saltus, 2011) based on the interpreted presence of drag, or wrench-style, folding exhibited by axes of the Cook Inlet anticlines as they approach the fault from the south (Plate 3). This interpretation has been challenged by recent field- and lidar-based fault mapping, which demonstrates that a series of Holocene geomorphic markers (e.g., stream channels, terrace margins and sand dunes) are offset vertically by the fault, but not laterally (Koehler et al., 2012b); at least not within the horizontal detection limit of lidar data. These new studies provide robust evidence that, at least in terms of Holocene activity, the Castle Mountain fault is best characterized as a north-dipping reverse fault with only a minor component of permissible right-slip. Koehler et al. (2012b) report a vertical uplift rate of ~0.020 in/yr (0.5 mm/yr).

2.4.4.2 *Lake Clark fault*

The Lake Clark fault is an approximately 154-mi-long (248-km-long) right-oblique reverse fault that extends northeastward from Lake Clark in the Aleutian Mountains to its terminus near the Beluga River (Plate 3). From this point, the Castle Mountain fault continues along the same trend northeastward through the Talketna Mountains (Koehler and Reger, 2011). Published literature documents approximately 1,640 to 3,280 ft (500 to 1000 m) of reverse motion along the Lake Clark fault based on the displacement of Tertiary formations, and 3 to 16 mi (5 to 26 km) of right lateral offset since the Eocene (Plafker et al., 1975; Detterman et al., 1976; Haeussler and Saltus, 2004).

Owing to the apparent along-strike continuity, it has been questioned whether the Lake Clark fault and the known-active Castle Mountain fault could be related fault segments. However, there is evidence for at least four Holocene earthquakes on the Castle Mountain fault, while evidence of Quaternary activity on the Lake Clark fault is ambiguous (Plafker et al., 1975; Schmoll and Yehle, 1987; Haeussler and Saltus, 2004; Koehler and Reger, 2011). Initial studies by Plafker et al. (1975) documented no apparent offset of topographic features or glacial deposits, while later work by Schmoll and Yehle (1987) inferred that faulting does offset moraines of early Naptowne age (approximately 60 to 130 thousand years ago) in the vicinity of Lone Ridge on the northwest side of Cook Inlet.

Recent work by Koehler and Reger (2011) concluded that no definitive geomorphic evidence exists to indicate offset of the early Naptowne age glacial deposits. The absence of definitive evidence may suggest the fault has a relatively low rate of activity and likely has not generated a surface rupturing earthquake since at least 60 thousand years ago (Koehler and Reger, 2011). According to the Alaska Quaternary Fault and Fold database (QFF) (Koehler et al., 2012a), the Lake Clark fault has been classified as a suspicious feature with a "slip rate that cannot be determined using geologic reasoning".

2.4.4.3 *The Denali fault*

The Denali fault defines the northern margin of the Southern Alaska block (Haeussler, 2008; [Plate 2](#)), and has been a major structural component of Alaska since it formed as a crustal suture during the Late Jurassic to early Cretaceous (Ridgeway et al., 2002). Offset of 56 million-year-old metamorphic and intrusive rocks suggests at least 249 mi (399 km) of total right-lateral displacement along the fault (Nokleberg et al., 1985). Offset is further constrained in the Denali region where the 38 million-year-old Mt. Foraker pluton is displaced 24 mi (38 km) from the McGonagal Pluton (Reed and Lamphere, 1974).

In 2002, the Denali fault produced a **M** 7.9 earthquake, the largest strike-slip earthquake to occur in North America in almost 150 years (Eberhart-Phillips et al., 2003). Detailed studies of offset glacial features along the fault following the 2002 earthquake have demonstrated a clear westward decrease in the Quaternary slip rate along the fault (Matmon et al., 2006; Meriaux et al., 2009).

Shaking from the 2002 **M** 7.9 earthquake was described as “light” in the Nikiski-Kenai area (USGS, 2011): An intensity of IV based on the Modified Mercalli Intensity (MMI) Scale (USGS, 1989). Light shaking is described as: “Felt indoors by many, outdoors by few during the day. At night, some awakened. Dishes, windows, doors disturbed; walls make cracking sound. Sensation like heavy truck striking building. Standing motor cars rocked noticeably.”

The Denali fault lies outside the north margin of the 124 mi (200 km) site radius that defines study region ([Plate 3](#)). However, because of its regional significance and seismogenic potential, it is described here for completeness. Previous analysis shows that the contribution of this fault to ground motions at the site is minimal, and that its contribution to the hazard at the site is insignificant (Fugro-McClelland, 2012a). The low ground shaking hazard at the site from this fault source is attributed to its great distance, and its subvertical dip.

To confirm the results of these earlier studies, a sensitivity analysis was performed to evaluate the contribution of the Denali fault to the hazard and the response spectra at the project site. The analysis is presented in [Appendix B](#). Results from the sensitivity analysis confirm that the Denali fault does not affect the estimated ground motion hazard at the project site, and that exclusion of this fault from the source model has a defensible and robust basis.

3.0 SEISMIC SOURCE CHARACTERIZATION

3.1 Introduction

Available information regarding the seismogenic features of southern Alaska and the Aleutian subduction zone was evaluated to develop a seismic source model for calculation of probabilistic earthquake ground motions at the Nikiski site.

Potential earthquake sources were identified and characterized based on the following data: (1) peer-reviewed literature, (2) published geologic maps, (3) historical seismicity, (4) geospatial data (e.g., topography and bathymetry), (5) proprietary 2D seismic reflection data, (6) Fugro (Fugro Report No. 04.10140334-7) 2D seismic reflection data collected for AKLNG, and (7) unpublished reports.

The seismic source model includes four categories or types of seismic sources, each representing a part of the seismic source model, and each requiring a different characterization of seismic source parameters or treatment in the PSHA calculations. The four types of seismic sources identified in the study region include the following:

1. Great megathrust earthquakes produced by coupling at the subduction interface, and defined by the geometric components of the subduction interface.
2. Intermediate and deep intraslab seismicity associated with the subducted Pacific Plate, or “slab”. This source originates at depths greater than about 12 mi (20 km) at the Aleutian-Alaskan trench, and then deepens to the northwest beneath Cook Inlet to greater than 31 mi (50 km) (Ratchkovski and Hansen, 2002).
3. Shallow crustal line sources, which include known seismogenic faults within the upper crust of the North America plate. Examples of these types of sources are the blind thrust/reverse faults that core the anticlines in upper Cook Inlet, the Castle Mountain fault, and Lake Clark fault.
4. Shallow crustal areal sources, which capture seismicity not attributable to any known crustal fault sources in the North America plate. This source includes contributions based on the rate of observed seismicity in the broader region surrounding the site.

Subduction interface and shallow crustal fault sources (items 1 and 3 from above) were individually characterized from paleoseismic, geophysical and geologic information ([Section 3.0](#)), and are represented in the PSHA calculations ([Section 4.0](#)) as fault sources. Intraslab and shallow crustal seismicity were characterized based on observed seismicity rates and are represented in the PSHA as distributed areal sources.

In the PSHA calculations, the subduction interface and the fault sources are modeled as planar sources and are characterized in terms of geometry, magnitude, recurrence, and fault activity parameters — as required for probabilistic seismic hazard analysis. The intraslab and shallow crustal seismicity are modeled as smoothed gridded sources with grid spacing of 0.1° in latitude and longitude. Many components of the subduction zone model follow Wesson et al. (2007).

In the text that follows, [Section 3.2](#) discusses the characterization of the subduction interface, [Section 3.3](#) discusses the intraslab sources, [Section 3.4](#) provides a detailed description of the crustal fault sources, and [Section 3.5](#) discusses upper crustal gridded areal seismicity sources.

3.2 Aleutian Subduction Zone Interface

The Aleutian subduction interface, a source of great earthquakes ($\geq M 8.0$) potentially affecting the study region, is modeled in three sections and is based on the USGS model of slab contours and segmentation boundaries (Wesson et al., 2007). Model parameters used for the subduction zone sources are listed in [Table 3.1](#).

3.2.1 Interface Geometry

The geometry of the subduction interface sources is defined by the dip, dip direction, up-dip limit depth, and down-dip limit depth. The modeled geometries of sources S1, S2 and S3 are shown on [Plate 7](#). The S1 and S2 sections model the plate interface between the subducting Pacific Plate and the North America Plate, which was the source of the 1964 **M** 9.2 earthquake. S1 models the section under Kodiak Island, and S2 the section beneath the Kenai peninsula. Although the interface surface appears to be warped but continuous, the planar models used here require the division into two sections in order to model distances to the site correctly. The third section (S3) models the plate interface between the Yakutat microplate and the Pacific Plate. Each section is specified to rupture individually; S1 and S2 rupture on northwest-dipping planes, and S3 ruptures on a north-dipping near-horizontal plane. The sections of the plate interface model are as follows:

- S1: This section models the slab interface in the western portion of the estimated 1964 rupture zone, and is defined as a 199-mi-long by 118-mi-wide (320-km-long by 190-km-wide) plane dipping 6.0° to the northwest. Its western terminus parallels the western shore of Kodiak Island and the modeled interface plane extends up-dip to the subduction interface to the southeast. The shallowest southeastern edge of the fault plane is modeled at a depth of 12 mi (20 km) and deepens down-dip to 25 mi (40 km) depth at the northwestern edge.
- S2: This section models the eastern portion of the estimated 1964 rupture zone as an approximately 217-mi-long by 186-mi-wide (350-km-long by 300-km-wide) plane dipping 3.4° to the northwest. Its western terminus underlies the eastern boundary of the Kenai lowlands, and the modeled interface plane extends up-dip to the subduction interface to the southeast. The shallowest southeastern edge of the fault plane is modeled at a depth of 12 mi (20 km). At this same location, Wesson et al. (2007) modeled the down-dip edge of the

megathrust as deepening from 21 mi (33 km) at the northeast corner to 25 mi (40 km) at the southwest corner. S2 approximates this by fixing the down-dip (northwest) edge at 24 mi (38 km).

- S3: This section represents the subduction interface segment beneath the Yakutat microplate and the underlying Pacific plate at the eastern end of the Aleutian subduction zone. In this area, the predominantly convergent-style margin of the Aleutian-Alaskan arc becomes predominantly a transform-style margin of southeastern Alaska. The subduction interface in this segment is modeled as a 205-mi-long by 137-mi-wide (330-km-long by 220-km-wide) horizontal plane at 9 mi (15 km) depth. Approximate structural boundaries of this modeled plane are the western convergent portion of the Transition fault, Aleutian megathrust, Chugach-St. Elias fault, and Fairweather fault ([Plate 2](#)).

3.2.2 Interface Activity Rate Scenarios, Recurrence, and Magnitudes

Both time-independent and time-dependent rates were used for the interface **M** 9.2 S2 source. A time-dependent occurrence rate for a seismic source is based on the concept of a regular time interval between large events. The more recently a large earthquake occurred, the longer the time until the next earthquake, and vice versa. Because the 1964 **M**9.2 event occurred only 50 years ago, and its repeat time appears to be about 535 years on average (Shennan et al., 2014), it was judged that some credence should be given to the idea that during the life of the structure the annual rate of occurrence will be less than the time-independent rate of 1/535 per year. Time-dependent versus Poissonian (non-time-dependent) models were weighted 0.33 and 0.67, respectively.

Following Wesson et al. (2007) and the time-dependent analysis presented in this report, the following maximum magnitude events and rates are assigned to the subduction interface sections:

- S1: **M** 8.8, with a time-independent (Poissonian) annual rate of 1/650 assigned;
- S2: **M** 9.2, with a rate of 1/802 assigned. This is the result of a time-independent (Poissonian) annual rate of 1/535 based on paleoseismic investigations (Carver and Plafker, 2008) weighted 0.67, and a time-dependent rate of 8.66e-06 weighted 0.33, for an assumed 50-year exposure period for the facility ([Appendix A](#));
- S3: **M** 7 – 8.1, annual rates determined by a truncated exponential recurrence with **M** \geq 7 rate of 1/303 and b-value of 0.666.

The **M** 7 to 8 non-Yakutat interface earthquakes are modeled as exponentially distributed according to rates in Wesson et al. (2007). The *a* and *b* Gutenberg-Richter recurrence parameters for this source were taken from their Table 3. Because in that Table *a*-values are for the entire Aleutian arc, they were scaled by the proportional areas of S1 plus S2. A slip rate was then

calculated that produced the same seismicity rate as the scaled a-value. Earthquakes in this magnitude range are modeled as occurring on the fault planes defined by S1 and S2.

Interface earthquakes in the **M** 5 to **M** 7 range are modeled as gridded, smoothed seismicity. As described in Wesson et al. (2007), this model is created by sorting seismicity into 0.1° bins, and performing Gaussian smoothing with a correlation distance (Frankel, 1995) of 47 mi (75 km). The grid sources were placed at a depth of 3 mi (5 km), as in Wesson et al. (2007).

3.3 Intraslab Source

Intraslab seismicity associated with the Aleutian Subduction Zone in the study region comprises Benioff zone seismicity with focal depths between 31 to 75 mi (50 and 120 km), associated with the subducting Pacific slab. For the intraslab source, we used the Wesson et al. (2007) model, which consists of gridded seismicity for two depth levels: 31 to 50 mi (50 to 80 km) (Plate 8) and 50 to 75 mi (80 to 120 km) (Plate 9) with a magnitude range of 5.0 to 8.0. Following Wesson et al. (2007), the depth for the 31-50 mi (50-80 km) sources was set at 37 mi (60 km), and 56 mi (90 km) for the 50 to 75 mi (80 to 120 km) points. The grid selection extent is defined as all points north of latitude 54.5N and east of longitude 162W.

This seismicity is modeled as a truncated exponential distribution with the b-value shown in Table 3 of Wesson et al. (2007), and the incremental a-value for each grid point contained in the grid files obtained from the USGS website:

(<http://earthquake.usgs.gov/hazards/products/ak/2007/software/AK2007Inputs.zip>).

3.4 Shallow Crustal Fault Sources

Twenty-two crustal faults that represent potential sources of seismic activity and strong ground shaking within the site region are included in the source model (Tables 3.2 and 3.3). Modeled fault sources consist of three structural features and/or provinces: (1) blind thrust and reverse faults that underlie anticlines in upper Cook Inlet (F1 through F15, F21 and F22, Plate 10); (2) the Castle Mountain fault (F16 through F18, Plate 11); and (3) the Lake Clark fault (F19 and F20, Plate 11). Parameters used to model the seismic sources included dip magnitude, dip direction, depth of the seismogenic zone, depth to the tip of the blind fault, slip rate, and potential earthquake magnitude.

Of the structures in the source model, only the Castle Mountain fault (F16 to F18) has documented historical surface ruptures and a well-constrained paleoseismic history. The Lake Clark fault (F19 and F20) is considered a potential seismic source because of its structural continuity with the known-active Castle Mountain fault and its inclusion in the Alaska Quaternary fault and fold database (QFF; Koehler et al., 2012a). Fault-cored folds in the upper Cook Inlet (F1 through F17, F21 and F22) are considered potential seismic sources because of spatially-associated historical seismicity (Flores and Doser, 2005), and the presence and deformation of Quaternary-aged growth strata interpreted on the fold flanks (Haeussler et al., 2000).

Geometric properties of the shallow crustal sources underlying the Cook Inlet anticlines have been updated in this study based on (1) interpretation of proprietary 2D seismic reflection data within the structural extent area ([Plate 12](#)), and (2) review of publically-available scientific literature. New constraints on these shallow crustal sources include fault location, length, dip magnitude, dip direction, depth of blind fault tips, and maximum moment magnitudes. We used a logic-tree approach to assign weighted distributions for each of the fault parameters listed above. Uncertainty in fault length is not considered in this update due to a lack of information available to support alternative scenarios.

Parameters obtained from the best-constrained structures were applied uniformly to the poorly characterized structures. The latter occur in areas where data are either sparse, unavailable or of poor quality. By extrapolating parameters between faults, we assume that deformation occurs uniformly across Cook Inlet and is predominantly contractional. These assumptions are somewhat simplified, but were made based on the similar orientations of the fold axes, and the roughly perpendicular orientations of the folds with respect to the maximum compressive stress axis in upper Cook Inlet (e.g., Haeussler et al., 2000; Bruhn and Haeussler, 2006; Flores and Doser, 2005).

A preferred M_{max} is calculated for the Castle Mountain fault based on the magnitude-area formula from Wells and Coppersmith (1994). Given the poor characterization of the remaining sources, we follow the precedent of prior published studies (Haeussler et al., 2000; Wong et al., 2008) and calculate a preferred M_{max} based on length-scaling relationships developed in Wells and Coppersmith (1994). Only a single magnitude estimate is used for these sources. Thus, the recurrence model can be defined as a maximum moment model.

Characteristics of the 22 fault sources are shown in [Tables 3.2 and 3.3](#), and their modeled map-trace locations and geometries are shown on [Plates 10 and 11](#).

3.4.1 Cook Inlet fault-cored folds

Seventeen shallow fault sources (F1 through F15, F21 and F22) are modeled within Cook Inlet. These sources define steeply- to moderately-dipping blind reverse faults that core or underlie the Cook Inlet anticlines (Haeussler et al., 2000; Bruhn and Haeussler, 2006). Prior to this study, the anticline axes from the QFF (Koehler et al., 2012a) were used as proxies for locating and defining the lengths of underlying faults. In the current study, we update these parameters based on expression of subsurface faulting (or lack thereof) interpreted from the industry and AKLNG seismic reflection data, and from review of scientific literature and unpublished technical reports.

Industry seismic reflection data were reviewed by Fugro in the data room at ConocoPhillips' (CoP) in Anchorage, Alaska during the week of 05 October 2015. These data supplement other CoP 2D seismic reflection data, which were reviewed by Fugro in 2012 for the earlier AKLNG siting study (Fugro-McClelland 2012b). The locations of the 2D seismic reflection lines reviewed in this study

are shown in (Plate 12). Because of commercial concerns, Fugro was allowed to view and take screen captures (JPEG and TIFF format) of the data, but could not retain the native SEGY files.

Fault location

For the purposes of this study, the term fault location refers to the spatial coordinates of the tip-line or up-dip extent of the blind reverse faults that underlie the Cook Inlet anticlines. Because the faults within the structural extent are blind, the tip-lines lie well below sea level.

To establish XY coordinates for the source model, screen-grabs of the vertical seismic displays collected in Alaska were georeferenced in ArcGIS using the end point locations of the corresponding seismic reflection acquisition lines. Locations of the acquisition lines were also established by georeferencing base maps showing the lines relative to geographic features. Subsurface picks on key structural elements interpreted on the reflection panels (e.g., fault tip lines, fold hinges and down-dip points along fault planes) were projected vertically to the surface, akin to an earthquake epicenter map, and attributed as point shapefiles.

To define the depth coordinates, two-way travel times (in milliseconds) of fault tip picks were depth-converted on a point-by-point basis using a velocity model developed from the 2015 onshore seismic reflection program (Fugro Report No. 04.10140334-7). These values were subtracted from ground surface elevation obtained from a composite digital elevation model (DEM) created by Fugro to derive absolute elevation. The Fugro DEM is a compilation of multiple elevation and bathymetric datasets, which include: (1) NOAA's AFSC/RACE Cook Inlet bathymetry data (Zimmerman and Prescott, 2014); (2) Fugro's high-resolution multi-beam echo sounder bathymetry data collected for the AKLNG project immediately offshore from the site (Fugro Report No. 04.10140334-7); (3) onshore topography from USGS NED 30-m data (USGS, 1999) for shoreline and terrain areas away from the site; (4) approximately 2.5-meter-resolution lidar digital elevation data (USGS, 2008) for the larger area surrounding the site; and (5) approximately 1-meter-resolution lidar digital elevation data provided by the Client for the area directly surrounding the site.

There was some scatter in the fault-tip pick locations due to epistemic uncertainty regarding the ability to identify or resolve the shallowest offset seismic reflection. To account for the scatter, a qualitative or visual-based "best-fit" fault tip-line was generated through the scattering of points, and was used to define the line geometry of that structure in the seismic source model (Plate 10).

For structures that lacked adequate industry seismic reflection coverage, fault locations were based on the published traces of corresponding anticline axes (Koehler et al., 2012a). These structures include: Falls Creek–Ninilchik anticline (F1), Kasilof anticline (F2), West Fork anticline (F6), Nicolai Creek anticline (F10), Moquawkie anticline (F11), Ivan River anticline (F14), Stump Lake anticline (F15), Sterling anticline (F21), and Trading Bay–North Trading Bay anticline (F22).

A key result of the seismic reflection interpretation effort is that the fault tip-lines have been shifted laterally away from the overlying fold axes. For example, the distance to the tip-line of the Middle Ground Shoal fault (F7), which lies west of the Site and represents the closest seismic source, has decreased by approximately 2 miles (3.2 kilometers) compared to the closest distance used in Phase 1 PSHA for that fault. To the east, the distance to the tip-line of the Kenai–Cannery Loop fault (F3), the next closest seismic source, has decreased by approximately 3 miles (5 kilometers). This result is consistent with fault-fold models (e.g., Suppe and Medwedeff, 1990; Allmendinger, 1998), which demonstrate that tips of blind contractional faults typically underlie the hinge lines between the anticline forelimb and adjacent synclinal flat, and not the fold crest ([Plate 13](#)).

Fault length

Fault lengths used in the previous seismic source model (Fugro Report No. 04.10140094-6) were based on the published lengths of the Cook Inlet anticline axes from the QFF (Koehler et al., 2012a). In this update to the source model, individual fault lengths were determined based on review of the industry seismic reflection data. These data were used to confirm or refine the published fault length values and evaluate potential structural connectivity, if any, between adjacent structures (e.g., the Middle Ground Shoal and Granite Point anticlines). In areas of inadequate seismic reflection coverage, some structures were linked (i.e., they have the potential to rupture together) if: (1) overlying fold terminations lay within a few kilometers of one another, (2) fold axes can be reasonably projected along strike into one another, (3) published literature suggests a potential structural link, and/or (4) the likelihood of structural connectivity cannot be confidently negated. Final fault lengths are presented in [Table 3.2](#).

Updates to the source model were made to the following structures: Kenai-Cannery Loop anticline (F3), Swanson River anticline (F4), Beaver Creek anticline (F5), Middle Ground Shoal–Granite Point anticlines (F7), McArthur River–Redoubt Shoal anticlines (F8), West McArthur River anticline (F9), North Cook Inlet anticline (F12), Beluga River–Lewis River anticlines (F13), and Trading Bay–North Trading Bay anticlines (F22).

The most notable changes in fault lengths include:

- The Middle Ground Shoal and Granite Point fault-fold system (F7) has a combined length of 42 miles (67 km), which is approximately 1.8 miles (3 km) longer than in the 2015 Phase 1 model (Fugro Report No. 04.10140094-6). The increase in length is based on the presence of low-amplitude folding of reflectors along strike and beyond where the fold terminations are shown on published maps (e.g., Koehler et al., 2012a). Similar to previous studies (Haeussler et al., 2000; Haeussler and Saltus, 2011; and the Phase 1 PSHA study (Fugro Report No. 04.10140094-6)), the Middle Ground Shoal and Granite Point anticlines are modeled as a single structure because both folds overlie an interpreted through-going master fault. The master fault is east vergent (i.e., it dips to the west), while the folds are

west vergent (i.e., they are asymmetric in profile view, with the steeper limb on the west side of the fold). The fold vergence is controlled by an east-dipping backthrust that roots into the master fault at depth (Plate 14). Based on the interpreted fault geometry in profile 203-290 (Plate 14), the McArthur River-Redoubt Shoal (F8) and West McArthur River (F9) faults (Plate 10) are also backthrusts that root into the master fault at depth. Reverse motion on the master fault has generated an east-side-down step in the top of Mesozoic basement (Plates 5 and 14). The Middle Ground Shoal and Granite Point anticlines formed above this step on the hinge line of what becomes a monocline at depth (below approximately 3000 msec Two-Way Travel Time (TWTT) on Plate 14). This fault system has been interpreted in the literature as a basement-cored fault-propagation fold (Haeussler et al., 2000; Bruhn and Haeussler, 2006) (Plate 15) or fault-bend fold (Frankforter and Waugaman, 2013; Plate 16), where the antithetic fault acts as a de facto roof thrust above an east-directed basement wedge.

- The Kenai-Cannery Loop fault-fold system (F3) was extended 15 miles (24 km) to the north, yielding a maximum length of approximately 28 miles (48 km). The increase in length is based on inferred continuity between an east-dipping (i.e., west-vergent) master fault that underlies both the Kenai-Cannery Loop anticline in the south and a monocline that was mapped in the seismic reflection data to the north (Plate 12). The monocline is interpreted in line p3890-10 (Plate 12), north of which there is no available reflection data. The overall geometry and structural style of the Kenai-Cannery Loop fault system is analogous to the Middle Ground Shoal–Granite Point system, but the net transport direction is to the west. Based on this relationship, we interpret the Middle Ground Shoal–Granite Point and Kenai-Cannery Loop structures as defining an inward-vergent fault system, with the Site located in the intervening synclinal flat. This is shown in a conceptual cross section across upper Cook Inlet at the latitude of the Site (Plate 17), and is based on interpretation of the available seismic reflection profiles.
- The length of the Beaver Creek anticline (F5) was reduced by approximately 4 miles (7 km), yielding a maximum length of approximately 7 miles (11 km). The length of this structure is constrained by industry lines ms-11 and ms-14 (Plate 12), which show no evidence of tilting along the projection of the fold axis. The lack of deformation thereby provides a maximum possible fault length, placing the limits of this structure beyond the extent of the structural mapping boundary (Plate 12).
- Trading Bay and North Trading Bay anticlines are linked into a single seismic source (F22) based on their proximity, which yields a fault length of approximately 8 miles (14 km).
- Beluga River and Lewis River anticlines are linked into a single seismic source (F13) based on suggestions in published literature (Haeussler and Saltus, 2011; Haeussler et al., 2000), which yields a fault length of approximately 22 miles (35 km).

- The West McArthur River anticline (F9) was extended slightly to the north based on its expression on industry seismic line 203-220 (there is no available reflection data north of this line). Despite the proximity and similarity in trends, we do not link this structure to the Trading Bay–North Trading Bay source (F22) based on arguments made by Haeussler and Saltus (2011).

Depth to fault tip

Blind faults that comprise sources F1 through F15, F21 and F22 by definition remain at some depth below the surface (Haeussler et al., 2000; Bruhn and Haeussler, 2006). Bruhn and Haeussler (2006) converted two-way travel time to depth in seismic reflection data to provide estimated fault tip depths for five structures: Middle Ground Shoal anticline (F7), McArthur River-Redoubt Shoal anticline (F8), West McArthur River anticline (F9), North Cook Inlet anticline (F12), and Beluga River anticline (F13). Corresponding fault tip depths are 1.7 mi (2.7 km), 0.7 mi (1.1 km), 1.3 mi (2.1 km), 2.1 mi (3.3 km), and 0.7 mi (1.1 km), respectively. We supplemented these values where we have coverage by the industry seismic data. Fault tip depths were calculated and updated for Kenai-Cannery Loop (F3), Swanson River (F4), Middle Ground Shoal–Granite Point (F7), McArthur River-Redoubt Shoal (F8), and West McArthur River fault sources (F9) (Table 3.2). Fault dip depth measurements were made in TWTT and converted to elevation using velocity-to-depth curves from onshore deep seismic survey (Fugro Report No. 04.10140334-7) and the compilation digital elevation model described above. It is difficult to directly compare the velocity model used in this analysis to previous Cook Inlet seismic reflection studies (Haeussler et al., 2000; Bruhn and Haeussler, 2006) because the authors of these studies do not explicitly state what values they used in their model. The only comparison comes from the Beluga anticline field, which lies beyond the northern boundary of the Structural Mapping Area. There, Haeussler et al. (2000) report fault tip-lines located “around 1.25 s TWT (1040 m).” This time-to-depth comparison indicates that, at least in that area, their velocity model for the upper kilometer is approximately 1,664 m/sec. For comparison, for the upper 1 kilometer of crust within the Structural Mapping extent, the velocity models used in this study range from a minimum of 1,525 m/s to a maximum of 2,377 m/s. The fault tip depths used in the seismic source model are calculated averages sampled from along the entire length of the structure, or where there is overlapping seismic reflection data.

Given the lack of available data for the remaining structures, and for those that lie outside the structural extent boundary, a uniform fault-tip depth of one kilometer was assigned. This approach was applied to the following sources: F1, F2, F5, F6, F10-F15, F21, and F22 (Table 3.2).

Fault dip

To calculate dip values for the fault sources, measurements were made in milliseconds (TWTT) along the down-dip extent points, and were then depth-converted using the procedure described above.

Fault dip data for sources F1 through F15, F21, and F22 are predominantly based on published literature. For faults coring the Kenai-Cannery Loop anticline (F3), Swanson River anticline (F4), Middle Ground Shoal–Granite Point anticline (F7), McArthur River-Redoubt Shoal anticline (F8), and West McArthur River anticline (F9), industry seismic data were used to calculate representative dip values. A single seismic line was examined for the Kasilof anticline (F2) to help further constrain weighting of dip parameters.

The dip range of these structures was determined using trigonometric relationships on the fault tip depths and on measurements of arbitrary down-dip points. The dips were calculated using each of the different velocity models, which yield a total of 9 dip values per fault. The calculated dip values for each structure were collated to provide average, minimum and maximum values. These values were used to determine the model parameters (Table 3.2). Additionally, the dip values were binned in increments of 5 degrees and a histogram was generated for the dip values for each structure. The histogram values were used to constrain the range of admissible dips as well as for the weighting scheme for the corresponding logic tree branch (Table 3.2).

Bruhn and Haeussler (2006) used seismic reflection data to construct cross-sections and assess dip angles for the faults below the Middle Ground Shoal anticline (F7), McArthur River-Redoubt Shoal anticline (F8), West McArthur River anticline (F9), the North Cook Inlet anticline (F12), and Beluga River anticline (F13). The corresponding dip values were: 45-55°, 55-80°, 70-90°, 55-62°, and 55-60°, respectively. Where appropriate, these values were revised where industry data were available, but were used directly for characterizing sources that lacked industry data coverage. For these latter faults (sources F1, F2, F5, and F9 thru F15), we considered an equally weighted distribution of fault dips (the weighting is shown in parentheses) that included the following: 45° (0.3), 60° (0.4), and 75° (0.3). Koehler et al. (2012a) list a vertical dip for the Swanson River anticline (F4). This value is incorporated into the source model by weighting the corresponding logic tree branch in favor of steeper dip angles: 60° (0.3), 75° (0.3), and 90° (0.4) (Table 3.2). The same scheme was adopted the Sterling anticline (F21).

Fault dip direction

The Cook Inlet faults and folds have variable geometries and vergence directions (Haeussler et al., 2000; Bruhn and Haeussler, 2006; Fugro-McClelland, 2012b; Phase 1 PSHA, Fugro Report No. 04.10140094-6; Fugro, 2015b). Dip directions used in the fault model are based on: (1) cross-sections from published scientific literature and unpublished technical reports (e.g., Haeussler et al., 2000; Bruhn and Haeussler, 2006), (2) fault dip directions observed directly in the industry seismic reflection data, and (3) indirect inference based on the overlying fold geometries and structural relations imaged in the industry seismic reflection data.

Published cross-sections and available industry data indicate that a majority of the folds on the western side of upper Cook Inlet basin are underlain by southeast-dipping faults (i.e., the folds are

west vergent). These folds include the McArthur River-Redoubt Shoal (F8), West McArthur River (F9), Beluga River (F13), and Trading Bay–North Trading Bay (F22) (Plate 10). As described above, structural relations require that the primary fault-transport direction on this side of the basin is to the east, opposite to the direction of fold vergence. Thus, many, if not all, of these east-dipping structures are antithetic structures, or backthrusts, that either root directly into the master ramp (e.g., the Middle Ground Shoal fault) or adjacent decollement that lies east of the ramp-flat transition (Frankforter and Waugaman, 2013; Plate 16). Thus, we assume that all of the faults on the west side of the basin, other than the one underlying the Middle Ground Shoal anticline, are southeast dipping. These structures include the Nicolai Creek anticline (F10), Trading Bay–North Trading Bay anticline (F22), Moquawkie anticline (F11), and Ivan River anticline (F14) (Plate 10 and Table 3.2).

Available industry data indicate that folds on the eastern side of upper Cook Inlet are underlain by faults that consistently dip to the southeast (e.g., Fugro-McClelland, 2012b). These folds include the Falls Creek-Ninilchik anticline (F1), Kasilof anticline (F2), Kenai-Cannery loop anticline (F3), Swanson River anticline (F4), and Beaver Creek anticline (F5). For sources where no subsurface data are available, we assign a southeast dip direction to match the structural trends of the surrounding folds. These latter sources are the West Fork anticline (F6) and Sterling anticline (F21) (Plate 10 and Table 3.2).

Depth of seismogenic zone

Seismic reflection and well data collected by the oil and gas industry show that several of the blind faults in upper Cook Inlet extend into the Mesozoic basement (i.e., they are so called “thick-skinned” faults). There is no data that conclusively shows whether or not these faults penetrate the entire thickness of the seismogenic crust (~22 mi [35 km]) (Haeussler et al., 2000; Bruhn and Haeussler 2006). However, Flores and Doser (2005) provide a cross section through upper Cook Inlet showing relocated historical seismicity collected over a thirty-five-year period in the greater Anchorage area. The cross section is located very near the site and passes through all of the closest line sources. While there are no alignments of seismicity or obvious correlations between earthquakes and any individual mapped structure, a key observation is that the density of earthquakes is clearly greatest between depths of approximately 9 to 15 mi (15 to 25 km), and then abruptly decreases. This depth ranges corresponds to the upper portion of an inferred serpentinite body (Saltus et al., 2001), which would provide a logical detachment surface, or decollement, for the Cook Inlet fault-folds. Given the lack of other compelling data to constrain the deeper structure, and the fact that these are basement-involved structures, we follow the scheme of Wong et al. (2008), and assign maximum fault-penetration depths of 9, 12 and 16 miles (15, 20 and 25 km, respectively).

Slip rate

Haeussler et al. (2000) approximated slip rates for the Middle Ground Shoal, Granite Point and North Cook Inlet anticlines based on fold properties measured on cross-sections (e.g., structural relief, shortening amounts and fault dip) and with assumptions about the onset of deformation in the Cook Inlet basin. Approximate slip rates for the Middle Ground Shoal and Granite Point anticlines vary from 0.015 to 0.107 in/yr (0.39 to 2.72 mm/yr) depending on the age of onset of deformation (11.2 to 1.6 Ma); while slip rates on the North Cook Inlet anticline vary from 0.002 to 0.011 in/yr (0.04 to 0.27 mm/yr) (Haeussler et al., 2000). Tighter folding observed along the Middle Ground Shoal anticline may reflect these higher slip rates; conversely, broader, less developed folding observed along the North Cook Inlet anticline may reflect lower slip rates.

Following Wong et al. (2008), we consider a weighted (value shown in parentheses) slip rate distribution of 0.015 in/yr [0.39 mm/yr] (0.2), 0.032 in/yr [0.82 mm/yr] (0.6), and 0.107 in/yr [2.72 mm/yr] (0.2), which assumes the onset of deformation along the Middle Ground Shoal and Granite Point anticlines (F7) began at 5.3 Ma (Haeussler et al., 2000). Similarly along the North Cook Inlet anticline (F12) we consider a weighted (value shown in parentheses) slip rate distribution of 0.002 in/yr [0.04 mm/yr] (0.2), 0.003 in/yr [0.08 mm/yr] (0.6), and 0.011 in/yr [0.27 mm/yr] (0.2), which also assumes that the onset of deformation began at 5.3 Ma (Haeussler et al., 2000).

The remaining blind fault sources within the upper Cook Inlet fold belt (F1 through F6, F8 through F11, and F13 thru F15) have been interpreted in the published literature (Haeussler and Saltus, 2011) as being less developed structures, similar to the North Cook Inlet anticline. Accordingly, a weighted slip rate distribution (value shown in parentheses) is assigned that is analogous to the North Cook Inlet anticline: 0.002 in/yr [0.04 mm/yr] (0.2), 0.003 in/yr [0.08 mm/yr] (0.6), and 0.011 in/yr [0.27 mm/yr] (0.2) ([Table 3.2](#)).

3.4.2 Castle Mountain-Lake Clark fault system

Collectively, the Castle Mountain and Lake Clark faults define a somewhat arcuate, approximately 280-mi-long (450-km-long) fault system that bounds the Cook Inlet basin on the north, and separates the Alaska and Aleutian ranges ([Plates 3 and 11](#)). The two faults are associated because they lie along strike of one another. However, based on results from multiple studies (discussed in more detail above and in the following subsections), their late Quaternary tectonic histories are quite different: Paleoseismic studies on the Castle Mountain fault show it has had at least four surface-rupturing earthquakes during the Holocene, while the Lake Clark fault has had none. For this reason, the possibility of a through-going rupture between these two faults is not considered in this study. The Lake Clark fault is included herein as a seismic source because it is listed in the Alaska QFF — it is included because of its along-strike continuity with the Castle Mountain fault.

3.4.2.1 *Castle Mountain fault*

Based on published literature (Plafker et al., 1994a, 1994b; Lahr et al., 1980; Flores and Doser, 2005) we divide the Castle Mountain fault (F16 to F18) into an eastern and western segment. Surface lengths for each segment were derived from mapped traces in the QFF (Koehler et al., 2012a).

Fault sources F16 to F18 ([Plate 11](#)) represent separate rupture scenarios of the Castle Mountain fault: a rupture of the full extent of the Castle Mountain fault (F16), a high slip-rate and a low slip-rate scenario on the western Castle Mountain fault segment (F17), and a rupture scenario of the eastern Castle Mountain fault and Caribou fault extension (F18). The modeled geometry and sense of slip for the fault is steeply dipping (80° for all scenarios).

A paleoseismic study by Haeussler et al. (2000) indicates reverse motion on the fault, however focal mechanisms from historic earthquakes indicate predominantly right-lateral shear (Lahr et al., 1986; Haeussler et al., 2002). Koehler et al. (2012b) present geomorphic evidence that demonstrates that the style of motion across the fault during the Holocene is contractional. While there may be a component of dextral motion, it is not detectable within the resolution of the lidar data or ground measurements (Koehler, personal communication). Based on these recent observations, we model the Castle Mountain fault as a reverse fault. Including a strike-slip component would make a negligible difference to ground motions at the site and be slightly less conservative. Consequently, we model the sense of motion across the fault as being purely reverse ([Table 3.3](#)). We consider the depth of the seismogenic zone for this fault to be 12 mi (20 km) based on published literature related to the 1984 **M5.7** earthquake in Sutton, Alaska (Lahr et al., 1980).

Estimates of fault slip rates along the Castle Mountain fault are based on published paleoseismologic and contemporary seismologic investigations (Fuchs, 1980; Willis et al., 2007; Wesson et al., 2007; Koehler and Reger, 2011; Matmon et al., 2006; Meriaux et al., 2009; Haeussler et al., 2000; Haeussler and Saltus, 2011; Wong et al., 2008). A mean slip rate of 0.02 in/yr (0.5 mm/yr) was used for scenarios involving both the Eastern Castle Mountain fault and the entire Castle Mountain fault (sources F18 and F16, respectively). Source F17 is modeled using two equally weighted slip scenarios (0.11 in/yr [2.9 mm/yr] mean rate; 0.02 in/yr [0.5 mm/yr] mean rate) to reflect disagreement in the published literature over activity rates of the western segment of the Castle Mountain fault (Willis et al., 2007; Wesson et al., 2007; Koehler and Reger, 2011).

3.4.2.2 *Lake Clark fault*

The Lake Clark fault consists of two segments, F19 and F20 ([Plate 11](#)). Surface lengths for these segments were derived from their mapped traces in the QFF ([Table 3.3](#)) (Koehler et al., 2012a). The boundary between the eastern (F19) and western (F20) strand is in an area of apparent structural complexity approximately 25 mi (40 km) east of Lake Clark (Koehler et al., 2012a).

Surface lengths for the segmented Lake Clark fault sources (F19 and F20) were derived from mapped traces in the QFF ([Table 3.3](#)) (Koehler et al., 2012a).

Although vertical offsets of 1,600 to 3,300 ft (490 to 100 m) within Tertiary formations are noted along the Lake Clark fault in the published literature (Plafker et al., 1975; Detterman et al., 1976), strike-slip motion is considered the dominant structural style based on the association with the Castle Mountain fault and the regional tectonic setting (Haeussler et al., 2000; Bruhn and Haeussler, 2006). It is unknown how or if this characterization of the fault might change given the more recent studies by Koehler et al. (2012b) that show the Castle Mountain fault as a predominantly reverse structure. To a certain extent this becomes irrelevant because there is a negligible difference to ground motions at the site if the Lake Clark fault is modeled as a predominantly reverse fault versus a predominantly strike-slip fault. Following Wong et al. (2008), we consider the following weighted (in parentheses) fault dips: 75° (0.5) and 90° (0.5). Only steep dips are considered in the model because of the straight map trace of the fault and the steep dips documented on the nearby Castle Mountain fault. The fault dip direction is modeled as northwest dipping. Additionally, we consider fault penetration depths of 9, 12, and 16 mi (15, 20, and 25 km) (Wong et al., 2008).

Slip-rate measurements for the Lake Clark fault derived from offset Eocene intrusive units, range from 3 to 16 mi (5 to 26 km) of right lateral separation (Plafker et al., 1975; Haeussler and Saltus, 2004). Plafker et al. (1975) estimated 3+0.6 mi (5+1 km) of offset of a 38.6 m.y. intrusive unit associated within the Talkeetna formation, resulting in an Eocene slip rate of 0.004 in/yr (0.1 mm/yr). Later studies by Haeussler and Saltus (2004) estimated 16 mi (26 km) of offset of magnetic anomalies within a 34-38 m.y. intrusive unit, resulting in an Eocene slip rate of 0.03 in/yr (0.7 mm/yr). Following Wong et al. (2008) and based on the ambiguous evidence for Quaternary activity on the fault (Plafker et al., 1975; Schmoll and Yehle, 1987; Koehler and Reger, 2011) we consider the following weighted (in parentheses) slip rates: 0.0004 in/yr [0.01 mm/yr] (0.2), 0.004 in/yr [0.1 mm/yr] (0.6), and 0.028 in/yr [0.7 mm/yr] (0.2).

Table 3.1: Subduction Zone Seismic Sources

Study ID	Name	Faulting Type	M distribution	Dip (deg.)	Dip direction	Depth Range in mi (km)	Activity Rate	Weight	b-value	Magnitude Range (M _w)	Citation
S1a	Kodiak Island Megathrust	Thrust	Maximum Moment	6	NW	12.5 - 25 (20 - 40)	1/650 (Annual, Poissonian)	1	-	8.8	Wesson et al. (2007)
S1b	Kodiak Island Megathrust	Thrust	Truncated exponential	6	NW	12.5 - 25 (20 - 40)	slip rate = 0.880 mm/yr (0.0346 in/yr)	1	0.689	7.0 - 8.0	Wesson et al. (2007)
S2a	Prince William Sound Megathrust	Thrust	Maximum Moment	3.4	NW	12.5 - 23.8 (20 - 38)	1/535 (Annual, Poissonian)	0.67	-	9.2	Wesson et al. (2007), Carver and Plafker (2008)
							8.66e-6 (Annual, Time-dependent)	0.33			Appendix A
S2b	Prince William Sound Megathrust	Thrust	Truncated exponential	3.4	NW	12.5 - 23.8 (20 - 38)	slip rate = 0.880 mm/yr (0.0346 in/yr)	1	0.689	7.0 - 8.0	Wesson et al. (2007)
S3	Yakutat Megathrust	Thrust	Truncated exponential	0.27	N	8.8 - 9.4 (14 - 15)	slip rate = 0.400 mm/yr (0.0157 in/yr)	1	0.666	7.0 - 8.1	Wesson et al. (2007)
MT	Megathrust	Strike Slip	Truncated exponential	0	-	3.1 (5)	Gaussian-smoothed grid	1	0.816	5.0 - 7.0	Wesson et al. (2007)
IS1	Intraslab - Intermediate	Normal	Truncated exponential	0	NW	31 - 50 (50 - 80) ¹	Gaussian-smoothed grid	1	0.858	5.0 - 8.0	Wesson et al. (2007)
IS2	Intraslab - Deep	Normal	Truncated exponential	0	NW	50 - 75 (80 - 120) ²	Gaussian-smoothed grid	1	1.007	5.0 - 8.0	Wesson et al. (2007)

¹Representative depth values used in PSHA per Wesson et al 2007 for Intraslab – Intermediate is 37.5 mi (60 km).

²Representative depth values used in PSHA per Wesson et al 2007 for Intraslab – Deep is 56.3 mi (90 km).



Table 3.2: Cook Inlet Basin Upper Plate Fault Sources

Study ID	Name	Faulting Type	M relation	Magnitude Frequency distribution	Dip (deg.)	Weight	Dip direction	Depth max in mi (km)	Weight	Depth to fault tip in mi (km)	Weight	Slip Rate in in/yr (mm/yr)	Weight	Fault Length in mi (km)	Maximum magnitude (M _w)	Citations
F1	Falls Creek-Ninilchik anticline	Reverse	WC94, M-L*, Reverse	Maximum Moment	45	0.3	SE	9.4 (15)	0.3	0.625 (1)	1	0.0016 (0.04)	0.2	16.9 (27)	6.7	Haeussler et al., 2000; Bruhn and Haeussler, 2006; Haeussler and Saltus, 2011; Koehler et al., 2012a; FMMG, 2012b
					60	0.4	SE	12.5 (20)	0.4			0.0031 (0.08)	0.6	16.9 (27)		
					75	0.3	SE	15.6 (25)	0.3			0.0106 (0.27)	0.2	16.9 (27)		
F2	Kasilof anticline	Reverse	WC94, M-L*, Reverse	Maximum Moment	45	0.2	SE	9.4 (15)	0.3	0.625 (1)	1	0.0016 (0.04)	0.2	5.6 (9)	6.2	Haeussler et al., 2000; Bruhn and Haeussler, 2006; Haeussler and Saltus, 2011; Koehler et al., 2012a; FMMG, 2012b
					60	0.2	SE	12.5 (20)	0.4			0.0031 (0.08)	0.6	5.6 (9)		
					75	0.6	SE	15.6 (25)	0.3			0.0106 (0.27)	0.2	5.6 (9)		
F3	Kenai-Cannery loop anticline	Reverse	WC94, M-L*, Reverse	Maximum Moment	45	0.1	SE	9.4 (15)	0.3	1.875 (3)	1	0.0016 (0.04)	0.2	30 (48)	7.1	Haeussler et al., 2000; Bruhn and Haeussler, 2006; Haeussler and Saltus, 2011; Koehler et al., 2012a; FMMG, 2012b
					60	0.7	SE	12.5 (20)	0.4			0.0031 (0.08)	0.6	30 (48)		
					75	0.2	SE	15.6 (25)	0.3			0.0106 (0.27)	0.2	30 (48)		
F4	Swanson River anticline	Reverse	WC94, M-L*, Reverse	Maximum Moment	50	0.6	SE	9.4 (15)	0.3	0.438 (0.7)	1	0.0016 (0.04)	0.2	24.4 (39)	6.9	Haeussler et al., 2000; Bruhn and Haeussler, 2006; Haeussler and Saltus, 2011; Koehler et al., 2012a; FMMG, 2012b
					65	0.3	SE	12.5 (20)	0.4			0.0031 (0.08)	0.6	24.4 (39)		
					80	0.1	SE	15.6 (25)	0.3			0.0106 (0.27)	0.2	24.4 (39)		
F5	Beaver Creek anticline	Reverse	WC94, M-L*, Reverse	Maximum Moment	45	0.3	SE	9.4 (15)	0.3	0.625 (1)	1	0.0016 (0.04)	0.2	4.4 (7)	6.0	Haeussler et al., 2000; Bruhn and Haeussler, 2006; Wong et al., 2008; Haeussler and Saltus, 2011; Koehler et al., 2012a
					60	0.4	SE	12.5 (20)	0.4			0.0031 (0.08)	0.6	4.4 (7)		
					75	0.3	SE	15.6 (25)	0.3			0.0106 (0.27)	0.2	4.4 (7)		
F6	West Fork anticline	Reverse	WC94, M-L*, Reverse	Maximum Moment	45	0.3	SE	9.4 (15)	0.3	0.625 (1)	1	0.0016 (0.04)	0.2	6.9 (11)	6.3	Haeussler et al., 2000; Bruhn and Haeussler, 2006; Haeussler and Saltus, 2011; Koehler et al., 2012a
					60	0.4	SE	12.5 (20)	0.4			0.0031 (0.08)	0.6	6.9 (11)		
					75	0.3	SE	15.6 (25)	0.3			0.0106 (0.27)	0.2	6.9 (11)		
F7	Middle Ground Shoal anticline + Granite Point anticline	Reverse	WC94, M-L*, Reverse	Maximum Moment	50	0.6	NW	9.4 (15)	0.3	0.875 (1.4)	1	0.0154 (0.39)	0.2	41.9 (67)	7.2	Haeussler et al., 2000; Bruhn and Haeussler, 2006; Wong et al., 2008; Haeussler and Saltus, 2011; Koehler et al., 2012a
					60	0.2	NW	12.5 (20)	0.4			0.0323 (0.82)	0.6	41.9 (67)		
					70	0.2	NW	15.6 (25)	0.3			0.1071 (2.72)	0.2	41.9 (67)		
F8	McArthur Redoubt River-Shoal	Reverse	WC94, M-L*, Reverse	Maximum Moment			SE	9.4 (15)	0.3	1 (1.6)	1	0.0016 (0.04)	0.2	16.9 (27)	6.7	Haeussler et al., 2000; Bruhn and Haeussler, 2006; Haeussler and



Study ID	Name	Faulting Type	M relation	Magnitude Frequency distribution	Dip (deg.)	Weight	Dip direction	Depth max in mi (km)	Weight	Depth to fault tip in mi (km)	Weight	Slip Rate in in/yr (mm/yr)	Weight	Fault Length in mi (km)	Maximum magnitude (M _w)	Citations
	anticline				60	0.3	SE	12.5 (20)	0.4			0.0031 (0.08)	0.6	16.9 (27)		Saltus, 2011; Koehler et al., 2012a
					75	0.7	SE	15.6 (25)	0.3			0.0106 (0.27)	0.2	16.9 (27)		
F9	West McArthur River anticline	Reverse	WC94, M-L*, Reverse	Maximum Moment	45	0.1	SE	9.4 (15)	0.3	0.938 (1.5)	1	0.0016 (0.04)	0.2	11.9 (19)	6.6	Haeussler et al., 2000; Bruhn and Haeussler, 2006; Haeussler and Saltus, 2011; Koehler et al., 2012a
					60	0.2	SE	12.5 (20)	0.4			0.0031 (0.08)	0.6	11.9 (19)		
					75	0.7	SE	15.6 (25)	0.3			0.0106 (0.27)	0.2	11.9 (19)		
F10	Nicolai Creek anticline	Reverse	WC94, M-L*, Reverse	Maximum Moment	45	0.3	SE	9.4 (15)	0.3	0.625 (1)	1	0.0016 (0.04)	0.2	4.4 (7)	6.0	Bruhn and Haeussler, 2006; Haeussler and Saltus, 2011; Koehler et al., 2012a
					60	0.4	SE	12.5 (20)	0.4			0.0031 (0.08)	0.6	4.4 (7)		
					75	0.3	SE	15.6 (25)	0.3			0.0106 (0.27)	0.2	4.4 (7)		
F11	Moquawkie anticline	Reverse	WC94, M-L*, Reverse	Maximum Moment	45	0.3	NW	9.4 (15)	0.3	0.625 (1)	1	0.0016 (0.04)	0.2	7.5 (12)	6.3	Haeussler et al., 2000; Bruhn and Haeussler, 2006; Haeussler and Saltus, 2011; Koehler et al., 2012a
					60	0.4	NW	12.5 (20)	0.4			0.0031 (0.08)	0.6	7.5 (12)		
					75	0.3	NW	15.6 (25)	0.3			0.0106 (0.27)	0.2	7.5 (12)		
F12	North Cook Inlet anticline	Reverse	WC94, M-L*, Reverse	Maximum Moment	45	0.3	SE	9.4 (15)	0.3	0.625 (1)	1	0.0016 (0.04)	0.2	24.4 (39)	6.9	Haeussler et al., 2000; Bruhn and Haeussler, 2006; Wong et al., 2008; Haeussler and Saltus, 2011; Koehler et al., 2012a
					60	0.4	SE	12.5 (20)	0.4			0.0031 (0.08)	0.6	24.4 (39)		
					75	0.3	SE	15.6 (25)	0.3			0.0106 (0.27)	0.2	24.4 (39)		
F13	Beluga River anticline + Lewis River anticline	Reverse	WC94, M-L*, Reverse	Maximum Moment	45	0.3	SE	9.4 (15)	0.3	0.625 (1)	1	0.0016 (0.04)	0.2	21.9 (35)	6.9	Haeussler et al., 2000; Bruhn and Haeussler, 2006; Wong et al., 2008; Haeussler and Saltus, 2011; Koehler et al., 2012a
					60	0.4	SE	12.5 (20)	0.4			0.0031 (0.08)	0.6	21.9 (35)		
					75	0.3	SE	15.6 (25)	0.3			0.0106 (0.27)	0.2	21.9 (35)		
F14	Ivan River anticline	Reverse	WC94, M-L*, Reverse	Maximum Moment	45	0.3	NW	9.4 (15)	0.3	0.625 (1)	1	0.0016 (0.04)	0.2	6.9 (11)	6.3	Haeussler et al., 2000; Bruhn and Haeussler, 2006; Wong et al., 2008; Haeussler and Saltus, 2011; Koehler et al., 2012a
					60	0.4	NW	12.5 (20)	0.4			0.0031 (0.08)	0.6	6.9 (11)		
					75	0.3	NW	15.6 (25)	0.3			0.0106 (0.27)	0.2	6.9 (11)		



F15	Stump Lake anticline	Reverse	WC94, M-L*, Reverse	Maximum Moment	45	0.3	NW	9.4 (15)	0.3	0.625 (1)	1	0.0016 (0.04)	0.2	4.4 (7)	6.0	Haeussler et al., 2000; Bruhn and Haeussler, 2006; Haeussler and Saltus, 2011; Koehler et al., 2012a
					60	0.4	NW	12.5 (20)	0.4			0.0031 (0.08)	0.6	4.4 (7)		
					75	0.3	NW	25	0.3			0.0106 (0.27)	0.2	4.4 (7)		
F21	Sterling anticline	Reverse	WC94, M-L*, Reverse	Maximum Moment	60	0.3	SE	9.4 (15)	0.3	0.625 (1)	1	0.0016 (0.04)	0.2	6.3 (10)	6.2	Haeussler et al., 2000; Bruhn and Haeussler, 2006; Haeussler and Saltus, 2011; Koehler et al., 2012; FCL, 2012
					75	0.3	SE	12.5 (20)	0.4			0.0031 (0.08)	0.6	6.3 (10)		
					90	0.4	SE	15.6 (25)	0.3			0.0106 (0.27)	0.2	6.3 (10)		
F22	Trading Bay + North Trading Bay anticline	Reverse	WC94, M-L*, Reverse	Maximum Moment	45	0.3	SE	9.4 (15)	0.3	0.625 (1)	1	0.0016 (0.04)	0.2	8.8 (14)	6.4	Haeussler et al., 2000; Bruhn and Haeussler, 2006; Haeussler and Saltus, 2011; Koehler et al., 2012
					60	0.4	SE	12.5 (20)	0.4			0.0031 (0.08)	0.6	8.8 (14)		
					75	0.3	SE	15.6 (25)	0.3			0.0106 (0.27)	0.2	8.8 (14)		

* Due to uncertainty of structure depth and orientations, Wong et al. (2008) and Haeussler et al. (2000) use the WC94, M-L, Reverse (Rupture length-magnitude) relation to determine M_w characteristic. We repeat the usage of inferred earthquake moment magnitude (M_w) herein.

Table 3.3: Non-Cook Inlet Basin Upper Plate Fault Sources

Study ID	Name	Faulting Type	M relation	Dip (deg.)	Depth range in mi (km)	Geometry Weight	Slip Rate in in/yr (mm/yr)	Mean Slip Rate in in/yr (mm/yr)	Slip Rate Weight	Slip Rate Distribution Type	Length in mi (km)	Area in mi ² (km ²)	Maximum magnitude (M _w)
F16	Castle Mountain – Entire fault	Reverse	WC94, M-L**, Reverse	80 NW	0.0 - 12.5 (0.0 - 20.0)	1	0.0197 (0.5)	0.0197 (0.5)	1.0	Uniform	118.5 (189.6)	1506 (3856)	7.8
F17	Castle Mountain West fault	Reverse	WC94, M-L**, Reverse	80 NW	0.0 - 12.5 (0.0 - 20.0)	0.5	0.0827 - 0.1417 (2.1 - 3.6)	0.1142 (2.9)	0.5	Uniform	38.4 (61.4)	490 (1253)	7.2
							0.0157 - 0.0236 (0.4 - 0.6)	0.0197 (0.5)	0.5				
F18	Castle Mountain East fault	Reverse	WC94, M-L**, Reverse	80 NW	0.0 - 12.5 (0.0 to 20.0)	0.5	0.0197 (0.5)	0.0197 (0.5)	1.0	none	80.4 (128.6)	1016 (2602)	7.6

Study ID	Name	Faulting Type	M relation	Magnitude Frequency Distribution	Dip (deg.)	Weight	Dip direction	Depth max in mi (km)	Weight	Depth to fault tip in mi (km)	Weight	Slip Rate in in/yr (mm/yr)	Weight	Fault Length in mi (km)	Maximum magnitude (M _w)	Citation
F19	Lake Clark fault east	Strike-slip	WC94, M-L**, Strike-slip	Maximum Moment	75	0.5	NW	9.4 (15)	0.3	-	1	0.0004 (0.01)	0.2	75 (120)	7.5	Plafker et al., 1975; Schmoll and Yehle, 1987; Haeussler and Saltus, 2004; Wong et al., 2008; Haeussler and Saltus, 2011; Koehler and Reger, 2011; Koehler et al., 2012a
					90	0.5	NW	12.5 (20)	0.4			0.0039 (0.1)	0.6	75 (120)		
								15.6 (25)	0.3			0.0276 (0.7)	0.2	75 (120)		
F20	Lake Clark fault west	Strike-slip	WC94, M-L**, Strike-slip	Maximum Moment	75	0.5	NW	9.4 (15)	0.3	-	1	0.0004 (0.01)	0.2	80 (128)	7.5	Plafker et al., 1975; Schmoll and Yehle, 1987; Haeussler and Saltus, 2004; Wong et al., 2008; Haeussler and Saltus, 2011; Koehler and Reger, 2011; Koehler et al., 2012a
					90	0.5	NW	12.5 (20)	0.4			0.0039 (0.1)	0.6	80 (128)		
								15.6 (25)	0.3			0.0276 (0.7)	0.2	80 (128)		

** Magnitude relationships: (WC94¹, M-L, Reverse): $M_{max}=5.00+1.22*\log(\text{surface rupture length of reverse fault})$, or equivalent WC94 relation (M-A and M-W),
 (WC94¹, M-L, Strike-slip): $M_{max}=5.16+1.12*\log(\text{surface rupture length of strike-slip fault})$, or equivalent WC94 relation (M-A and M-W)

¹ WC94: Wells, D.L. and Coppersmith, K.J., 1994

3.4.3 Excluded Faults

Numerous faults are presented in the neotectonics maps of Alaska (Plafker et al., 1994) that are not included in the discussion and study source model above. These faults are generally not shown in the QFF (Koehler et al., 2012a). These faults were excluded because of a lack of supporting information (e.g., activity levels, location, spatial persistence, and relation to seismic events) or because the reported activity of the fault was very low (<0.02 in/yr / <0.5 mm/yr) and the fault was far from the site.

The Bruin Bay fault and the Border Ranges faults, two prominent crustal structures in the site vicinity, were excluded from this study because there is no evidence for Holocene faulting along either structure. The Border Range fault is considered a Tertiary normal fault; the Bruin Bay fault is a reverse fault whose age of last movement is not clear.

Additional faults excluded for this study include: the Chugach-St. Elias fault, the Kodiak Shelf fault zone, the Hicks Creek fault, the Matanuska Glacier fault, the Kenai lineament, the Ragged Mountain fault, the Patton Bay and Hanning Bay faults, and the Hinchinbrook Island, Hawkins Island, and Cordova mainland faults. The Salamatof Road fault was not included in the source model because it is interpreted as a non-seismogenic fault. This conclusion is based on lateral continuity of seismic reflections across the mapped trace of this structure, as imaged during the onshore geophysics campaign of the AKLNG project (Fugro, 2015e).

The Denali fault is not included as a seismic source for this study. To confirm the earlier result, a sensitivity analysis was performed to evaluate the Denali fault contribution to the hazard and the response spectra at the project site. The analysis is presented in [Appendix B](#) and confirms that exclusion of Denali fault from the seismic source model is supported because it does not affect the estimated ground motion hazard at the project site.

3.5 **Upper Crustal Areal Source**

In addition to the upper crustal seismic sources described above, upper crustal areal seismicity in the study region is included in the seismic source model. Areal seismicity captures seismic events that are not attributable to a known structure. In the study region, the shallow dip of the subducting Pacific slab and uncertainty in computed hypocentral depths, make it unfeasible to separate upper crustal sources from megathrust interface sources. Consequently, shallow slab seismicity (i.e., earthquakes with focal depths of 0 to 31 mi [0 to 50 km]) is modeled using the USGS slab seismicity model for shallow earthquakes that are not associated with the megathrust interface (Wesson et al., 2007).

3.6 Earthquake Recurrence and Activity Rates

3.6.1 Introduction

Two different earthquake recurrence models were used to characterize the various shallow crustal, intermediate, and deep gridded sources as well as the fault sources in the seismotectonic model, including:

- The activities of the shallow, intermediate, and intraplate gridded seismicity not associated with the Aleutian-Alaskan megathrust were modeled per the gridded seismicity model of Wesson et al. (2007) described in [Section 3.5.2](#) below.
- The activity of the fault sources was modeled by means of the fault slip rate in conjunction with the pure maximum moment magnitude model. This model assumes that all slip produces only the maximum magnitude. Smaller earthquakes are captured by the gridded seismicity model of Wesson et al. (2007).

The subsequent sections discuss the historical seismicity catalog used to develop the source parameters and the methodology employed to derive those parameters for the different source types.

3.6.2 Seismicity Catalog and Grid Source Models

A single upper crustal areal source (Zone A1 on Plate 18) covering the study region was utilized to represent shallow crustal seismicity (≤ 31 mi depth [≤ 50 km]) that is not related to either the megathrust or a known upper crustal structure. A1 is defined as a subset of the USGS smoothed seismicity grid model (Wesson et al., 2007), which is appropriate for non-megathrust seismicity that occurs between 0 and 31 mi (50 km) depth ([Plate 18](#)), latitudes 54.5N and 64N, and longitudes of 157W and 141W. Rates of seismicity in A1 are contained in the gridded seismicity model of Wesson et al. (2007) and the b-value in their Table 3. Gridded incremental values of occurrence of **M** 6.0 per 100 square kilometers per year in the study region range from interval lows of 0.030e-4 to 0.100e-4, to interval highs of 0.300e-4 to 1.000e-4.

To generate their grid source models, Wesson et al. (2007) utilized updated estimates of smoothed seismicity derived from the following combined catalogs: (1) Engdahl and Villaseñor's International Association for Seismology and Physics of the Earth's Interior (IASPEI) project, (2) Stover and Coffman's Seismicity of the United States, (3) the US Geological Survey Preliminary Determination of Epicenters (PDE), (4) the International Seismological Centre (ISC), and (5) the Alaska Earthquake Information Center (AEIC). Source catalogs spanning 1898 through 2004 were ranked subjectively to derive preferred focal coordinates and moment magnitudes for each event. Where moment magnitudes were listed, those values were used. Other magnitudes were converted to moment magnitude using published relations (Utsu, 2002; Sipkin, 2003).

Wesson et al. (2007) declustered the combined catalog using the Gardner and Knopoff (1974) algorithm as described in Wesson et al. (1999a; 1999b) and Frankel et al. (1996; 2002).

Published aftershock studies are available for 12 of the largest mainshocks in the combined catalog, which are listed below. For the following earthquakes and intervals, Wesson et al. (2007) removed aftershocks on the basis of the published studies rather than using Gardner and Knopoff's (1974) time-distance windows:

- 1949 0822 Queen Charlotte (**M** 8.1), 1,000 days;
- 1957 0309 Great Aleutian (**M** 8.6), 1,500 days;
- 1958 0710 Fairweather (**M** 7.7), 500 days;
- 1964 0328 Great Alaskan (**M** 9.2), 1,500 days;
- 1965 0204 Rat Islands (**M** 8.7), 1,300 days;
- 1972 0730 Sitka (**M** 7.6), 500 days;
- 1979 0228 St. Elias (**M** 7.5), 600 days;
- 1986 0507 Andreanof Island (**M** 8.0), 1,000 days;
- 1987 1130 Gulf of Alaska (**M** 7.9), 750 days;
- 1988 0306 Gulf of Alaska (**M** 7.8), 750 days; and
- 2002 1103 Denali fault (**M** 7.9), 500 days.

Declustering reduced the 1898 to 2004 combined catalog from approximately 21,000 magnitude ≥ 4.0 records to approximately 7,500 mainshocks. Overall completeness levels were determined as:

- \geq magnitude 4.5 since 1964;
- \geq magnitude 6.0 since 1932; and
- \geq magnitude 6.9 since 1898.

Wesson et al. (2007) model the smoothed seismicity with an assumed exponential magnitude-frequency distribution:

$$\log_{10}N = a - b \mathbf{M}, \quad (3-1)$$

where

N = the number of earthquakes per year in a magnitude interval,

\mathbf{M} = moment magnitude, and

a and b = parameters, determined using Weichert's (1980) method for estimating a and b values in catalogs with variable completeness levels.

Earthquakes not associated with the megathrust were considered in three groups:

- depth 0-31 mi (0-50 km) not associated with megathrust;
- depth >31-50 mi (50-80 km); and
- depth >50-75 mi (80-120 km).

Wesson et al. (2007) described the grid activity rate calculations as follows: "Earthquake activity rates were calculated in each cell of a 0.1° -long \times 0.1° -lat grid and smoothed using a two-dimensional Gaussian function with correlation distance g (Frankel, 1995): $b = 0.816$ and $g = 75$ km for earthquakes with depth ≥ 31 mi / 50 km [sic] not associated with the megathrust, $b = 0.858$ and $g = 31$ mi / 50 km for earthquakes with depth > 31 mi / 50 km and ≥ 50 mi / 80 km, and $b = 1.007$ and $g = 31$ mi / 50 km for earthquakes with depth > 50 mi / 80 km and ≥ 75 mi / 120 km."

Within the context of Wesson et al. (2007), it appears that the statement " $b = 0.816$ and $g = 75$ km for earthquakes with depth ≥ 31 mi / 50 km not associated with the megathrust" is a misprint that should properly read " $b = 0.816$ and $g = 47$ mi / 75 km for earthquakes with depth ≤ 31 mi / 50 km not associated with the megathrust." If a revision or correction to Wesson et al. (2007) exists, it has not been found. This information is noted here for sake of clarity, but it ultimately does not affect the study region model usage of the gridded seismicity model, as it is the end model of Wesson et al. (2007) that was utilized herein; Fugro has not recreated the model based on the parameters published above.

4.0 PSHA METHODOLOGY

4.1 PSHA Framework

The methodology for Probabilistic Seismic Hazard Analysis (PSHA) is illustrated schematically on [Plate 19](#) and includes the following components:

1. Characterization of the seismic sources within a specified radius (124 miles / 200 km for the current report) around the site. This leads to the development of a seismotectonic model for use in subsequent PSHA evaluations. The characterization includes:
 - a. Source geometry and location;
 - b. Source type (e.g. shallow crustal, subduction, etc.) and style of faulting (e.g., normal, strike-slip, reverse, etc.);
 - c. Magnitude potential (i.e., range of earthquake sizes possible on each source) and magnitude distribution (i.e., typically characterized using a magnitude probability density function);
2. Earthquake magnitude recurrence: this is a characterization of the annual rate at which earthquakes of a specified magnitude or greater occur in each source. Depending on the source type, the magnitude recurrence is estimated based on: (i) the long term slip rate (e.g., for planar fault sources) or (ii) regression on the historic seismicity (e.g., for aerial sources).
3. Characterization of ground motion attenuation in each source based on the geologic environment and source types: This is described by a Ground Motion Prediction Equation, or GMPE (a.k.a “attenuation relationship” or “attenuation model”).
4. Performing PSHA using as input the seismotectonic model developed in the previous step in combination with the GMPEs selected for the specific environment, to estimate the ground motion hazard at the site. This is expressed in terms of the annual frequency of exceeding a given spectral acceleration at the project site (i.e., annual hazard curves). This information can also be shown in the form of uniform hazard spectra (UHS) which correspond to spectral acceleration having the same probability of exceedance across all structural periods. The UHS are typically used by different design codes to define the design spectra.
5. Deaggregation of seismic hazard in terms of magnitude, distance, number of standard deviations, seismic source, etc. to compute the relative contribution of different earthquake scenarios to the hazard at the site.

4.1.1 PSHA Calculations

Computation of the seismic hazard (Step 4 described above) involves the combination of uncertainties in earthquake size, location, frequency, and resulting ground motions. The estimated annual rate at which the ground motion, A , will exceed a particular value, a , is computed by (Cornell, 1968):

$$\lambda[A > a] = \sum_{i=1}^{N_{source}} N(M_{min}) \iint P[A > a | m, r] f_M(m) f_R(r) dm dr \quad (4-1)$$

where N_{source} is the total number of fault and areal sources, $N(M_{min})$ is the annual rate of earthquakes with magnitude greater than or equal to M_{min} , $P[A > a | m, r]$ is the probability of the ground motion, A , exceeding the threshold value, a , given the earthquake magnitude and distance from the fault, and $f_M(m)$ and $f_R(r)$ are probability density functions describing the variability in magnitude and distance.

The computation of this integral is carried out numerically. By assuming that earthquake occurrence can be modeled as a Poisson process, the probability of exceedance in a specified exposure period (typically corresponding to the useful life of a project) may be estimated as follows (Yegian, 1979):

$$P[A > a, t] = 1 - e^{-[\lambda(a)t]} \quad (4-2)$$

where $P[A > a, t]$ is the conditional probability of the spectral acceleration (A) exceeding a specified acceleration (a) during a time interval (t) given that an earthquake will occur, and $\lambda(a)$ is the mean annual rate of exceedance of the specified acceleration level.

4.2 Treatment of Uncertainty

When performing PSHA, there exists uncertainty with regards to the seismic source characterization (earthquake size, type, and distribution in space in time) as well as ground motion amplitude at the project site resulting from a given earthquake scenario. This uncertainty is in part due to inherent randomness in the natural process (aleatory variability) and in part due to uncertainty in the modeling of the process (epistemic uncertainty).

Aleatory variability is accounted for in the probability density function (PDF) of continuous random variables such as spectral acceleration given a magnitude and distance, or earthquake magnitude given a rupture dimension.

Epistemic uncertainty is accounted for through a logic tree approach. This approach is used to take into consideration uncertainty with respect to parameters that are used in the seismic hazard analyses. Such parameters may be the maximum magnitude on a fault, the long-term slip rate, the median ground motion given an earthquake scenario, and the magnitude probability density

function. The following list describes the parameters for which epistemic uncertainty is described in the logic tree (a generic illustration of which is given in [Plate 20](#)):

- Fault segmentation. Multi-segment rupture was considered along the Castle Mountain Fault ([Table 3.3](#)).
- Dip angle of the planar fault sources. Up to three different dip angles were considered for the planar fault sources. These were weighted according to the relative confidence in the estimates ([Tables 3.2 and 3.3](#)).
- Depth of the planar fault sources. Three different seismogenic depths were considered for the planar fault sources. These were weighted according to the relative confidence in the estimates ([Tables 3.2 and 3.3](#)).
- Magnitude recurrence. Up to two different magnitude recurrence models were used for the interface sources as discussed in [Section 3.0](#). Example probability density functions (PDF) and cumulative probability density functions for the truncated exponential and maximum magnitude models is provided in [Section 5.3](#).
- Time Dependence. Both time-dependent and time-independent models with suitable weights were used for the interface source S2.
- Slip rate on the planar fault sources. Three different slip rates were considered for the planar fault sources. These were weighted according to the relative confidence in the estimates ([Tables 3.2 and 3.3](#)).
- Ground motion prediction equations (GMPEs). Four Next Generation Attenuation (NGA West 2) relationships (Bozorgnia et al., 2014), with equal weights, were used to model all shallow crustal sources (including shallow crustal background seismicity sources and planar fault sources). Three subduction relationships were used to model all subduction interface and intraslab sources. Within the subduction relationships, BC Hydro (BC Hydro, 2012; Abrahamson et al., 2015) relationship was used with a weight of 0.5, other two relationships were used with a weight of 0.25 each. The aleatory variability (σ) has also been taken into account in the ground motion prediction equations. The GMPEs adopted for this study are described in [Section 5.4](#).

4.3 Implementation

Probabilistic seismic hazard analyses were carried out using the computer program HAZ43 (Abrahamson, 2013). This program was developed by Dr. Abrahamson, and it has been validated using all test cases presented in the PSHA Validation Project performed by the Pacific Earthquake Engineering Research (PEER) Center's Lifelines Program (Thomas et al., 2010).

The hazard calculation described by [Equation 4-1](#) is carried by discretizing the distribution on earthquake magnitude, location, and shaking amplitude with the following assumptions: (1) The magnitude distribution per planar fault source is sampled at intervals of 0.01 magnitude units; (2) The variability in ground motion amplitude for a given earthquake scenario is truncated at ± 3 standard deviations.

4.4 Near Source and Directivity Effects

Near-source effects for relatively large magnitude earthquakes are typically considered for distances from the fault of about 15 km or less. These effects are usually referred to as forward, neutral, and backward directivity conditions. In general, forward directivity is associated with the fault rupturing towards the site, and backward directivity conditions with the fault rupturing away from the site. Near-source effects are accounted for in this study by using the recently developed Bayless and Somerville directivity model (in Spudich et al., 2013) as part of the NGA West 2 project. Bayless and Somerville present an improved version of the older Somerville et al. (1997) and Abrahamson (2000) directivity model, which retains that model's computational simplicity but updates the model with new data and a better functional form including rupture-length denormalization, a modified dependence on site azimuth, use of azimuth tapers to obviate the need for an excluded zone, and extension of the algorithm to allow directivity calculations for complicated, noncontiguous rupture zones. Additionally, the Bayless and Somerville model explicitly developed directivity models for fault-normal (FN) and fault-parallel (FP) components. The calculation of near-source effects is implemented probabilistically by randomizing the location of the earthquake hypocenter given a rupture area.

The AKLNG project site is located close to two identified seismic fault sources, F3 Kenai – Cannery loop Anticline and F7 Middle Ground Shoal Anticline and Granite Point Anticline. Hence, near-source effects were taken into consideration in the analyses.

5.0 SEISMIC HAZARD ANALYSES

5.1 Project Location

Probabilistic seismic hazard analyses (PSHA) were conducted for four representative onshore locations and four representative nearshore locations in order to capture spatial variability of the ground motions within the project area. (Plate 21). The geographical coordinates of the locations used for the seismic hazard analyses are tabulated in Table 5.1. The closest distance from the onshore site 4 and the nearshore site 1 to the seismic sources described in Section 3.0 are summarized in Table 5.2. The 2002 Denali earthquake, which was included in a sensitivity study in Appendix B to confirm exclusion from the analyses, was at a distance of 144 miles (232 km) from Onshore Site 3.

Table 5.1: Coordinates of Representative Locations

Location	Latitude (degrees)	Longitude (degrees)
Onshore Site 1	60.66486	-151.35769
Onshore Site 2	60.65455	-151.34953
Onshore Site 3	60.67554	-151.36764
Onshore Site 4	60.66120	-151.36600
Nearshore Site 1	60.65763	-151.38643
Nearshore Site 2	60.66965	-151.38962
Nearshore Site 3	60.66132	-151.37457
Nearshore Site 4	60.64981	-151.37039

Table 5.2: Closest Distance to Seismic Sources

Source	Closest Distance in miles (km)	
	Onshore Site 4	Nearshore Site 1
F1 Falls Creek-Ninilchik Anticline	28.8 (46.1)	28.6 (45.8)
F2 Kasilof Anticline	20.5 (32.8)	20.2 (32.3)
F3 Kenai – Cannery loop Anticline	5.7 (9.1)	6.2 (9.9)
F4 Swanson River Anticline	12.9 (20.6)	13.6 (21.7)
F5 Beaver Creek Anticline	11.1 (17.7)	11.7 (18.7)
F6 West Fork Anticline	16.9 (27.1)	17.4 (27.9)
F7 Middle Ground Shoal Anticline and Granite Point Anticline	4.4 (7.0)	3.8 (6.0)
F8 McArthur River-Redoubt Shoal Anticline	9.6 (15.4)	9.1 (14.6)
F9 West McArthur River Anticline	10.9 (17.4)	10.4 (16.7)
F10 Nicolai Creek Anticline	22.6 (36.1)	22.8 (36.4)
F11 Moquawkie Anticline	27.8 (44.4)	28.0 (44.8)
F12 North Cook Inlet Anticline	13.4 (21.4)	13.9 (22.2)
F13 Beluga River Anticline and Lewis River Anticline	29.5 (47.2)	30.0 (48.0)
F14 Ivan River Anticline	42.6 (68.1)	43.0 (68.8)
F15 Stump Lake Anticline	45.9 (73.4)	46.4 (74.3)
F16 Castle Mountain – Entire Fault	46.4 (74.2)	46.8 (74.9)
F17 Castle Mountain West Fault	46.4 (74.3)	46.8 (74.9)
F18 Castle Mountain East Fault	92.9 (148.6)	93.5 (149.6)
F19 Lake Clark Fault East	37.3 (59.6)	37.2 (59.5)
F20 Lake Clark Fault West	56.6 (90.6)	55.9 (89.5)
F21 Sterling Anticline	14.3 (22.8)	14.8 (23.6)
F22 Trading Bay and North Trading Bay Anticline	12.8 (20.4)	12.8 (20.4)
S1 Interface Subduction - Kodiak Island	124.4 (199.0)	124.0 (198.4)
S2 Interface Subduction - Price William Sound	43.9 (70.2)	44.3 (70.9)
S3 Interface Subduction - Yakutat	214.5 (343.2)	215.3 (344.4)
MT Megathrust Gridded Seismicity	28.6 (45.8)	29.3 (46.8)
IS60 Intraslab Subduction, depth 37 mi (60 km)	37.3 (60.0)	37.3 (60.0)
IS120 Intraslab Subduction, depth 74 mi (120 km)	55.9 (90.0)	55.9 (90.0)

5.2 Site Classification

Dynamic subsurface conditions were characterized by means of: (1) 8 Phase 1 onshore borings which included downhole seismic shear wave velocity logging and presented in the Geotechnical Data report (Fugro Report No. 04.10140094-8), (2) 18 Phase 2 onshore borings which included downhole seismic shear wave velocity logging and presented in the Onshore Geotechnical Data report (Fugro Report No. 04.10140334-8), (3) 9 nearshore borings which included downhole seismic shear wave velocity logging performed during Phase 2 and presented in the Marine Geotechnical Data report (Fugro Report No. 04.10140334-9), and (4) Interferometric Multichannel Analysis of Surface Waves (IMASW) data presented in the Onshore Geophysical Survey Report (Fugro Report No. 04.10140334-7). In addition, a number of Standard Penetration Test (SPT) based empirical correlations were used to estimate either G_{max} or V_s for all 87 onshore and 25 nearshore borings performed at the project site. The empirical correlations between SPT blow counts and shear wave velocity (or small strain shear modulus) for sands and clays that were considered are summarized in [Table 5.3](#). Based on the available data (field logs and boring logs), the subsurface conditions generally consist of sandy gravel to gravelly sand in the top approximately 26 ft depth, underlain by poorly graded sand to a depth of approximately 65 ft. Interlayered sandy/clayey deposits were typically found at deeper depths (>65 ft). A detailed description of subsurface conditions in the onshore areas is provided in the Onshore and the Marine Geotechnical Data Reports for the project (Fugro Reports No. 04.10140334-8 and No. 04.10140334-9, respectively). [Plate 22](#) presents a summary of measured shear wave velocity data obtained from the 26 downhole seismic shear wave velocity tests in the onshore project area. Estimated time-averaged shear wave velocities (V_{s30}), at the ground surface, for the twenty-six downhole measurements are in the range of 685 ft/s (209 m/s) to 1181 ft/s (360 m/s), with an average of approximately 912 ft/s (278 m/s). Similarly, [Plate 23](#) presents a summary of measured shear wave velocity data obtained from the 9 downhole seismic shear wave velocity tests in the nearshore project area. Estimated time-averaged shear wave velocities (V_{s30}), at the ground surface, for the nine downhole measurements are in the range of 817 ft/s (249 m/s) to 941 ft/s (287 m/s), with an average of approximately 876 ft/s (267 m/s). Based on this, the seismic hazard analyses were performed, for the onshore as well as nearshore locations, at the ground surface with a time-weighted average shear wave velocity of 885 ft/s (270 m/s) corresponding to site class D per ASCE 7-05. [Plate 24](#) presents a summary of all measured shear wave velocity data obtained from the downhole seismic shear wave velocity tests in the onshore and the nearshore project area during Phases 1 and 2.

Table 5.3: Empirical Correlations for Shear Wave Velocity

Reference	Soil Type	Correlated Parameters	Correlations
Brandenburg et al. (2010)	All	SPT blow count (N_{60}) Effective vertical stress, σ'_v	$\ln(V_s) = \beta_0 + \beta_1 \ln(N_{60}) + \beta_2 \ln(\sigma'_v) + \eta + \varepsilon$ where V_s – Shear wave velocity in m/s $\beta_0, \beta_1, \beta_2, \eta$, and ε – Regression parameters depend on soil type
Wair et al. (2012)	All	SPT blow count (N_{60}) Effective vertical stress, σ'_v	$V_s = a \cdot N_{60}^b \cdot \sigma'_v{}^c \cdot d$ where V_s – Shear wave velocity in m/s a, b , and c – Regression parameters depend on soil type d – Age Scaling Factor

5.3 Magnitude Probability Density Functions

The recurrence of earthquakes in a region is modeled by means of magnitude recurrence relationships, $N(M)$. Those relationships describe the annual rate at which earthquakes with magnitudes equal to or greater than M occur on a given source or region and may be estimated through the following equation:

$$N(M) = N(M_{min}) \cdot \int_M^{M_{max}} f_m(m) \cdot dm \quad (5-1)$$

As suggested by this equation, the following information is required for each areal or fault source to develop its magnitude recurrence relationship:

- The magnitude probability density function, $f(m)$, which describes the relative number of large, moderate and small magnitude earthquakes occurring on the source.
- The activity rate, $N(M_{min})$ which describes the annual number of earthquakes on a source larger than a minimum magnitude of engineering interest, M_{min} .

Different magnitude distributions are typically used for areal sources (background gridded seismicity sources) compared to fault sources which have been observed to generate earthquakes in a preferred magnitude range. As discussed in [Section 3.0 \(Tables 3.1 to 3.3\)](#), two different magnitude probability density functions (PDF) were used to model the relative rate of occurrence of different magnitudes of the seismogenic sources: (a) the truncated exponential (Gutenberg-Richter) model is used for shallow crustal and subduction background gridded seismicity sources (MT, IS1, and IS2) as well as interface subduction sources S1b, S2b, and S3, and (b) the maximum magnitude (pure characteristic) model is used for planar fault sources as well as

interface subduction sources S1a and S2a that are capable of generating megathrust events ($M > 8.5$).

Example probability density functions (PDF) and cumulative probability density functions for the truncated exponential and maximum magnitude (pure characteristic) models are shown on [Plates 25 and 26](#), respectively. For this comparison, a characteristic magnitude of 7.75 was assumed. This magnitude was also used as the maximum magnitude in the truncated exponential model. The characteristic model was assumed to have a truncated normal distribution with maximum and minimum magnitudes of ± 0.24 units about the characteristic magnitude and a standard deviation of 0.12. This distribution represents the aleatory variability in the magnitude potential of any given source. The pure characteristic (maximum magnitude) model has the highest probability density around the characteristic magnitude while zero density is assigned to smaller magnitudes. The differences in the probability density between the two models translate to significantly different recurrence relationships. [Plate 26](#) shows the annual recurrence predicted using the two models in combination with a slip rate of 0.039 in/yr (1.0 mm/year), a fault area of 38564 mi² (100,000 km²) and a b-value of 1.0. The truncated exponential model estimates the occurrence of earthquakes for a range of magnitudes, with the smaller magnitude earthquakes occurring more frequently compared to the larger ones. Conversely, the pure characteristic (maximum magnitude) model which estimates larger frequency of occurrence for the characteristic magnitude earthquake. It is important to note that an areal source overlaps the planar fault source. In this way, the majority of characteristic earthquakes are concentrated along the fault plane while smaller and moderate magnitude earthquakes are distributed evenly over a broader zone.

5.4 Horizontal Ground Motion Prediction Equations

The attenuation of seismic waves from a seismogenic source to the site was modeled using horizontal Ground Motion Prediction Equations (GMPEs). These empirical relationships should model the type of rupture mechanism as well as the regional geology to properly estimate site-specific strong ground motion.

The project area lies in an active plate margin region, with shallow crustal as well as interface and intraslab subduction sources. Accordingly, shallow crustal as well as interface and intraslab relationships were selected for the project. These relationships include the recently developed Next Generation Attenuation (NGA West 2) relationships for the shallow crustal sources (Bozorgnia et al., 2014), and relationships for interface and deep intraslab subduction sources based on interface/megathrust and intraslab events worldwide. Improvements in the NGA West 2 GMPEs compared to the NGA West 1 GMPEs (Power et al., 2008) include among others: (a) an expanded earthquake database, especially in large distance and small magnitude range; (b) increase in total number of earthquakes (a total of 161 additional moderate-to-large world-wide earthquakes and 266 small-to-moderate magnitude California earthquakes were added to the NGA West 2 earthquake database); (c) improvements to the “small magnitude” scaling of the GMPEs; (d)

improvements to the “large distance” scaling of the GMPEs; and (e) improvements in the quality of site data and shear wave velocity classification. The relationships used for the project and their corresponding weights are presented in [Table 5.4](#). Idriss (2014) was not adopted since it is not applicable to V_{s30} values less than 1476 ft/s (450 m/s). The remaining four NGA West 2 relationships were weighted equally for the analyses, as there was no justification to provide unequal weighting. Within the subduction relationships, BC Hydro (2012) with the adjustments recommended by Abrahamson et al. (2015) is the preferred model because it is based on a much larger data set that includes all of the data used by Zhao et al. (2006), and uses the Atkinson and Macias (2009) simulation result to constrain the break in the magnitude scaling at high magnitudes. Hence, a higher weight was assigned to that relationship. The BC Hydro (2012) relationship used in this study has included the adjustments recommended by Abrahamson et al. (2015) for the magnitude scaling parameter ΔC_1 for the larger magnitude interface and intraslab events.

Table 5.4: Selected Ground Motion Prediction Equations

Sources	GMPE	Weight
Shallow Crustal Sources (Faults F1 through F20 and Shallow Crustal Background Seismicity)	Abrahamson et al. (2014)	0.25
	Boore et al. (2014)	0.25
	Campbell and Bozorgnia (2014)	0.25
	Chiou and Youngs (2014)	0.25
Interface - Megathrust (Interface Segments S1, S2, S3 and MT Megathrust Gridded Seismicity)	BC Hydro (2012) with the adjustments recommended by Abrahamson et al. (2015)	0.50
	Zhao et al (2006)	0.25
	Atkinson and Macias (2009)	0.25
Intraslab Subduction Sources (IS60 and IS120)	BC Hydro (2012) with the adjustments recommended by Abrahamson et al. (2015)	0.50
	Zhao et al (2006)	0.25
	Atkinson and Boore (2003)	0.25

5.5 Definition of Design Level Events

Per the input from EMALL, National Fire Protection Agency (NFPA) 59A 2006 and ASCE 7-05 have been adopted for the ground motion development for the project. NFPA-59A 2006 has adopted the provisions of ASCE 7-05. According to the requirements of the National Fire Protection Agency (NFPA) 59A 2006 ground motions are developed for two levels:

- The OBE (Operating Basis Earthquake) defined as mean hazard ground motion with a 10 percent probability of exceedance within a 50-year period (475 year return period), and
- The Safe Shutdown Earthquake defined as the “Maximum Considered Earthquake” (MCE) ground motion per ASCE 7-05.

Evaluating the MCE involves a combination of both probabilistic and deterministic analyses. The MCE corresponds to the lesser of: (a) ground motions that have a 2 percent probability of exceedance during a 50-year design life (i.e., return period of 2,475 years), Section 21.2.1 of ASCE 7-05; and (b) 150% of the largest median 5 percent damped spectral response acceleration at that period for characteristic earthquakes on all known active faults within the region (Section 21.2.2 of ASCE 7-05).

Per ASCE 7-05 requirements, ground motions are developed for two levels: (a) Maximum Considered Earthquake (MCE), and (b) Design Earthquake (abbreviated for this project as DE to distinguish from other shaking levels) is defined as 2/3 of MCE, along with some other checks pertaining to spectral shape.

In addition, spectra have also been developed per the requirements of NFPA 59A 2013 and ASCE 7-10, per the request of EMALL. Those results are presented in [Appendix C](#).

5.6 Extending the Design Spectra to Long Periods

The NGA West 2 GMPEs have been developed for structural periods up to 10 seconds. However, subduction GMPEs have been defined to periods of up to 3, 5, and 10 seconds for Atkinson and Boore (2003), Zhao et al (2006), and BC Hydro (2012) with Abrahamson et al. (2015) adjustments GMPEs, respectively. Because of the limitations in applicable periods for Atkinson and Boore (2003) and Zhao et al (2006) subduction models, the UHS could only be defined up to 3 seconds using the full PSHA logic tree. A well-established methodology to extend a design spectrum to longer periods is not available in the literature. However, there appears to be consensus among the scientific community (e.g., NEHRP, 2003) that in the absence of data at long periods design response spectra (not GMPEs) can be extended based on a constant spectral velocity assumption for the intermediate periods and a constant spectral displacement assumption for long periods. For design purposes the “corner period”, marking the transition between constant spectral velocity and constant spectral displacement is a function of the earthquake magnitude and has been tabulated by NEHRP (2003). For this study, the corner period was estimated based on magnitudes of the contributing sources to the hazard at long periods. Based on deaggregation results, majority of long period hazard stems from large magnitude ($M > 7.5$) earthquakes. The long-period transition period T_L for the project area determined according to ASCE 7-05 is 16 seconds. Accordingly, a corner period greater than 10 s was selected for that region. The UHS were extended from 3 to 10 s assuming constant structural velocity.

5.7 Probabilistic Seismic Hazard Analyses Results

Results from the probabilistic seismic hazard analyses are presented in terms of horizontal design response spectra at the ground surface with a time-weighted average shear wave velocity (V_{s30}) value of 885 ft/s (270 m/s) for the planned LNG facility locations (i.e., onshore sites 1 to 4 and nearshore sites 1 to 4). [Plates 27 and 28](#) present the estimated 5-percent damped horizontal response spectra for onshore sites 1 to 4 for 475 and 2475 year return period events, respectively. As shown on the plates, ground motions results are generally similar for those four locations, with differences in spectral values less than 1% for the 475-year event and 2% for the 2475-year events. Similar results are observed for the four nearshore sites in [Plates 29 and 30](#). Hence, onshore site 4 and nearshore site 1 ([Plate 21](#)) are selected as representative locations for the development of design spectra for the onshore and the nearshore LNG facilities, respectively.

[Plate 31](#) compares the estimated 5-percent damped horizontal response spectra for onshore site 4 to and nearshore site 1 for 475 and 2475 year return period events. Ground motions results are generally similar for the onshore and the nearshore locations, with differences in spectral values less than 1% for the 475-year event and up to 2% for the 2475-year events. [Plate 32](#) compares the estimated 5-percent damped horizontal response spectra for onshore site 4 to and the onshore Phase 1 PSHA results (Fugro Report No. 04.10140094-6) for 475 and 2475 year return period events. The onshore horizontal response spectra from the current study are similar to the Phase 1 onshore PSHA results (Fugro Report No. 04.10140094-6), being lower approximately 2% at PGA and 0% at structural period $T = 3$ secs for the 475-year event and lower approximately 3% at PGA and higher by 2% at structural period $T = 3$ secs for the 2475-year events. Those small differences could be attributed to the refined seismotectonic model and the updated BC Hydro (2012) with the adjustments recommended by Abrahamson et al. (2015) used in the current study.

5.7.1 Seismic Hazard Curves

[Plates 33 and 34](#) present the total mean hazard curves for structural periods ranging from PGA to 3 seconds corresponding to onshore site 4, and nearshore site 1. These hazard curves represent the total mean hazard from combining all seismic sources and GMPEs.

5.7.2 Horizontal Uniform Hazard Response Spectra (UHRS)

[Plates 35 and 36](#) present the mean horizontal uniform hazard acceleration response spectra (UHRS) for return periods of 475 and 2475-year return period spectra for onshore site 4 and nearshore site 1, respectively, with no directivity effects. These UHRS were computed based on the total mean hazard curves presented on the total mean hazard curves similar to [Plates 33 and 34](#). As shown on the figures, ground motions results are very similar for those these locations.

[Plates 37 and 38](#) present the 475 and 2475-year return period spectra (5% damping) for the onshore and the nearshore locations, incorporating near-source directivity effects. The results are

shown for no directivity (ND) and fault normal (FN) and fault parallel (FP) directivity conditions. In general, near source effects are associated with structural periods longer than 0.6 seconds. For both the onshore and nearshore sites, in the period range of 0.5 to 1.5 s, the FN spectrum is identical to the ND for both the 475-year event and the 2475-year return period event. At longer structural periods (i.e., $T > 1.5$ sec), the FN spectrum is approximately 1% to 2% higher than the ND spectrum for the 475-year event. For the 2475-year return period event, the FN spectrum is approximately 3% to 6% higher than the ND spectrum at longer structural periods (i.e., $T > 1.5$ sec). The fault parallel (FP) spectrum is approximately identical to the ND spectrum up to the period of 1.5 secs and is 0 to 1% higher than the ND spectrum at longer periods for the 475-year event. For the 2475-year return period event, the FP spectrum is approximately 1% to 3% higher than the ND spectrum at longer structural periods (i.e., $T > 1.5$ sec). The spectral ordinates of horizontal uniform hazard spectra (UHS) for different return periods for site class D condition ($V_{s30} = 885$ ft/s) for the onshore and nearshore sites are tabulated in [Tables 5-5 through 5-8](#) for No Directivity, Fault Normal, Fault Parallel, and Average Directivity conditions, respectively. [Plate 39](#) presents the FN/ND and FP/ND ratios for 475 and 2475 years.

Table 5.5: Horizontal Response Spectra (5% damping) for 475 and 2475-year Events for the Onshore and Nearshore Sites with No Directivity, for Site Class D ($V_{s30} = 885$ ft/s)

Period (sec)	Spectral Acceleration 475-year event – Onshore Site (g)	Spectral Acceleration 475-year event – Nearshore Site (g)	Spectral Acceleration 2475-year event – Onshore Site (g)	Spectral Acceleration 2475-year event – Nearshore Site (g)
PGA	0.528	0.528	0.897	0.900
0.03	0.567	0.568	0.985	0.989
0.075	0.754	0.756	1.311	1.314
0.1	0.903	0.904	1.576	1.579
0.15	1.042	1.043	1.810	1.815
0.2	1.133	1.134	1.966	1.972
0.3	1.113	1.116	1.975	1.986
0.5	0.916	0.918	1.685	1.701
0.75	0.674	0.675	1.274	1.289
1	0.530	0.531	1.017	1.031
1.5	0.333	0.334	0.682	0.693
2	0.241	0.241	0.510	0.519
3	0.148	0.148	0.328	0.334
4	0.111	0.111	0.246	0.250
5	0.089	0.089	0.197	0.200
6	0.074	0.074	0.164	0.167
7	0.063	0.064	0.141	0.143
8	0.055	0.056	0.123	0.125
9	0.049	0.049	0.109	0.111
10	0.044	0.044	0.098	0.100

Table 5.6: Horizontal Response Spectra (5% damping) for 475 and 2475-year Events for the Onshore and Nearshore Sites with Fault Normal Directivity, for Site Class D ($V_{s30} = 885$ ft/s)

Period (sec)	Spectral Acceleration 475-year event – Onshore Site (g)	Spectral Acceleration 475-year event – Nearshore Site (g)	Spectral Acceleration 2475-year event – Onshore Site (g)	Spectral Acceleration 2475-year event – Nearshore Site (g)
PGA	0.528	0.528	0.897	0.900
0.03	0.567	0.568	0.985	0.989
0.075	0.754	0.756	1.311	1.314
0.1	0.903	0.904	1.576	1.579
0.15	1.042	1.043	1.810	1.815
0.2	1.133	1.134	1.966	1.972
0.3	1.113	1.116	1.975	1.986
0.5	0.916	0.918	1.685	1.701
0.75	0.674	0.675	1.274	1.289
1	0.530	0.531	1.017	1.031
1.5	0.333	0.334	0.682	0.693
2	0.243	0.244	0.528	0.537
3	0.150	0.150	0.351	0.357
4	0.112	0.112	0.260	0.265
5	0.090	0.090	0.209	0.213
6	0.075	0.075	0.174	0.177
7	0.064	0.064	0.150	0.152
8	0.056	0.056	0.130	0.132
9	0.050	0.050	0.116	0.118
10	0.045	0.045	0.104	0.106

Table 5.7: Horizontal Response Spectra (5% damping) for 475 and 2475-year Events for the Onshore and Nearshore Sites with Fault Parallel Directivity, for Site Class D ($V_{s30} = 885$ ft/s)

Period (sec)	Spectral Acceleration 475-year event – Onshore Site (g)	Spectral Acceleration 475-year event – Nearshore Site (g)	Spectral Acceleration 2475-year event – Onshore Site (g)	Spectral Acceleration 2475-year event – Nearshore Site (g)
PGA	0.528	0.528	0.897	0.900
0.03	0.567	0.568	0.985	0.989
0.075	0.754	0.756	1.311	1.314
0.1	0.903	0.904	1.576	1.579
0.15	1.042	1.043	1.810	1.815
0.2	1.133	1.134	1.966	1.972
0.3	1.113	1.116	1.975	1.986
0.5	0.916	0.918	1.685	1.701
0.75	0.674	0.675	1.274	1.289
1	0.530	0.531	1.017	1.031
1.5	0.333	0.334	0.682	0.693
2	0.242	0.243	0.519	0.528
3	0.149	0.150	0.341	0.347
4	0.111	0.112	0.254	0.258
5	0.089	0.089	0.202	0.205
6	0.074	0.074	0.169	0.172
7	0.064	0.064	0.145	0.148
8	0.056	0.056	0.127	0.129
9	0.049	0.050	0.113	0.115
10	0.045	0.045	0.102	0.103

Table 5.8: Horizontal Response Spectra (5% damping) for 475 and 2475-year Events for the Onshore and Nearshore Sites with Average Directivity, for Site Class D ($V_{s30} = 885$ ft/s)

Period (sec)	Spectral Acceleration 475-year event – Onshore Site (g)	Spectral Acceleration 475-year event – Nearshore Site (g)	Spectral Acceleration 2475-year event – Onshore Site (g)	Spectral Acceleration 2475-year event – Nearshore Site (g)
PGA	0.528	0.528	0.897	0.900
0.03	0.567	0.568	0.985	0.989
0.075	0.754	0.756	1.311	1.314
0.1	0.903	0.904	1.576	1.579
0.15	1.042	1.043	1.810	1.815
0.2	1.133	1.134	1.966	1.972
0.3	1.113	1.116	1.975	1.986
0.5	0.916	0.918	1.685	1.701
0.75	0.674	0.675	1.274	1.289
1	0.530	0.531	1.017	1.031
1.5	0.333	0.334	0.682	0.693
2	0.242	0.243	0.524	0.533
3	0.149	0.150	0.346	0.352
4	0.112	0.112	0.257	0.262
5	0.089	0.090	0.205	0.209
6	0.074	0.075	0.172	0.174
7	0.064	0.064	0.147	0.150
8	0.056	0.056	0.128	0.130
9	0.050	0.050	0.114	0.116
10	0.045	0.045	0.103	0.105

5.7.3 Seismic Hazard Deaggregation by Seismic Source

Plates 40 to 42 present the seismic source contribution to the total mean hazard for PGA, structural period of 1 second ($Sa [T=1.0s]$) and 3 seconds ($Sa [T=3.0s]$), respectively, for the onshore location. For short structural periods (i.e. PGA) the seismic hazard is dominated by intermediate depth to deep intraslab sources for both 475- and 2475-year return periods. At longer structural periods (i.e. 1 and 3 seconds) contribution from the interface subduction source (S2-Prince William Sound), is also significant. Only one local fault, F7 - Middle Ground Shoal Anticline

and Granite Point Anticline, is seen to contribute (up to 32%) for the return periods considered. Fault F7 has a mean slip rate of 0.0437 in/yr (1.11 mm/yr) compared to the other local faults with mean slip rates on the order of 0.0043 in/yr (0.11 mm/yr). Similar results are presented on [Plates 43 to 45](#) for the nearshore Location.

[Plates 46 and 47](#) present bar plots illustrating the fractional contribution to the total mean hazard from different seismic sources for 475- and 2475-year return periods for the onshore location. Similar results are presented on [Plates 48 and 49](#) for the nearshore location.

As shown on [Plate 46](#), for the 475-year return period, at both short and long periods hazard is dominated by intraslab source (62% for PGA, 36% for T=1 sec and 28% for T=3 sec). Contribution from S2 Interface - Price William Sound is about 8% at PGA, 20% at T=1 sec and 30% at T=3 sec. Middle Ground Shoal Anticline and Granite Point Anticline (F7) planar source contributes about 8% at PGA, about 17% at T=1.0 sec and about 19% at T=3 sec. Finally, the contribution from the shallow crustal background gridded seismicity and mega thrust gridded seismicity sources are in the range of 6 to 13%. In general, similar results are obtained for the 2475-year return period event on [Plate 47](#), except decreased contribution from background gridded seismicity sources and increased contribution from interface subduction source—S2 and Middle Ground Shoal Anticline and Granite Point Anticline (F7) planar source at long periods (reaching about 24% and 30% at T=1 sec, respectively). Also, increased contribution (~36%) from interface subduction source S2 (Prince William Sound) was observed at T=3 sec for the 2,475-year event. Similar contributions to the onshore location is observed at the nearshore location within 1% difference for the 475-year event ([Plate 48](#)). For the 2475-year return period event at the nearshore location, the Middle Ground Shoal Anticline and Granite Point Anticline (F7) planar source has an increased contribution of up to 4% at T=3 sec in comparison to the onshore location ([Plate 49](#)).

5.7.4 Seismic Hazard Deaggregation by Earthquake Magnitude, Distance and Epsilon

[Plate 50](#) presents the seismic hazard deaggregation with respect to earthquake magnitude, distance, and epsilon for PGA, structural period of 1 second and structural period of 3 seconds, for 475- and 2475-year return periods, respectively, for the onshore location. Similar results for the nearshore location are presented in [Plate 51](#).

In general, for the return period of 475 years for both short and longer structural periods the seismic hazard at the project site is controlled by mainly three scenarios: (a) intermediate to large magnitude (i.e., 7.0 to 8.0) events at distances between about 31 to 93 mi (50 km to 150 km) associated with the intermediate depth to deep intraslab sources, (b) larger magnitudes between 9 to 9.2 at distances between about 31 to 62 mi (50 km to 100 km) attributed to the megathrust events on S2 interface (Prince William Sound), and (c) and intermediate to large magnitude events (i.e., 7 to 7.5) at distances about 3.1 to 6.2 mi (5 to 10 km) from the project site associated primarily with Middle Ground Shoal Anticline and Granite Point Anticline (F7) planar source. For

longer structural periods (i.e., period of 1 and 3 seconds), the relative contribution from large magnitude (i.e., 7.0 to 8.0 and 9.0 to 9.2) events increases.

Similar trends are also observed for the longer return period of 2475 years, with generally larger contributions from larger epsilon (ϵ) values. Epsilon is the number of standard deviations that the estimated ground motion amplitude deviates from the estimated median ground motion amplitude. Thus, an epsilon of 1 indicates that the probabilistic value of the ground motion corresponds to a median plus one-standard-deviation value. These results are observed for both the onshore and nearshore location.

5.8 Comparison with Regional Studies

The results of the probabilistic seismic hazard analyses, using the seismotectonic model outlined in the current report, were compared with results from United States Geologic Survey (USGS) 2007 seismic hazard maps for Alaska (Wesson et al., 2007). The 2007 USGS study provide ground motion estimates at a regional scale at a bedrock horizon. In order to compare the results, generic amplification factors were used with the USGS spectra at rock level to estimate shaking at the competent soil horizon. Code based soil amplification ratios from ASCE 7-10 (ASCE, 2010) were used for this purpose. The short periods were amplified by 5 percent and long periods by 65 percent. [Plate 52](#) shows a comparison of site-specific spectra from this study for the onshore location and 2007 USGS study. As shown on the plate, the site-specific study is generally similar to the USGS study for 975-year return period at structural periods greater than 0.5 seconds. Differences in UHS can be associated with:

- Ground motion prediction equations: The current study uses NGA West 2 (Bozorgnia et al., 2014) relationships for the shallow crustal sources, BC Hydro (2012) with Abrahamson et al. (2015) adjustments, Zhao et al (2006) and Atkinson and Macias (2009) relationships for the interface sources and BC Hydro (2012) with Abrahamson et al. (2015) adjustments, Zhao et al. (2006) and Atkinson and Boore (2003) relationships for the intraslab sources, as shown on [Table 5.4](#). The 2007 USGS study used Youngs et al 1997 (interface) and Sadigh et al. (1997) for the Megathrust and Transition fault, Abrahamson and Silva (1997), Boore et al (1997), Sadigh et al (1997) and Campbell and Bozorgnia (2003) for shallow crustal source and Youngs et al. (1997) and Atkinson and Boore (2003) for deeper earthquakes. The GMPEs used in this study are based on significantly larger earthquake databases than those used in the 2007 USGS study. The subduction and NGA West-2 relationships used in this study have also been adopted by USGS in their updated 2014 seismic hazard maps (Petersen et al., 2014).
- Seismic source characterization (geometry and magnitude recurrence): Seismic source geometry and maximum magnitude potential are very similar for both studies with the exception of faults F1 through F15, F21 and F22 which were not included in the USGS

study. As these faults do not significantly contribute to the hazard, differences in source geometry and maximum magnitude potential is not seen as a significant factor contributing to the differences in UHS, apart from the contribution of Fault F7. Also, as stated in [Section 2.0](#), the June 23, 2014 Rat Islands event is the largest intraslab earthquake to be included in the historic catalog for the Alaska-Aleutian arc. The occurrence of this event caused the M_{\max} of intraslab events to be raised to **M** 8.0, from the M_{\max} of 7.5 used in the 2007 USGS study.

- Magnitude recurrence of the megathrust earthquakes: The 2007 USGS study uses a time-independent model. Due to the large release of energy from the **M**9.2 earthquake just 50 years ago it was deemed appropriate to give some weight to time-dependent renewal models for the S2 subduction interface source. The time-dependent models effectively reduces the earthquake recurrence and hazard on these sources. Hence, the current study uses a combination of time-independent and time-dependent models for the interface source S2. The USGS model assumes the hazard from this source does not change in time, which results in an increase of hazard as compared to the time-dependent model.

5.9 Horizontal Ground Motions per NFPA 59A 2006 / ASCE 7-05

5.9.1 Operational Basis Earthquake (OBE)

As presented in [Section 5.7](#), the onshore and nearshore response spectra for the 475-year return period event are nearly identical. Hence, the OBE spectrum developed for the nearshore location is proposed as representative for the project site. The OBE spectra for fault normal (FN) and fault parallel components (FP) are presented for structural analyses purposes. [Plate 53](#) presents the acceleration response spectra (fault normal (FN) and fault parallel (FP) components) at ground surface ($V_{s30} = 885$ ft/s) for OBE (475-years return period) for the project facilities and [Table 5.9](#) tabulates the spectral ordinates of the OBE spectra. As shown in [Plate 49](#), the OBE spectra for FN and FP components are very similar.

Table 5.9: 5-percent Damped Horizontal Acceleration Response Spectrum at Ground Surface for OBE per NFPA 59A 2006, $V_{s30} = 885$ ft/s

Period (sec)	Spectral Acceleration for Operating Basis Earthquake (OBE) for the Onshore and Nearshore Locations – Fault Normal (FN), g	Spectral Acceleration for Operating Basis Earthquake (OBE) for the Onshore and Nearshore Locations – Fault Parallel (FP), g
PGA	0.528	0.528
0.03	0.568	0.568
0.075	0.756	0.756
0.1	0.904	0.904
0.15	1.043	1.043
0.2	1.134	1.134
0.3	1.116	1.116
0.5	0.918	0.918
0.75	0.675	0.675
1	0.531	0.531
1.5	0.334	0.334
2	0.244	0.243
3	0.150	0.150
4	0.112	0.112
5	0.090	0.089
6	0.075	0.074
7	0.064	0.064
8	0.056	0.056
9	0.050	0.050
10	0.045	0.045

5.9.2 Maximum Considered Earthquake (MCE) / Safe Shutdown Earthquake (SSE)

Both probabilistic and deterministic analyses were conducted to estimate the Maximum Considered Earthquake (MCE) ground motion, per the definition in ASCE 7-05. The probabilistic 5-percent damped horizontal response spectra were developed for the Alaska LNG Project site for return period of 2,475 years. The deterministic earthquake response spectrum was calculated as the 150% of the largest median 5 percent damped spectral response acceleration at that period for

characteristic earthquakes on all known active faults within the region. Deterministic analyses for three earthquake scenarios: (1) the planar fault F7 (Middle Ground Shoal anticline and Granite Point anticline), (2) the planar fault F3 (Kenai – Cannery loop Anticline), and (3) the S2 interface (Prince William Sound) were conducted using the attenuation relationships according to [Table 5.4](#). Due to the close proximity of faults F3 and F7 to the onshore and nearshore facility locations, separate deterministic analyses were performed for the onshore and nearshore sites. The deterministic S2 interface subduction scenario assumed a magnitude (M_w) of 9.2 earthquake and a rupture distance (R) of 43.8 mi (70.1 km) for the onshore site and 44.3 mi (70.9 km) for the nearshore site. The deterministic planar fault F3 scenario assumed a magnitude of 7.1 and a rupture distance of 5.8 mi (9.2 km) for the onshore site and 6.3 mi (10.1 km) for the nearshore site, while the deterministic planar fault F7 scenario assumed a magnitude of 7.2 and a rupture distance of 4.4 mi (7.1 km) for the onshore site and 3.8 mi (6.1 km) for the nearshore site. [Plates 54 and 55](#) present the development of the 150% median deterministic response spectrum without directivity effects for the onshore and the nearshore locations, respectively. As shown on both [Plates 54 and 55](#), the deterministic spectrum is controlled by the planar fault F7 scenario at all periods.

[Plate 56](#) presents the procedure of development of acceleration response spectra for the Maximum Considered Earthquake (MCE) for Site Class D, $V_{s30} = 885$ ft/s for the onshore location for the fault normal (FN) component. The plate shows: (a) the UHS corresponding to a return period of 2,475-years (i.e., 2 percent probability of exceedance in 50 years) for the Fault Normal (FN) condition; (b) the 150% median deterministic spectrum calculated for the characteristic magnitude events, from [Plate 54](#) and incorporating the fault normal directivity effects using the FN/ND ratios estimated in PSHA for the 2475-year event ([Plate 39](#)), (c) the deterministic limit spectrum per ASCE 7-05, Section 21.2; and (d) the resulting project fault normal (FN) MCE spectrum for the onshore location. Per the ASCE 7-05 guidelines, deterministic MCE spectrum is the highest of the 150% median deterministic spectrum and the deterministic limit spectrum. Site specific MCE spectrum is the lowest of UHS corresponding to a return period of 2,475-years (i.e., 2 percent probability of exceedance in 50 years) and the deterministic MCE spectrum. As shown on the plate, the MCE spectral acceleration is controlled by the probabilistic site-specific spectrum at short periods (less than 0.09 sec), by the 150% median deterministic spectrum for periods between 1 to 3 secs, and by the ASCE 7-05 deterministic limit at the remaining periods. Similar results are presented on [Plate 57](#) for the onshore location for the fault parallel (FP) component. [Table 5.10](#) tabulates the smoothed spectral ordinates of the 5-percent damped horizontal spectra for SSE for the onshore location, for fault normal and fault parallel components.

[Plates 58 and 59](#) present the procedure of development of acceleration response spectra for the Maximum Considered Earthquake (MCE) for Site Class D, $V_{s30} = 885$ ft/s for the nearshore location for the fault normal (FN) and fault parallel (FP) component, respectively. For the nearshore location, the MCE spectral acceleration is controlled by the probabilistic site-specific spectrum at short periods (less than 0.09 sec), by the 150% median deterministic spectrum for periods between

0.25 to 0.35 secs and 1 to 4 secs and by the ASCE 7-05 deterministic limit spectrum at the remaining periods. The final SSE nearshore spectra were smoothed for the development of spectrally matched motions by increasing uniformly the plateau of the spectra to the maximum value as presented on [Plate 60](#). [Table 5.11](#) tabulates the smoothed spectral ordinates of the 5-percent damped horizontal spectra for SSE for the nearshore location, fault normal and fault parallel components. [Plate 61](#) compares the estimated Maximum Considered Earthquake (MCE) Spectra (fault normal and fault parallel) at ground surface ($V_{s30} = 885$ ft/s) per ASCE 7-05 estimated for the onshore location to those for the nearshore location. Ground motions results are generally similar for the onshore and the nearshore locations. Both the fault normal and fault parallel MCE spectra for the nearshore location are approximately 6% to 7% higher than the corresponding spectra of the onshore location for structural periods $T = 1$ to $T = 3$ secs, due to the prevailing deterministic scenario at this period range. [Plate 62](#) presents the comparison of Maximum Considered Earthquake (MCE) Spectra (fault normal and fault parallel) at ground surface ($V_{s30} = 885$ ft/s) per ASCE 7-05 estimated for the representative onshore location to the onshore Phase 1 PSHA Results ($V_{s30} = 900$ ft/s) (Fugro Report No. 04.10140094-6).

Table 5.10: 5-percent Damped Horizontal Acceleration Response Spectrum for the Onshore Location for SSE/MCE at the Ground Surface per NFPA 59A 2006 / ASCE 7-05, $V_{s30} = 885$ ft/s

Period (sec)	Spectral Acceleration Fault Normal (FN), (g)	Spectral Acceleration Fault Parallel (FP), (g)
PGA	0.897	0.897
0.03	0.985	0.985
0.09	1.491	1.491
0.1	1.500	1.500
0.15	1.500	1.500
0.2	1.500	1.500
0.3	1.500	1.500
0.5	1.500	1.500
0.6	1.500	1.500
0.75	1.200	1.200
1	0.900	0.900
1.5	0.625	0.625
2	0.479	0.472
3	0.311	0.302
4	0.225	0.225
5	0.180	0.180
6	0.150	0.150
7	0.129	0.129
8	0.113	0.113
9	0.100	0.100
10	0.090	0.090

Table 5.11: 5-percent Damped Smoothed Horizontal Acceleration Response Spectrum for the Nearshore Location for SSE/MCE at the Ground Surface per NFPA 59A 2006 / ASCE 7-05, $V_{s30} = 885$ ft/s

Period (sec)	Spectral Acceleration Fault Normal (FN), (g)	Spectral Acceleration Fault Parallel (FP), (g)
PGA	0.901	0.901
0.03	0.990	0.990
0.09	1.496	1.496
0.1	1.533	1.533
0.15	1.533	1.533
0.2	1.533	1.533
0.3	1.533	1.533
0.5	1.533	1.533
0.6	1.533	1.533
0.75	1.200	1.200
1	0.961	0.961
1.5	0.671	0.671
2	0.515	0.506
3	0.334	0.324
4	0.225	0.225
5	0.180	0.180
6	0.150	0.150
7	0.129	0.129
8	0.113	0.113
9	0.100	0.100
10	0.090	0.090

5.9.3 Design Earthquake (DE) Spectrum

The aforementioned PSHA analyses were conducted for subsurface conditions with a time-weighted average shear wave velocity (V_{s30}) of 885 ft/s. ASCE 7-05 provides a procedure for the development of the “design spectrum” at the same soil conditions with those from the Maximum Considered Earthquake (MCE). The development of the “design spectrum” at ground surface ($V_{s30} = 885$ ft/s) per ASCE 7-05 is shown on [Plate 63](#) for the onshore location for the fault normal (FN)

component: (a) the onshore MCE fault normal component; and (b) 2/3 the onshore MCE fault normal component for Site Class D which is the project DE spectrum. The developed spectrum cannot be less than 80% of the general spectrum (Section 11.4.5 of ASCE 7-05). The ASCE 7-05 DE spectrum is two thirds of the site-specific MCE spectrum. Similar results are presented on [Plate 64](#) for the onshore location for the fault parallel (FN) component. [Table 5.12](#) tabulates the spectral ordinates of the 5-percent damped horizontal spectrum for DE for the onshore location, fault normal and fault parallel components.

[Plates 65 and 66](#) present the procedure of development of acceleration response spectra for the Maximum Considered Earthquake (MCE) for Site Class D, $V_{s30} = 885$ ft/s for the nearshore location for the fault normal (FN) and fault parallel (FP) component, respectively. The ASCE 7-05 DE spectrum is two thirds of the site-specific nearshore MCE spectrum for both the fault normal and fault parallel components. [Table 5.13](#) tabulates the spectral ordinates of the 5-percent damped horizontal spectra for DE for the nearshore location, for fault normal and fault parallel components.

[Plate 67](#) presents the summary results of horizontal acceleration response spectra for OBE and SSE for planned onshore facilities at the ground surface with a time-weighted average shear wave velocity (V_{s30}) of 885 ft/s per NFPA 59A 2006 ground motion requirements. Similar results are presented on [Plate 68](#) for MCE and DE at the ground surface with a time-weighted average shear wave velocity (V_{s30}) of 885 ft/s per ASCE 7-05 ground motion requirements. [Plates 69 and 70](#) show similar results for the nearshore facilities. Horizontal Ground Motions per IBC (2012) / NFPA 59A 2013 are presented in [Appendix C](#).

Table 5.12: 5-percent Damped Horizontal Acceleration Response Spectrum for the Onshore Location for Design Earthquake (DE) at the Ground Surface per ASCE 7-05, $V_{s30} = 885$ ft/s

Period (sec)	Spectral Acceleration – Fault Normal (FN), (g)	Spectral Acceleration – Fault Parallel (FP), (g)
PGA	0.598	0.598
0.03	0.657	0.657
0.09	0.994	0.994
0.1	1.000	1.000
0.15	1.000	1.000
0.2	1.000	1.000
0.3	1.000	1.000
0.5	1.000	1.000
0.6	1.000	1.000
0.75	0.800	0.800
1	0.600	0.600
1.5	0.417	0.417
2	0.320	0.314
3	0.207	0.201
4	0.150	0.150
5	0.120	0.120
6	0.100	0.100
7	0.086	0.086
8	0.075	0.075
9	0.067	0.067
10	0.060	0.060

Table 5.13: 5-percent Damped Horizontal Acceleration Response Spectrum for the Nearshore Location for Design Earthquake (DE) at the Ground Surface per ASCE 7-05, $V_{s30} = 885$ ft/s

Period (sec)	Spectral Acceleration – Fault Normal (FN), (g)	Spectral Acceleration – Fault Parallel (FP), (g)
PGA	0.601	0.601
0.03	0.660	0.660
0.09	0.998	0.998
0.1	1.022	1.022
0.15	1.022	1.022
0.2	1.022	1.022
0.3	1.022	1.022
0.5	1.022	1.022
0.6	1.022	1.022
0.75	0.800	0.800
1	0.640	0.640
1.5	0.447	0.447
2	0.343	0.337
3	0.223	0.216
4	0.150	0.150
5	0.120	0.120
6	0.100	0.100
7	0.086	0.086
8	0.075	0.075
9	0.067	0.067
10	0.060	0.060

5.10 Vertical Ground Motions per NFPA 59A 2006 / ASCE 7-05

Robust ground motion prediction equations for vertical ground motions and V/H ratios are not currently available in the literature for the subduction seismic environment similar to that of AKLNG project region. Hazard deaggregation results ([Plates 46 through 49](#)) show that short period ground motion hazard at the project site is primarily associated with the intraslab subduction sources. Gülerce and Abrahamson (2011) developed V/H ratios using existing V/H relations for shallow crustal earthquakes based on the site V_{s30} from the PEER-NGA West 1 database. However, such a

published V/H model is currently not available for intraslab subduction events. Therefore, in consultation with EMALL, the V/H ratios for the project site were developed based on recorded data from the Alaska region. Fugro selected shallow crustal recordings from Alaska and downloaded them from the Pacific Earthquake Engineering Research (PEER) Center NGA motion database website. These motions corresponded to free-field conditions and Site Class D classification per NEHRP (2003). In addition, more motions were selected from the Network for Earthquake Engineering Simulation (NEES) at UCSB site for the Delaney Park Downhole Array Station in Alaska. [Tables 5.14 and 5.15](#) present the downloaded motions recorded in Alaska for Site Class D and rupture distance up to 31 mi (50 km) from the Delaney Park Downhole Array Station and the Pacific Earthquake Engineering Research (PEER) Center NGA motion database website, respectively.

Table 5.14: List of Acceleration Records in Alaska for Site Class D and Rupture Distance up to 31 mi / 50 km from the Delaney Park Downhole Array Station

Earthquake ID	Year	Month	Day	Max PGA (g)	Magnitude (M _L)	Epicentral Distance mi (km)	Source Depth mi (km)
5047474	2005	2	16	0.014	4.74	7.93 (12.69)	21.75 (34.80)
6208470	2006	7	27	0.036	4.7	8.29 (13.26)	22.49 (35.99)
12137460	2012	5	16	0.019	4.6	6.77 (10.83)	38.58 (61.72)
9097480	2009	4	7	0.015	4.8	17.49 (27.98)	20.64 (33.03)
10263490	2010	9	20	0.032	4.9	12.92 (20.67)	28.39 (45.43)
12339002	2012	12	4	0.026	5.8	27.68 (44.29)	33.25 (53.20)
10097460	2010	4	7	0.004	4.6	26.71 (42.73)	22.08 (35.32)

Table 5.15: List of Acceleration Records in Alaska for Site Class D and Rupture Distance up to 31 mi / 50 km from the Pacific Earthquake Engineering Research (PEER) Center NGA Motion Database

Earthquake ID	Year	Month	Day	Max PGA (g)	Magnitude (M _w)	Rupture Distance	Source Depth
						mi (km)	mi (km)
2114	2002	11	3	0.333	7.9	0.11 (0.18)	5.6 (8.9)
2111	2002	11	3	0.109	7.9	26.9 (42.99)	5.6 (8.9)

Plate 71 presents the results for the V/H ratios for distances ranging from 0-31 mi (0-50 km). The average and the median of the V/H ratios are also provided on the Plate. The plate also provides the lower threshold of one half per NPFA-59A (2006) guidelines. The recommended V/H ratios used in the present study was developed as a smooth envelope of the median of the recorded events for Site Class D in Alaska for distances from 0-31 mi (0-50 km). The recommended V/H ratios used herein are tabulated in Table 5.16.

Table 5.16: Recommended V/H Ratios for the Development of Vertical Spectra for Site Class D at the Project Site

Period (sec)	V/H
PGA	0.770
0.03	0.930
0.075	1.310
0.1	1.179
0.15	0.980
0.2	0.846
0.3	0.630
0.5	0.500
0.75	0.500
1	0.500
1.5	0.500
2	0.500
3	0.500
4	0.500
5	0.500
6	0.500
7	0.500
8	0.500
9	0.500
10	0.500

The vertical response spectra at surface for SSE / MCE and OBE, were developed by applying V/H ratios developed above for site class D to the horizontal response spectra of average directivity at surface. The vertical response spectrum DE at surface was estimated as two-thirds of MCE per ASCE 7-05 guidelines. [Plate 72](#) presents the vertical acceleration spectra at the ground surface estimated for SSE and OBE for the planned onshore and nearshore facilities, per NFPA-59A 2006 ground motion requirements. [Table 5.17](#) lists the spectral ordinates of the vertical SSE and OBE spectra at surface for the planned onshore and nearshore facilities.

[Plate 73](#) presents the vertical acceleration spectra at the ground surface estimated for Maximum Considered Earthquake (MCE) and Design Earthquake (DE) for planned onshore and nearshore

facilities, per ASCE 7-05 ground motion requirements. [Table 5.18](#) lists the spectral ordinates of the vertical MCE and DE spectra at surface for the planned onshore and nearshore facilities.

Table 5.17: 5%-damped Vertical Spectra at Ground Surface per NFPA-59A 2006

Period (seconds)	Spectral Acceleration for OBE Level for the Onshore and Nearshore Locations (g)	Spectral Acceleration for SSE Level for the Onshore Location (g)	Spectral Acceleration for SSE Level for the Nearshore Location (g)
0.01	0.407	0.691	0.694
0.03	0.528	0.916	0.921
0.075	0.990	1.788	1.795
0.1	1.066	1.769	1.769
0.15	1.022	1.470	1.470
0.2	0.960	1.269	1.269
0.3	0.703	0.945	0.966
0.5	0.459	0.750	0.750
0.75	0.338	0.600	0.600
1	0.266	0.450	0.480
1.5	0.167	0.313	0.335
2	0.122	0.238	0.255
3	0.075	0.153	0.164
4	0.056	0.113	0.113
5	0.045	0.090	0.090
6	0.037	0.075	0.075
7	0.032	0.064	0.064
8	0.028	0.056	0.056
9	0.025	0.050	0.050
10	0.023	0.045	0.045

Table 5.18: 5%-damped Vertical Spectra at Ground Surface per ASCE 7-05

Period (seconds)	Spectral Acceleration for MCE Level - Onshore Site (g)	Spectral Acceleration for MCE Level - Nearshore Site (g)	Spectral Acceleration for DE Level - Onshore Site (g)	Spectral Acceleration for DE Level - Nearshore Site (g)
0.01	0.691	0.694	0.461	0.463
0.03	0.916	0.921	0.611	0.614
0.075	1.788	1.795	1.192	1.196
0.1	1.769	1.769	1.179	1.179
0.15	1.470	1.470	0.980	0.980
0.2	1.269	1.269	0.846	0.846
0.3	0.945	0.966	0.630	0.644
0.5	0.750	0.750	0.500	0.500
0.75	0.600	0.600	0.400	0.400
1	0.450	0.480	0.300	0.320
1.5	0.313	0.335	0.208	0.224
2	0.238	0.255	0.159	0.170
3	0.153	0.164	0.102	0.110
4	0.113	0.113	0.075	0.075
5	0.090	0.090	0.060	0.060
6	0.075	0.075	0.050	0.050
7	0.064	0.064	0.043	0.043
8	0.056	0.056	0.038	0.038
9	0.050	0.050	0.033	0.033
10	0.045	0.045	0.030	0.030

6.0 DEVELOPMENT OF GROUND ACCELERATION TIME HISTORIES

6.1 Ground Motion Selection

Five sets (each with three components) of accelerograms were selected and spectrally matched to ground surface ($V_{s30} = 885$ ft/s) OBE and SSE spectra per NFPA 59A 2006 guidelines.

[Appendix D](#) presents similar results for per the NFPA 59A 2013 guidelines. Typically, the main considerations while selecting the time histories are: (1) design earthquake parameters (magnitude and distance) resulting from hazard deaggregation, (2) the overall shape of the response spectra relative to the target spectrum, (3) earthquake source mechanism, (4) subsurface conditions at the recording station, (5) significant duration ($D_{5_{95}}$), and (6) frequency content of the time histories.

The deaggregation results in [Section 5.0](#) show that the seismic hazard is mainly controlled by three scenarios in both short and long structural periods: (a) larger magnitudes between 9 to 9.2 at distances typically about 31 to 62 mi (50 km to 100 km) associated with the S2 Interface - Prince William Sound, (b) intermediate to large magnitude (i.e., 7.0 to 8.0) events at distances between about 31 to 93 mi (50 km to 150 km) primarily associated with the intermediate depth and deep intraslab sources, and (c) intermediate to large magnitude events (i.e., 7 to 7.5) at short distances about 3.1 to 6.2 mi (5 to 10 km) associated with the Middle Ground Shoal Anticline and Granite Point Anticline (F7) planar source. Ground motion time histories were selected accordingly. As mentioned above, the primary considerations in selection of ground motion time histories included magnitude and distance ranges of the contributing scenarios, overall spectral shape, earthquake source mechanism and subsurface conditions at the recording station.

One set of recording from **M** 7.14 Duzce 1999 earthquake was selected, to represent ground motions associated with the intermediate to large magnitude shallow crustal earthquake at relatively short distance (attributed to fault F7 - Middle Ground Shoal Anticline and Granite Point Anticline). To incorporate near-source and rupture directivity effects due to fault F7, the original recorded Duzce motions were rotated to resolve a set of fault-normal and fault-parallel horizontal components and these motions were then used generate the design acceleration time histories for OBE and SSE/MCE events. Remaining four sets of recordings were selected to represent ground motions associated with the intermediate to larger magnitude subduction earthquakes. One megathrust (interface) recording from **M** 8.8 Chile earthquake was selected to represent the ground motions associated with the larger magnitude mega thrust interface earthquakes. We note that very few deep intraplate, large magnitude subduction earthquake recordings are available worldwide, especially recordings with compatible spectral shapes with the target OBE and SSE level spectra developed for the project site. Therefore, the available records in the database to select from were limited. Hence, in addition to one intraslab recording (**M** 7.6 El Salvador, 2001), we included another interface recording from, **M** 8.1 Mexico 1985 earthquake and a larger

magnitude shallow crustal recording from **M** 7.9 Denali 2002 earthquake that were in agreement with the magnitude-distance deaggregation of the seismic hazard and in general compliance with all the other seed ground motion selection criteria. It is noted that the recent 2011 Tohoku ground motions were considered, but the recorded spectral shapes were quite different than the ones developed for this project. Shallow crustal recordings (Duzce and Denali) were selected and downloaded from the Pacific Earthquake Engineering Research (PEER) Center NGA motion database website (<http://ngawest2.berkeley.edu/>). Seed time histories of subduction events were downloaded from the Consortium of Organizations for Strong-Motion Observations Systems (COSMOS) Virtual Data Center website (<http://strongmotioncenter.org/vdc/scripts/default.plx>). **Table 6.1** summarizes the relevant parameters of the selected seed time histories.

Table 6.1: Summary of Selected Seed Motion Characteristics

Earthquake	Station	Magnitude/Style of Faulting	Distance in mi (km)	V_{s30} in ft/s (m/s) / Soil Type	Motion ID	PGA (g)	Longest Usable Period (s)	D_{5-75} / D_{5-95}^1 (s)
Duzce, 1999	Duzce	7.14/Strike-slip	4.1 (6.6)	925 (282)	DZCFN	0.40	10.0	7.3 / 11.1
					DZCFP	0.52		7.0 / 10.9
					DZC-UP	0.35		5.8 / 11.0
Denali, 2002	Camp (Temp)	7.90/Strike Slip	31.2 (49.9)	1310 (399.4)	Carlo-090	0.10	12.8	12.6 / 24.3
					Carlo-360	0.08		10.2 / 19.3
					Carlo-UP	0.07		11.5 / 21.7
Mexico, 1985	La Union	8.1/Subduction-Interface	52.1 (83.9)	Rock	UNIO-N00W	0.17	10.0 ²	14.9 / 24.3
					UNIO-N90W	0.15		16.5 / 26.4
					UNIO-UP	0.14		16.8 / 27.6
El Salvador, 2001	Cutuco	7.6/ Subduction-Intraslab	70.8 (114)	Acid Pyroclastic, Volcanic Epiclastics	CTO-180	0.09	10.0 ²	18.1 / 27.3
					CTO-270	0.08		18.8 / 28.6
					CTO-UP	0.06		20.6 / 29.9
Chile, 2010	Santiago La Florida	8.8/Subduction-Interface	59.7 (96.1)	Unknown	MEP-EW	0.17	10.0 ²	27.5 / 41.3
					MEP-NS	0.24		25.5 / 39.8
					MEP-V	0.13		32.8 / 50.1

¹ Duration based on the time interval between the points at which 5% and 75% (D_{5-75}) / 5% and 95% (D_{5-95}) of the total energy was recorded.

² Longest usable frequency after filtering.

6.2 Approach

6.2.1 Modification of Selected Seed Motions

Acceleration time histories at the ground surface (two horizontal and one vertical components) were generated for the project area by spectrally matching recorded acceleration time histories to the OBE and SSE target spectra developed from PSHA (shown on [Plates 67, 70 and 72](#)) according to the ASCE 4-98 spectral matching criteria. A time-domain spectral matching procedure was used to better preserve the characteristics of the seed time histories. The procedure usually involves the following steps:

- Rotation of original motions to obtain motions in the FN and FP directions
- Spectral matching of the motions to the target spectra;
- Baseline correction of the spectrally matched motions; and
- Validation per the ASCE 4-98 requirements.

6.2.2 Rotation of Original Motions to FN and FP Components

As mentioned earlier, the original recorded Duzce horizontal time histories were rotated to resolve the fault normal and fault parallel components. For the Duzce motion, the orientation of the strike of the fault is parallel to the DZC270 component. Since the remaining four sets of recordings were selected to represent ground motions associated with the intermediate to larger magnitude subduction earthquakes at larger distances and the directivity effects are insignificant for those recordings, the seed time histories were not rotated.

6.2.3 Time-Domain Spectral Matching

A time-domain spectral matching procedure was adopted for this project. Time-domain spectral matching adds finite wavelets in the time domain to decrease the spectral deficiencies between the seed motion and the target spectra. The result is a realistic looking time history that preserves the seed motion characteristics while generally achieving a close match with the target frequency spectra at all spectral ordinates.

The time-domain spectral matching was accomplished using the computer code RSPMATCH written by Abrahamson (2003), which generally follows the algorithm as set forth by Lilhanand and Tseng (1988). As stated above, this code calculates the spectral differences between a response spectrum and a target spectrum, and then adds wavelets in the time domain to alter the frequency content to reduce the differences.

The quality of the results is measured by the tolerance to which the matched motions converge toward the target spectrum, and how well the matched motions compare to the original motions in the time domain. In particular, the matched displacement and velocity time histories should look reasonable and reflect some of the predominant characteristics of the original motions.

6.2.4 Baseline Correction

A final baseline correction was necessary to remove any permanent offset imposed on the time history through the spectral matching procedure. This baseline correction was carried out by fitting an n^{th} order polynomial (where $n = 4$ to 10) to the displacement time history. The second derivative of this polynomial is then subtracted from the acceleration time history.

6.2.5 Validation per the ASCE 4-98 Requirements

Per the request of EMALL, the final spectrally matched motions were checked against the ASCE 4-98 criteria (in Section 2.3) for time histories. If the spectrally matched acceleration time history failed one criterion, then the matching was rejected and a new spectral match was performed. When all three components of a motion were matched, the cross-correlation coefficients between the time history components were calculated according to:

$$\text{Corr}(x,y) = [\sum (x-m_x)(y-m_y)/n]/(\sigma_x \sigma_y) \quad (6-1)$$

where x and y are the acceleration amplitudes for each of two components, m_x and m_y are their means (which are effectively zero), n is the number of time steps in each time history, the summation is done over all time steps, and σ_x and σ_y are the standard deviations of x and y . This calculation is made using the CORREL function within Excel. Two time histories are considered statistically independent when the absolute value of the correlation coefficient does not exceed 0.3, per ASCE 4-98.

6.3 Spectrally Matched Motions Per NFPA 59A 2006

The spectrally matched motions for OBE level per NFPA 59A 2006 are shown on [Plates 74 through 88](#), which includes plots showing the target spectrum, acceleration response spectra for the seed motion as well as the matched motion for 5% damping. Also shown are plots of the associated acceleration, velocity, and displacement time histories of the seed motions and matched motions. Similar set of results for SSE level per NFPA 59A 2006 are shown on [Plates 89 through 103](#) and [Plates 104 through 118](#) for the onshore and nearshore locations, respectively. Spectrally matched motions per NFPA 59A 2013 are presented in [Appendix D](#).

The significant duration (D_{5-95}) of the spectrally matched horizontal ground motions were compared to the deterministic estimates using empirical relationships (Abrahamson and Silva, 1996 and Bommer et al., 2009) on [Plates 119 through 121](#) for OBE and SSE levels per NFPA 59A 2006 for the onshore and nearshore locations, respectively. The empirical relationship proposed by Bommer et al. (2009) uses the PEER earthquake dataset which includes the 2002 Denali, 1999 Chi-Chi, and 1999 Turkey earthquakes. Abrahamson and Silva (1996) based on a seismic catalogue for shallow crustal motions up Northridge 1994 event, proposed two functional forms for significant duration, with a magnitude-dependent and magnitude-independent stress drop. The magnitude-dependent stress drop is used herein. Deterministic duration estimates were computed for the following three controlling scenarios (a) $M_w = 9.2$ at distance of 43.8 mi (70 km), (b) $M_w = 8.0$

at distance of 37.5 mi (60 km), and (c) $M_w = 7.2$ at distance of 6.2 mi (10 km). Overall, the range of significant duration of the matched motions is representative of the range corresponding to the earthquake scenarios controlling the ground motion hazard at the site. Furthermore, the average strong motion duration of the 10 spectrally matched ground motions (shown with the thick black dash line) compares well with the average of median estimates (shown with the solid yellow line).

[Appendix E](#) presents results in graphical form of: (i) the acceleration, velocity and displacement time histories, (ii) the normalized cumulative energy, (iii) the target and the calculated response spectra, (iv) the fourier amplitude spectrum, (v) the power spectra density function of each matched component of the motions and also presents the cross-correlation coefficients of the components of each motion. These results indicate that all requirements per ASCE 4-98 are met for the spectral matching at both OBE and SSE level per NFPA 59A 2006.

7.0 REFERENCES

- AEIC (Alaska Earthquake Information Center), 2013. AEIC Earthquake database search. AEIC Earthquake Database Search -The database contains earthquake locations from 01/1898 through 12/31/2015 (http://www.aeic.alaska.edu/html_docs/db2catalog.html, last accessed February, 2016)
- Abe, K., 1984, Magnitudes of large shallow earthquakes from 1904 to 1980: Physics of the Earth and Planetary Interiors, v. 27, p. 72–92.
- Abrahamson, N.A., 2000, Effects of Rupture Directivity on Probabilistic Seismic Hazard Analysis, Proc. Sixth International Conference on Seismic Zonation, Palm Springs, CA. November 12-15, 2000.
- Abrahamson, N.A., 2003, RSPMATCH Software.
- Abrahamson, N.A., 2013, HAZ43, Seismic Hazard Analysis Software.
- Abrahamson, N.A., and Silva, W.J., 1996, Empirical Ground Motion Models, Report prepared to Brookhaven National Laboratory.
- Abrahamson, N.A., Silva W.J., 1997, Empirical response spectral acceleration relations for shallow crustal earthquakes, Seismological Research Letters, Vol. 68, No. 1, pp 94-127.
- Abrahamson, N.A., Silva W.J., Kamai R. 2014, Summary of the ASK14 ground motion relation for active crustal regions, Earthquake Spectra, Vol 30, No 3, pp 1025-1055
- Abrahamson N.A., Gregor N., Addo K., 2015, BC Hydro Ground Motion Prediction Equations for Subduction Earthquakes, Earthquake Spectra, Preprint.
- American Society of Civil Engineers, 2000, ASCE Standard 4-98 – Seismic Analysis of Safety-related Nuclear Structures and Commentary, ASCE 4-98.
- American Society of Civil Engineers, 2006, ASCE Standard 7-05 – Minimum Design Loads for Buildings and Other Structures, ASCE 7-05
- American Society of Civil Engineers, 2010, ASCE Standard 7-10 – Minimum Design Loads for Buildings and Other Structures, ASCE 7-10.
- Alaska Oil and Gas Conservation Commission, 1994, 1994 Statistical report: 230 p.
- Allmendinger, R.W., 1998, Inverse and forward modeling of trishear fault-propagation folds: Tectonics, Vol. 17, p.640-656.
- ASCE 7-10 Supplement No.1, Minimum Design Loads for Building and Other Structures, Effective October 1, 2013, Chapter 21, pp. 13.
- Atkinson, G.M., and Boore, D.M., 2003, Empirical ground-motion relations for subduction zone earthquakes and their application to Cascadia and other regions: Bulletin of the Seismological Society of America, 93 (4), 1703–1729.

- Atkinson G., and Macias, M., 2009, Predicted ground motions for great interface earthquakes in the Cascadia subduction zone: *Bulletin of the Seismological Society of America*, 87, p. 97-113.
- BC Hydro, 2012, Dam Safety, Probabilistic seismic hazard analysis (PSHA) model, Volume 3: Ground motion characterization (GMC) model, Report No E658, Vol 3, November 2012.
- Berger, A. L., and Spotila, J. A., 2008, Denudation and deformation in a glaciated orogenic wedge: the St. Elias orogen, Alaska: *Geology* 36, p. 523–526.
- Berger, A. L., Spotila, J. A., Chapman, J., Pavlis, T. L., Enkelmann, F., and Buscher, J. T., 2008, Architecture, kinematics, and exhumation of a convergent orogenic wedge: a thermochronological investigation of tectonic-climatic interactions within the central St. Elias orogen, Alaska: *Earth Planet. Sci. Lett.* 270, p. 13–24.
- Bommer, J.J., Stafford, P.J., and Alarcon, J.E., 2009, Empirical Equations for the Prediction of Significant, Bracketed, and Uniform Duration of Earthquake Ground Motion," *Bulletin of the Seismological Society of America*, Vol 99, No. 6, pp. 3217-3233.
- Boore D.M., Joyner W., Fumal T., 1997, Equations for estimating horizontal response spectra and peak acceleration from Western North American earthquakes – a summary of recent work, *Seismological Research Letters*, Vol. 68, No. 1, pp 128-153.
- Boore D.M., Stewart J.P., Seyhan E., Atkinson G.M., 2014, NGA-West 2 Equations for Predicting PGA, PGV, and 5%-Damped PSA for Shallow Crustal Earthquakes, *Earthquake Spectra*, Vol 30, No 3, pp 1057-1085.
- Boss, R.F., Lennon, R.B., and Wilson B.W., 1976, Middle Ground Shoal oil field, Alaska, in Braunstein, J., ed., *North American oil and gas fields: American Association of Petroleum Geologists Memoir* 24, p. 1–22.
- Bozorgnia Y., Abrahamson N.A., Al Atik L., Ancheta T.D., Atkinson G.M., Baker J.W., Baltay A., Boore D.M., Campbell K.W., Chiou B.S.J., Darragh R., Day S., Donahue J., Graves R.W., Gregor N., Hanks T., Idriss I.M., Kamai R., Kishida T., Kottke A., Mahin S.A., Rezaeian S., Rowshandel B., Seyhan E., Shahi S., Shantz T., Silva W., Spudich P., Stewart J.P., Watson-Lamprey J., Wooddell K., Youngs R., 2014, "NGA-West2 Research Project", *Earthquake Spectra*, Vol 30, No 3, pp 973-987.
- Bradley, D.C., Kusky, T.M., Haeussler, P.J., Karl, S.M., and Donley, D.T., 1999, *Geology of the Seldovia quadrangle: US Geological Survey Open-File Report* 99-18, scale 1:250,000.
- Brandenburg, S.,J., Bellana, N., and Shantz, T., 2010, Shear Wave Velocity as a Statistical Function of Standard Penetration Test Resistance and Vertical Effective Stress at Caltrans Bridge Sites, Report No: PEER2010/03, Pacific Earthquake Engineering Research Center.
- Brocher, T.M., Fuis, G.S., Fisher, M.A., Plafker, G., Moses, J.M., Taber, J.J., and Christensen, N.I., 1994, Mapping the megathrust beneath the northern Gulf of Alaska using wide-angle seismic data: *J. Geophys. Res.*, 99(B6), p. 11,663–11,685.

- Bruhn, R.L., and Haeussler, P.J., 2006, Deformation driven by subduction and microplate collision: Geodynamics of Cook Inlet Basin, Alaska. *Geol. Soc. Amer. Bulletin*, v. 118, no. 3/4, p. 289-303.
- Bruns, T.R., 1983, Model for the origin of the Yakutat block, an accreting terrane in the northern Gulf of Alaska: *Geology*, v. 11, p. 718-721.
- Bucknam, R.C., and Hemphill-Haley, E., and Leopold, E.B., 1992, Abrupt uplift within the last 1,700 years at southern Puget Sound, Washington: *Science*, v. 258, p. 1611–1614.
- Calderwood, K.W., and Fackler, W.C., 1972, Proposed Stratigraphic Nomenclature for the Kenai Group, Cook Inlet Basin, Alaska: *A.A.P.G. Bull.*, v. 56, no. 4, April 1972.
- Campbell K.W., Bozorgnia Y., 2003, Updated nearsource ground-motion (attenuation) relations for the horizontal and vertical components of peak ground acceleration and acceleration response spectra, *Bulletin of the Seismological Society of America*, Vol 95, No 5, pp 314-331.
- Campbell K.W., Bozorgnia Y., 2014, NGA-West2 Ground Motion Model for the Average Horizontal Components of PGA, PGV, and 5% Damped Linear Acceleration Response Spectra, *Earthquake Spectra*, Vol 30, No 3, pp 1087-1115.
- Carver, G.A. and Plafker, G., 2008, Paleoseismicity and neotectonics of the Aleutian Subduction Zone - An overview, in Freymueller, J.T., Haeussler, P.J., Wesson, R.L., and Ekstrom, Goran, eds., 2008, *Active tectonics and seismic potential of Alaska: American Geophysical Union, Geophysical Monograph 179*, p. 83–108.
- Cedric, T., C. Ji, and R. Archuleta, 2014, The Rupture Process of the 2014 Rat Island Intermediate-Depth Earthquake with Relation to the Geodynamical Context of the Western Aleutian Arc, abstract submitted to Fall 2014 Meeting, American Geophysical Union.
- Chiou, B.S.J. and Youngs, R.R., 2014, Update of the Chiou and Youngs NGA Model for the Average Horizontal Component of Peak Ground Motion and Response Spectra, *Earthquake Spectra*, Vol 30, No 3, pp 1117-1153.
- Christensen and Beck, 1994, The rupture process and tectonic implications of the great 1964 Prince William Sound earthquake: *Pure & Applied Geophysics PAGEOPH* p.12
- Cornell, C.A., 1968, Engineering seismic risk analysis: *Bulletin of the Seismological Society of America*, Vol 58, No. 5, p. 1583-1606.
- Consortium of Organizations for Strong-Motion Observations Systems (COSMOS) Virtual Data Center website (<http://strongmotioncenter.org/vdc/scripts/default.plx>), last accessed on February, 2016)
- Cramer, C. H., M. D. Petersen, T. Cao, T. R. Topozada, and M. S. Reichle, 2000, A time-dependent probabilistic seismic-hazard model for California. *Bulletin of the Seismological Society of America* 90, 1–21.

- Crone, A.J., Personius, S.F., Craw, P.A., Haeussler, P.J., and Staff, L.A., 2004, The Susitna Glacier thrust fault — Characteristics of surface ruptures on the fault that initiated the 2002 Denali Fault earthquake: *Bulletin of the Seismological Society of America*, v. 94, no. 6, part B, p. 5–22.
- Csejtey, Béla, Jr., Cox, D.P., Evarts, R.C., Stricker, G.D., and Foster, H.L., 1982, The Cenozoic Denali fault system and the Cretaceous accretionary development of southern Alaska, *Journal of Geophysical Research*, v. 87, no. B5, p. 3741–3754.
- Detterman, R.L., Plafker, G., Hudson, T., Tysdal, R.G., and Pavoni, N., 1974, Surface geology and Holocene breaks along the Susitna segment of the Castle Mountain fault, Alaska: US Geological Survey Miscellaneous Field Studies Map MF-618, 1 sheet, scale 1:63,360.
- Detterman, R.L., Hudson, T., Plafker, G., Tysdal, R.G., and Hoare, J.M., 1976, Reconnaissance geologic map along Bruin Bay and Lake Clark Faults in Kenai and Tyonek quadrangles, Alaska: U.S. Geological Survey Open-File Map 76-477, 4 p., scale 1:250,000, 2 sheets.
- Eberhart-Phillips, D., Haeussler, P.J., Freymueller, J.T., Frankel, A.D., Rubin, C.M., Craw, P., Ratchkovski, N.A., Anderson, G., Carver, G.A., Crone, A.J., Dawson, T.E., Fletcher, H., Hansen, R., Harp, E.L., Harris, R.A., Hill, D.P., Hreinsdóttir, S., Jibson, R.W., Jones, L.M., Kayen, R., Keefer, D.K., Larsen, C.F., Moran, S.C., Personius, S.F., Plafker, G., Sherrod, B., Sieh, K., N., and Wallace, W. K., 2003, The 2002 Denali fault earthquake, Alaska: A large magnitude, slip-partitioned event: *Science*, 300(5622), pp. 1113-1118.
- Elliott, J. L., C. F. Larsen, J. T. Freymueller, and R. J. Motyka, 2010, Tectonic block motion and glacial isostatic adjustment in southeast Alaska and adjacent Canada constrained by GPS measurements, *J. Geophys. Res.*, 115, B09407.
- Fisher, M.A., Detterman, R.L., and Magoon, L.B., 1987, Tectonics and petroleum geology of the Cook-Shelikof basin, southern Alaska in Scholl, D.W., et al., eds., *Geology and resource potential of the continental margin of western North America and adjacent ocean basins, Beaufort Sea to Baja California*: Houston, Texas, Circum-Pacific Council for Energy and Mineral Resources Earth Science Series, v. 6, p. 213-228.
- Fisher, M. A., and Magoon, L. B., 1978, Geologic framework of lower Cook Inlet, Alaska: *The American Association of Petroleum Geologists Bulletin*, v. 62, no. 3, pp. 373-402.
- Fletcher, H.J., and Freymueller, J.T., 1999, New GPS constraints on the motion of the Yakutat terrane: *Geophys. Res. Lett.* 26, p. 3029–3032.
- Fletcher, H.J., and Freymueller, J.T., 2003, New constraints on the motion of the Fairweather fault, Alaska, from GPS observations: *Geol. Res. Lett.* 30, p. 3.
- Flores, C.F., and Doser, D.I., 2005, Shallow Seismicity of the Anchorage, Alaska, Region (1964 – 1999), *Bulletin of the Seismological Society of America*, Vol. 95, No. 5, pp. 1865-1879.
- Frankel, A. D., 1995, Mapping seismic hazard in the Central and Eastern United States: *Seismological Research Letters*, v. 66, no. 4, p. 8–21.

- Frankel, A. D., Mueller, C., Barnhard, T., Perkins, D., Leyendecker, E., Dickman, N., Hanson, S., and Hopper, M., 1996, National seismic-hazard maps, Documentation June 1996: US Geological Survey Open-File Report 96-532, 110 pages.
- Frankel, A. D., Petersen, M.D., Mueller, C.S., Haller, K.M., Wheeler, R.L., Leyendecker, E.V., Wesson, R.L., Harmsen, S.C., Cramer, C.H., Perkins, D.M., and Rukstales, K.S., 2002, Documentation for the 2002 update of the National Seismic Hazard Maps: U.S. Geological Survey Open-File Report 2002-420.
- Frankforter, M.J., and Waugaman, J.C., 2013, The Granite Point field, Cook Inlet, Alaska in Stone, D.M., and Hite, D.M., eds, Oil and Gas Fields of the Cook Inlet Basin, Alaska: AAPG Memoir 104, p. 263-290.
- Freymueller, J.T., Woodard, H., Cohen, S.C., Cross, R., Elliott, J., Larsen, C.F., Hreinsdottir, S., and Zweck, C., 2013, Active deformation processes in Alaska, based on 15 years of GPS measurements, *in* J.T. Freymueller, P.J. Haeussler, R.L. Wesson, and G. Ekstrom (eds.): Active Tectonics and Seismic Potential of Alaska, Geophysical Monograph Series, Vol. 179, 431 p.
- Fuchs, W.A., 1980, Tertiary tectonic history of the Castle Mountain–Caribou fault system in the Talkeetna Mountains, Alaska: Salt Lake City, University of Utah, Department of Geology and Geophysics, Ph.D. dissertation, 150 p.
- Fugro Consultants, Inc. (Fugro), 2015a, LNG Facilities Seismic Engineering Report, LNG facilities, Alaska LNG Project, Nikiski, Alaska, Report No. 04.10140334-13
- Fugro Consultants, Inc. (Fugro), 2015b, Pre-FEED Probabilistic Seismic Hazard Analysis Report, Onshore LNG facilities, Alaska LNG Project, Nikiski, Alaska, Rev B, Report No. 04.10140094-6.
- Fugro Consultants, Inc. (Fugro), 2015c, LNG Facilities Onshore Integrated Site Characterization and Geotechnical Engineering Report, Onshore LNG facilities, Alaska LNG Project, Nikiski, Alaska, Report No. 04.10140334-14.
- Fugro Consultants, Inc. (Fugro), 2015d, Study of the Beluga and SRS Anticlines, Upper Cook Inlet, Alaska, Alaska LNG Project, Report No. 04.79150016.
- Fugro Consultants, Inc. (Fugro), 2015e, LNG Facilities Onshore Geophysical Survey Report, Onshore LNG facilities, Alaska LNG Project, Nikiski, Alaska, Rev A, Report No. 04.10140334-7.
- Fugro Consultants, Inc. (Fugro), 2015f, Geotechnical Data Report, Onshore LNG facilities, Alaska LNG Project, Nikiski, Alaska, Report No. 04.10140094-8.
- Fugro Consultants, Inc. (Fugro), 2015g, LNG Facilities Onshore Geotechnical Data Report, Onshore LNG facilities, Alaska LNG Project, Nikiski, Alaska, Report No. 04.10140334-8.
- Fugro Consultants, Inc. (Fugro), 2015h, LNG Facilities Marine Geotechnical Data Report, Marine LNG facilities, Alaska LNG Project, Nikiski, Alaska, Report No. 04.10140334-9.

- Fugro-McClelland Marine Geosciences, Inc. (FMMG), 2012a, Geologic Study Potential LNG plant sites, south central Alaska, Report No. 0201-7173-2, prepared for Conoco-Phillips, Inc.
- Fugro-McClelland Marine Geosciences, Inc. (FMMG), 2012b, Geologic hazard study, tsunami and surface deformation assessment of potential LNG plant sites, south central Alaska, Addendum to Report No: 0201-7173-2, prepared for Conoco-Phillips, Inc.
- Gardner, J.K., and Knopoff, L., 1974, Is the sequence of earthquakes in southern California, with aftershocks removed, Poissonian?: *Bulletin of the Seismological Society of America*, v. 64, no. 5, p. 1363–1367.
- Glen, J.M.G., Schmidt, J., and Morin, R., 2007b, Gravity and magnetic character of south-central Alaska: Constraints on geologic and tectonic interpretations, and implications for mineral exploration, in Ridgway, K.D., Trop, J.M., Glen, J.M.G., and O'Neill, J.M., eds., *Tectonic Growth of a Collisional Continental Margin: Crustal Evolution of Southern Alaska*: Geological Society of America Special Paper 431, p. 593–622.
- Gülerce, Z. and Abrahamson, N.A., 2011, Site-Specific Design Spectra for Vertical Ground Motion, *Earthquake Spectra*, Vol. 27, No. 4, pp. 1023-1047.
- Haeussler, P.J., 1998, Surficial geologic map along the Castle Mountain fault between Houston and Hatcher Pass Road, Alaska: US Geological Survey Open-File Report OF-98-480, scale 1:25,000, 1 sheet.
- Haeussler, P. J., Bruhn, R.L. and Pratt, T.L., 2000, Potential seismic hazards and tectonics of upper Cook Inlet basin, Alaska, based on analysis of Pliocene and younger deformation, *Geol. Soc. Am. Bull.*, 112, p 1414-1429.
- Haeussler, P. J., Best, T.C., and Waythomas, C.F., 2002, Paleoseismology at high latitudes: Seismic disturbance of late Quaternary deposits along the Castle Mountain fault near Houston, Alaska, *Geol. Soc. Am. Bull.*, 114, 1296-1310, 1 plate.
- Haeussler, P.J., and Saltus, R.W., 2004, 26 km of offset on the Lake Clark fault since late Eocene time. U.S. Geological Survey Professional Paper 1709-A, p. 1-4.
- Haeussler, P.J., 2008, An overview of the neotectonics of interior Alaska—Far-field deformation from the Yakutat Microplate collision, in Freymueller, J.T., Haeussler, P.J., Wesson, R.L., and Ekstrom, Goran, eds., 2008, *Active tectonics and seismic potential of Alaska*: American Geophysical Union, Geophysical Monograph 179, p. 83–108.
- Haeussler, P.J., and Saltus, R.W., 2011, Location and Extent of Tertiary Structures in Cook Inlet Basin, Alaska, and Mantle Dynamics that Focus Deformation and Subsidence: USGS Professional Paper 1776-D, 26 p.
- Haeussler, P. J. , Schwartz, D.P., Dawson, T.E., Stenner, H.D., Lienkaemper, J.J., Sherrod, B., Cinti, F.R., Montone, P., Craw, P.A., Crone A.J., and Personius, S.F., 2004, Surface rupture and slip distribution of the Denali and Totschunda faults in the 3 November 2002 ML 7.9 earthquake, Alaska, *Bull. Seismol. Soc. Am.*, 94(6B), S23-S52.

- Hamilton, S. & Shennan, I., 2005, Late Holocene relative sea-level changes and the earthquake deformation cycle around upper Cook Inlet, Alaska. *Quaternary Science Reviews*. 2005;24:1479-1498.
- Hamilton, S., Shennan, I., Combellick, R., Mulholland, J. and Noble, C. 2005. Evidence for two great earthquakes at Anchorage, Alaska and implications for multiple great earthquakes through the Holocene. *Quaternary Science Reviews*, 24: 2050-2068.
- Hartman, D.C., Pessel, G.H., McGee, D.L., 1972, Kenai Group of Cook Inlet Basin, Alaska: State of Alaska Department of Natural Resources, Division of Geological and Geophysical Surveys, Energy Resources Section, Alaska Open File Report 349, 5 p.
- Hartman, D. C., G. H. Pessel, and D. L. McGee, 1974. Stratigraphy of the Kenai group, Cook Inlet, Alaska Div. Geol. Geophys. Surv. Open-File Rept. 49.
- Idriss I. M., 2014, An NGA-West2 Empirical Model for Estimating the Horizontal Spectral Values Generated by Shallow Crustal Earthquakes, *Earthquake Spectra*, Vol. 30, No. 3, pp. 1155-1177
- International Code Council, Inc., 2012, 2012 International Building Code (IBC)
- Johnson, S.Y., Potter, C.J., Armentrout, J.M., Miller, J.J., Finn, C., and Weaver, C.S., 1996, The southern Whidbey Island fault: An active structure in the Puget Lowland, Washington, *Geological Society of America Bulletin*, v. 108, p. 334-354.
- Karlstrom, T.N.V., 1964, Quaternary geology of the Kenai Lowland and Glacial history of the Cook Inlet region, Alaska: US Geological Survey Professional Paper 443, 69, p., 7 plates, various scales.
- Kelly, T.E., 1961, Photogeology—A quick, economical tool for oil hunters: *Oil and Gas Journal*, November 20, p. 265–272.
- Kelly, T.E., 1963, Geology and hydrocarbons in Cook Inlet basin, Alaska, in Childs, O.E., and Beebe, W.B., eds., *Backbone of the Americas: American Association of Petroleum Geologists Memoir 2*, p. 278–296.
- Kirschner, C.E., and Lyon, C.A., 1973, Stratigraphic and tectonic development of Cook Inlet petroleum province, in Pitcher, M.G., ed., *Arctic geology: American Association of Petroleum Geologists Memoir 19*, p. 396-407.
- Koehler, R.D. and Reger, R.D., 2011, Reconnaissance Evaluation of the Lake Clark Fault, Tyonek Area, Alaska, Division of Geological & Geophysical Surveys Preliminary Interpretive Report 2011-1.
- Koehler, R.D., Farrell, RE., Burns, P.A.C., and Combellick, R.A., 2012a, Quaternary faults and fold in Alaska: A digital database: Alaska Division of Geological & Geophysical Surveys Miscellaneous Publication 141, 31p., 1 sheet, scale 1:3,700,000.

- Koehler, R.D., Reger, R.D., and Frohman, R., 2012b, The Castle Mountain fault, south-central Alaska: New lidar-based observations on the sense of slip, Poster S53D-2530: Presented at the American Geophysical Union (AGU) annual meeting, December 3-7, 2012, San Francisco, CA.
- Lahr, J.C., Stephens, C.D., Hasegawa, H.S., Boatwright, John, and Plafker, George, 1980, Alaska seismic gap only partially filled by February 28, 1979 earthquake: *Science*, v. 207, p. 1351-1353.
- Lilhanand, K., and Tseng, W.S., 1988, "Development and Application of Realistic Earthquake Time Histories Compatible with Multiple Damping Response Spectra", 9th World Conf. Earthquake Engineering, Tokyo, Japan, Vol. II, p. 819-824.
- Luco, N., B.R. Ellingwood, R.O. Hamburger, J.D. Hooper, J.K. Kimball & C.A. Kircher, 2007, "Risk-Targeted versus Current Seismic Design Maps for the Conterminous United States," Proceedings of the 2007 Structural Engineers Association of California Convention, Lake Tahoe, CA, pp. 163-175.
- Magoon, L.B., Adkinson, W.L., and Egbert, R.M., 1976, Map showing geology, wildcat wells, Tertiary plant fossil localities, K-Ar age dates, and petroleum operations, Cook Inlet area, Alaska: US Geological Survey Miscellaneous Investigations Series Map I-1019, scale 1:250 000.
- Matthews, M. V., W. L. Ellsworth, and P. A. Reasenber, 2002, A Brownian Model for Recurrent Earthquakes. *Bulletin of the Seismological Society of America*, 92, 2233-2250.
- Matmon, A., Schwartz, D.P., Haeussler, P.J., Finkel, R., Lienkaemper, J.J., Stenner, H.D., and Dawson, T.E., 2006, Denali fault slip rates and Holocene-late Pleistocene kinematics of central Alaska: *Geology*, v. 34, p. 645-648.
- Meigs, A., and Sauber, J., 2000, Southern Alaska as an example of the long-term consequences of mountain building under the influence of glaciers: *Quat. Sci. Rev.* 19, p. 1543-1562.
- Mériaux, A.S, Sieh, K, Finkel, R.C., Rubin, C.M., Taylor, M.H., Meltzner, A.J., and Ryerson, F.J., 2009, Kinematic behavior of southern Alaska constrained by westward decreasing postglacial slip rates on the Denali Fault, Alaska: *Journal of Geophysical Research*, v. 114, B03404.
- Montgomery, D. R., 2002, Valley formation by fluvial and glacial erosion: *Geology* 30, p. 65.
- National Fire Protection Association (NFPA), 2006, Standard for the production, storage, and handling of liquefied natural gas (LNG), NFPA 59A, 2006 Edition.
- National Fire Protection Association (NFPA), 2013, Standard for the production, storage, and handling of liquefied natural gas (LNG), NFPA 59A.
- National Geophysical Data Center (NGDC), 2012, Record of significant earthquake: http://www.ngdc.noaa.gov/nndc/struts/results?eq_0=2964&t=101650&s=13&d=22,26,13,12&nd=display, last accessed February, 2016.

- (NEHRP), Recommended Provisions for Seismic Regulations for New Buildings and Other Structures (FEMA 450), 2003 Edition
- Nelson, S.W., Dumoulin, J.A., and Miller, M.L., 1985, Geologic map of the Chugach National Forest: US Geological Survey Miscellaneous Field Studies Map MF-1645B, scale 1:250,000.
- Network for Earthquake Engineering Simulation at the University of California, Santa Barbara. Data repository available online at <http://www.nees.ucsb.edu/> (last accessed February, 2016)
- Nishenko, S. P and Jacob, K. H., 1990, Seismic Potential of the Queen-Charlotte-Alaska-Aleutian Seismic Zone, *Journal of Geophysical Research-Solid Earth and Planets*, Volume 95, Issue B3, p.2511-2532.
- Nokleberg, W. J., Jones, D.L., and Silberling, N.J., 1985, Origin and tectonic evolution of the Maclaren and Wrangellia terranes, eastern Alaska Range: *Alaska*, *Geol. Soc. Am. Bull.*, 96, p. 1251-1270.
- Pacific Earthquake Engineering Research (PEER) Center NGA motion database website (<http://ngawest2.berkeley.edu/>), last accessed on February, 2016
- Page, R.A., Biswas, N.N., Lahr, J.C., Pulpan, H., 1991, Seismicity of continental Alaska, in Slemmons, D.B., Engdahl, E.R., Zoback, M.R., and Blackwell, D.D., eds., *Neotectonics of North America: Boulder, Colorado, Geological Society of America, Decade Map Volume 1*, p. 47-68.
- Perry, S.E., Garver, J.I., and Ridgway, K.D., 2009, Transport of the Yakutat terrane, Southern Alaska: evidence from sediment petrology and detrital zircon fission-track and U/Pb double dating: *Journal of Geology*, v. 117, p. 156-173.
- Petersen, M. D., C. H. Cramer, and A. D. Frankel, 2002, Simulations of seismic hazard for the Pacific Northwest of the United States from earthquakes associated with the Cascadia subduction zone. *Pure and Applied Geophysics* 159, 2,147–2,168.
- Petersen, M.D., Moschetti, M.P., Powers, P.M., Mueller, C.S., Haller, K.M., Frankel, A.D., Zeng, Yuehua, Rezaeian, Sanaz, Harmsen, S.C., Boyd, O.S., Field, Ned, Chen, Rui, Rukstales, K.S., Luco, Nico, Wheeler, R.L., Williams, R.A., and Olsen, A.H., 2014, "Documentation for the 2014 update of the United States national seismic hazard maps: U.S. Geological Survey Open-File Report 2014–1091", 243 p., <http://dx.doi.org/10.3133/ofr20141091>
- Plafker, George, 1967, Surface faults on Montague Island associated with the 1964 Alaska earthquake: *US Geological Survey Professional Paper* 543-G, 43 p.
- Plafker, G., Detterman, R.L., and Hudson, T., 1975, New data on the displacement history of the Lake Clark fault, in Yount, M.E. ed., *United States Geological Survey Alaska Program, 1975. U.S. Geological Survey Circular* 722, p 44-45.
- Plafker, G., 1987, Regional geology and petroleum potential of the northern Gulf of Alaska continental margin in Scholl, D. W., Grantz, A., and Vedder, J. G., eds., 1987, *Geology and*

- resource potential of the continental margin of western North America and adjacent ocean basins: Beaufort Sea to Baja California: Earth Science Series, Houston, Circum-Pacific Council for Energy and Mineral Resources, p. 229–268.
- Plafker, G., Moore, J.C., and Winkler, G.R., 1994a, Geology of the southern Alaska margin, in Plafker, G., and Berg, H.C., eds., The geology of Alaska: Boulder, Colorado, Geological Society of America, v. G-1, p. 389-449.
- Plafker, G., Gilpin, L. M., and Lahr, J.C., 1994b, Neotectonic map of Alaska, in Plafker, G., and Berg, H.C., eds., The geology of Alaska: Boulder, Colorado, Geological Society of America, v. G-1, plate 122, scale 1:2 500 000.
- Power, M., Chiou, B., Abrahamson, N., Bozorgnia, Y., Shantz, T., Roblee, C., 2008, An Overview of the NGA Project, Earthquake Spectra, Vol. 24, No. 1, pp. 3-21.
- Ratchkovski, N.A., Pujol, J., and Biswas, N.N., 1998, Relocation of shallow earthquakes in southern Alaska using Joint Hypocenter Determination method: Journal of Seismology 2, p. 87-102.
- Ratchkovski, N., and Hansen, R., 2002, New evidence for segmentation of the Alaska subduction zone: Bulletin of the Seismological Society of America, 92, p. 1754-1765.
- Reed, B. L., and Lanphere, M.A., 1974, Offset plutons and history of movement along the McKinley segment of the Denali fault system: Alaska, Geol. Soc. Am. Bull., 85, p. 1883-1892.
- Ridgway, K. D., Trop, J.M., Nokleberg, W.J., Davidson, C.M., and Eastham, K.R., 2002, Mesozoic and Cenozoic tectonics of the eastern and central Alaska Range: Progressive basin development and deformation in a suture zone: Geol. Soc. Am. Bull., 114, 1480-1504.
- Sadigh K., Chang C., Egan J., Makdisi F., Youngs R., 1997, Attenuation relationships for shallow crustal earthquakes based on California strong motion data, Seismological Research Letters, Vol. 68, No. 1, pp 180-189.
- Saltus, R.W., Haeussler, P.J., Bracken, R.E., Doucette, J.P., and Jachens, R.C., 2001, Anchorage urban region aeromagnetics (AURA) project—preliminary geophysical results: U.S. Geological Survey Open-File Report 01-0085, 23 p.
- Schmoll, H.R., and Yehle, L.A., 1987, Surficial geologic map of the northwestern quarter of the Tyonek A-4 quadrangle, south-central Alaska. U.S. Geological Survey Miscellaneous Field Studies Map MF-1934, scale 1:31,680.
- Shellenbaum, D.P., Gregersen L.S., and Delaney, P.R., 2010, Top Mesozoic unconformity depth map of the Cook Inlet Basin, Alaska, Alaska Division of Geological and Geophysical Surveys, Report of Investigations 2010-2, Sheet 1 of 1.
- Shennan, I. & Hamilton, S., 2006, Coseismic and pre-seismic subsidence associated with great earthquakes in Alaska. Quaternary Science Reviews, 25:1-8

- Shennan, I., Barlow, N., Carver, G., Davies, F., Garret, E., and Hocking E., 2014, Great tsunamigenic earthquakes during the past 1000 yr on the Alaska megathrust, *Geology*, v. 42, no. 8, p.687-690.
- Sipkin, S.A., 2003, A correction to body-wave magnitude mb based on moment magnitude Mw: *Seismological Research Letters*, v. 74, p. 739–742.
- Somerville, P.G., Smith, N.F., and Graves, R.W., 1997, Modifications of Empirical Strong Ground Motion Attenuation Relations to Include the Amplification and Duration Effects of Rupture Directivity, *Seismological Research Letters*, Vol. 68, No. 1.
- Spotila, J. A., Buscher, J. T., Meigs, A. J., and Reiners, P.W., 2004, Long-term glacial erosion of active mountain belts: example of the Chugach–St. Elias Range, Alaska: *Geology* 32, p. 501–504.
- Spudich P., Bayless J.R., Baker J.W., Chiou B.S.J., Rowshandel B., Shahi S.K., Somerville P., 2013, “Final Report of the NGA-West2 Directivity Working Group”, PEER Report 2013/09, May 2013.
- Stephens, C.D., Page, R.A., Lahr, J.C., and Fogleman, K.A., 1995, Crustal seismicity in the Anchorage region of Alaska: *Geological Society of America Abstracts with Programs*, v. 27, no. 5, p. 78–79.
- Stover, C.W., and Coffman, J.L., 1993, *Seismicity of the United States, 1568-1989 (Revised): US Geological Survey Professional Paper 1527*, 415 p.
- Sugiyama, Y., 1995, Geological background of the 1995 Hyogo–Ken Nambu (Kobe) earthquake: *Eos (Transactions, American Geophysical Union)*, v. 76, p. F371.
- Suppe, J., and Medwedeff, D. A., 1990, Geometry and kinematics of fault-propagation folding: *Ecolgae Geol. Helv.*, v. 83, no. 3, p. 409-454.
- Thomas, P., Wong, I., Abrahamson, N. 2010, “Verification of Probabilistic Seismic Hazard Analysis Computer Programs”, Pacific Earthquake Engineering Research Center, PEER Report 2010/106, College of Engineering, University of California, Berkeley, May 2010.
- Tysdal, R.G., and Case, J.E., 1979, Geologic map of the Seward and Blying Sound quadrangles, Alaska: US Geological Survey Miscellaneous Investigations Series Map I-1150, scale 1:250,000.
- U.S. Geological Survey (USGS), 1989, *The Severity of an Earthquake*: U. S. Government Printing Office, 1989-288-913.
- U.S. Geological Survey (USGS), 1999, National Elevation Dataset (30 meters), EROS Data Center.
- U.S. Geological Survey (USGS), 2008, National Elevation Dataset, 1/9 arc second (2.5 meters), LiDAR derived digital elevation model, EROS Data Center, Data obtained Sept 2014 from USGS.

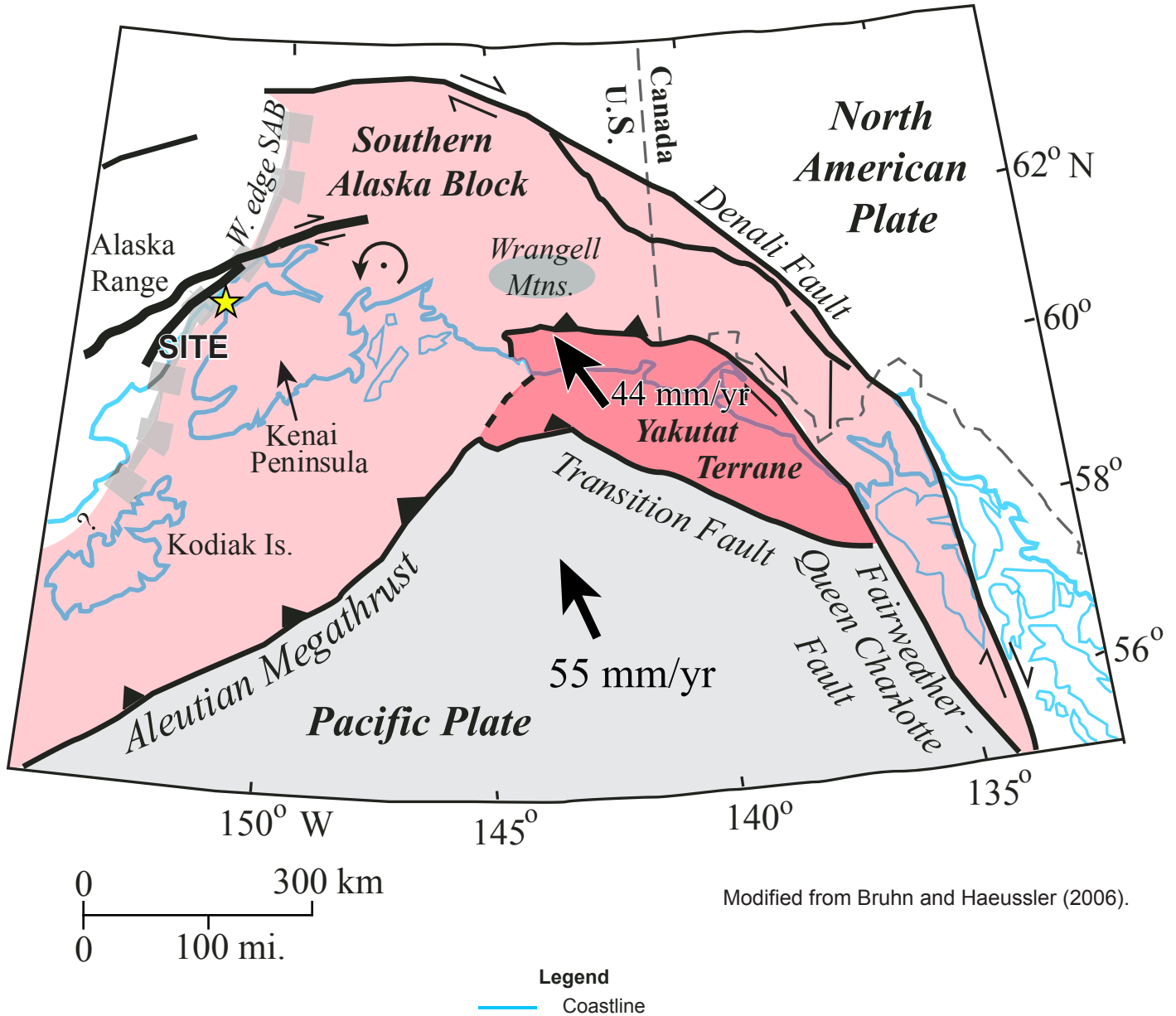
- U.S. Geological Survey (USGS), 2011, Denali M 7.9 Community Internet Intensity Map: <http://earthquake.usgs.gov/earthquakes/dyfi/events/ak/22614036/us/index.html>, last accessed February, 2016.
- Utsu, T., 2002, Relationships between magnitude scales, in Lee, W.H.K, Kanamori, H., Jennings, P.C., and Kisslinger, C., editors, International Handbook of Earthquake and Engineering Seismology: Academic Press, a division of Elsevier, two volumes, International Geophysics, v. 81-A, p. 733–746.
- Wair, B., DeJong, J., and Shantz, T., 2012, Guidelines for Estimation of Shear Wave Velocity Profiles, Report No: PEER2012/08, Pacific Earthquake Engineering Research Center.
- Weichert, D.H., 1980, Estimation of earthquake recurrence parameters for unequal observation periods for different magnitudes: Bulletin of the Seismological Society of America, v. 70, p. 1337–1356.
- Wesnousky, S.G., and Scholz, C.H., 1982, Deformation of an island arc: Rates of moment release and crustal shortening in intraplate Japan determined from seismicity and Quaternary fault data: Journal of Geophysical Research, v. 87, p. 6829–6852.
- Wells, D.L., and Coppersmith, K.J., 1994, Analysis of empirical relationships among magnitude, rupture length, rupture area, and surface displacement: Bulletin of the Seismological Society of America, v. 84, p. 974-1002.
- Wesson, R. L., Boyd, O. S., Mueller, C. S., Bufe, C. G., Frankel, A. D., Petersen, M. D., 2007, Revision of time-Independent probabilistic seismic hazard maps for Alaska: US Geological Survey Open-File Report 2007-1043.
- Wesson, R.L., Frankel, A.D., Mueller, C.S., and Harmsen, S., 1999a, Probabilistic seismic hazard maps of Alaska: US Geological Survey Open-File Report 99–36.
- Wesson, R.L., Frankel, A.D., Mueller, C.S., and Harmsen, S., 1999b, Probabilistic seismic hazard maps of Alaska: US Geological Survey Miscellaneous Investigations Series I–2679.
- Willis, J. B., Haeussler, P.J., Bruhn, R.L., and Willis, G.C., 2007, Holocene slip rate for the western segment of the Castle Mountain fault, Alaska, Bull. Seismol. Soc. Am., 97(3), 1019-1024.
- Wilson, F.H., Detterman, R.L., and DuBois, Gregory, 1999, Digital data for the geologic framework of the Alaska Peninsula, southwest Alaska, and the Alaska Peninsula terrane: US Geological Survey Open-File Report 99-317
- Wilson, F.H., Hults, C.P., Shew, N., and Labay, K.A., compilers, 2008, Digital data for Geology of the Prince William Sound and Kenai Peninsula region, Alaska – Including the Kenai, Seldovia, Seward, Blying Sound, Cordova, and Middleton Island 1:250,000-scale quadrangles: US Geological Survey Open-File Report 2008-1002 DRAFT, 48 p., 1 plate.
- Winkler, G.R., and Plafker, George, 1981, Geologic map and cross sections of the Cordova and Middleton Island quadrangles, southern Alaska: US Geological Survey Open-file Report 81-1164, scale 1:250,000.

- Winkler, G.R., and Plafker, George, 1993, Geologic map of the Cordova and Middleton Island quadrangles, southern Alaska: US Geological Survey Miscellaneous Investigations Map I-1984, scale 1:250,000.
- Wong, I., Dawson, T., Dober, M., Russon, L., Knudsen, K., Terra, F., 2008, Site-specific probabilistic and deterministic seismic hazard analyses and development of earthquake ground motions for the Port of Anchorage expansion project, Alaska: prepared for Terracon Consultants, Inc. by URS Corporation, Seismic Hazards Group.
- Yegian, M.K., 1979, Probabilistic Seismic Hazard Analysis: Report 13 of the Miscellaneous Paper S-73-1 series: State-of-the-art for assessing earthquake hazards in the United States, Vicksburg, US Army Corps of Engineers, Waterways Experiment Station.
- Youngs R., Chiou S., Silva W., Humphrey J., 1997, Strong ground-motion attenuation relationships for subduction zone earthquakes, *Seismological Research Letters*, Vol. 68, No. 1, pp 58-73.
- Zhao J.X., Zhang, J., Asano, A., Ohno, Y., Oouchi, T., Takahashi, T., Ogawa, H., Irikura, K., Thio, H., Somerville, P., Fukushima, Y., and Fukushima, Y., 2006, Attenuation relations of strong ground motion in Japan using site classification based on predominant period: *Bulletin of the Seismological Society of America*, v. 96, p. 898–913.
- Zimmerman and Prescott, 2014, AFSC/RACE: Cook Inlet Grid, National Oceanic and Atmosphere Administration (NOAA).

ILLUSTRATIONS

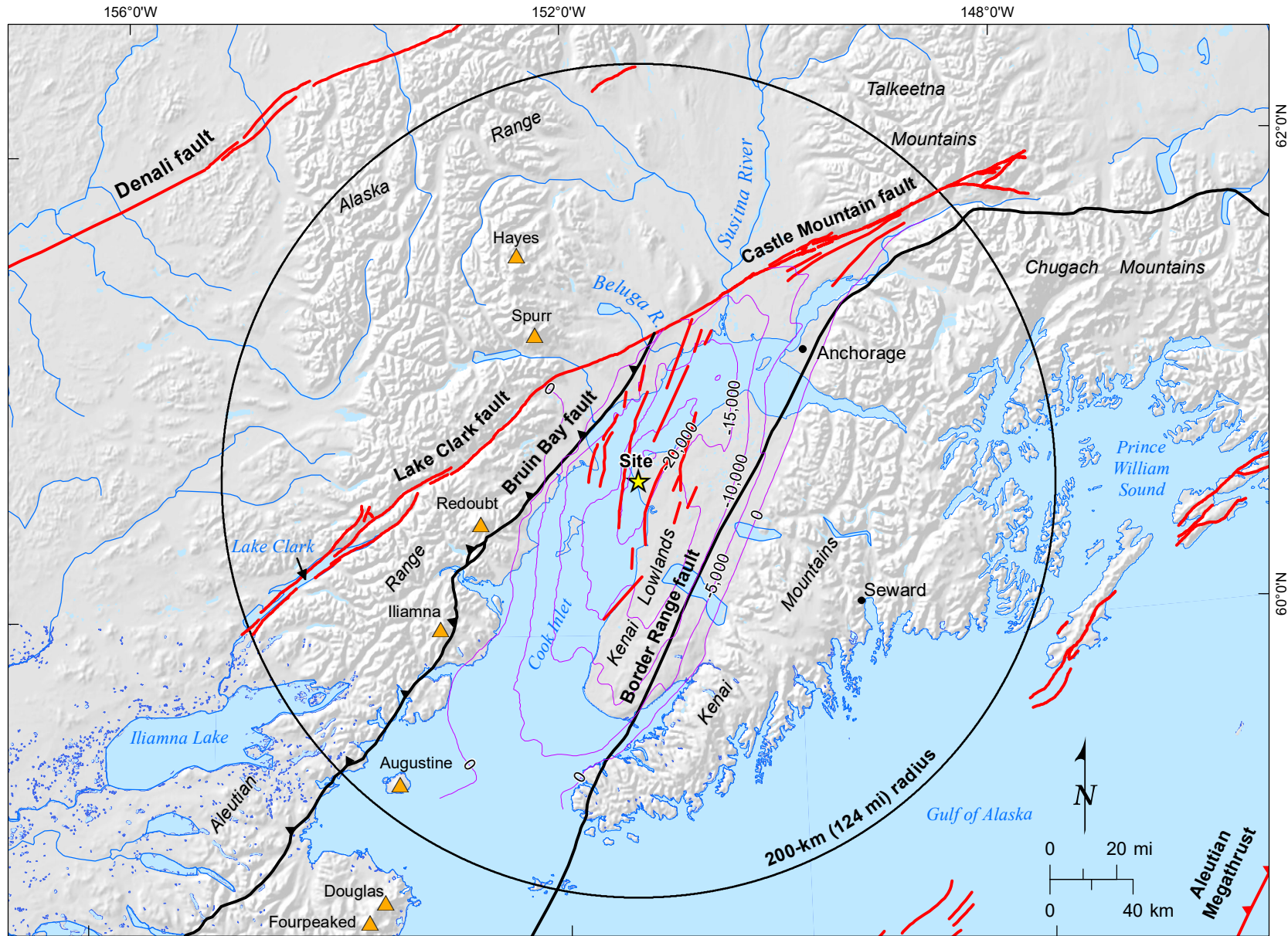


SITE LOCATION MAP
LNG FACILITIES
ALASKA LNG PROJECT
NIKISKI, ALASKA



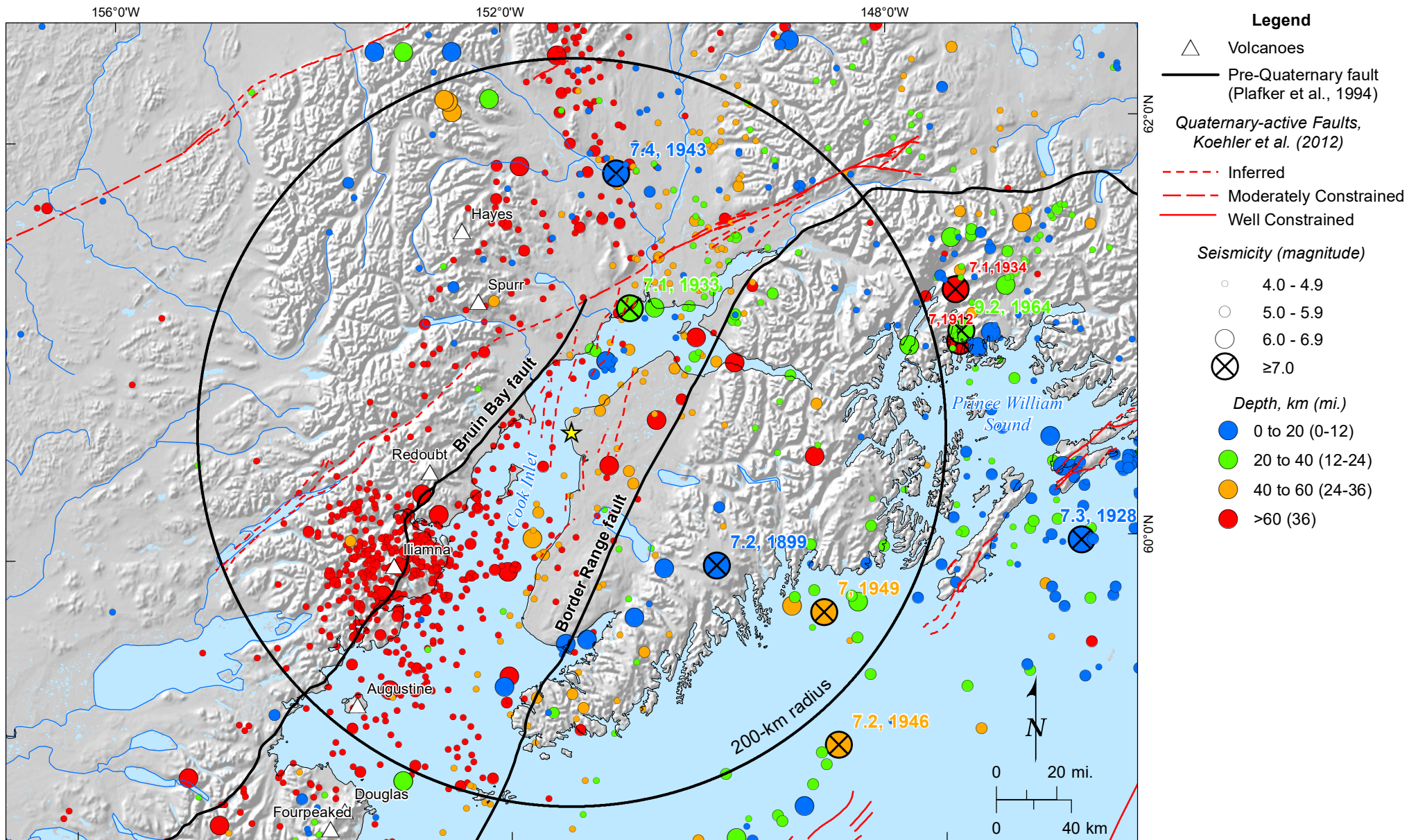
Modified from Bruhn and Haeussler (2006).

TECTONIC FRAMEWORK OF SOUTHERN ALASKA
 LNG FACILITIES
 ALASKA LNG PROJECT
 NIKISKI, ALASKA



- | | |
|---|--|
|  Pre-Quaternary fault (Plafker et al., 1994) |  Volcanoes |
|  Quaternary-active fault, Koehler et al. (2012), and this study |  Depth of Cook Inlet Basin, 5,000-foot contours (modified from Schellenbaum et al., 2010) |

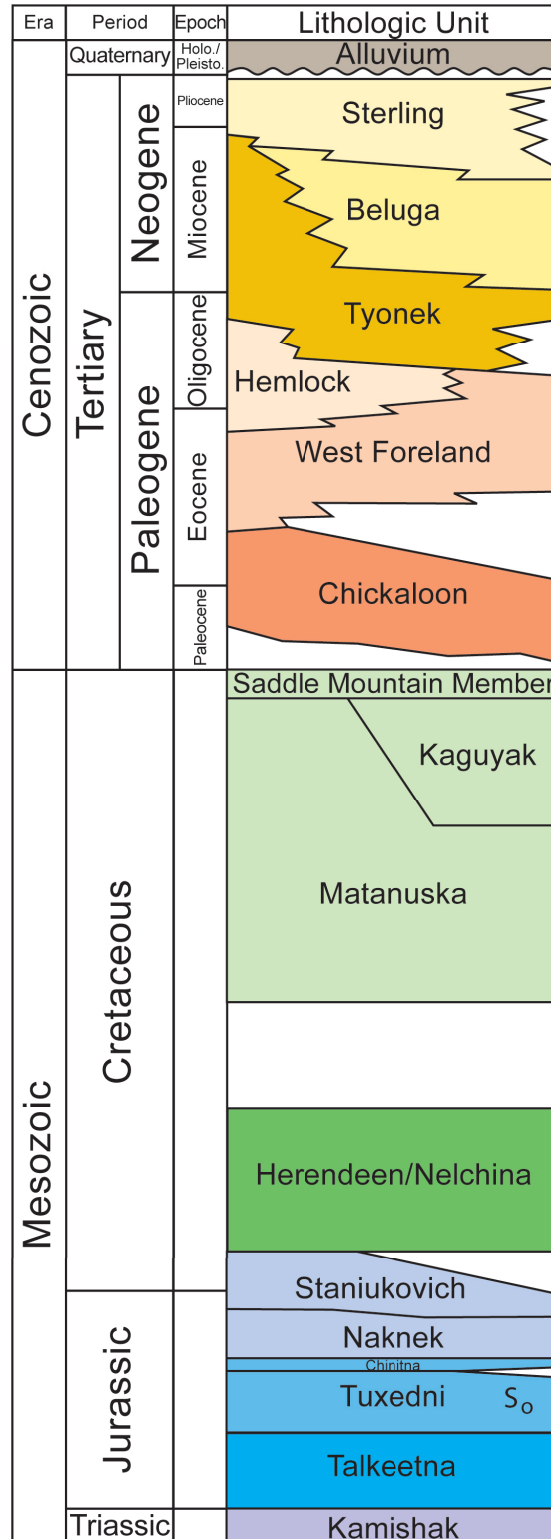
REGIONAL FAULT MAP
LNG FACILITIES
ALASKA LNG PROJECT
NIKISKI, ALASKA



Seismicity from AEIC (1899-2015)

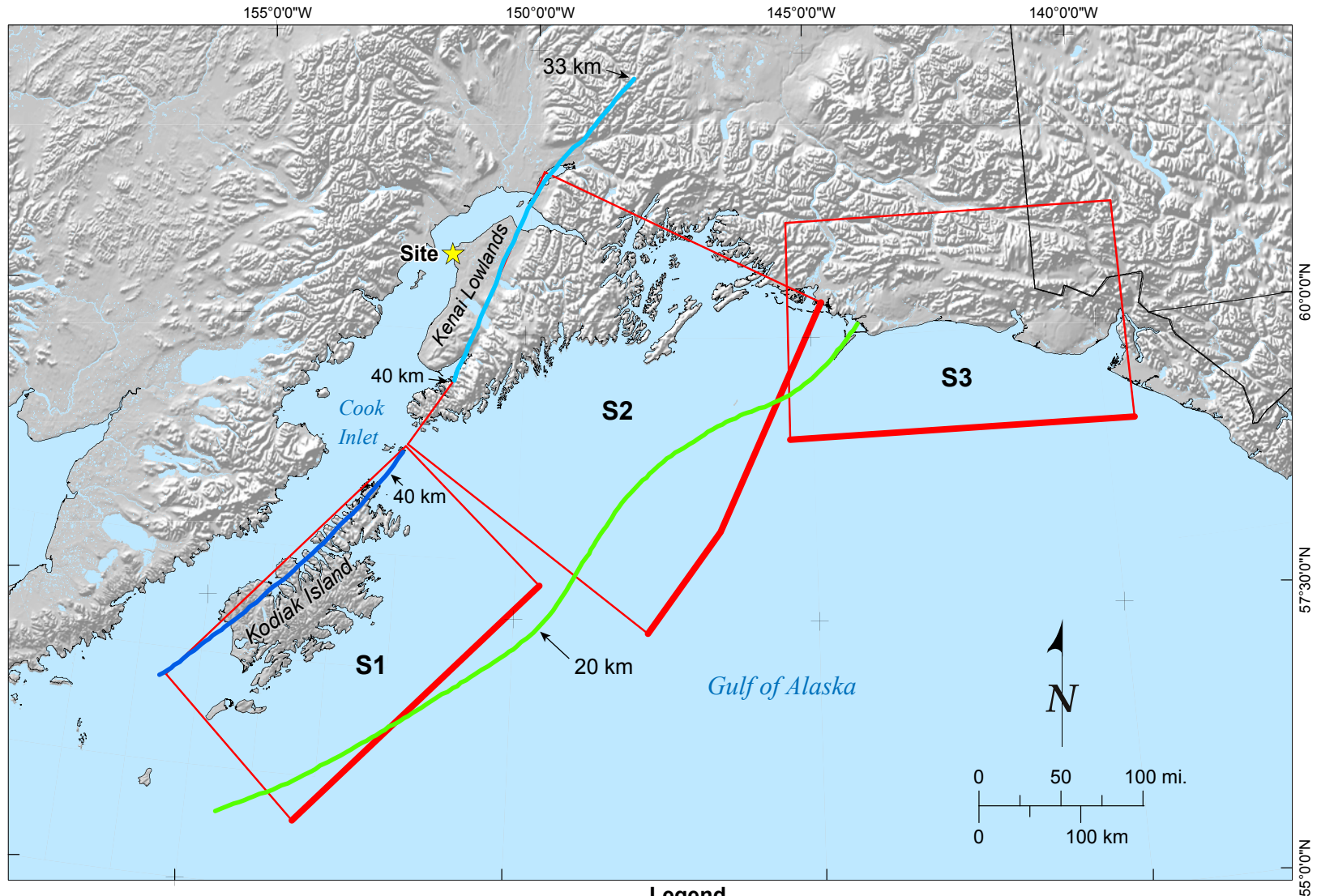
SEISMICITY MAP
 LNG FACILITIES
 ALASKA LNG PROJECT
 NIKISKI, ALASKA

P:\Projects\10_000010_140334_AKING_PreFEED_Phase2\05_Graphics\10_140334_PSHA\04_D-19_Regional_Seismicity.mxd; [reimberg, 5/19/2016]

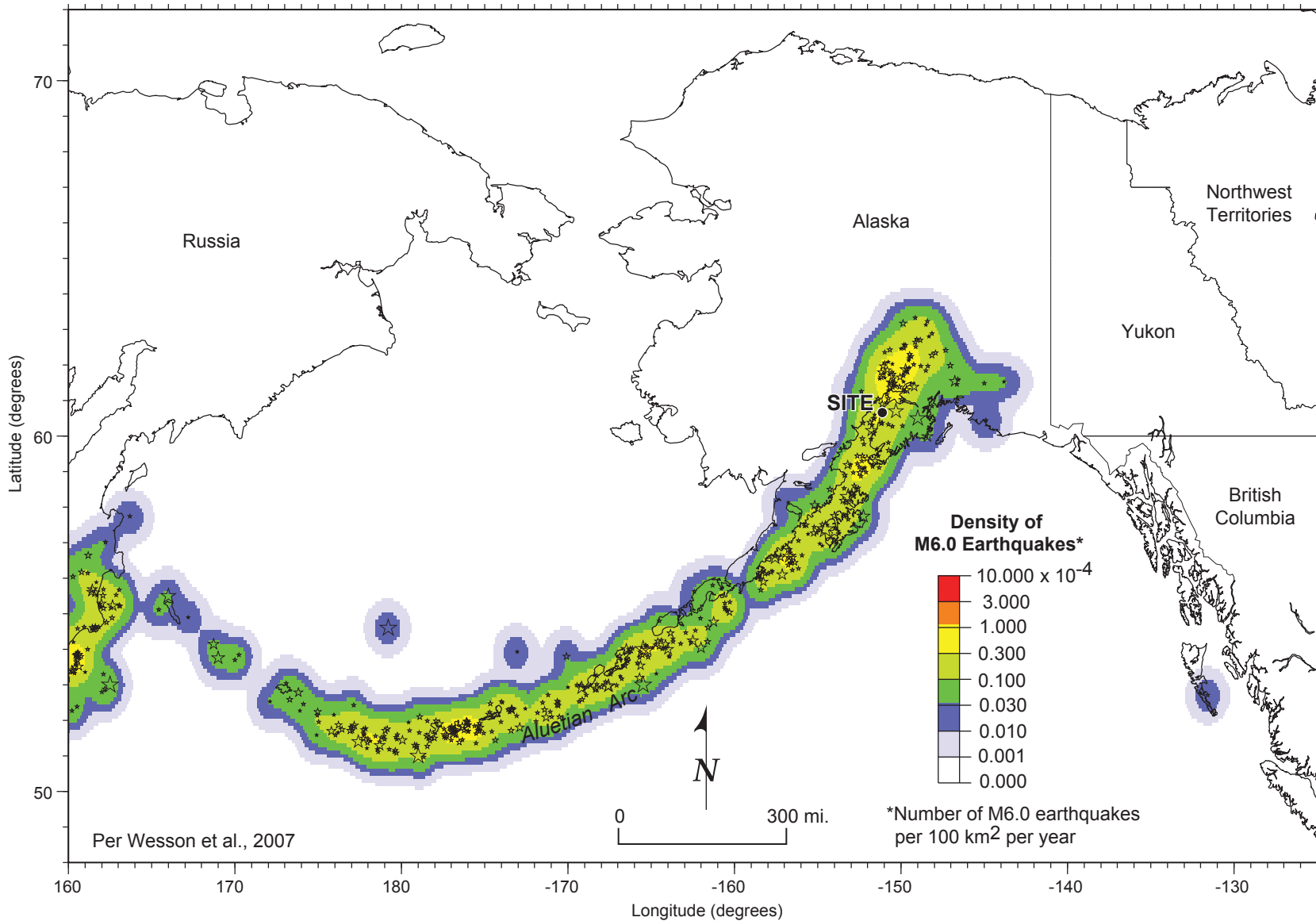


Modified from Enos and Maier, 2013.

STRATIGRAPHIC COLUMN OF COOK INLET BASIN
 LNG FACILITIES
 ALASKA LNG PROJECT
 NIKISKI, ALASKA

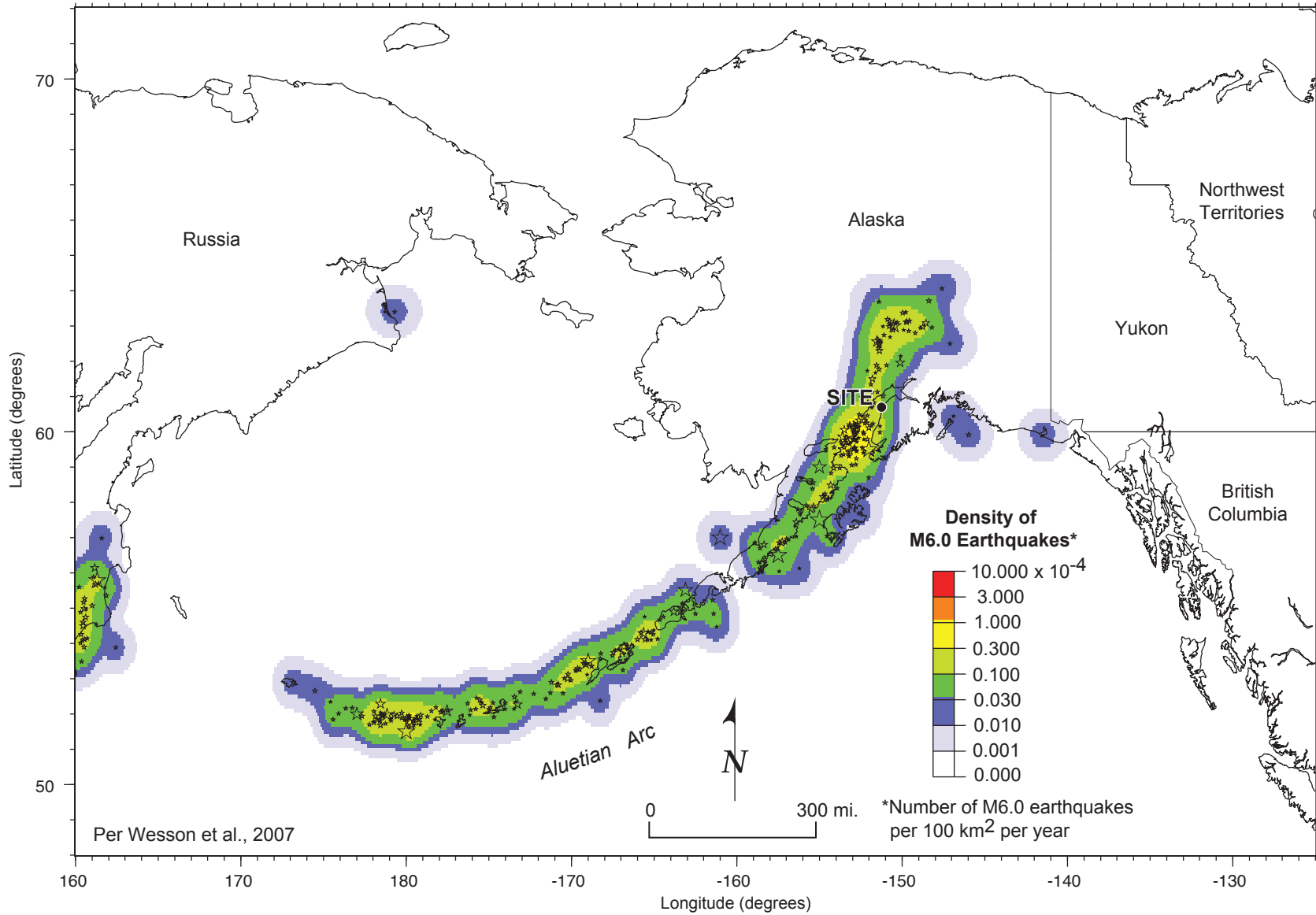


MEGATHRUST INTERFACE MODEL
 LNG FACILITIES
 ALASKA LNG PROJECT
 NIKISKI, ALASKA

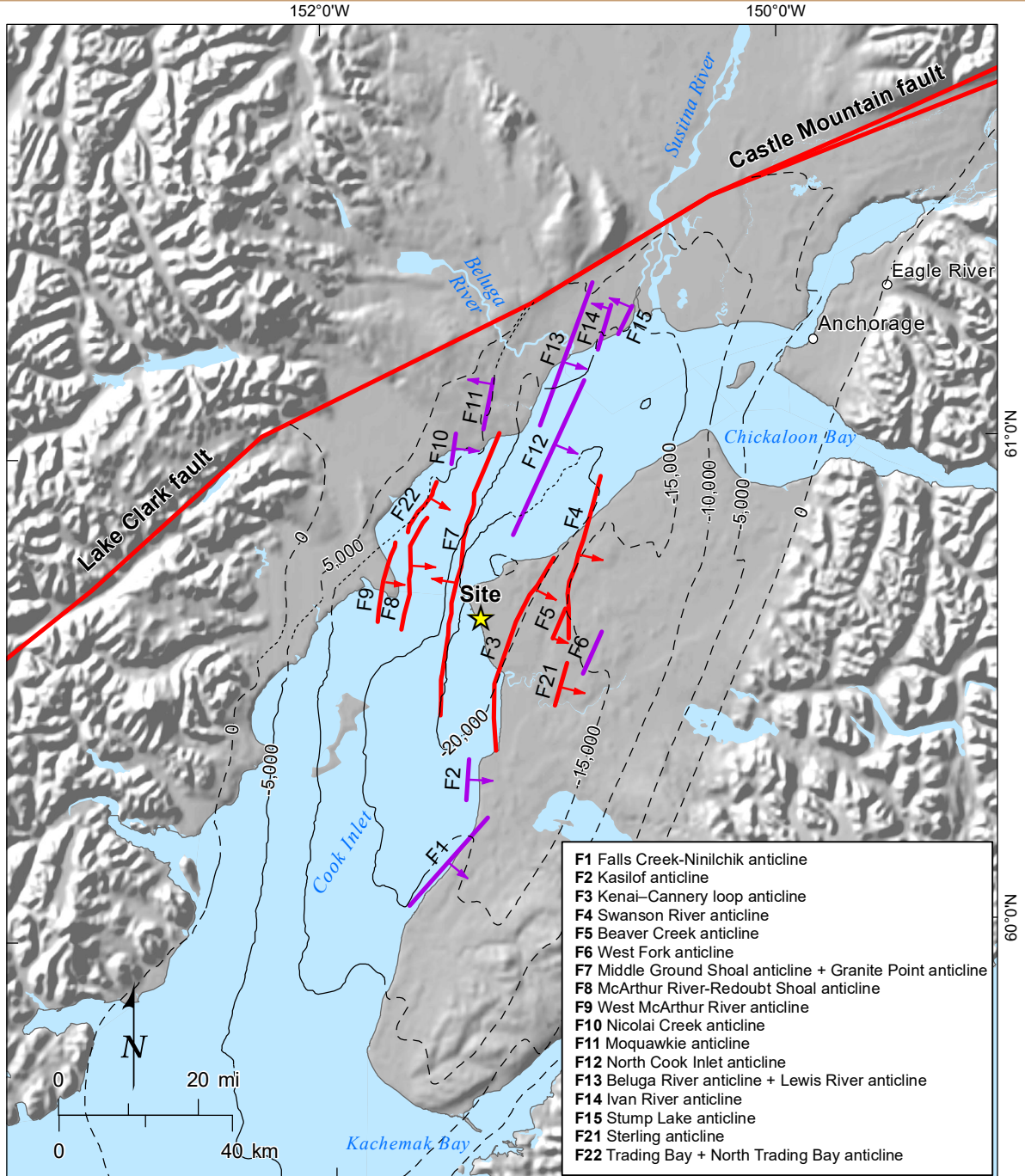


**WESSON ET AL (2007) MODEL OF INTRASLAB SEISMICITY
M6.0 EARTHQUAKES WITH DEPTHS OF 31 TO 50 MI (50 TO 80 KM)**

LNG FACILITIES
ALASKA LNG PROJECT
NIKISKI, ALASKA



**WESSON ET AL (2007) MODEL OF INTRASLAB SEISMICITY
M6.0 EARTHQUAKES WITH DEPTHS OF 50 TO 75 MI (80 TO 120 KM)
LNG FACILITIES
ALASKA LNG PROJECT
NIKISKI, ALASKA**



- F1 Falls Creek-Ninilchik anticline
- F2 Kasilof anticline
- F3 Kenai-Cannery loop anticline
- F4 Swanson River anticline
- F5 Beaver Creek anticline
- F6 West Fork anticline
- F7 Middle Ground Shoal anticline + Granite Point anticline
- F8 McArthur River-Redoubt Shoal anticline
- F9 West McArthur River anticline
- F10 Nicolai Creek anticline
- F11 Moquawkie anticline
- F12 North Cook Inlet anticline
- F13 Beluga River anticline + Lewis River anticline
- F14 Ivan River anticline
- F15 Stump Lake anticline
- F21 Sterling anticline
- F22 Trading Bay + North Trading Bay anticline

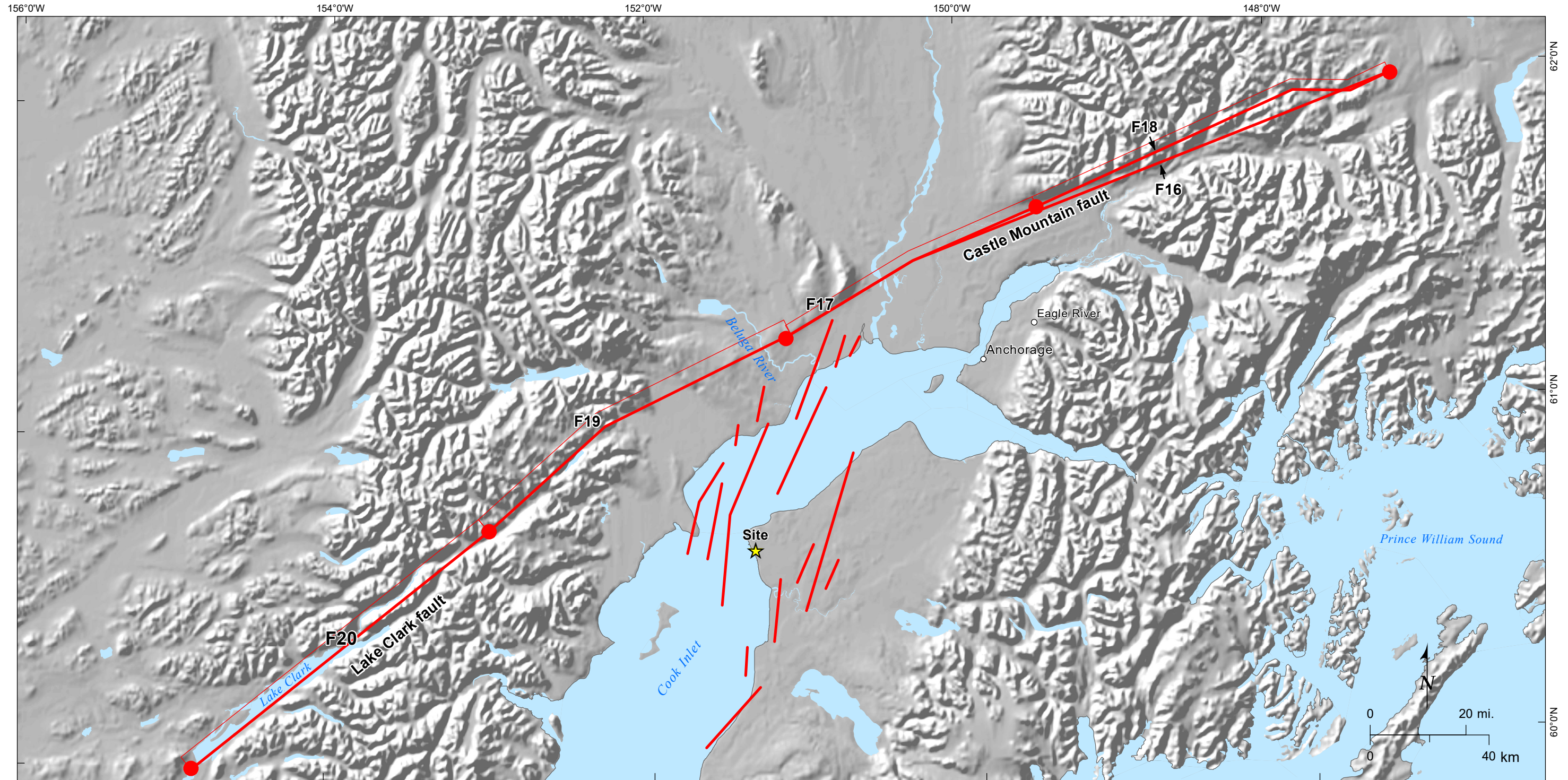
Legend

- Modeled Surface Projection of Blind Fault Tip-Line**
-  **F3** Based on mapping of seismic reflection data; arrow shows direction of dip
 -  **F1** Based on Koehler (2012); arrow shows direction of dip

Depth of Cook Inlet Basin, 5,000-foot Contours (modified from Schellenbaum et al., 2010)

-  Dashed where approximate
-  Solid where well located
-  Interpolated

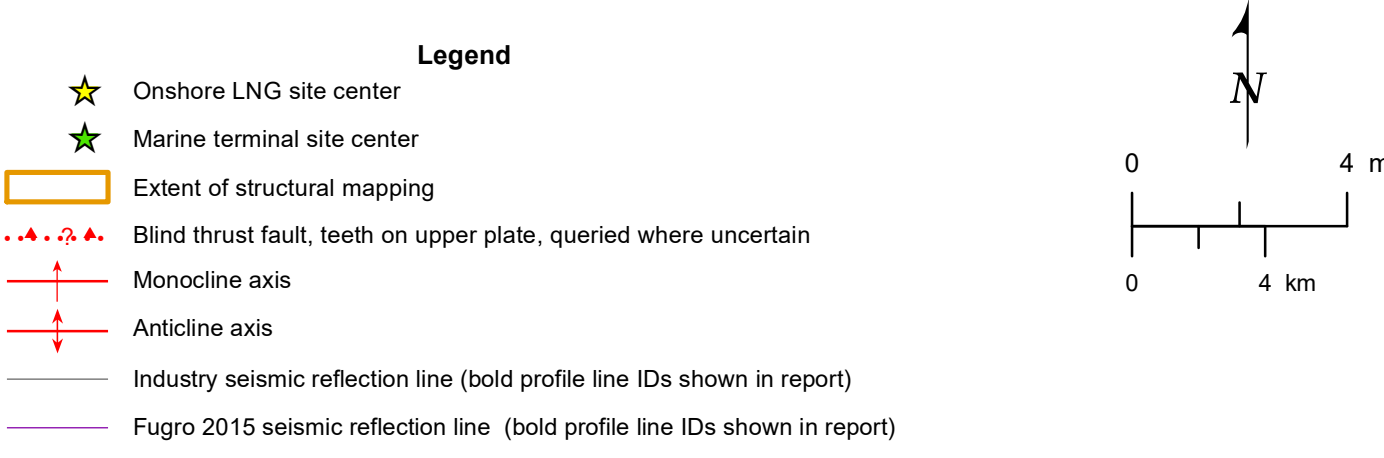
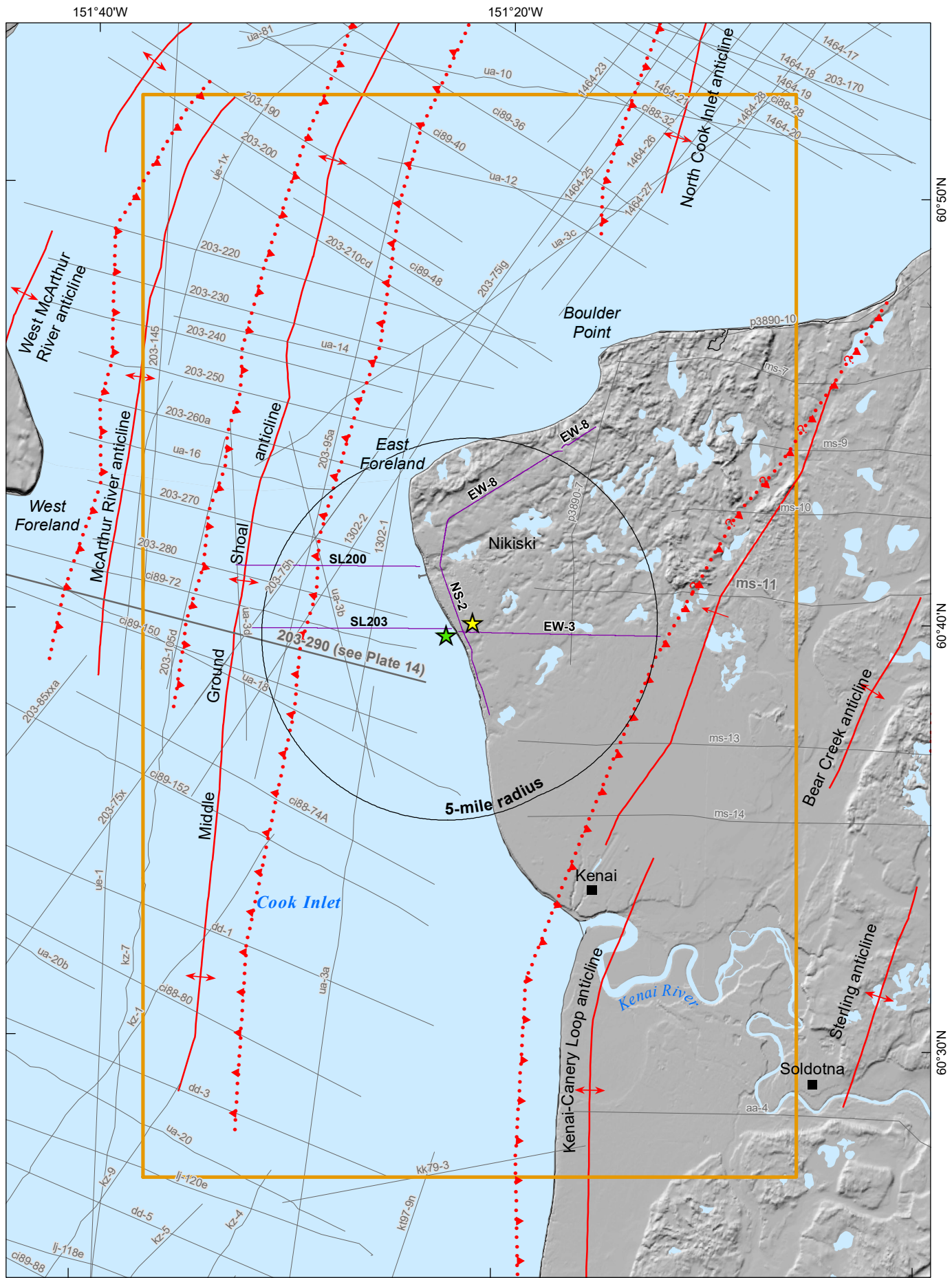
COOK INLET FAULT-CORED FOLD SOURCE MODEL
 LNG FACILITIES
 ALASKA LNG PROJECT
 NIKISKI, ALASKA



- Notes:
1. F19 and F20: Lake Clark fault
 2. F16, F17 and F18: Castle Mountain fault

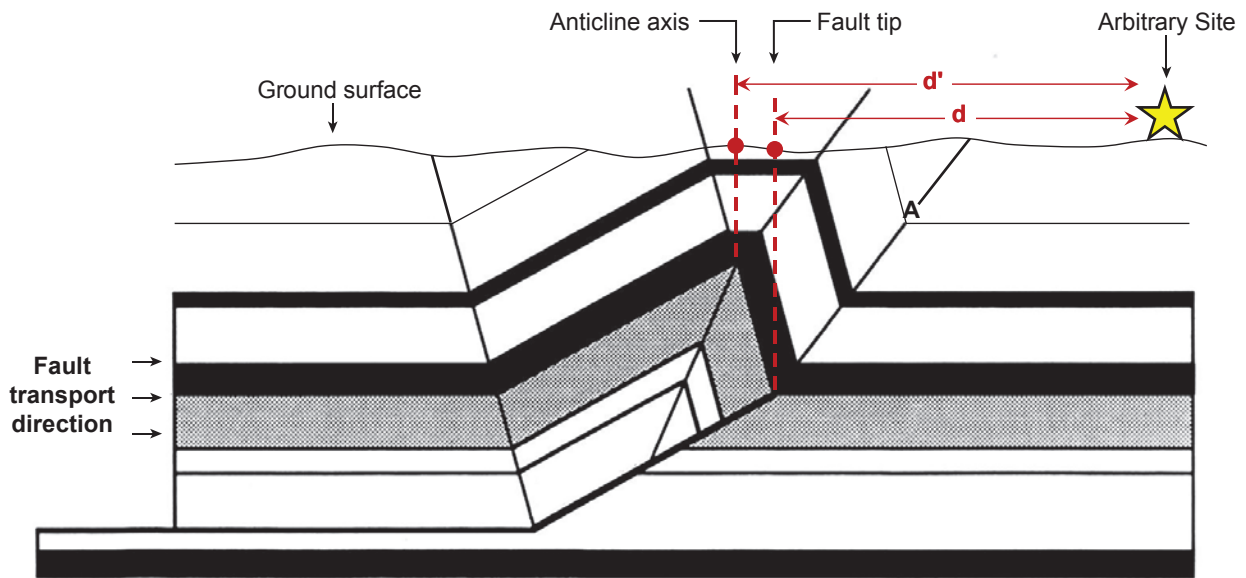
- Legend**
-  Surface fault trace with segment boundary
 -  Projection of fault plane at depth
 - F19** Source identification number

**NON-COOK INLET BASIN UPPER
 PLATE FAULT SOURCE MODEL**
 LNG FACILITIES
 ALASKA LNG PROJECT
 NIKISKI, ALASKA



FOLDS AND FAULTS MAPPED FROM SEISMIC REFLECTION DATA
 LNG FACILITIES
 ALASKA LNG PROJECT
 NIKISKI, ALASKA

P:\Projects\10_0000\10_140334_AK LNG_PrefEED_Phase205_Graphics\10_140334_PSHA12_D_345_FaultsFolds_SeismicLines_020416.mxd; jholmberg; 5/9/2016



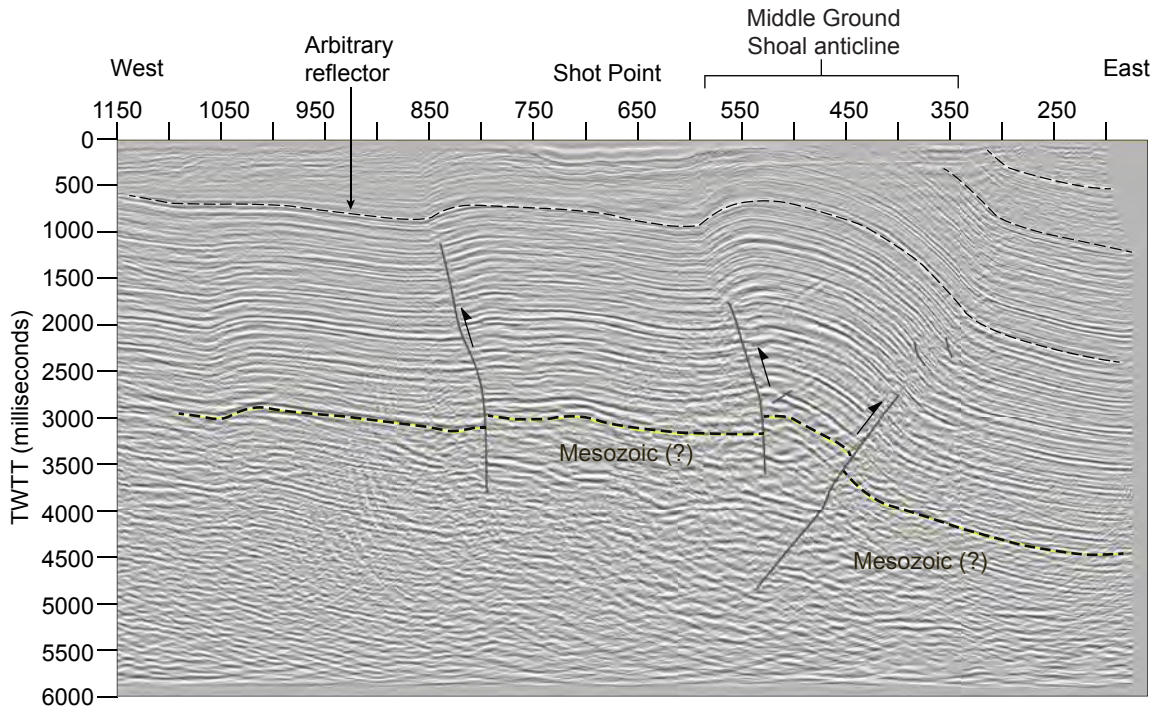
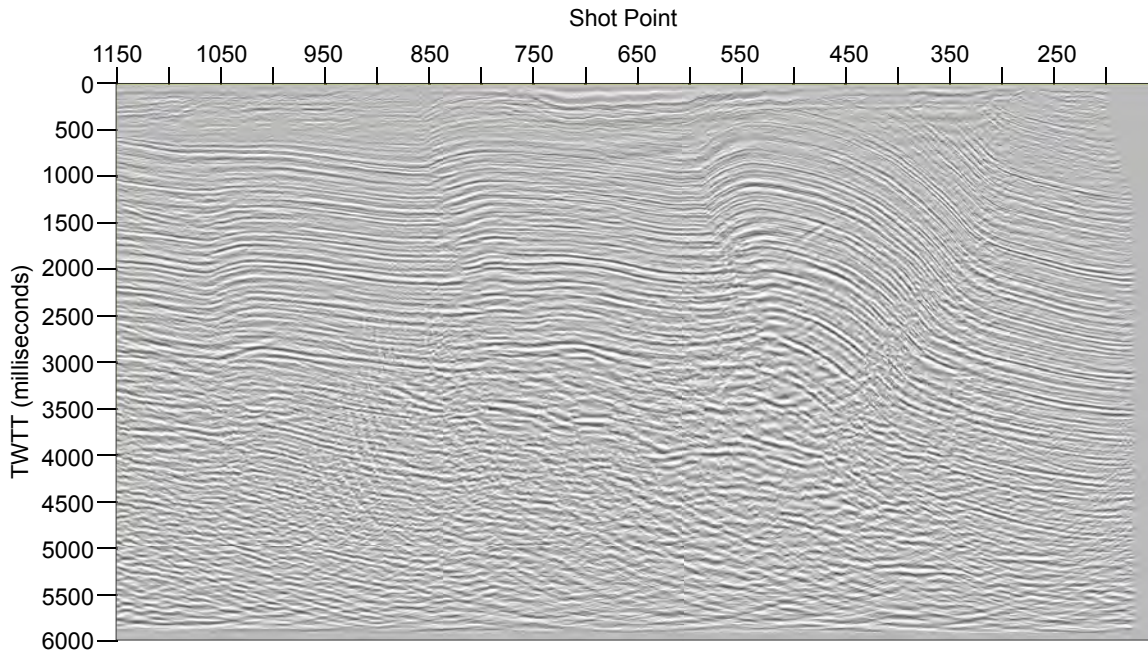
Modified from Suppe and Medwedeff (1990)

Note:

1. $d < d'$, where d and d' are the distances between the Site and the projected fault tip and anticline axis, respectively.
2. **A** = Axial hinge separating the anticline forelimb from the synclinal flat.
3. This diagram is meant to illustrate how the site-to-source distance would change in map view if the anticline axis (left-hand dot) was used as a proxy for fault tip location. This diagram does not accurately portray the depth of the fault tips, which would be the same in both scenarios.

f:\wbc-file\project\Projects\10_0000\10_140094_AK LNG_EIV_PrefEED\05_Graphics\10_140094_PSHA

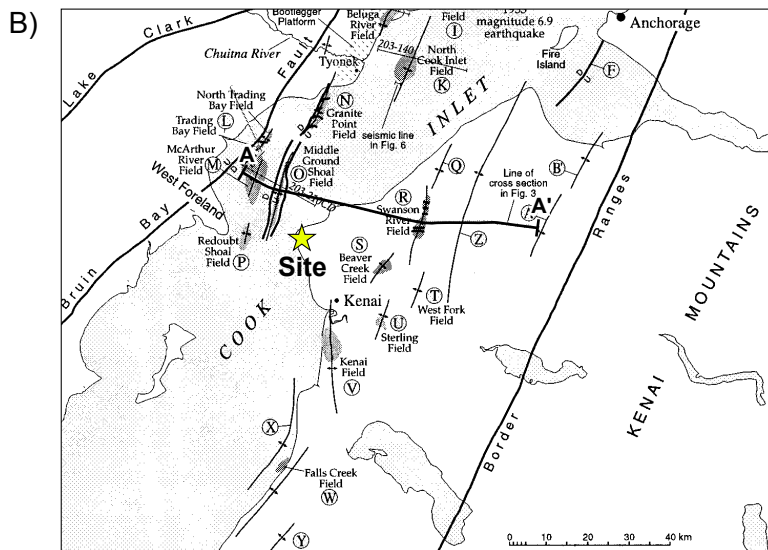
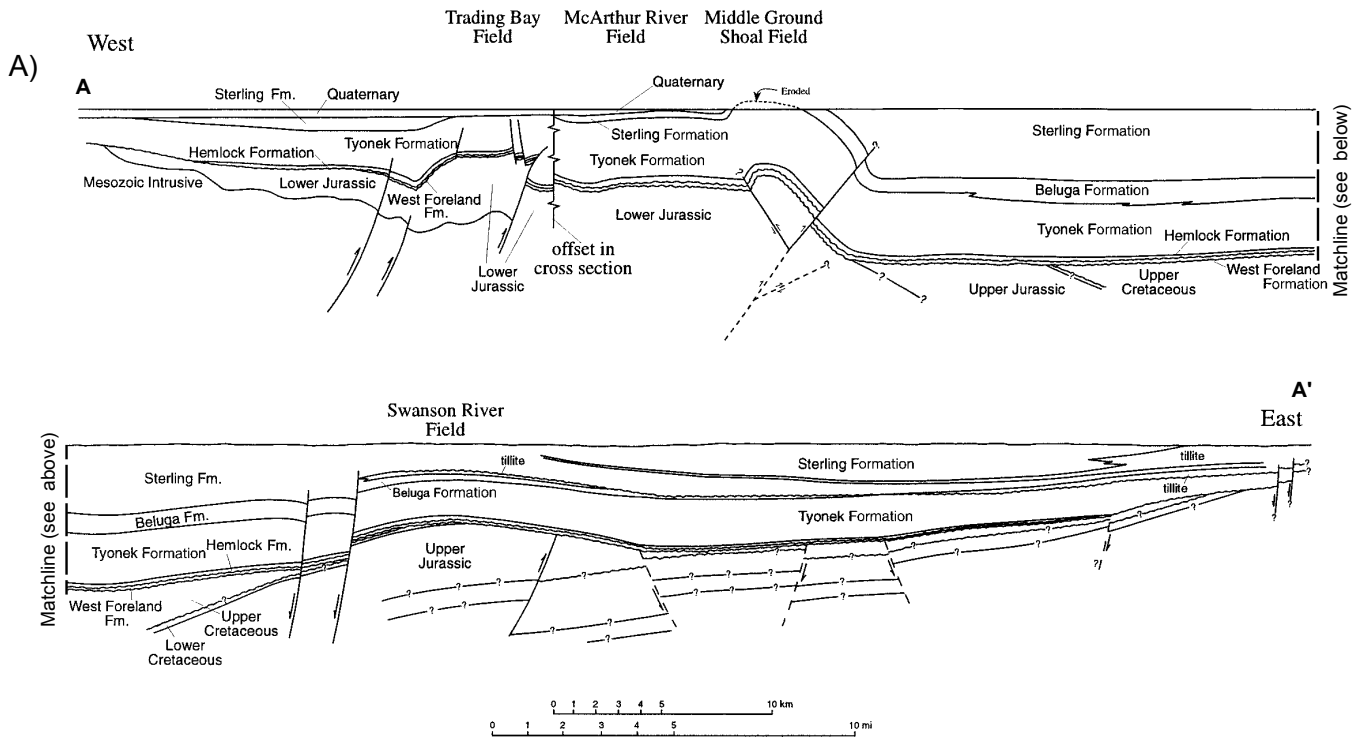
CONCEPTUAL FAULT-PROPAGATION FOLD MODEL
 LNG FACILITIES
 ALASKA LNG PROJECT
 NIKISKI, ALASKA



The information contained herein is ConocoPhillips "independent information," as defined in the June 30 2014 Alaska LNG Project Pre-FEED Joint Venture Agreement ("Pre-FEED JVA"), and is provided to Lead Party subject to the Pre-FEED JVA solely for the purpose of geohazard analysis, including probabilistic seismic hazard analysis, to support the Alaska LNG project's FERC filings.

For line location see Plate 12.

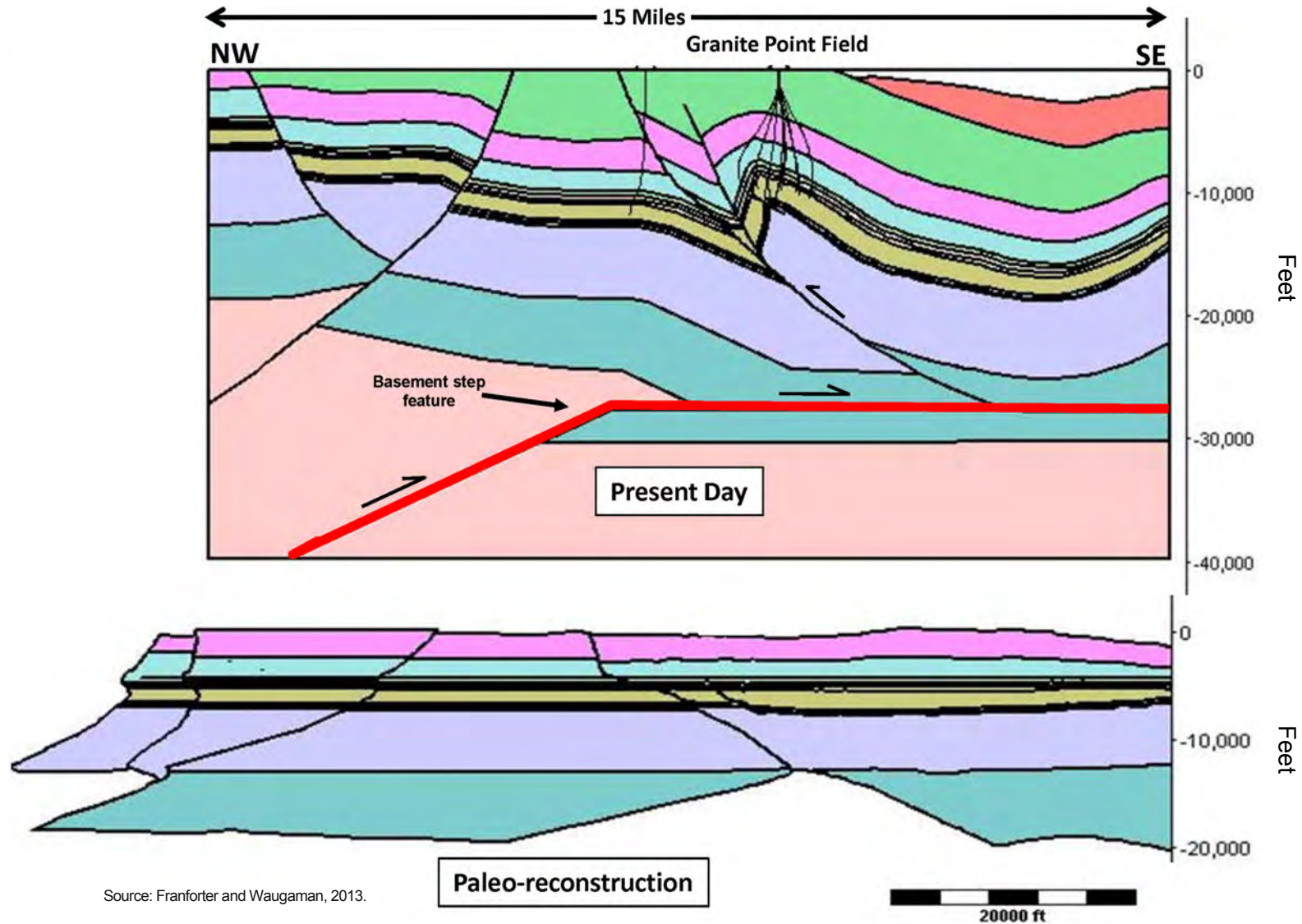
**SEISMIC REFLECTION LINE 203-290, SHOWING MIDDLE
 GROUND SHOAL FAULT-FOLD SYSTEM
 LNG FACILITIES
 ALASKA LNG PROJECT
 NIKISKI, ALASKA**



Legend
 A — A' Cross section location

A) Cross section with no vertical exaggeration of the Cook Inlet Basin from Boss et al. (1976) with interpretation of Middle Ground Shoal structure by Haeussler et al. (2000). B) Depth to the base of the Tertiary section between Middle Ground Shoal and Swanson River fields is based on interpretation of seismic reflection data by Haeussler et al. (2000). Figure modified from Haeussler et al. (2000).

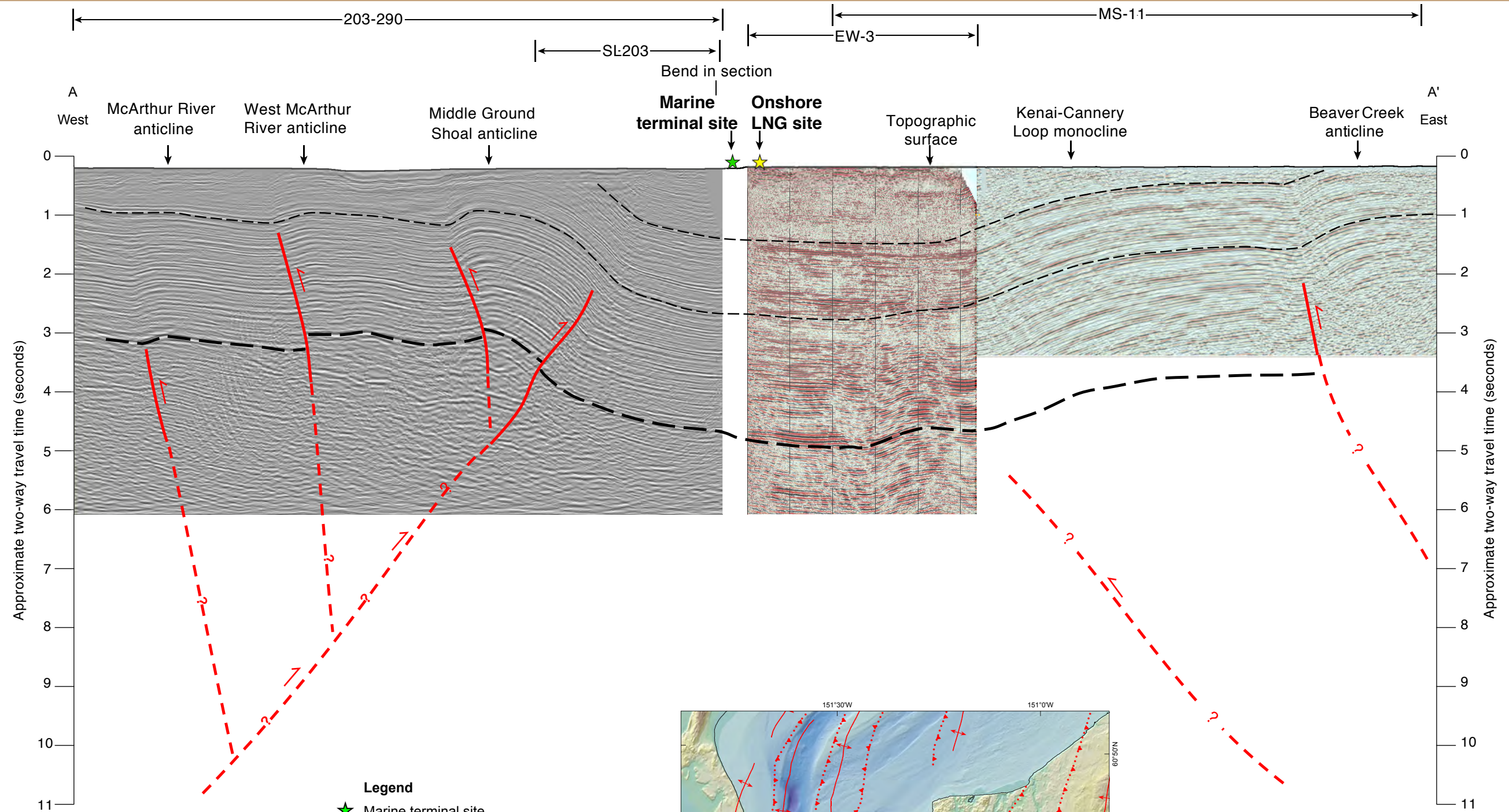
**CROSS-SECTION OF THE NORTHERN COOK INLET
 ONSHORE LNG FACILITIES
 ALASKA LNG PROJECT
 NIKISKI, ALASKA**



Paleo-reconstruction

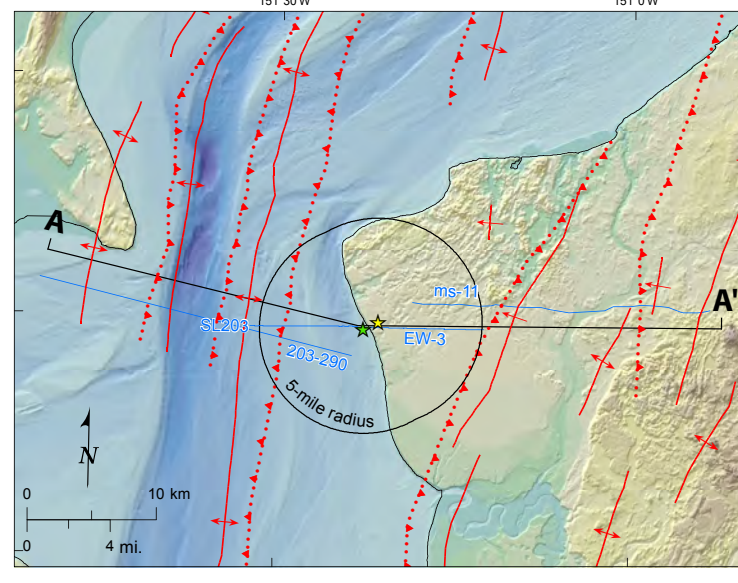
**DIAGRAMMATIC CROSS SECTION OF
THE GRANITE POINT ANTICLINE AREA
LNG FACILITIES
ALASKA LNG PROJECT
NIKISKI, ALASKA**

\\na-weller\project\Project\0_000010_140334_AK LNG_Prefeed_Phase2005_Graphics\0_140334_PSHA



- Legend**
- ★ Marine terminal site
 - ★ Site center
 - - - Structural form line within undifferentiated Tertiary units
 - - - Top of Mesozoic basement
 - - - Faults; dashed where inferred

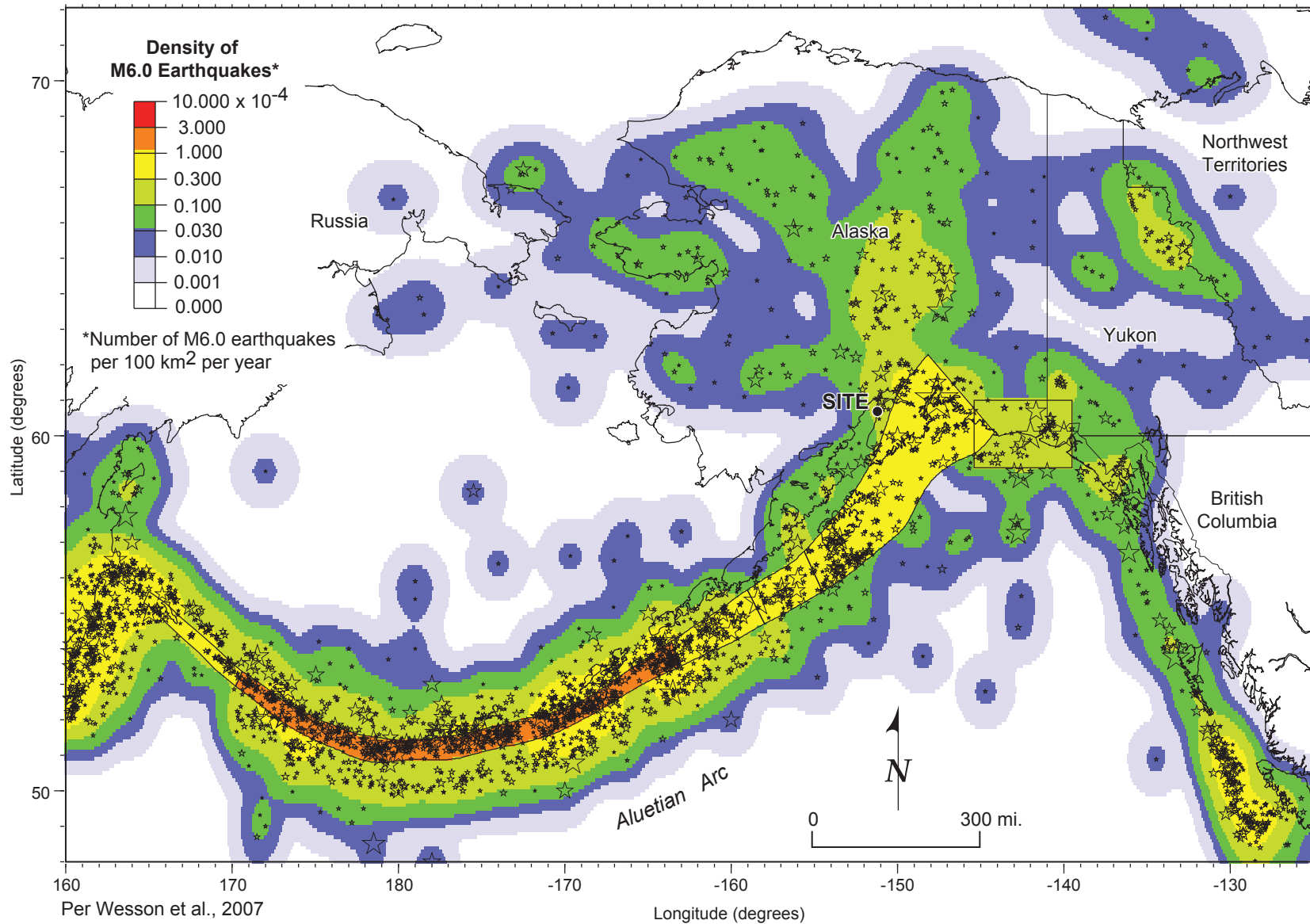
Notes:
 1. For conceptual purposes only.
 2. Horizontal and vertical are not to scale.



CONCEPTUAL CROSS SECTION OF UPPER COOK INLET BASIN AT THE LATITUDE OF THE SITE LNG FACILITIES ALASKA LNG PROJECT NIKISKI, ALASKA

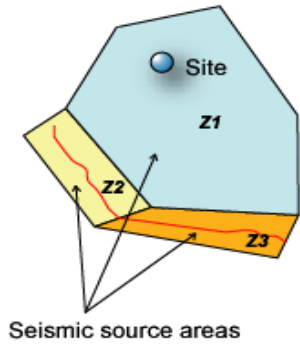
0 10,000 ft.
 Horizontal scale

f:\a\wc\files\project\Projects\10_0000\10_140334_AKLNG_PrefEED_Phase2\05_Graphics\10_140334_PSHA

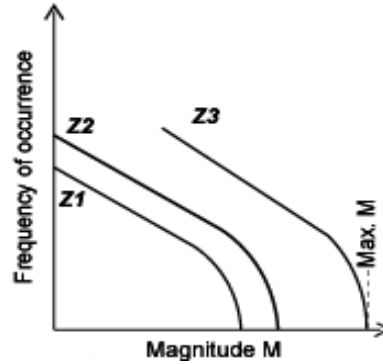


WESSON ET AL (2007) MODEL M6.0 EARTHQUAKE EVENTS NOT ASSOCIATED WITH MEGATHRUST EVENTS (0 to 31 MI / 0 TO 50 KM DEPTH) LNG FACILITIES ALASKA LNG PROJECT NIKISKI, ALASKA

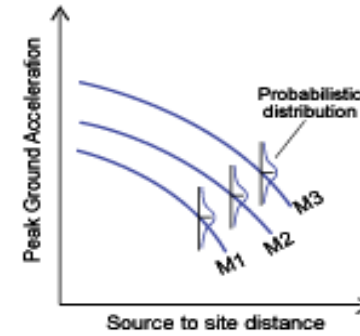
1. Define Seismic Sources



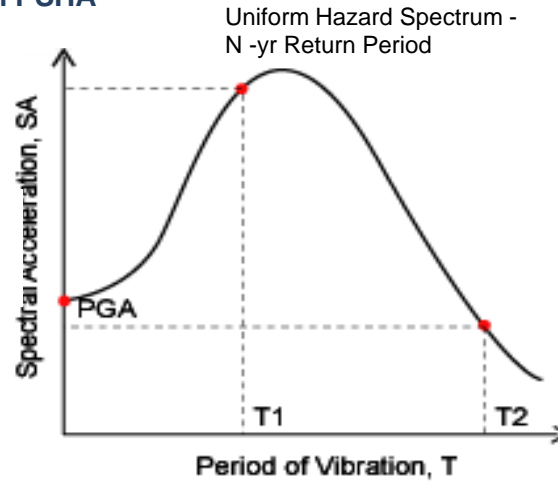
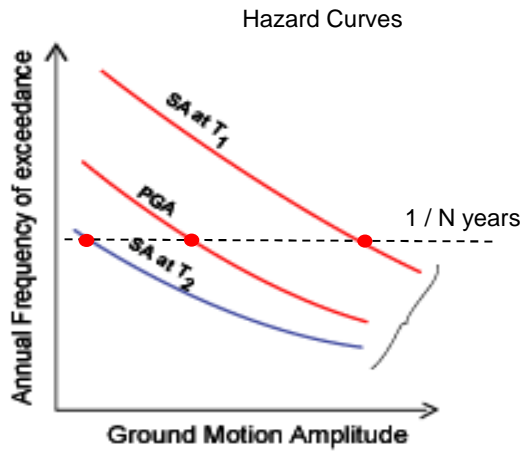
2. Characterize Magnitude Recurrence



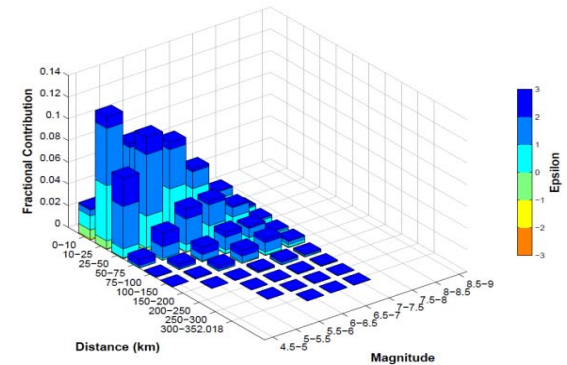
3. Characterize amplitude of ground motions for given eqk. scenario (GMPE)



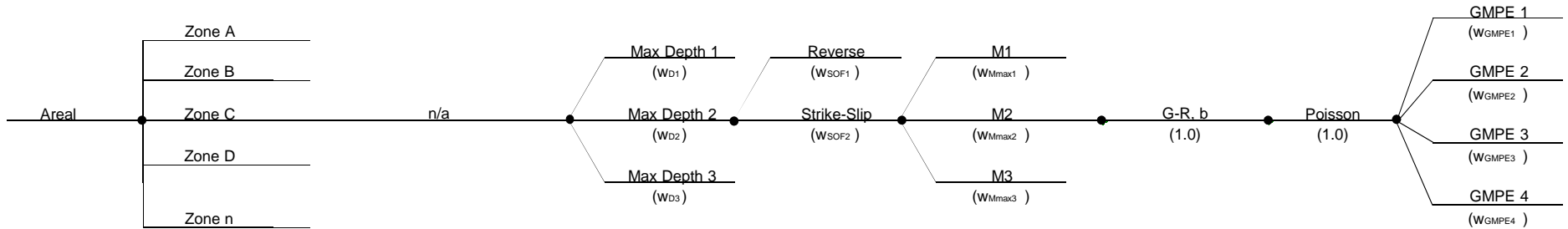
4. Perform PSHA



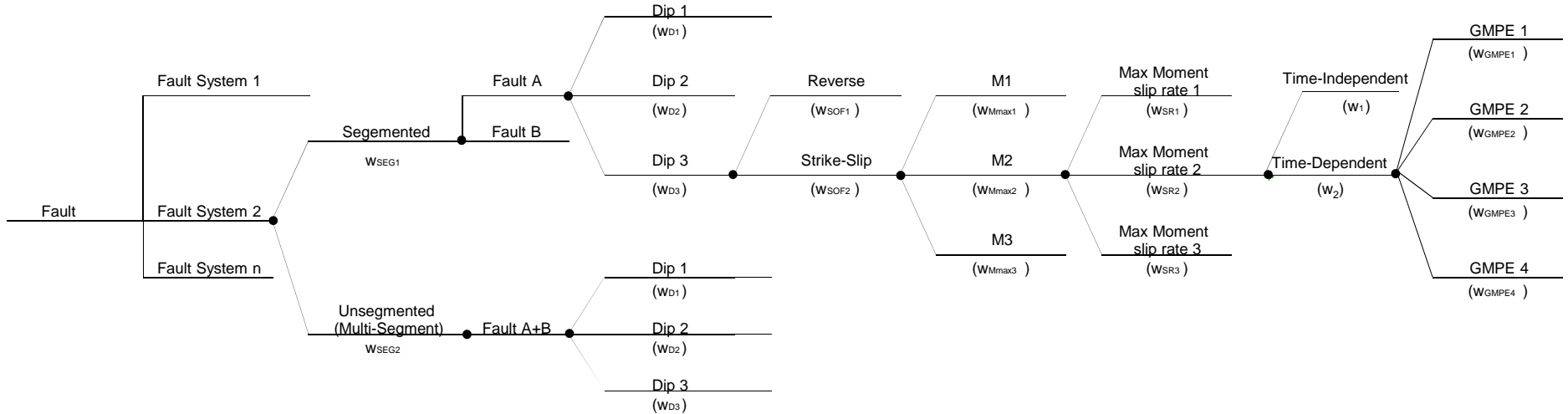
5. Deaggregation



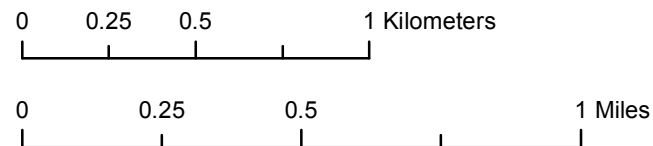
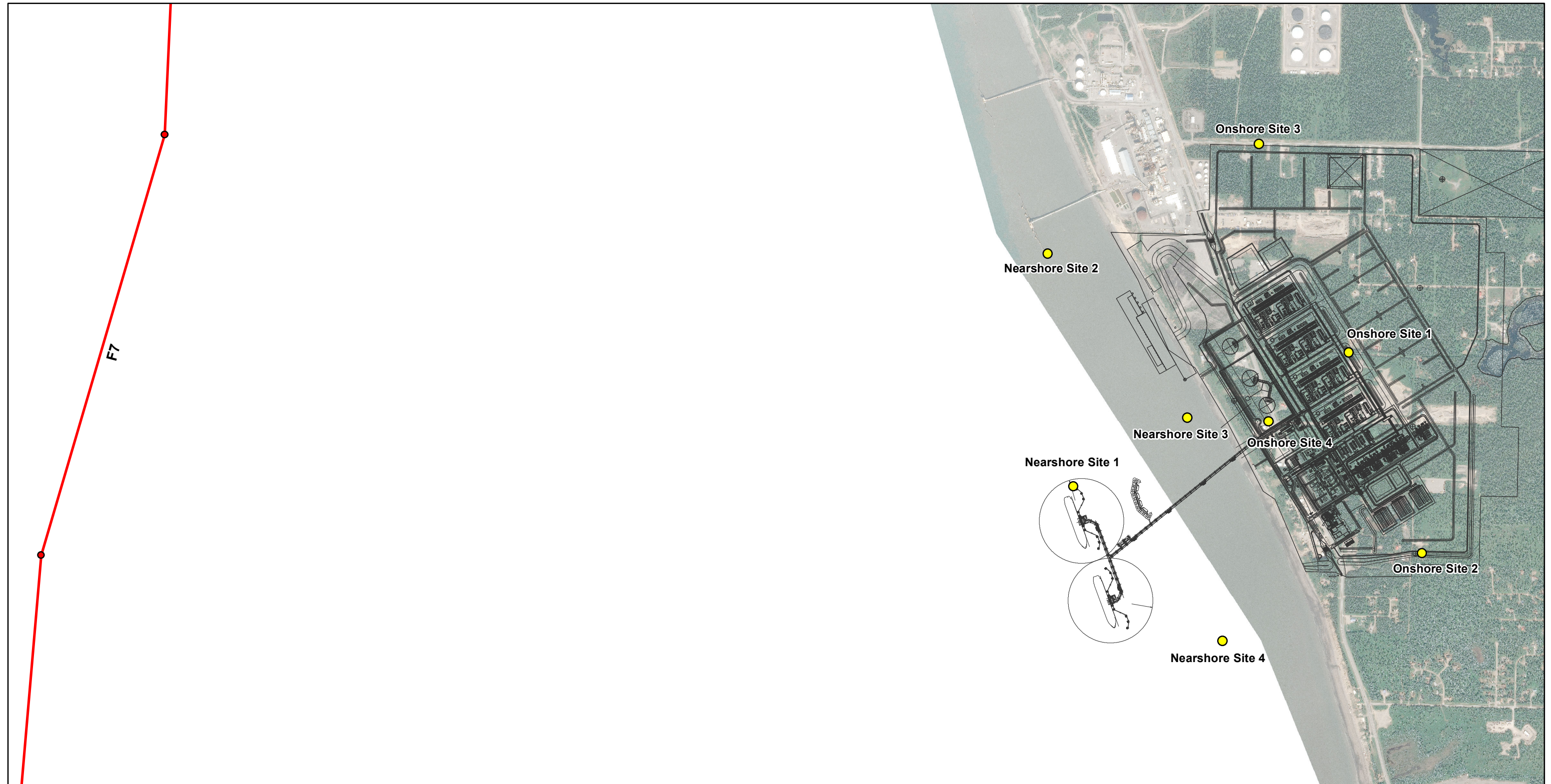
1. Source Type, Location, and Geometry					2. Earthquake Magnitude Distribution and Frequency			3. Ground Motion Prediction Equation
Source Type	Source	Segmentation	Source Geometry	Style of Faulting	Maximum Magnitude	Magnitude Recurrence	Time Dependence	



NOTE: This logic tree illustrates the modeling of epistemic uncertainty modeled in this project. Values and weights for specific seismic sources and sources of uncertainty are described in Section 3.

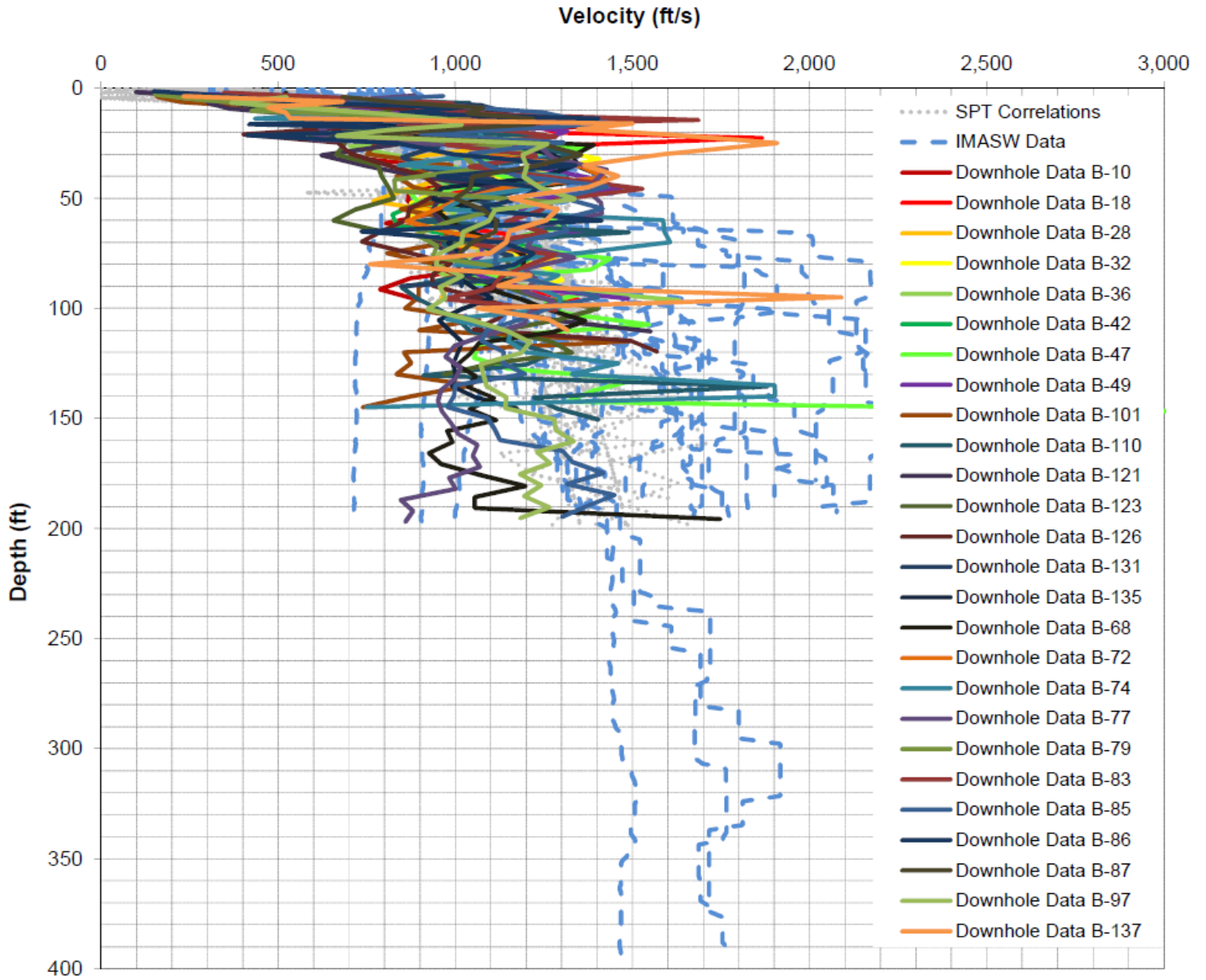


GENERIC LOGIC TREE FOR TREATMENT OF EPISTEMIC UNCERTAINTIES
 LNG FACILITIES
 ALASKA LNG PROJECT
 NIKISKI, ALASKA



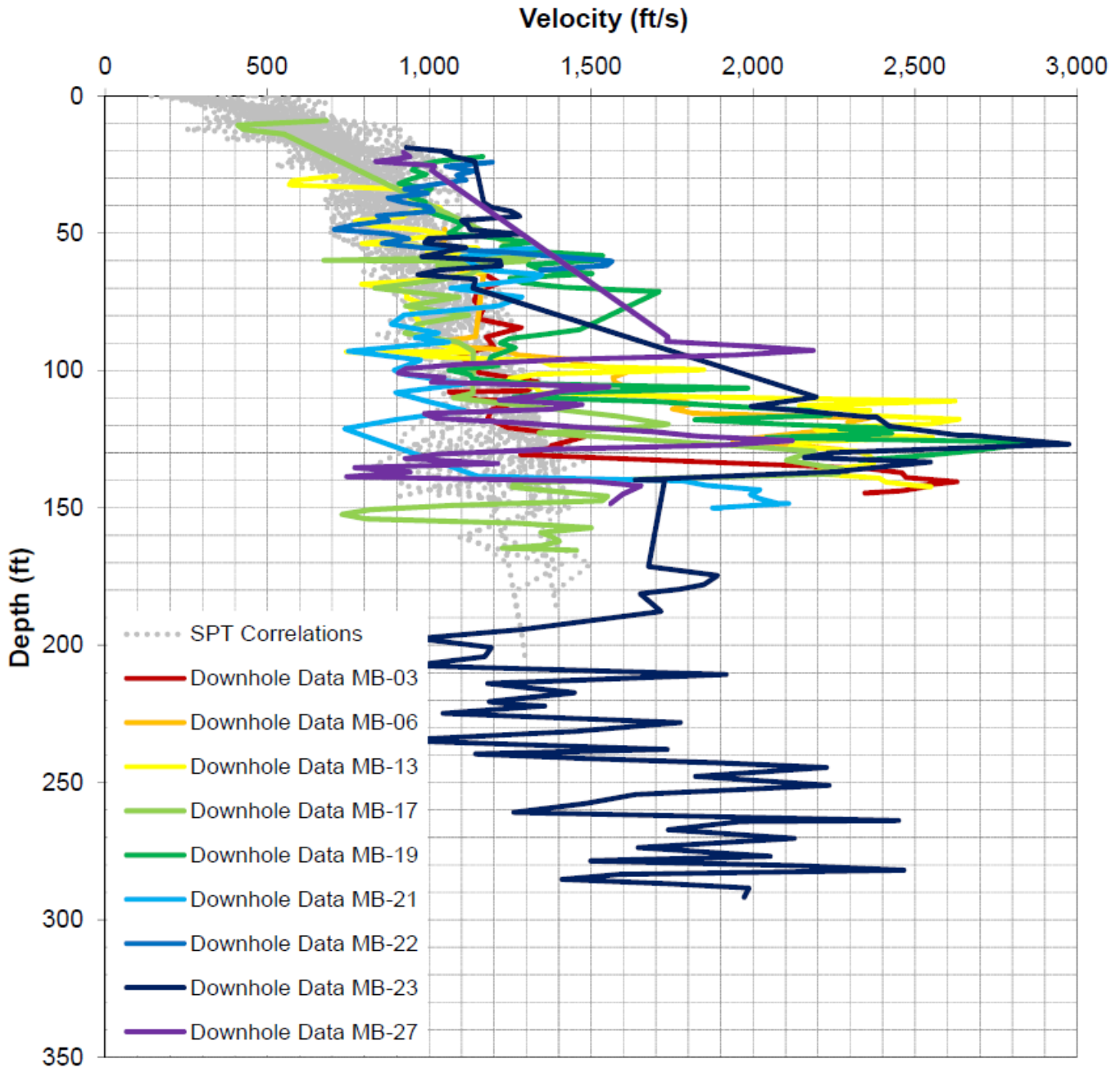
Legend
● Line Source
● PSHA Locations

PSHA LOCATIONS
LNG FACILITIES
ALASKA LNG PROJECT
NIKISKI, ALASKA



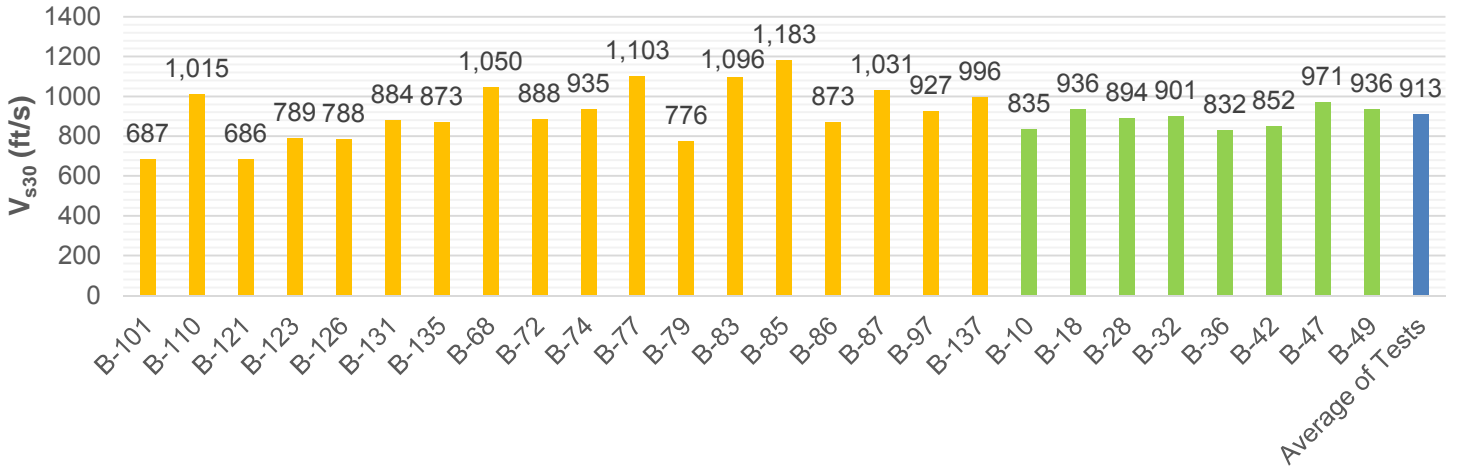
DEVELOPMENT OF SHEAR WAVE VELOCITY PROFILES FOR THE ONSHORE LNG FACILITIES

LNG FACILITIES
ALASKA LNG PROJECT
NIKISKI, ALASKA

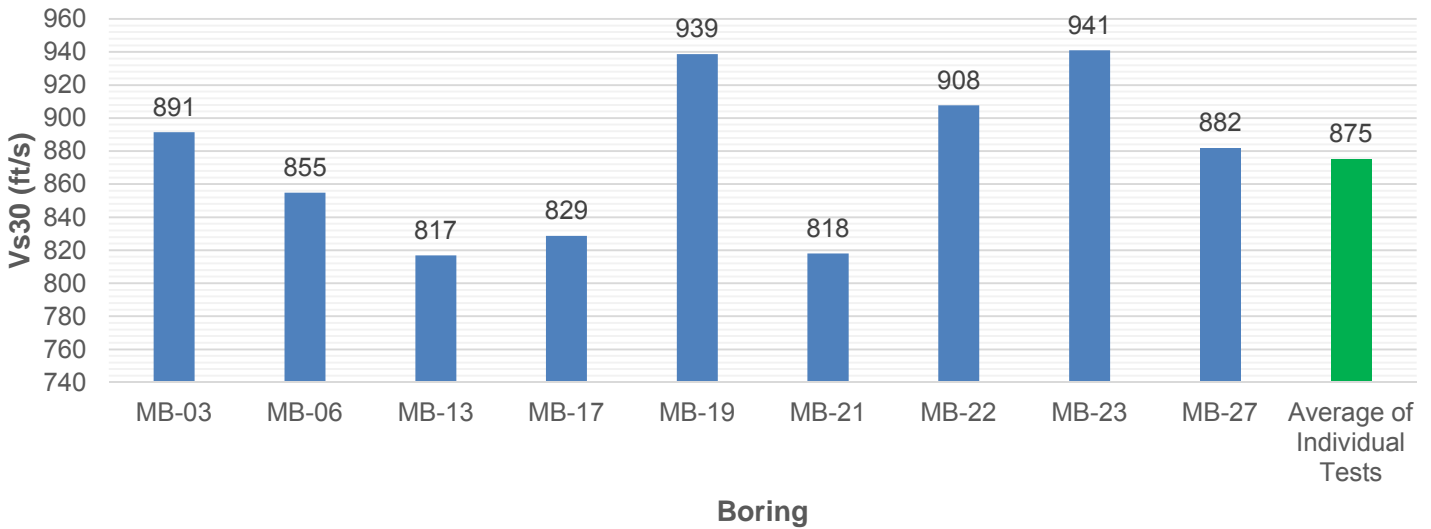


DEVELOPMENT OF SHEAR WAVE VELOCITY PROFILES FOR THE NEARSHORE LNG FACILITIES
LNG FACILITIES
ALASKA LNG PROJECT
NIKISKI, ALASKA

Phases 1&2 Onshore

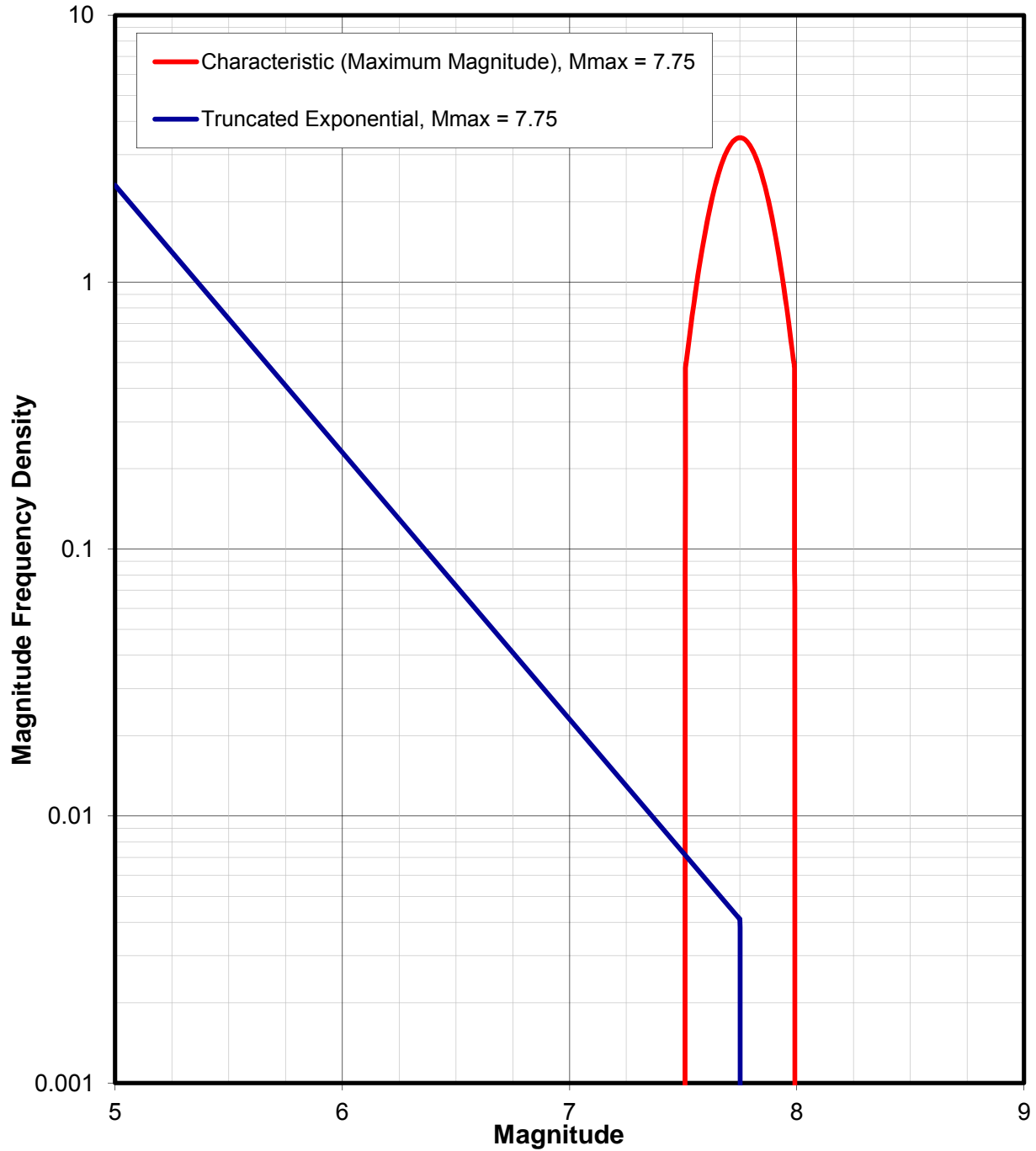


Phase 2 Nearshore



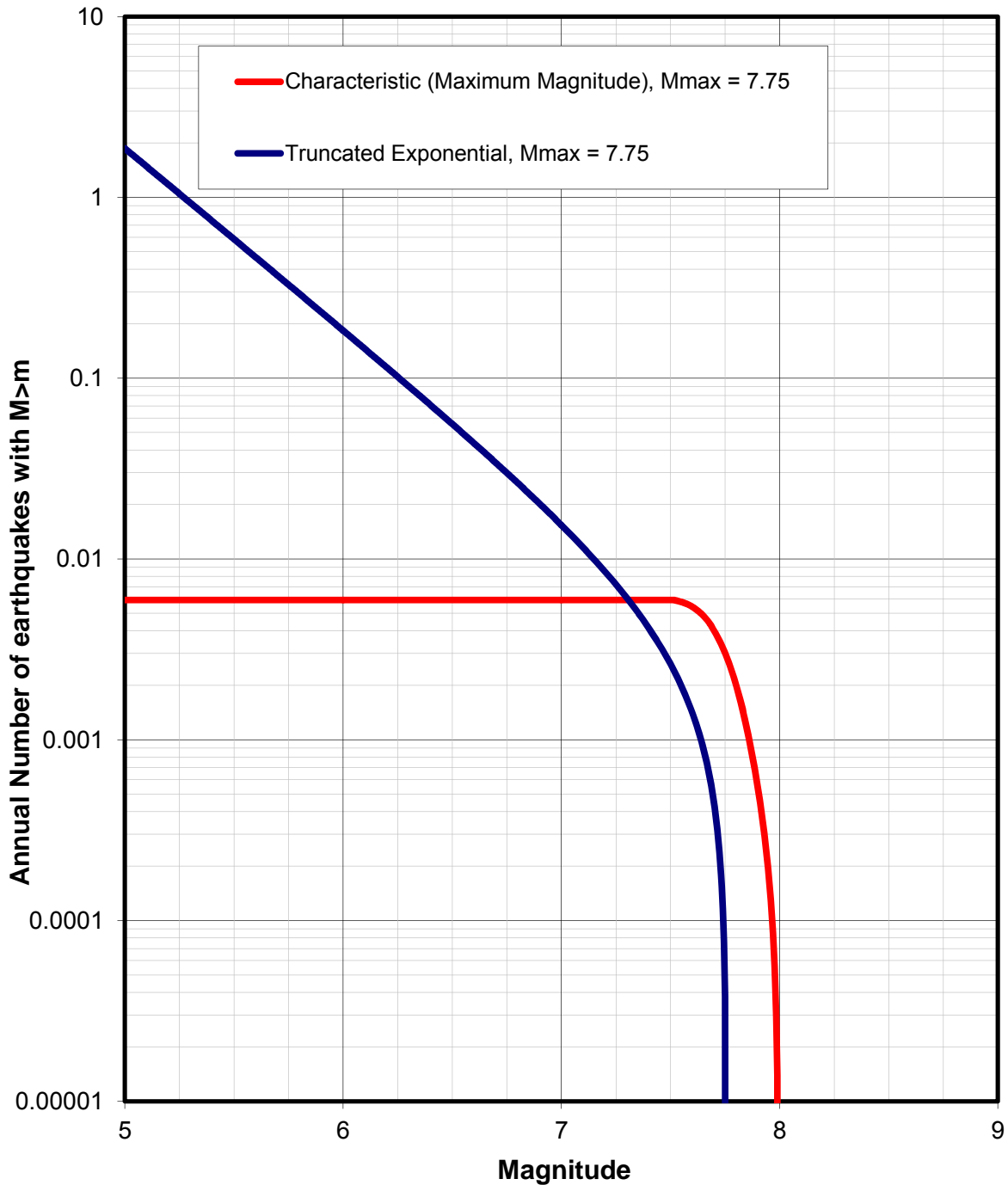
SUMMARY OF SHEAR WAVE VELOCITY DATA OBTAINED FROM DOWNHOLE SEISMIC SHEAR WAVE VELOCITY TESTS IN THE ONSHORE AND NEARSHORE PROJECT AREA DURING PHASES 1 AND 2

LNG FACILITIES
 ALASKA LNG PROJECT
 NIKISKI, ALASKA



EXAMPLE MAGNITUDE PROBABILITY DENSITY FUNCTIONS

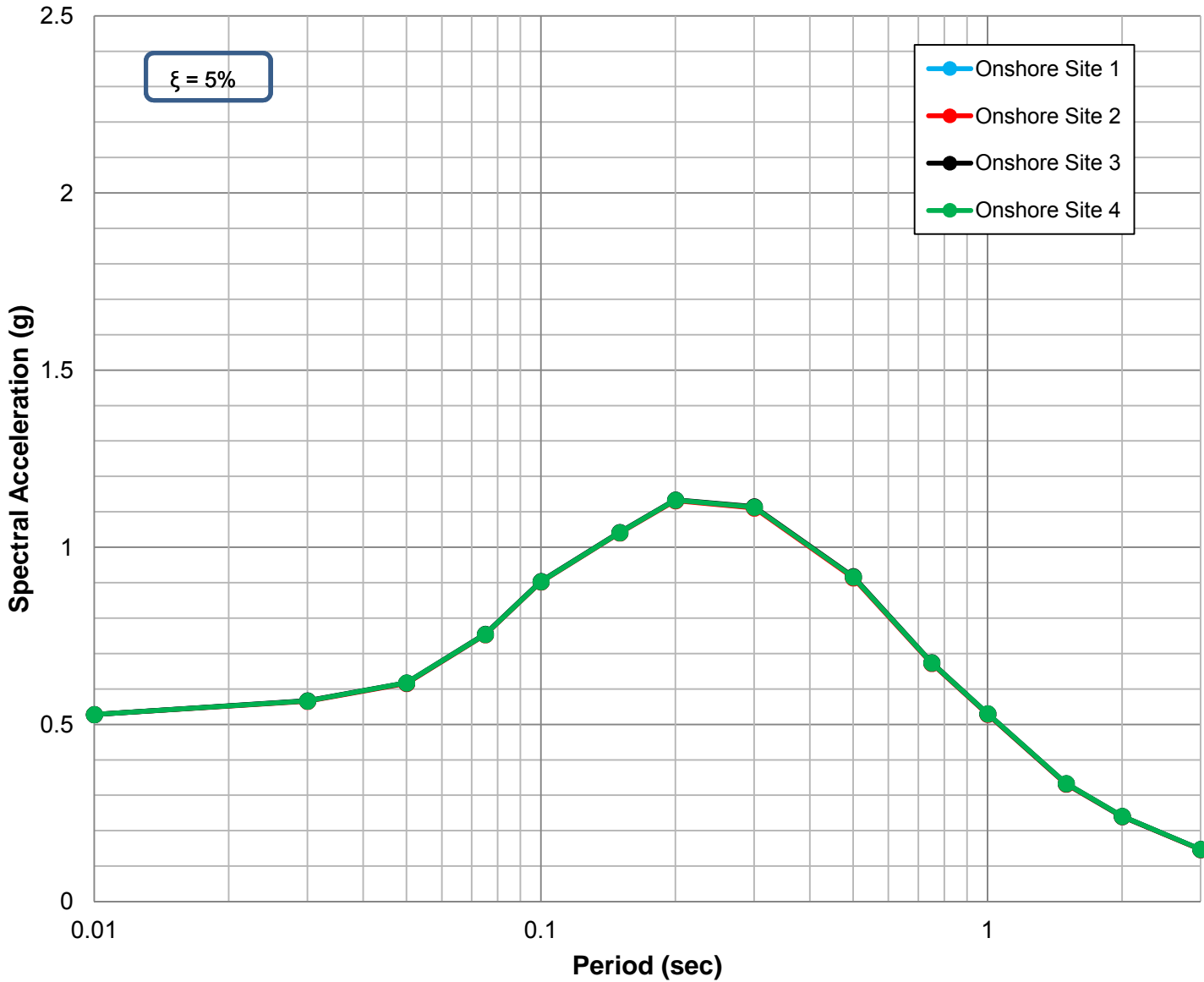
LNG FACILITIES
ALASKA LNG PROJECT
NIKISKI, ALASKA



EXAMPLE ANNUAL RECURRENCE PREDICTED BY DIFFERENT MAGNITUDE PDF MODELS

LNG FACILITIES
ALASKA LNG PROJECT
NIKISKI, ALASKA

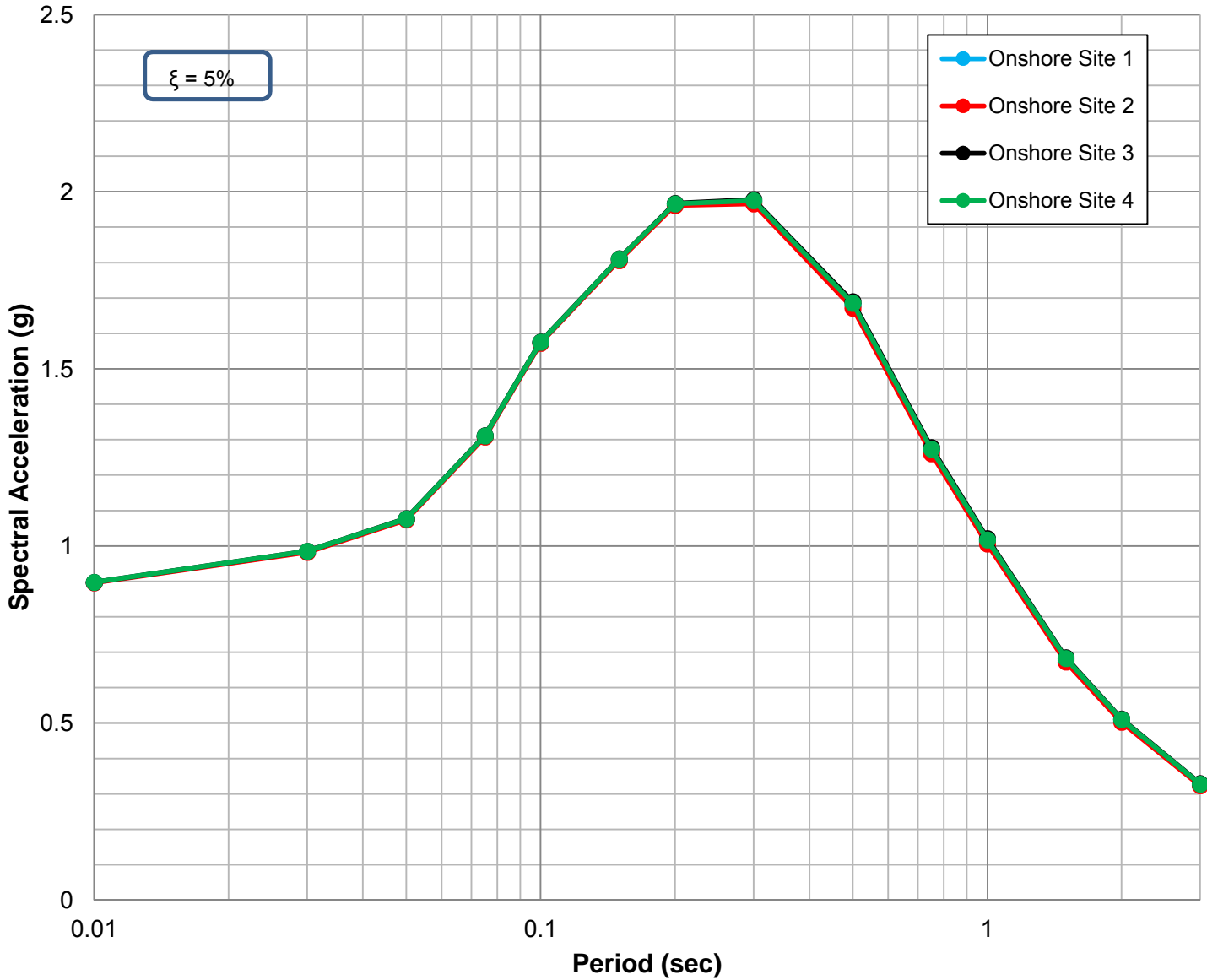
475-Year



475-YEAR RETURN PERIOD HORIZONTAL ACCELERATION RESPONSE SPECTRA ESTIMATED FOR THE REPRESENTATIVE ONSHORE LOCATIONS (VS30 = 885 FT/S)

LNG FACILITIES
ALASKA LNG PROJECT
NIKISKI, ALASKA

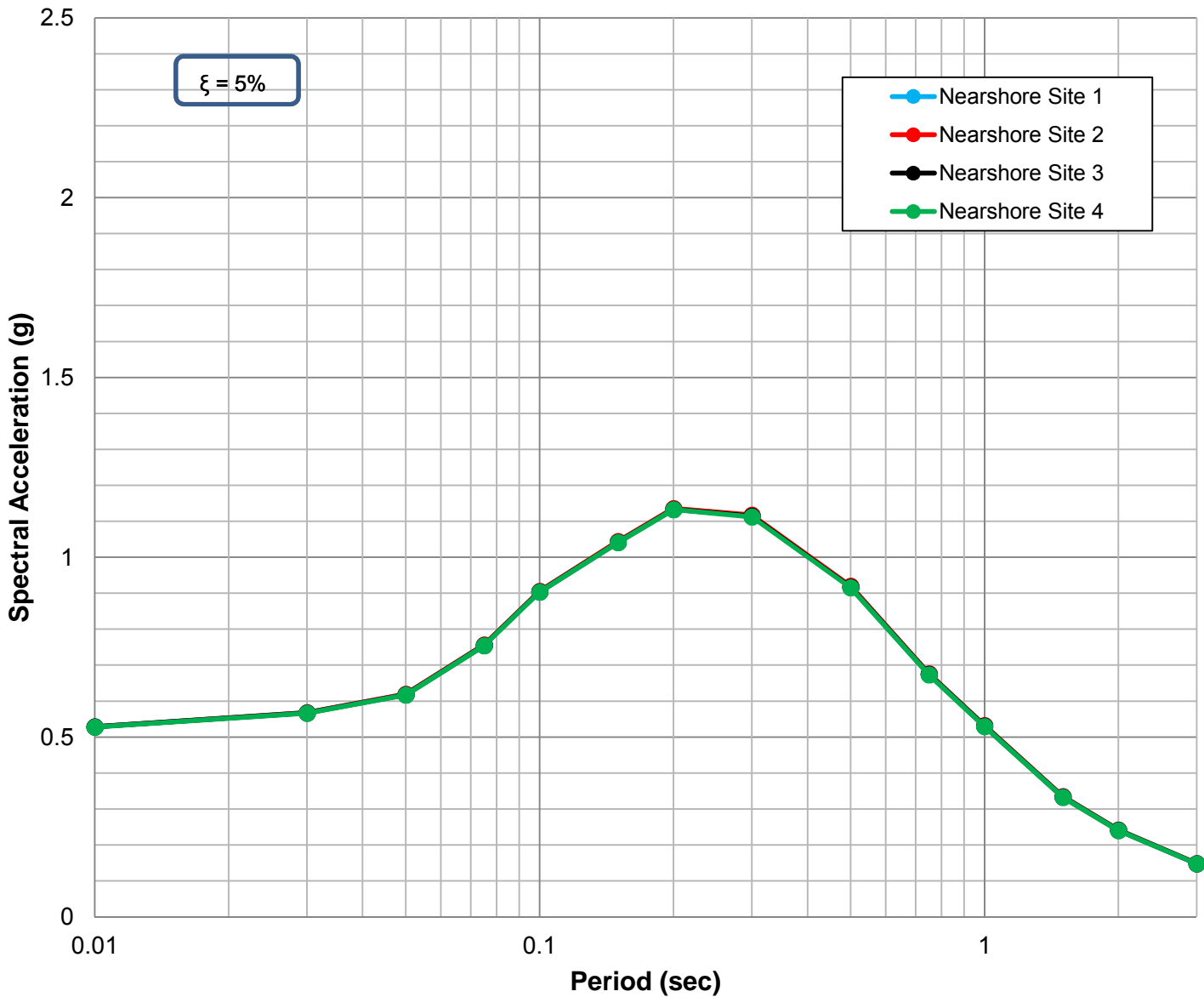
2475-Year



2475-YEAR RETURN PERIOD HORIZONTAL ACCELERATION RESPONSE SPECTRA ESTIMATED FOR THE REPRESENTATIVE ONSHORE LOCATIONS (VS30 = 885 FT/S)

LNG FACILITIES
ALASKA LNG PROJECT
NIKISKI, ALASKA

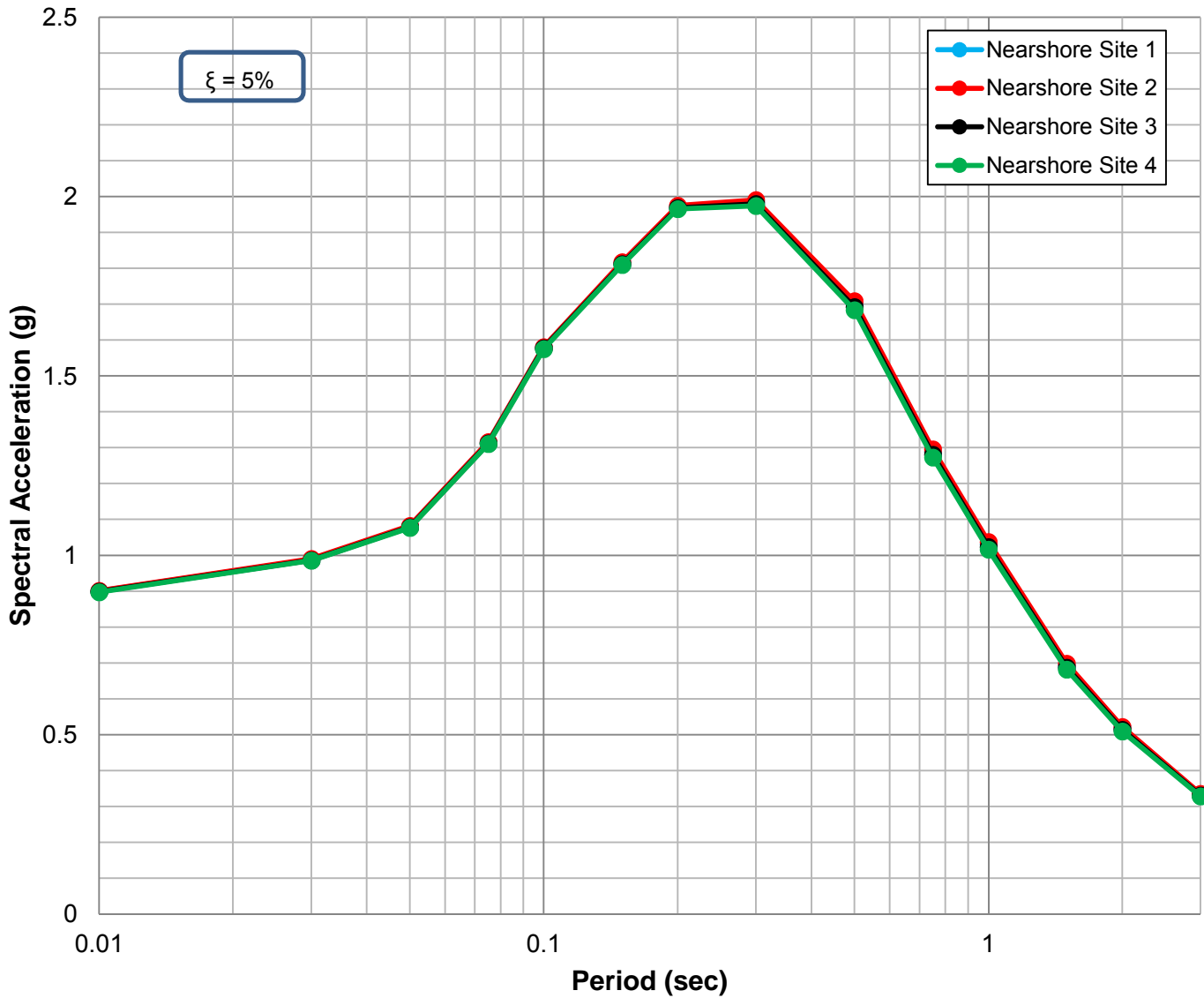
475-Year



475-YEAR RETURN PERIOD HORIZONTAL ACCELERATION RESPONSE SPECTRA ESTIMATED FOR THE REPRESENTATIVE NEARSHORE LOCATIONS (VS30 = 885 FT/S)

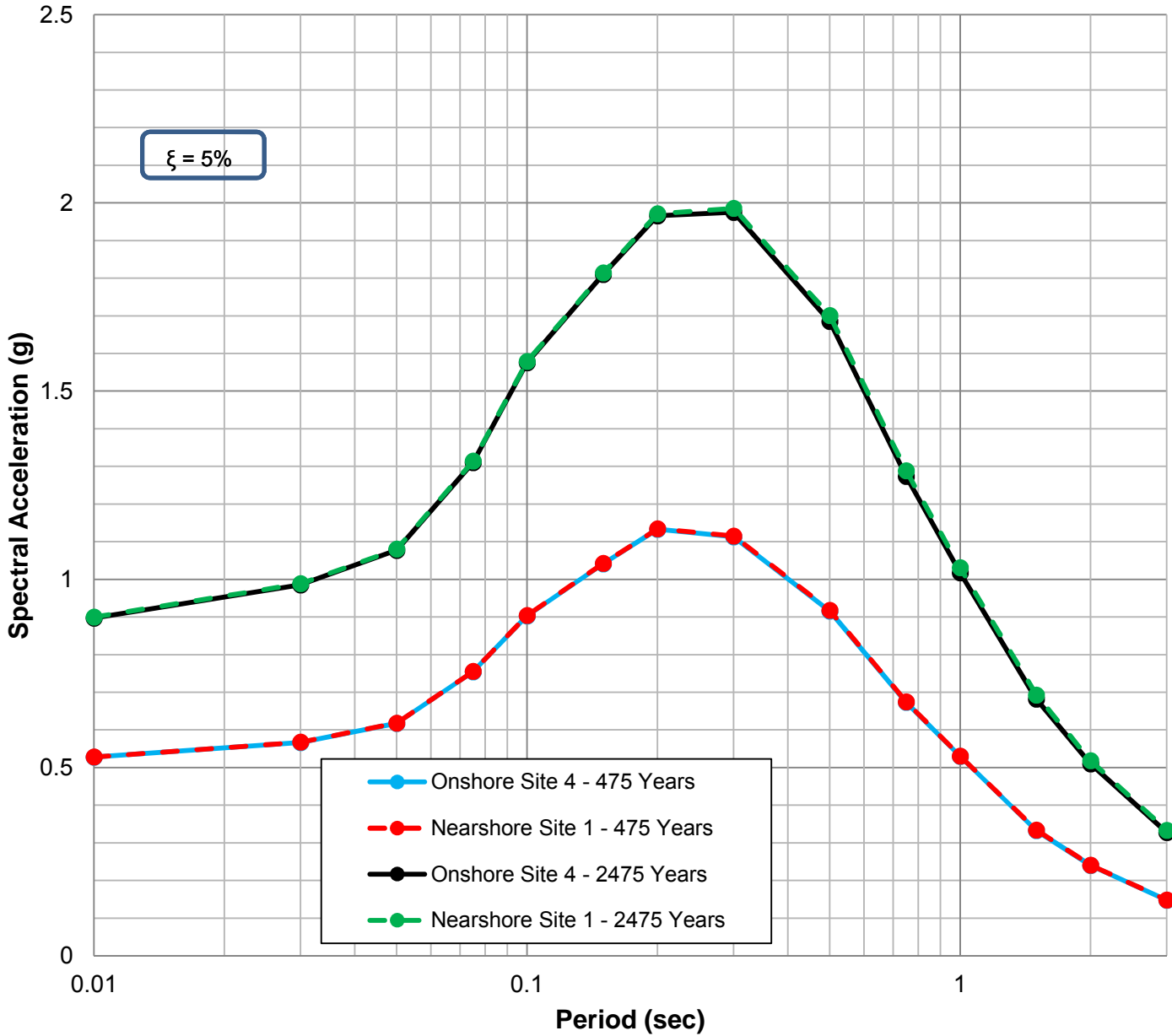
LNG FACILITIES
ALASKA LNG PROJECT
NIKISKI, ALASKA

2475-Year



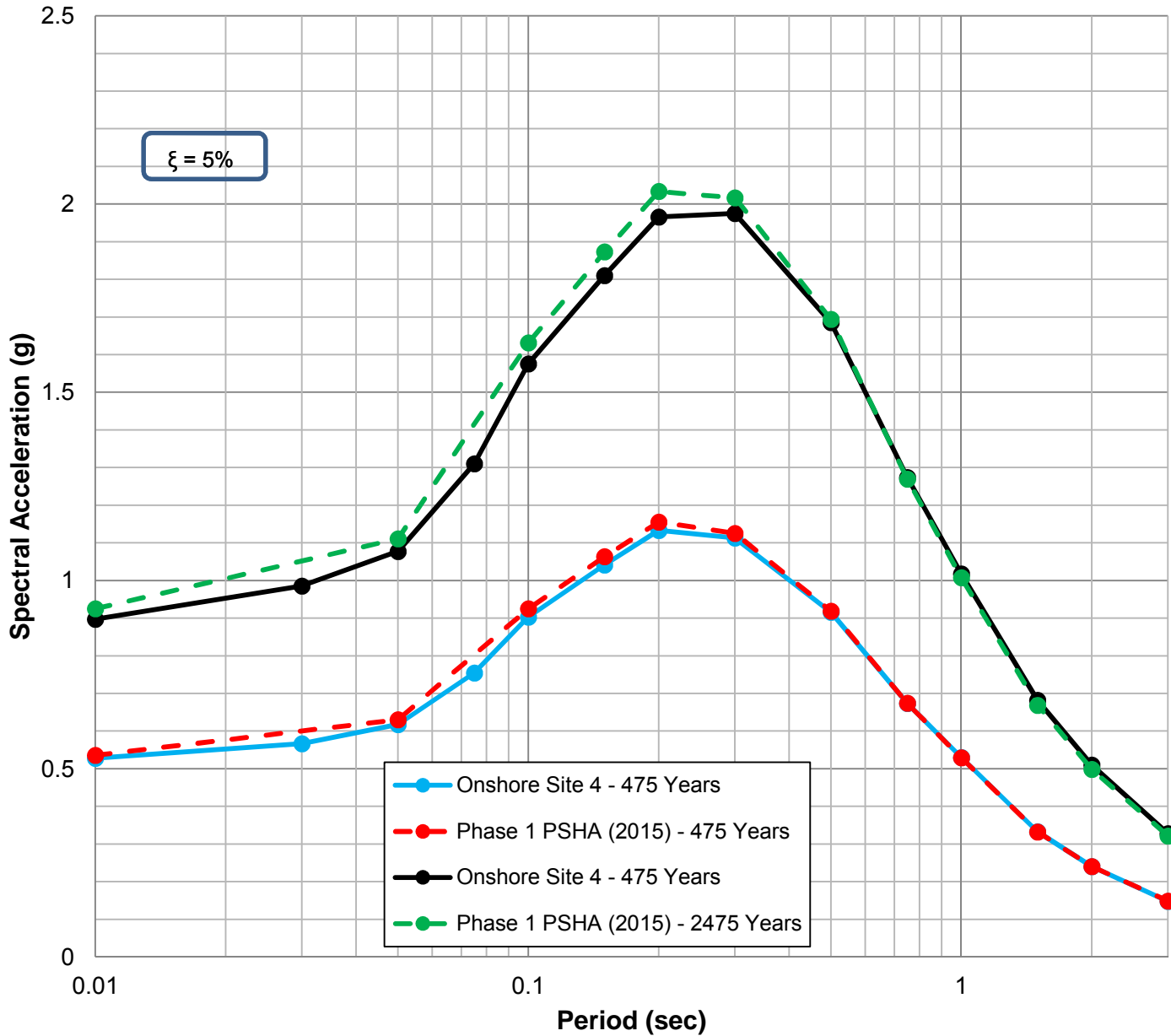
2475-YEAR RETURN PERIOD HORIZONTAL ACCELERATION RESPONSE SPECTRA ESTIMATED FOR THE REPRESENTATIVE NEARSHORE LOCATIONS (VS30 = 885 FT/S)

LNG FACILITIES
ALASKA LNG PROJECT
NIKISKI, ALASKA



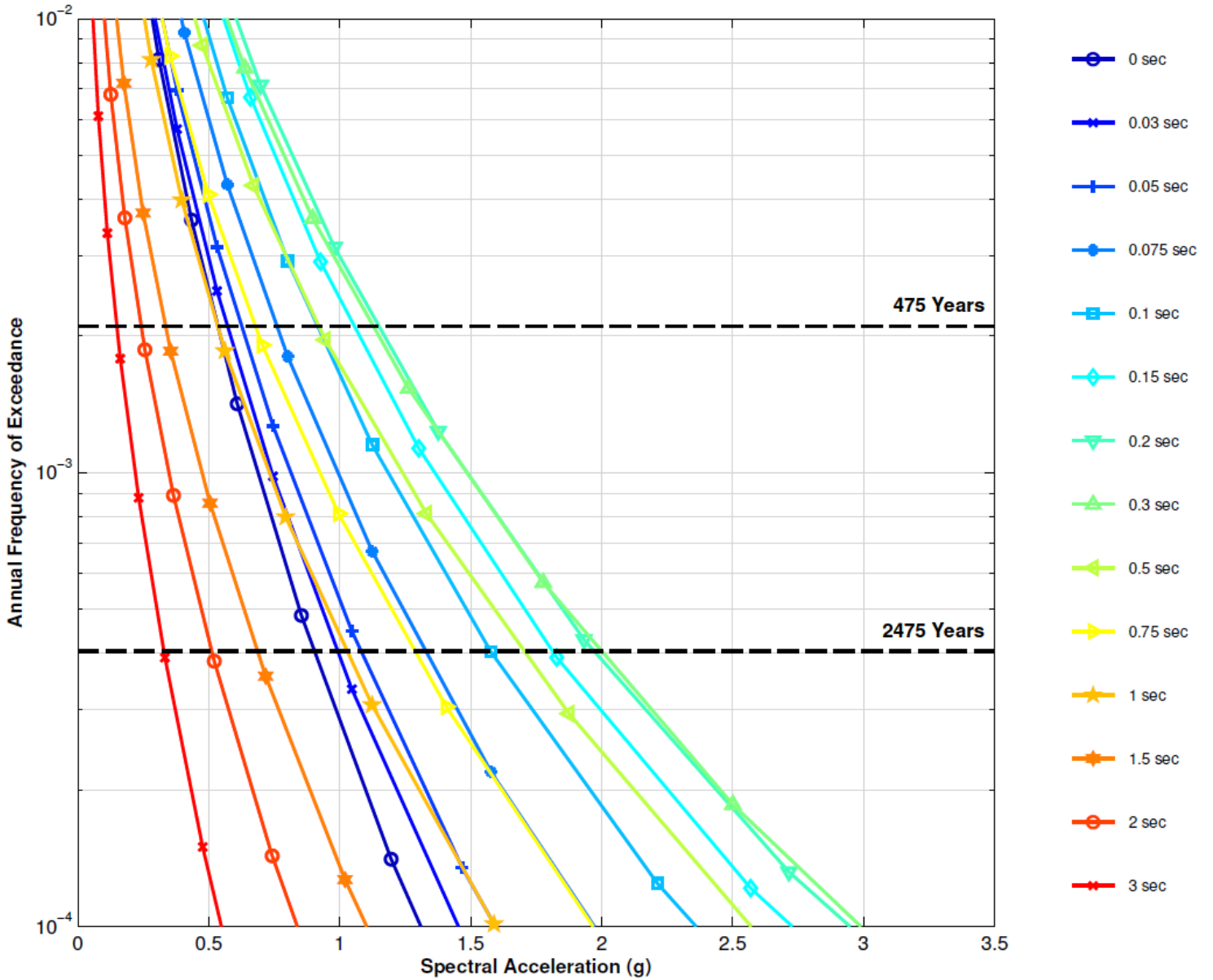
COMPARISON OF 475- AND 2475-YEAR RETURN PERIOD HORIZONTAL ACCELERATION RESPONSE SPECTRA ESTIMATED FOR THE REPRESENTATIVE ONSHORE AND NEARSHORE LOCATIONS (VS30 = 885 FT/S)

LNG FACILITIES
ALASKA LNG PROJECT
NIKISKI, ALASKA



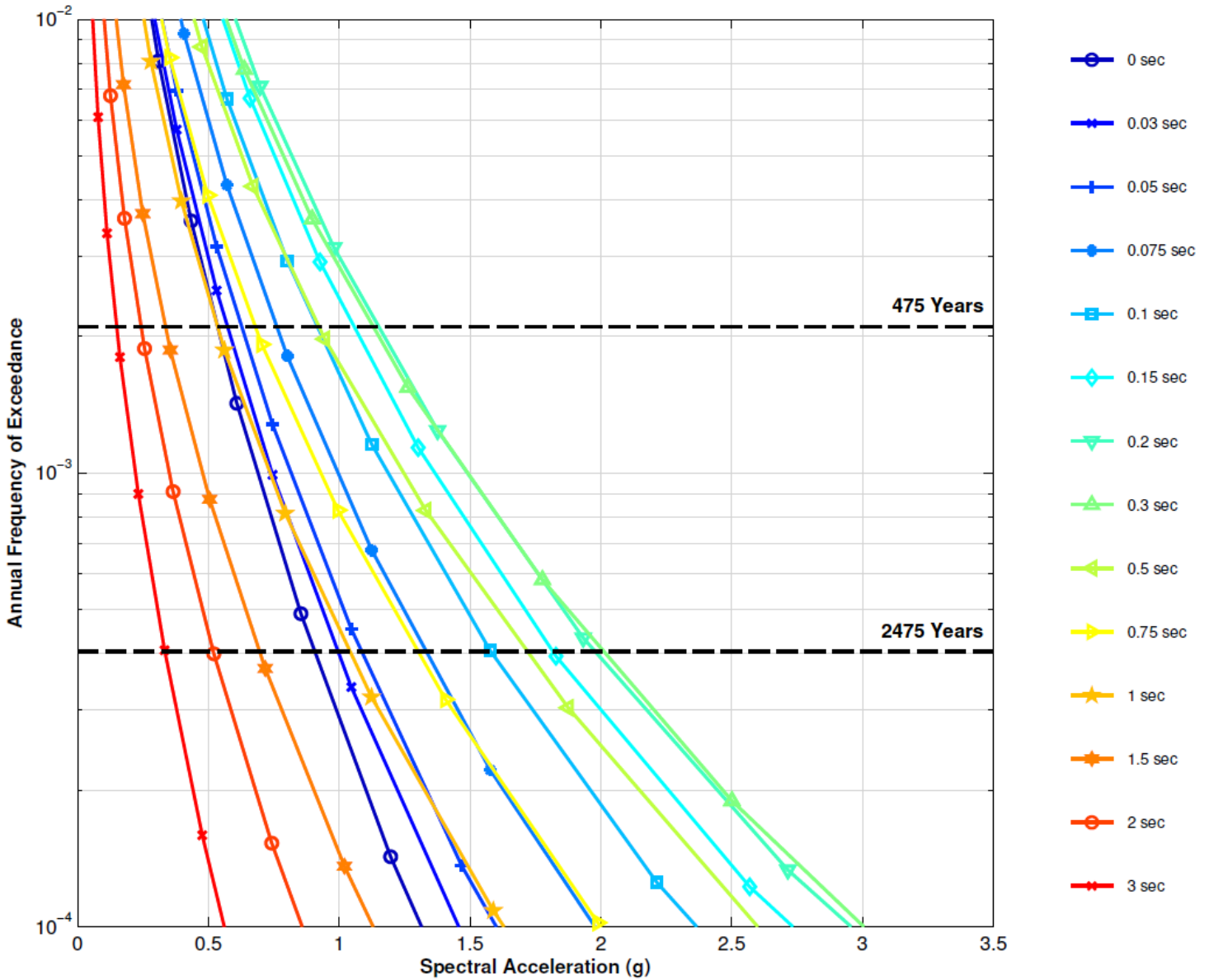
COMPARISON OF 475- AND 2475-YEAR RETURN PERIOD HORIZONTAL ACCELERATION RESPONSE SPECTRA ESTIMATED FOR THE REPRESENTATIVE ONSHORE LOCATION (VS30 = 885 FT/S) TO THE PHASE 1 PSHA RESULTS (VS30 = 900 FT/S)

LNG FACILITIES
ALASKA LNG PROJECT
NIKISKI, ALASKA



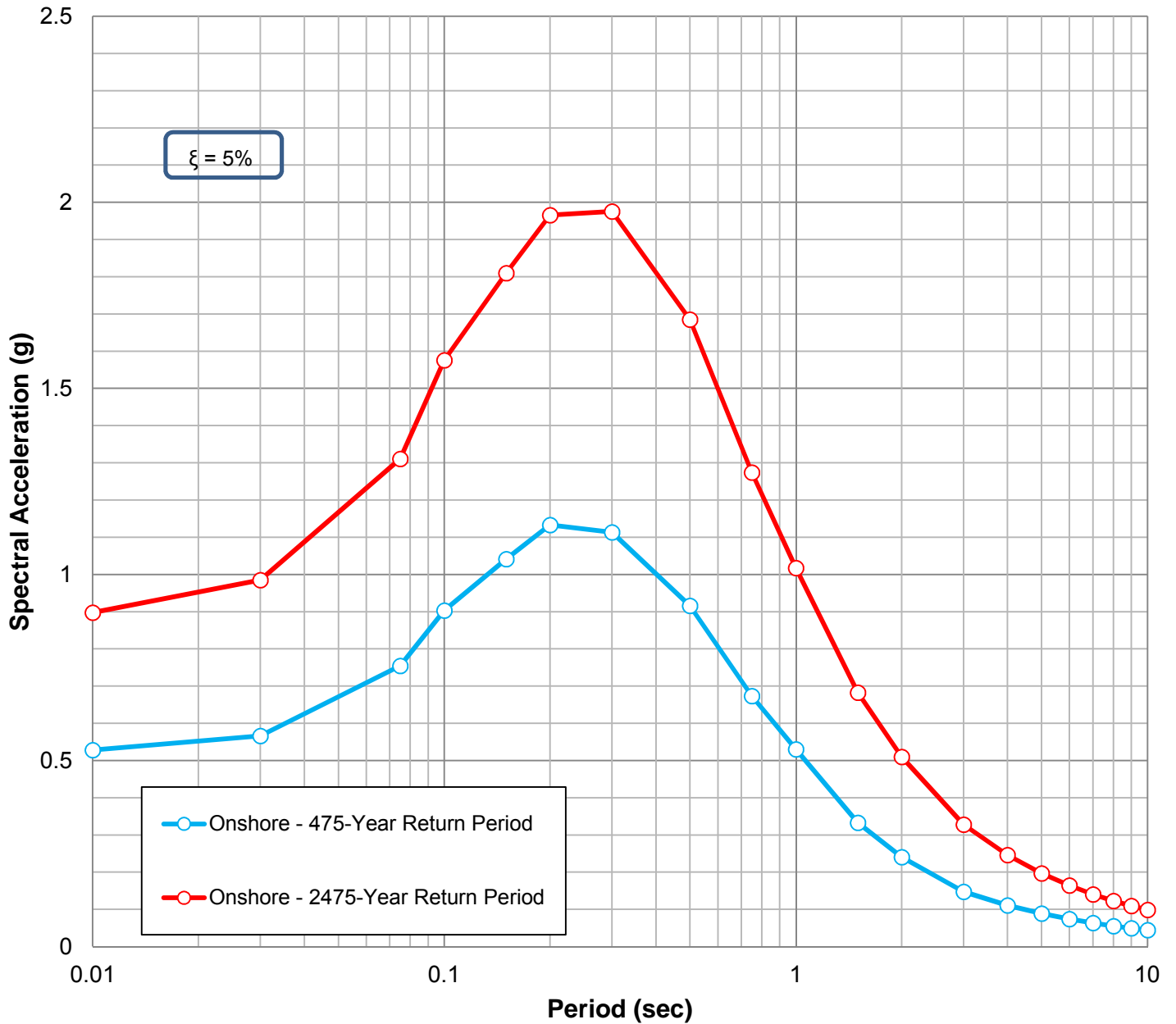
MEAN ANNUAL HAZARD CURVES AT DIFFERENT STRUCTURAL PERIODS FOR THE ONSHORE LOCATION - NO DIRECTIVITY (VS30 = 885 FT/S)

LNG FACILITIES
ALASKA LNG PROJECT
NIKISKI, ALASKA



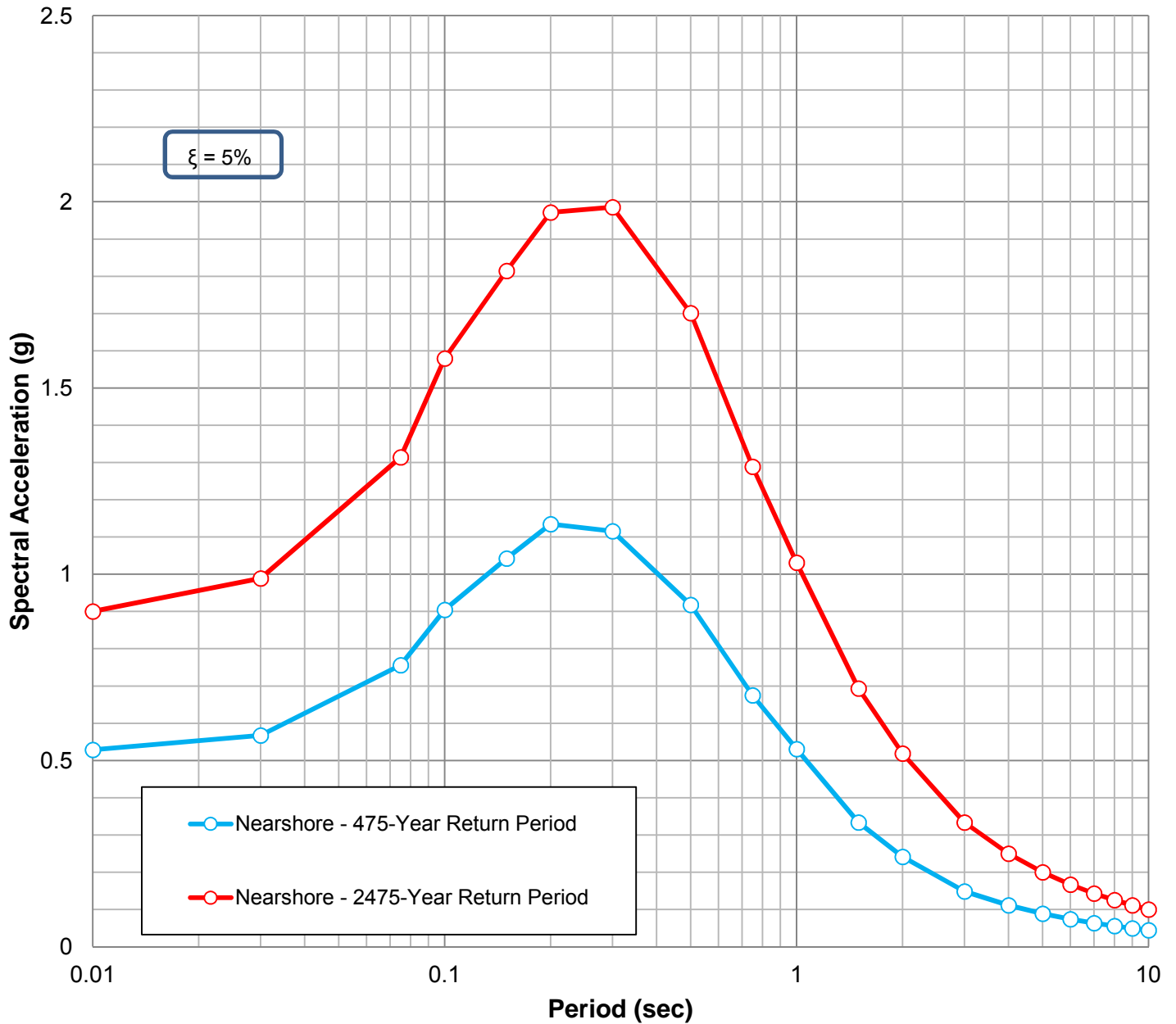
MEAN ANNUAL HAZARD CURVES AT DIFFERENT STRUCTURAL PERIODS FOR THE NEARSHORE LOCATION - NO DIRECTIVITY (VS30 = 885 FT/S)

LNG FACILITIES
ALASKA LNG PROJECT
NIKISKI, ALASKA



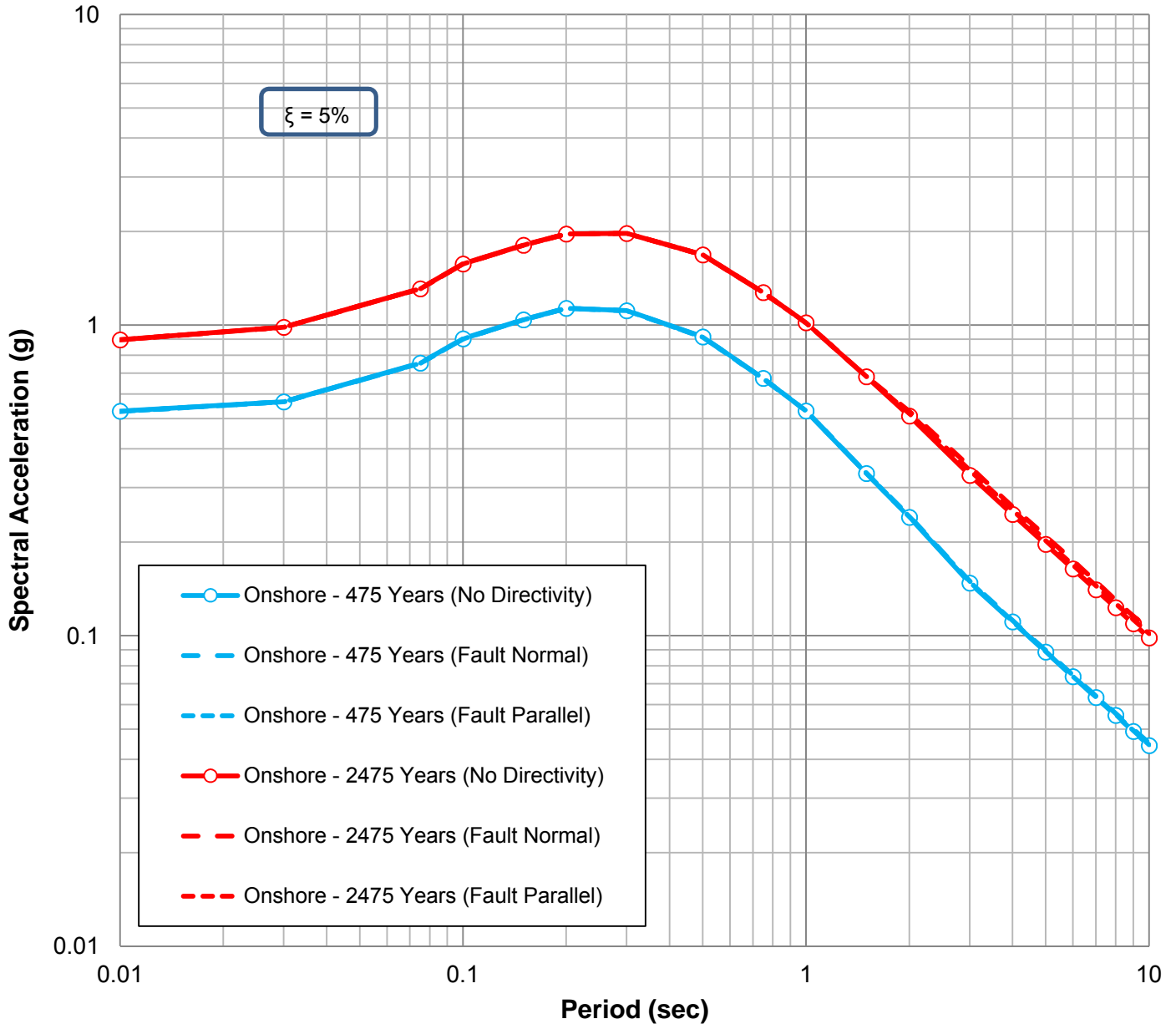
5-PERCENT DAMPED HORIZONTAL ACCELERATION RESPONSE SPECTRA FOR THE ONSHORE LOCATION FOR 475 AND 2475-YEAR RETURN PERIOD EVENTS - NO DIRECTIVITY (VS30 = 885 FT/S)

LNG FACILITIES
 ALASKA LNG PROJECT
 NIKISKI, ALASKA



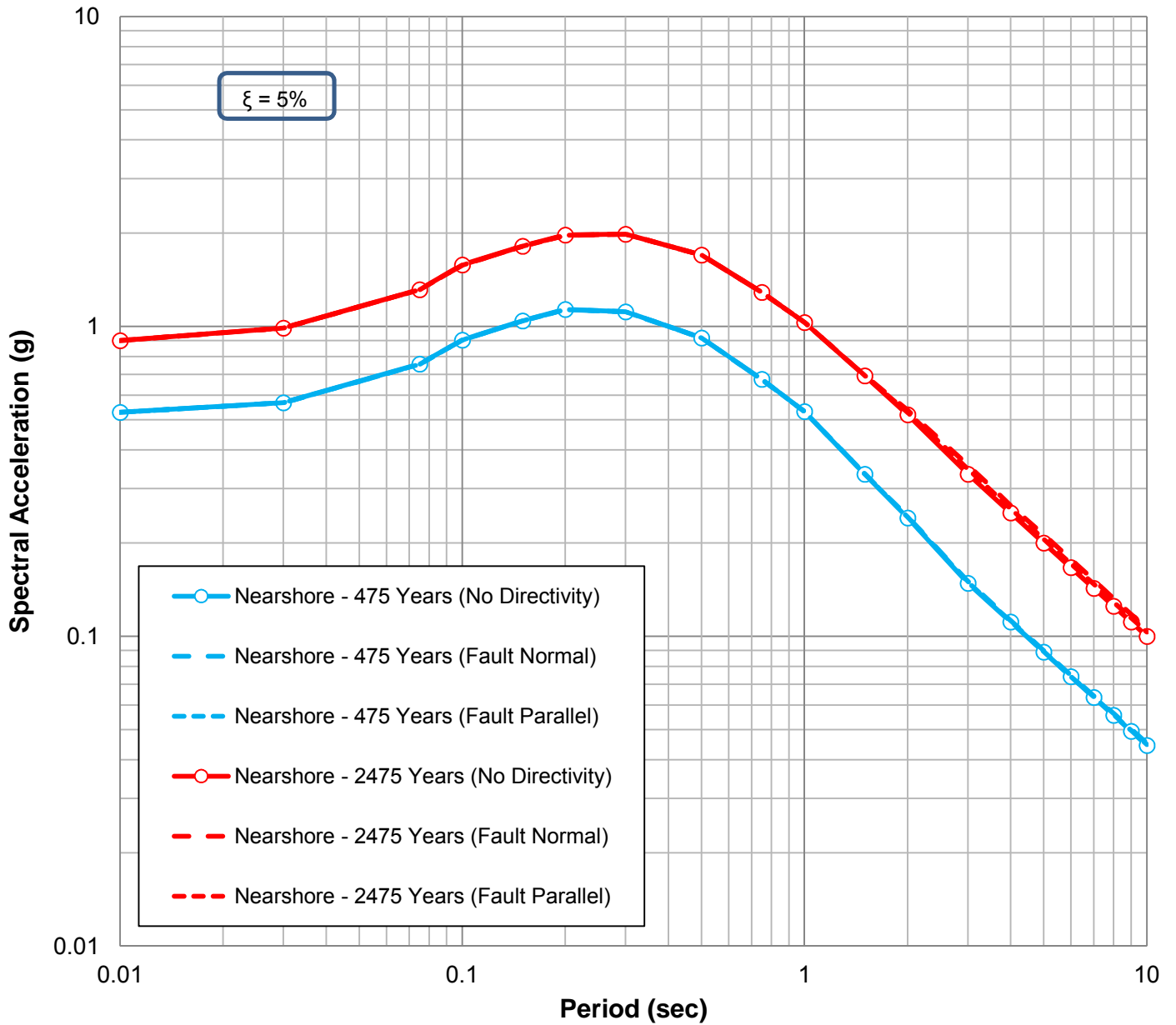
5-PERCENT DAMPED HORIZONTAL ACCELERATION RESPONSE SPECTRA FOR THE NEARSHORE LOCATION FOR 475 AND 2475-YEAR RETURN PERIOD EVENTS - NO DIRECTIVITY (VS30 = 885 FT/S)

LNG FACILITIES
ALASKA LNG PROJECT
NIKISKI, ALASKA



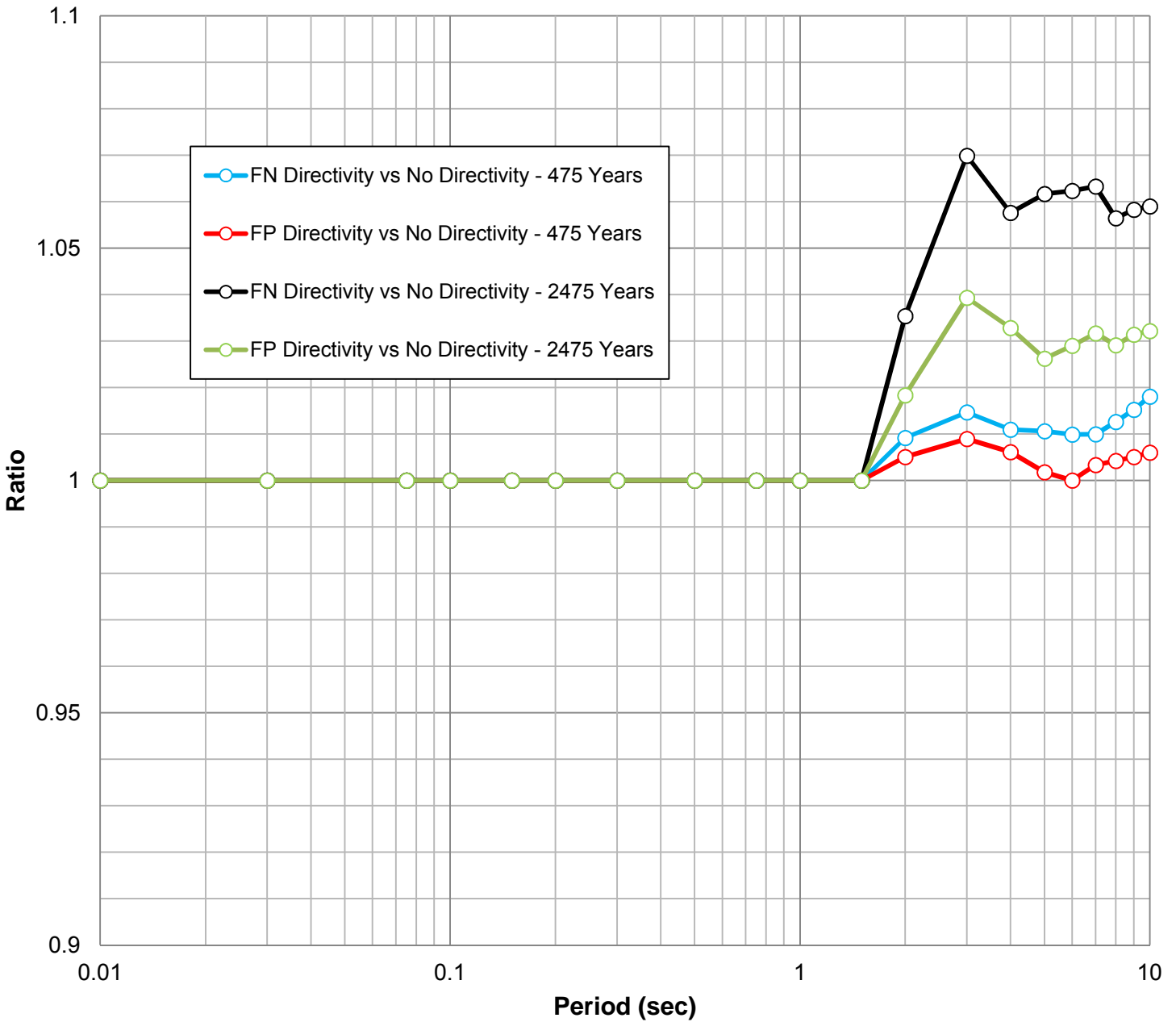
5-PERCENT DAMPED HORIZONTAL ACCELERATION RESPONSE SPECTRA FOR THE ONSHORE LOCATION FOR 475 AND 2475-YEAR RETURN PERIOD EVENTS - NO DIRECTIVITY (ND), FAULT NORMAL (FN) AND FAULT PARALLEL (FP) DIRECTIVITY EFFECTS (VS30 = 885 FT/S)

LNG FACILITIES
 ALASKA LNG PROJECT
 NIKISKI, ALASKA

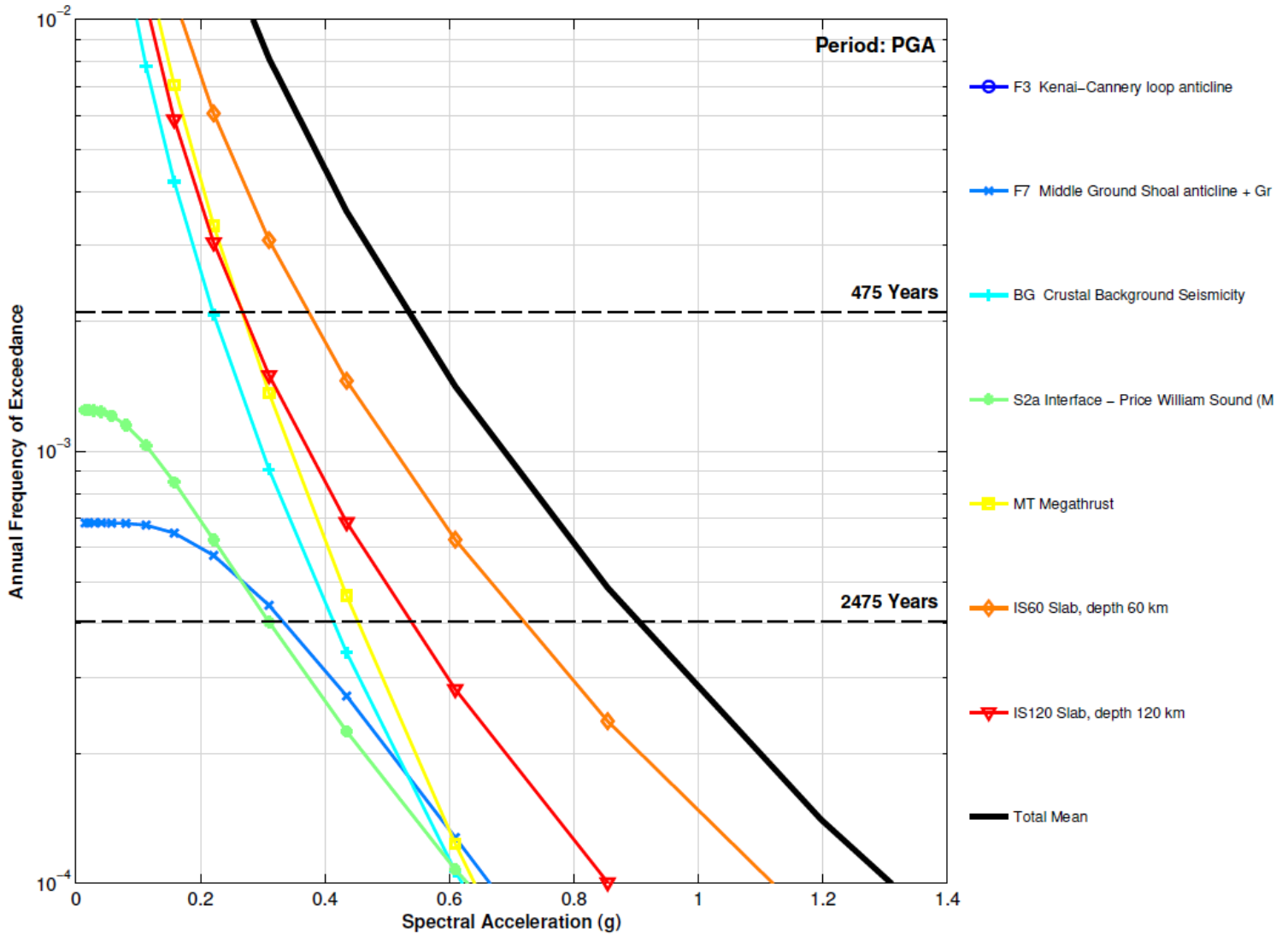


5-PERCENT DAMPED HORIZONTAL ACCELERATION RESPONSE SPECTRA FOR THE NEARSHORE LOCATION FOR 475 AND 2475-YEAR RETURN PERIOD EVENTS - NO DIRECTIVITY (ND), FAULT NORMAL (FN) AND FAULT PARALLEL (FP) DIRECTIVITY EFFECTS (VS30 = 885 FT/S)

LNG FACILITIES
 ALASKA LNG PROJECT
 NIKISKI, ALASKA

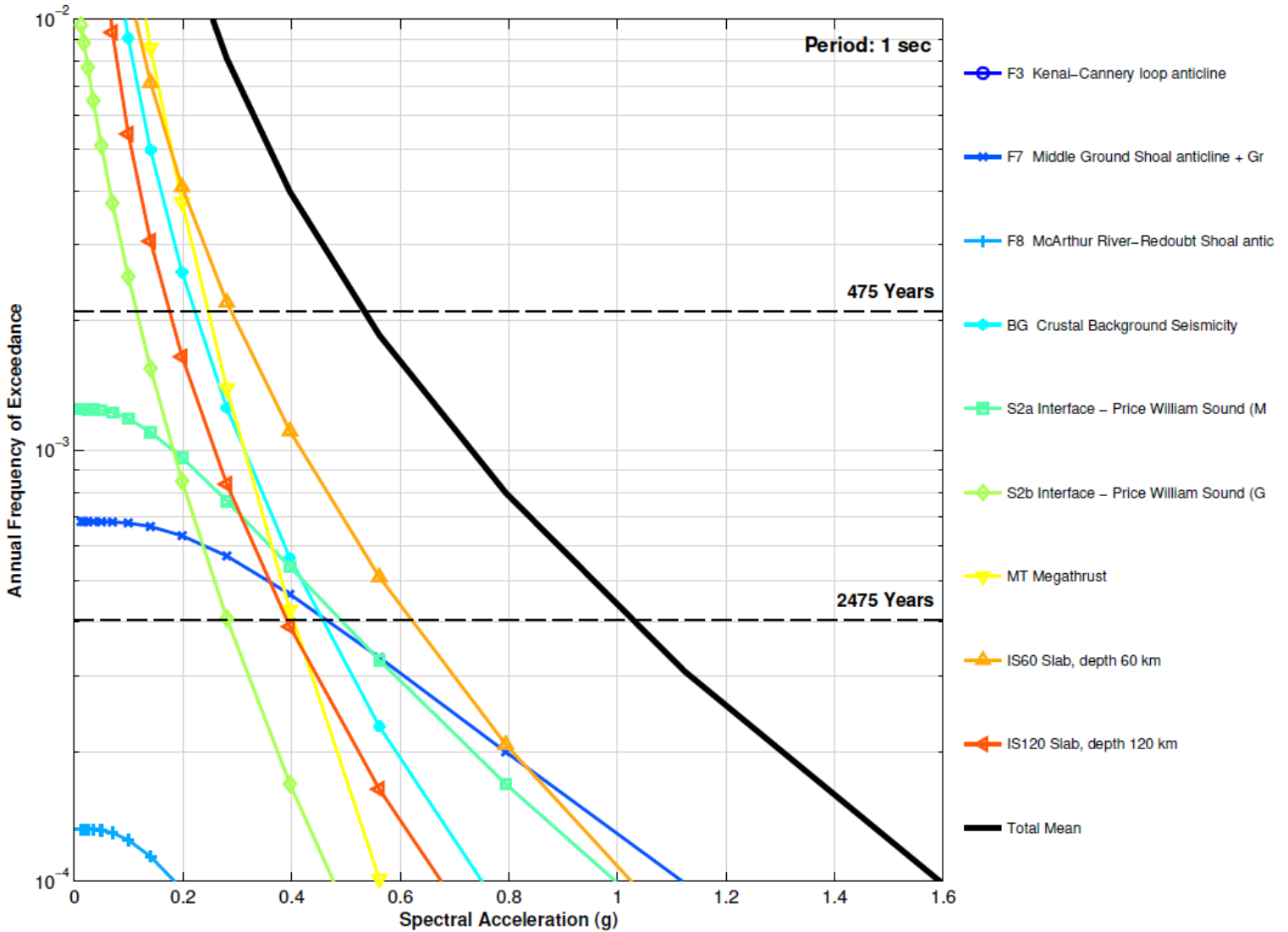


FN/ND AND FP/ND RATIOS FOR 475 AND 2475 YEARS
 LNG FACILITIES
 ALASKA LNG PROJECT
 NIKISKI, ALASKA



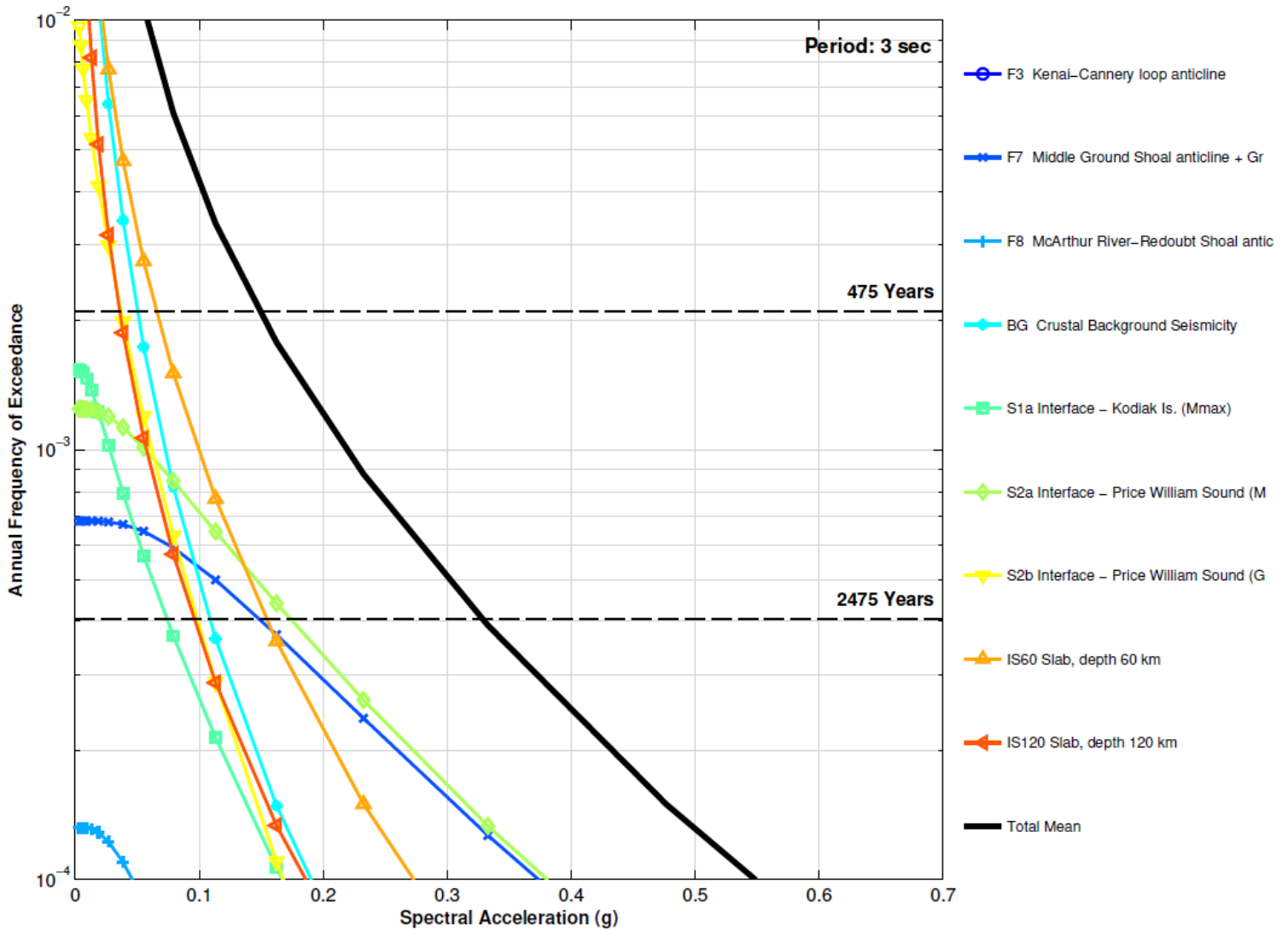
ANNUAL HAZARD CURVES PER SEISMIC SOURCE AT PGA - ONSHORE LOCATION (VS30 = 885 FT/S)

LNG FACILITIES
ALASKA LNG PROJECT
NIKISKI, ALASKA



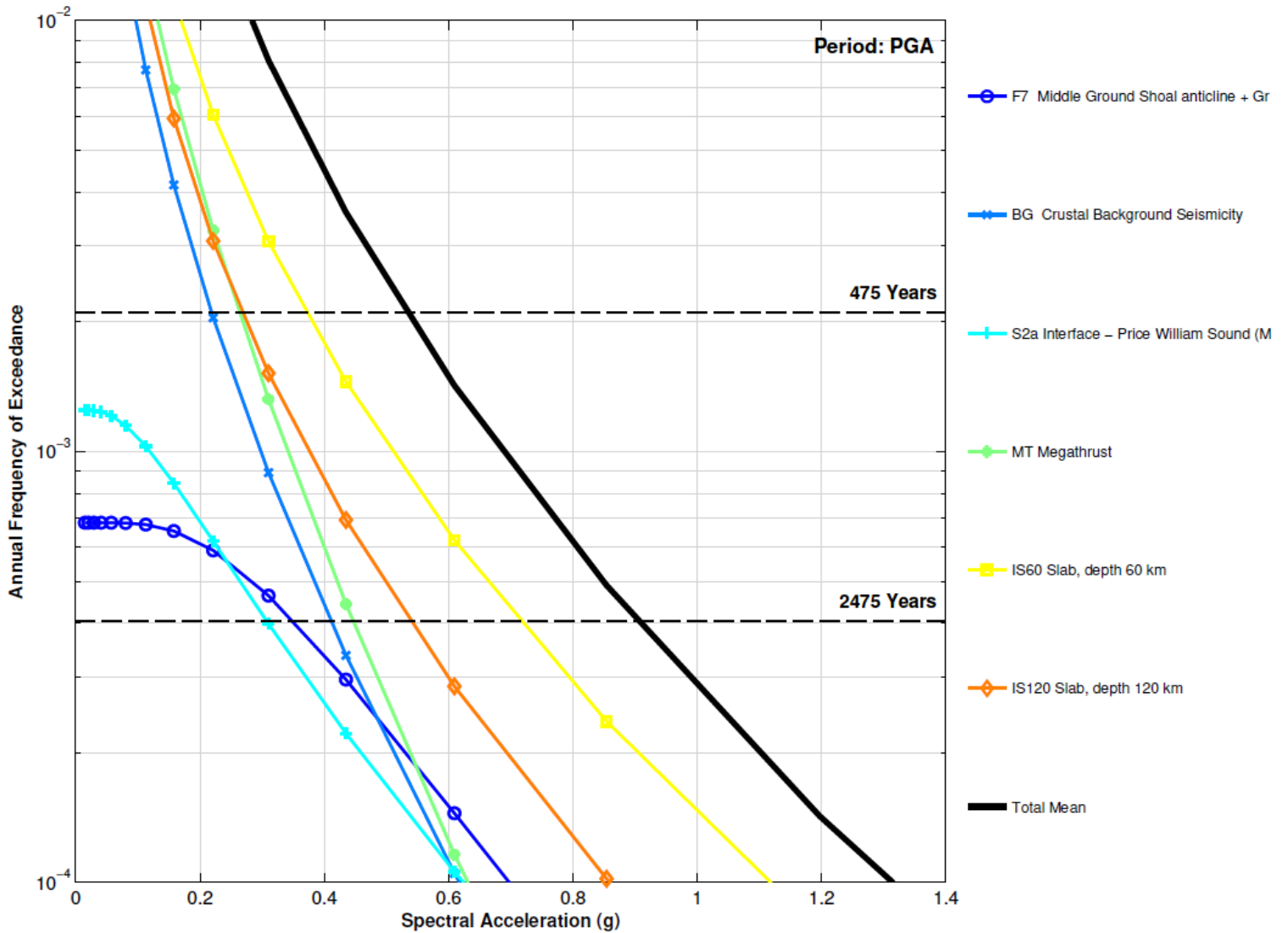
ANNUAL HAZARD CURVES PER SEISMIC SOURCE AT 1 SEC - ONSHORE LOCATION (VS30 = 885 FT/S)

LNG FACILITIES
 ALASKA LNG PROJECT
 NIKISKI, ALASKA



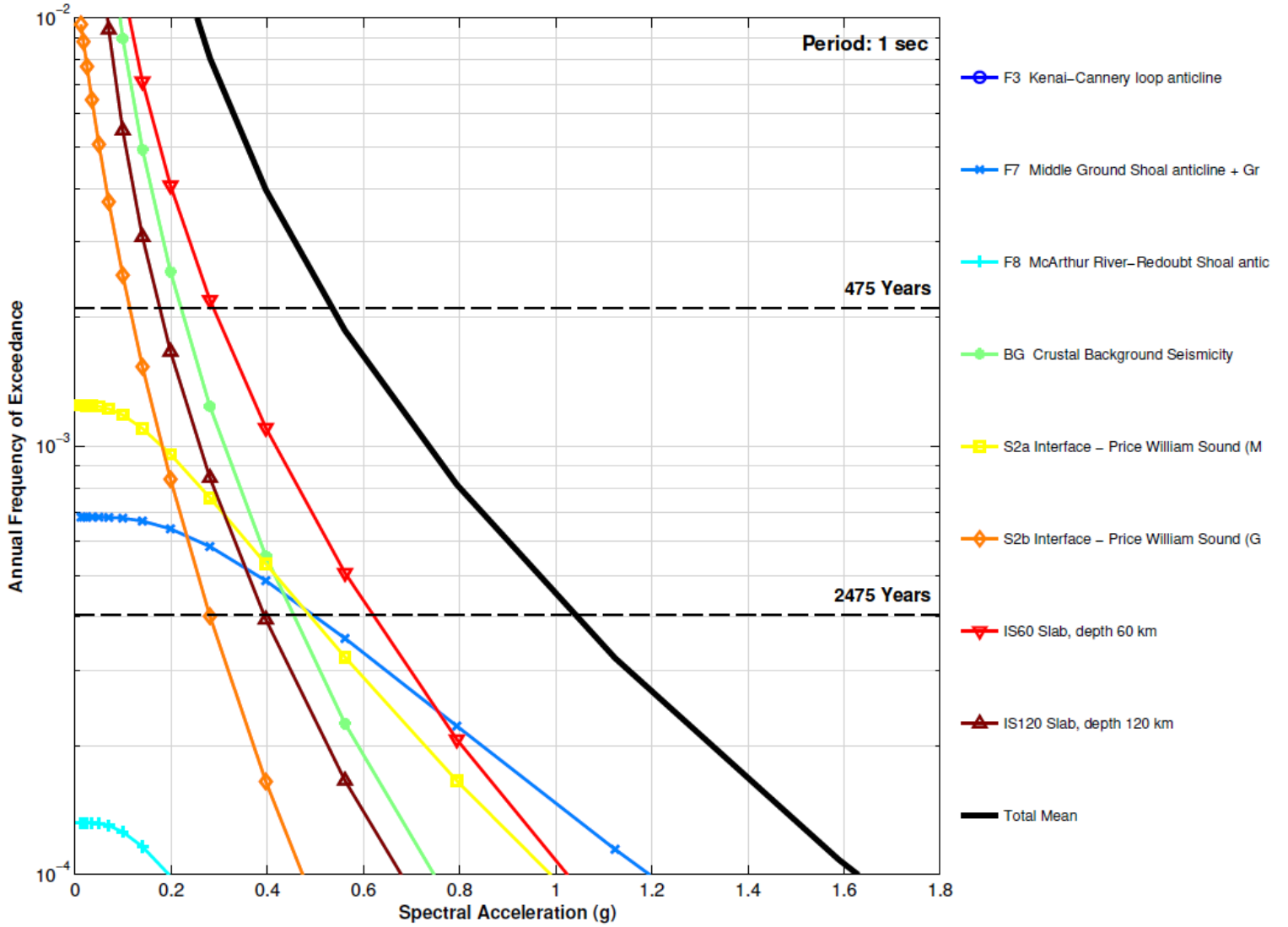
ANNUAL HAZARD CURVES PER SEISMIC SOURCE AT 3 SEC - ONSHORE LOCATION (VS30 = 885 FT/S)

LNG FACILITIES
 ALASKA LNG PROJECT
 NIKISKI, ALASKA



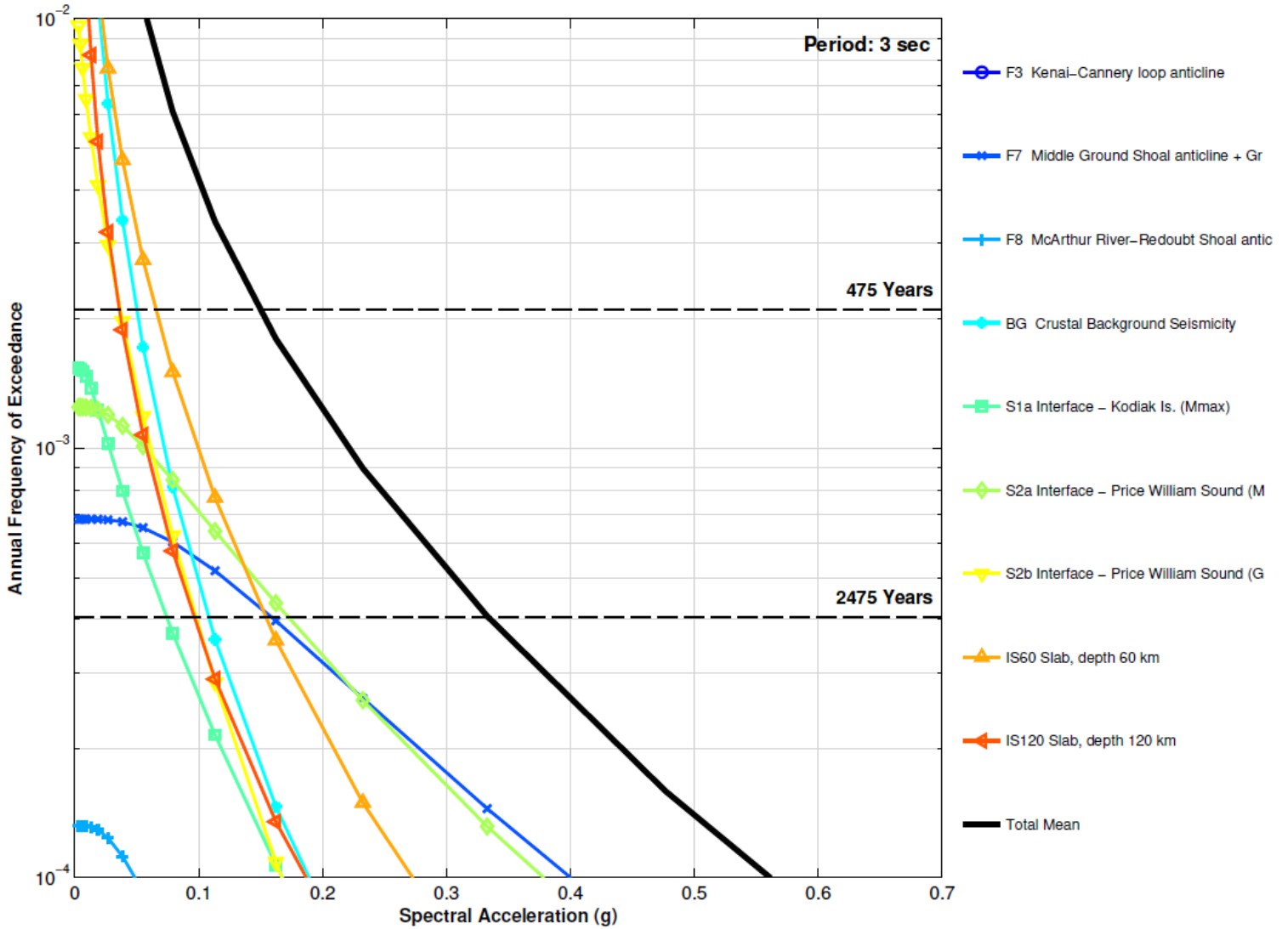
ANNUAL HAZARD CURVES PER SEISMIC SOURCE AT PGA - NEARSHORE LOCATION (VS30 = 885 FT/S)

LNG FACILITIES
ALASKA LNG PROJECT
NIKISKI, ALASKA



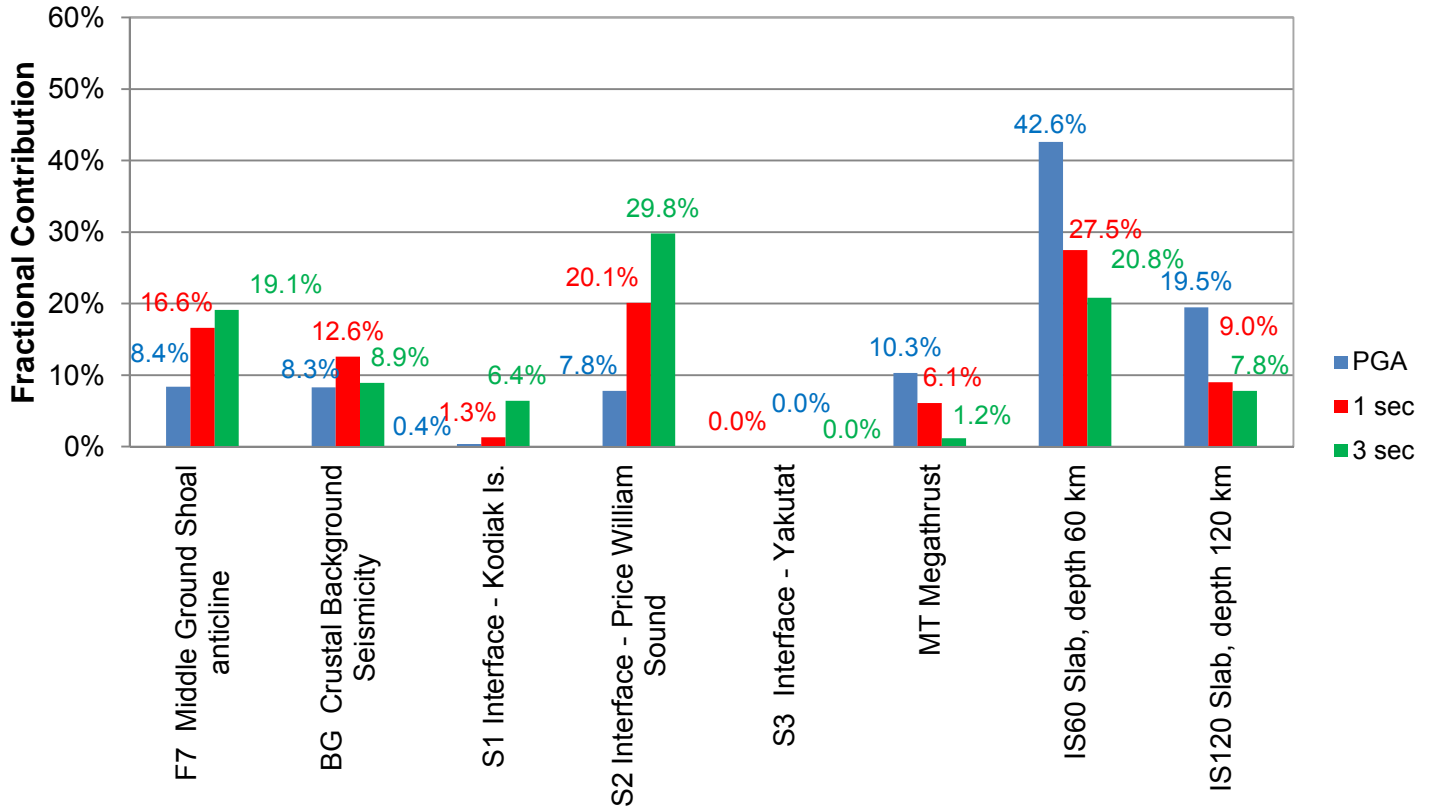
ANNUAL HAZARD CURVES PER SEISMIC SOURCE AT 1 SEC - NEARSHORE LOCATION (VS30 = 885 FT/S)

LNG FACILITIES
 ALASKA LNG PROJECT
 NIKISKI, ALASKA



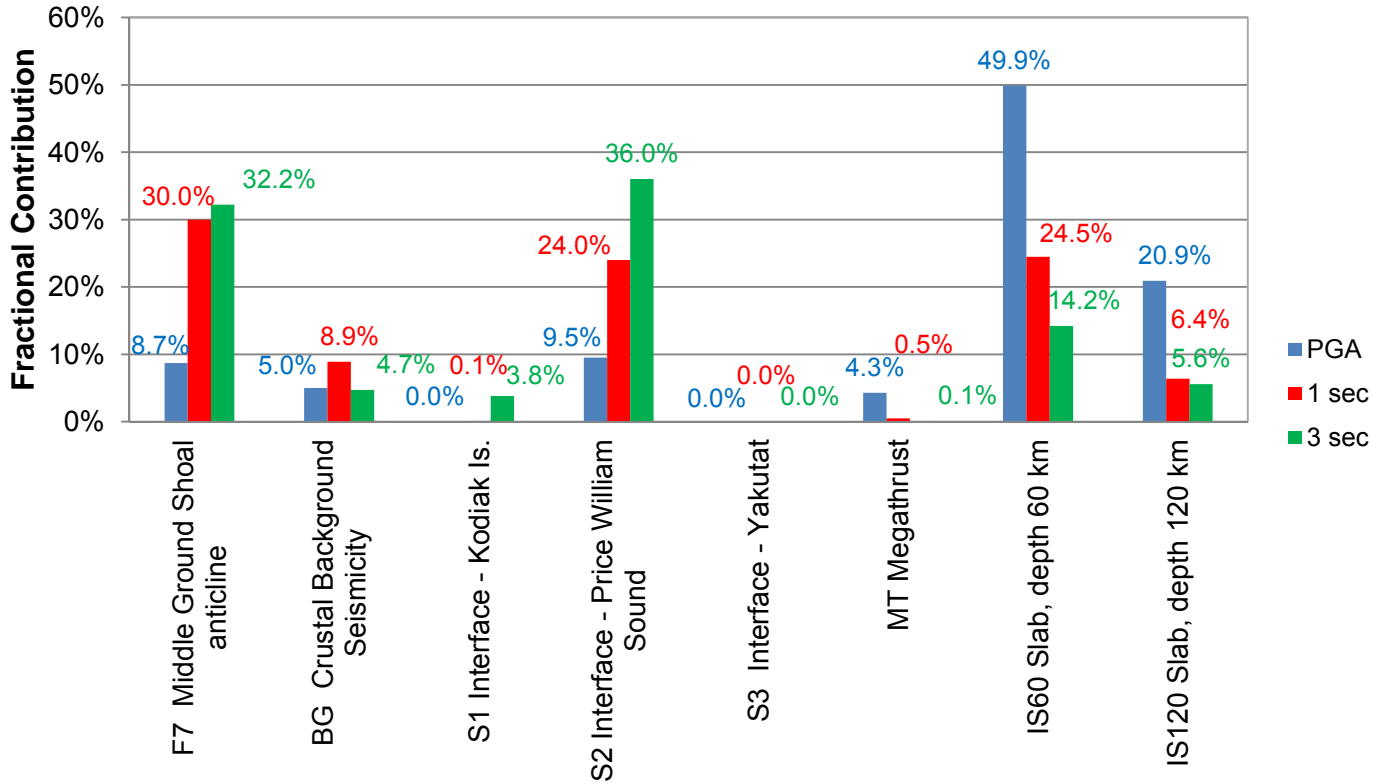
ANNUAL HAZARD CURVES PER SEISMIC SOURCE AT 3 SEC - NEARSHORE LOCATION (VS30 = 885 FT/S)

LNG FACILITIES
 ALASKA LNG PROJECT
 NIKISKI, ALASKA



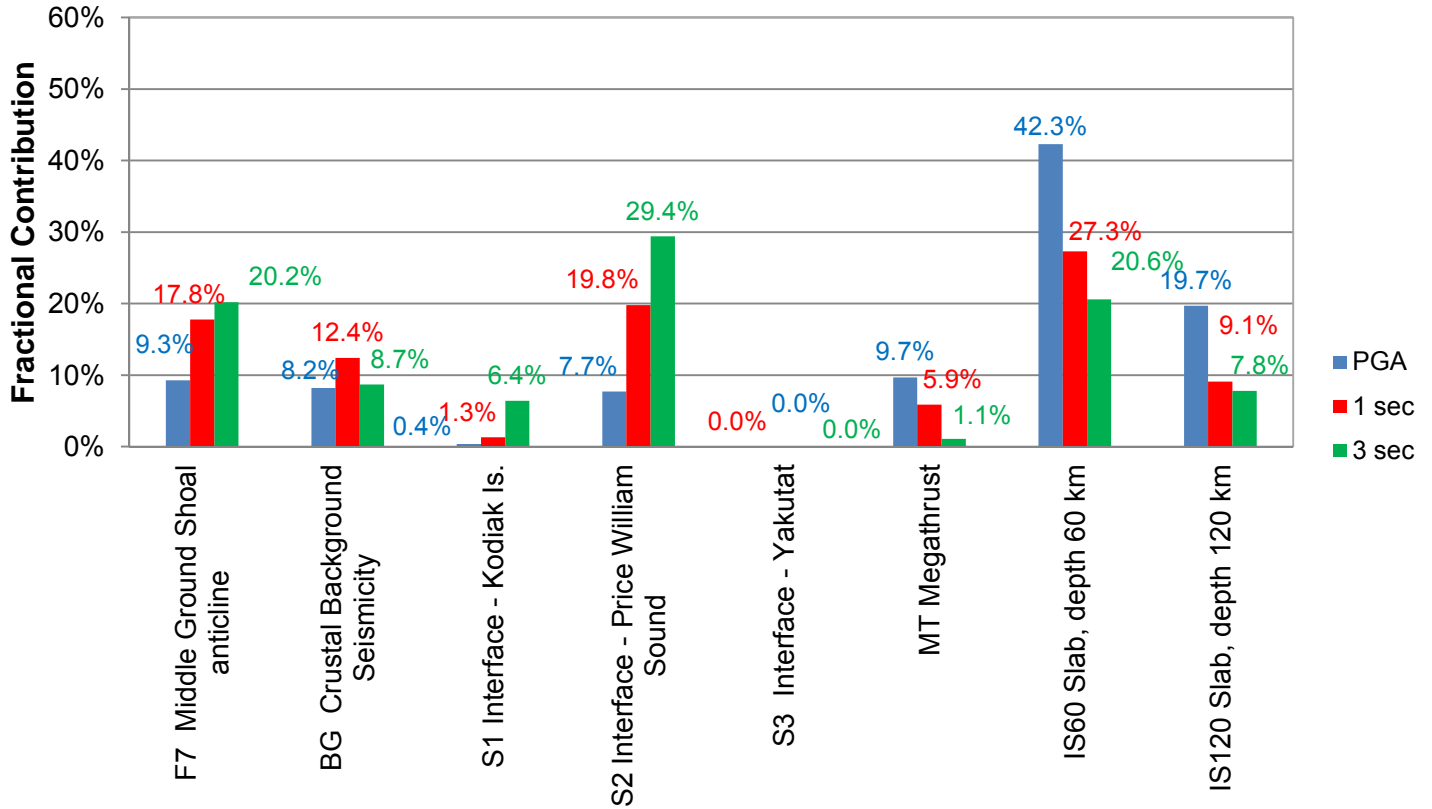
DEAGGREGATION OF THE HAZARD BY SEISMIC SOURCES FOR PGA, SA (T=1.0 SEC) AND SA (T=3.0 SEC), FOR 475-YEAR RETURN PERIOD - ONSHORE LOCATION (VS30 = 885 FT/S)

LNG FACILITIES
 ALASKA LNG PROJECT
 NIKISKI, ALASKA



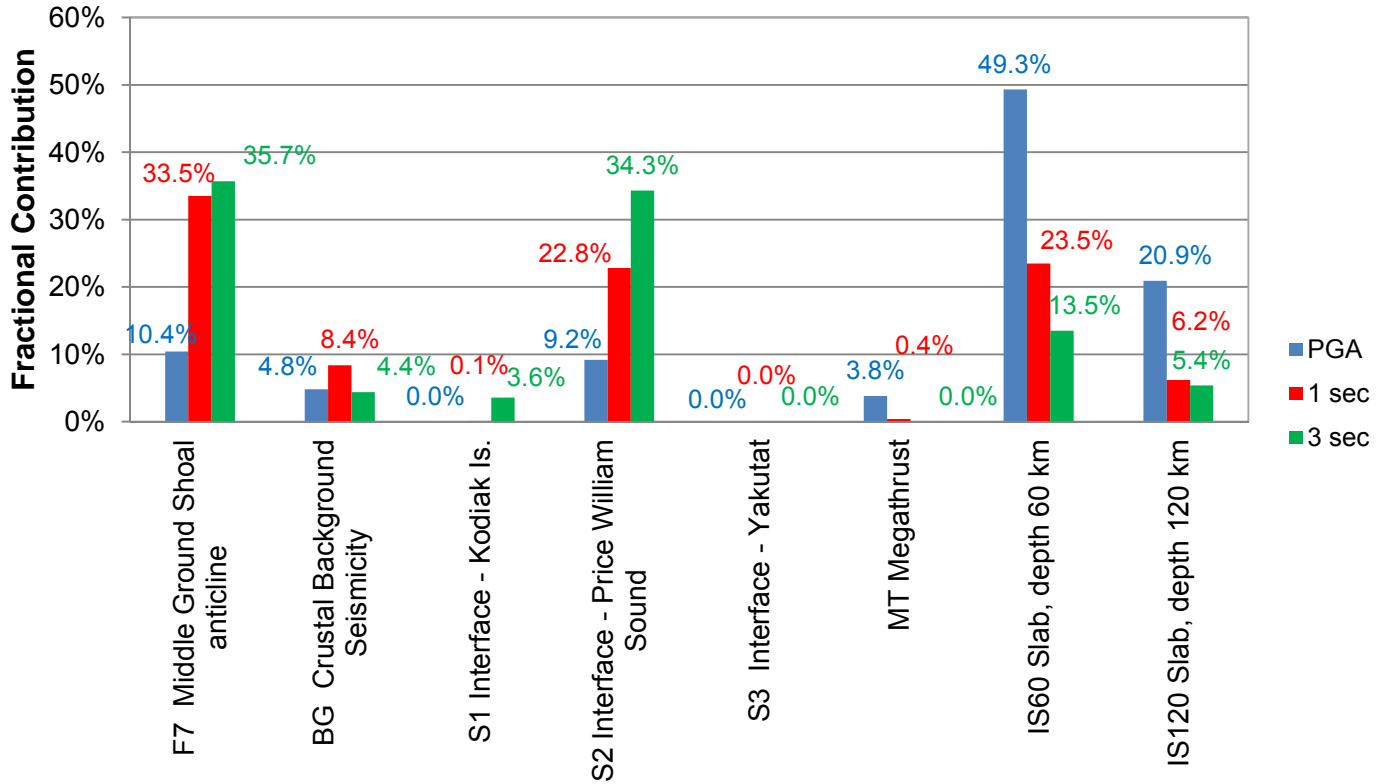
DEAGGREGATION OF THE HAZARD BY SEISMIC SOURCES FOR PGA, SA (T=1.0 SEC) AND SA (T=3.0 SEC), FOR 2475-YEAR RETURN PERIOD - ONSHORE LOCATION (VS30 = 885 FT/S)

LNG FACILITIES
 ALASKA LNG PROJECT
 NIKISKI, ALASKA



DEAGGREGATION OF THE HAZARD BY SEISMIC SOURCES FOR PGA, SA (T=1.0 SEC) AND SA (T=3.0 SEC), FOR 475-YEAR RETURN PERIOD - NEARSHORE LOCATION (VS30 = 885 FT/S)

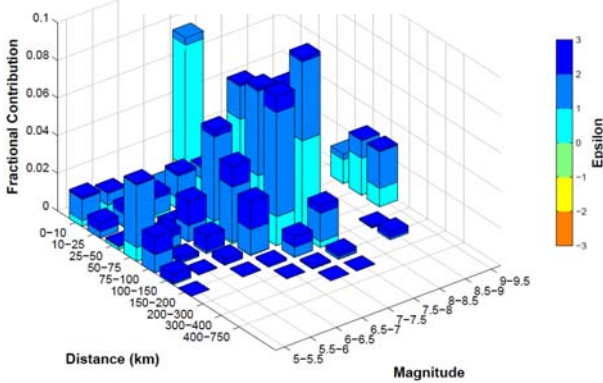
LNG FACILITIES
 ALASKA LNG PROJECT
 NIKISKI, ALASKA



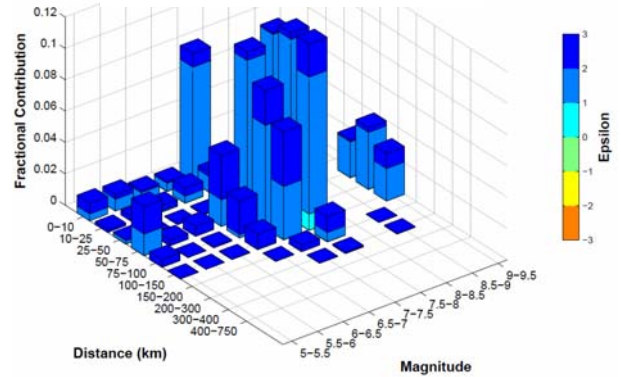
DEAGGREGATION OF THE HAZARD BY SEISMIC SOURCES FOR PGA, SA (T=1.0 SEC) AND SA (T=3.0 SEC), FOR 2475-YEAR RETURN PERIOD - NEARSHORE LOCATION (VS30 = 885 FT/S)

LNG FACILITIES
 ALASKA LNG PROJECT
 NIKISKI, ALASKA

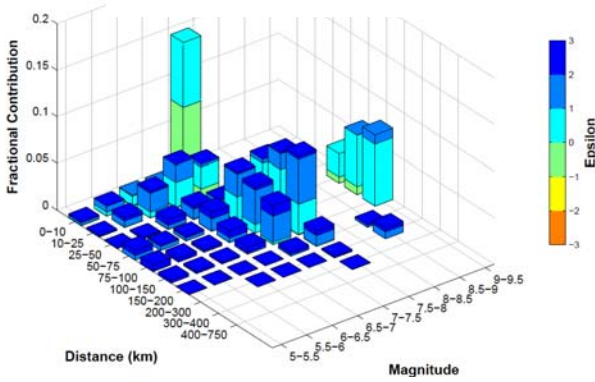
PGA
475-year Return Period



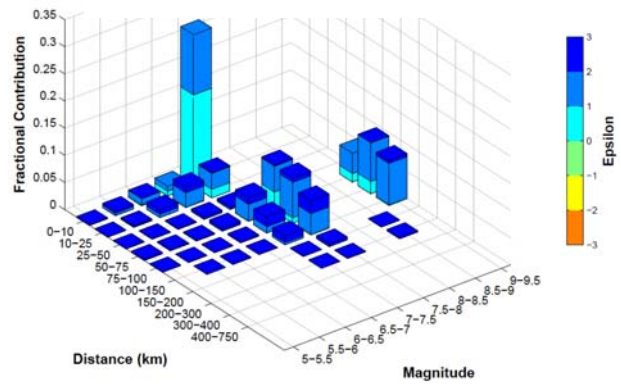
PGA
2475-year Return Period



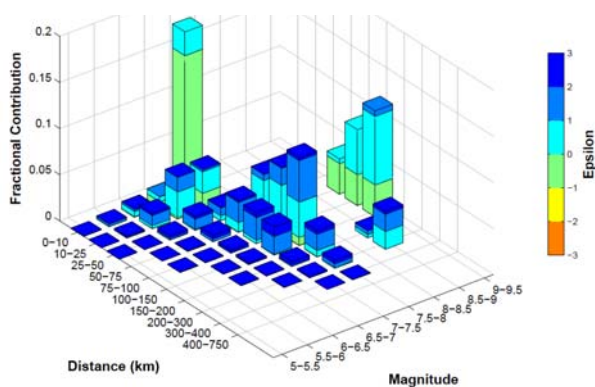
Sa (T=1.0 sec)
475-year Return Period



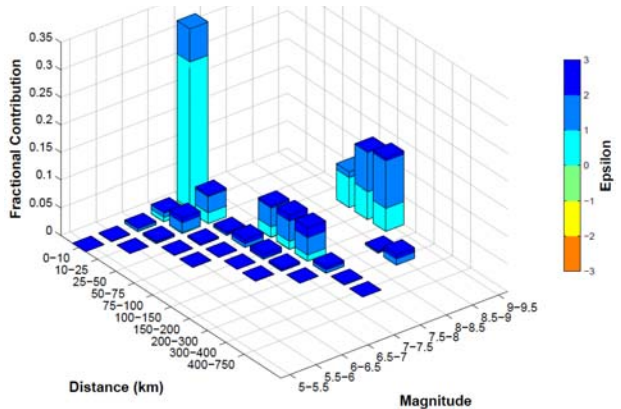
Sa (T=1.0 sec)
2475-year Return Period



Sa (T=3.0 sec)
475-year Return Period



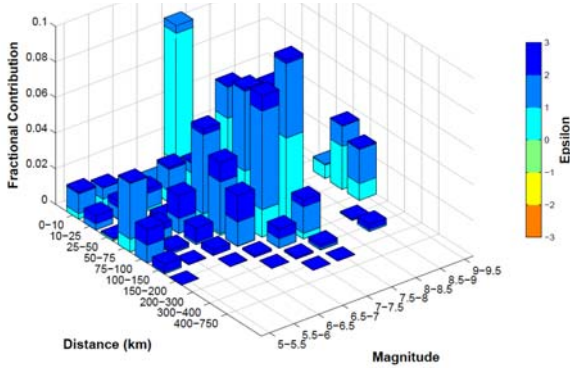
Sa (T=3.0 sec)
2475-year Return Period



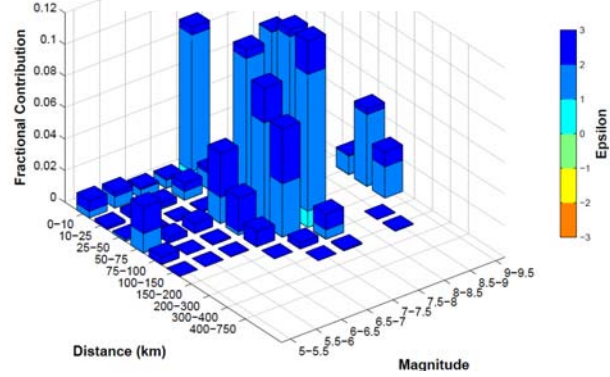
DEAGGREGATION OF THE HAZARD BY MAGNITUDE AND DISTANCE - ONSHORE LOCATION (VS30 = 885 FT/S)

LNG FACILITIES
ALASKA LNG PROJECT
NIKISKI, ALASKA

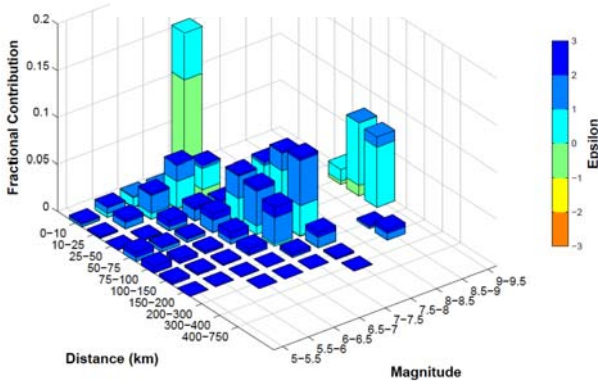
PGA
475-year Return Period



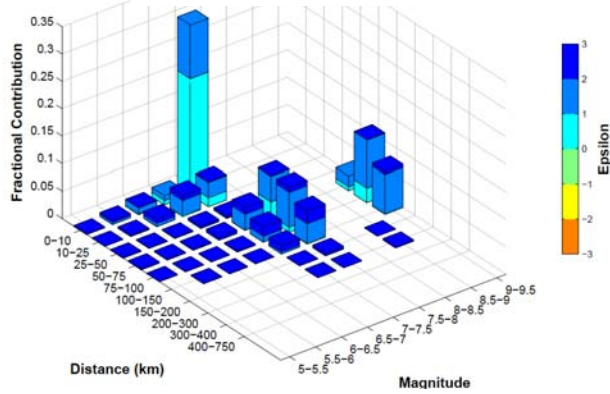
PGA
2475-year Return Period



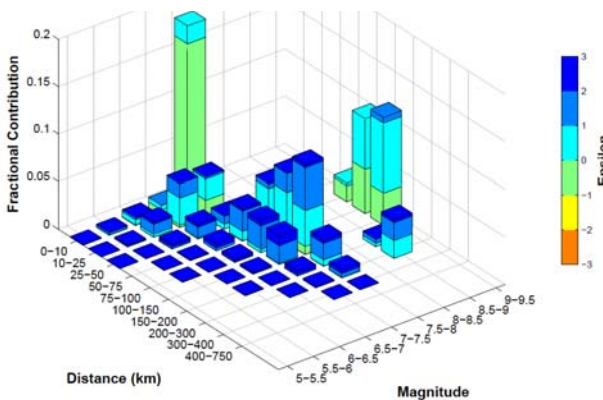
Sa (T=1.0 sec)
475-year Return Period



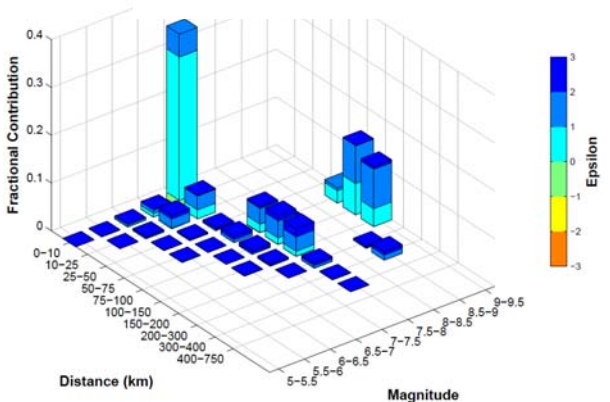
Sa (T=1.0 sec)
2475-year Return Period



Sa (T=3.0 sec)
475-year Return Period



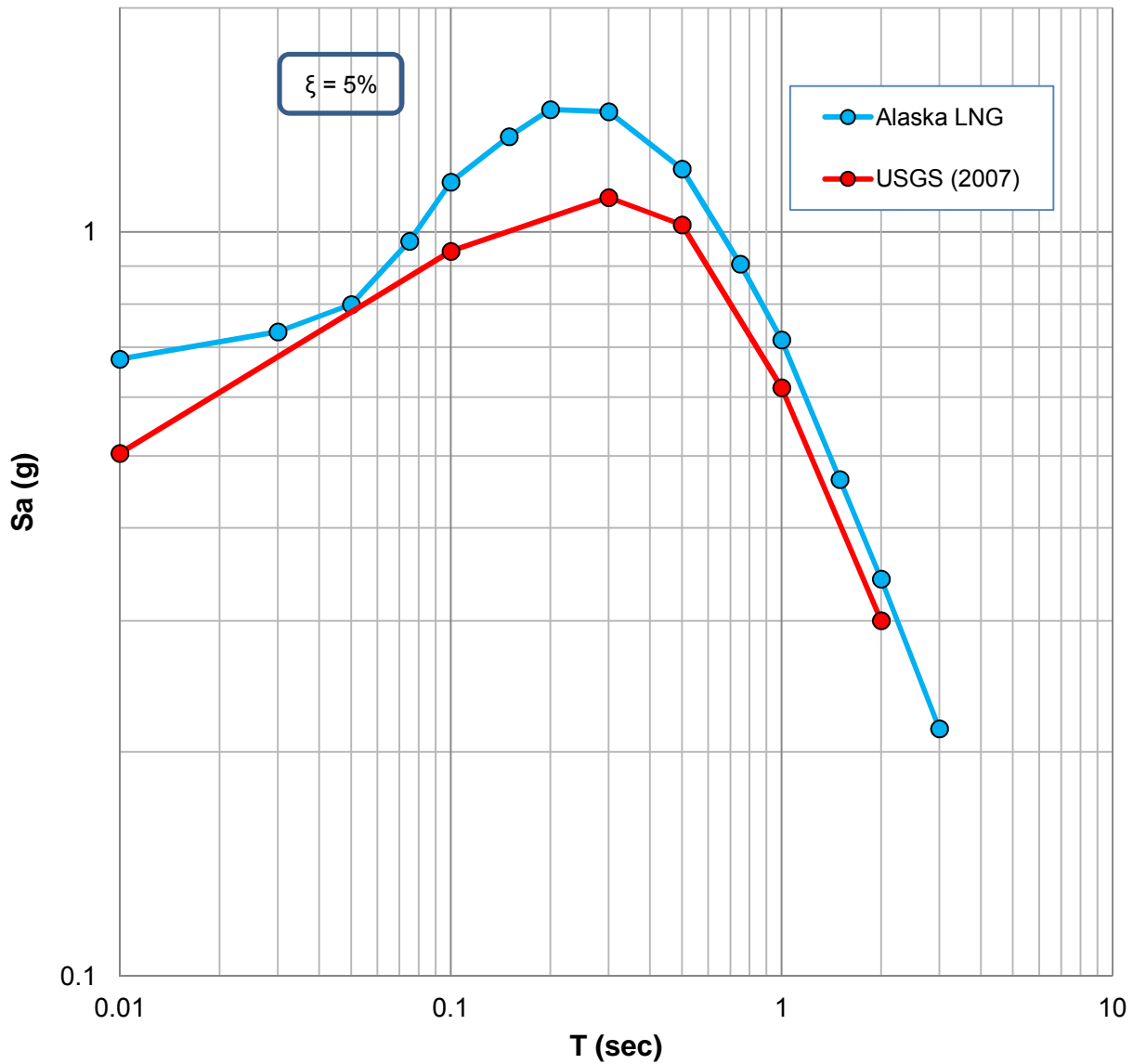
Sa (T=3.0 sec)
2475-year Return Period



**DEAGGREGATION OF THE HAZARD BY MAGNITUDE AND DISTANCE - NEARSHORE LOCATION
(VS30 = 885 FT/S)**

LNG FACILITIES
ALASKA LNG PROJECT
NIKISKI, ALASKA

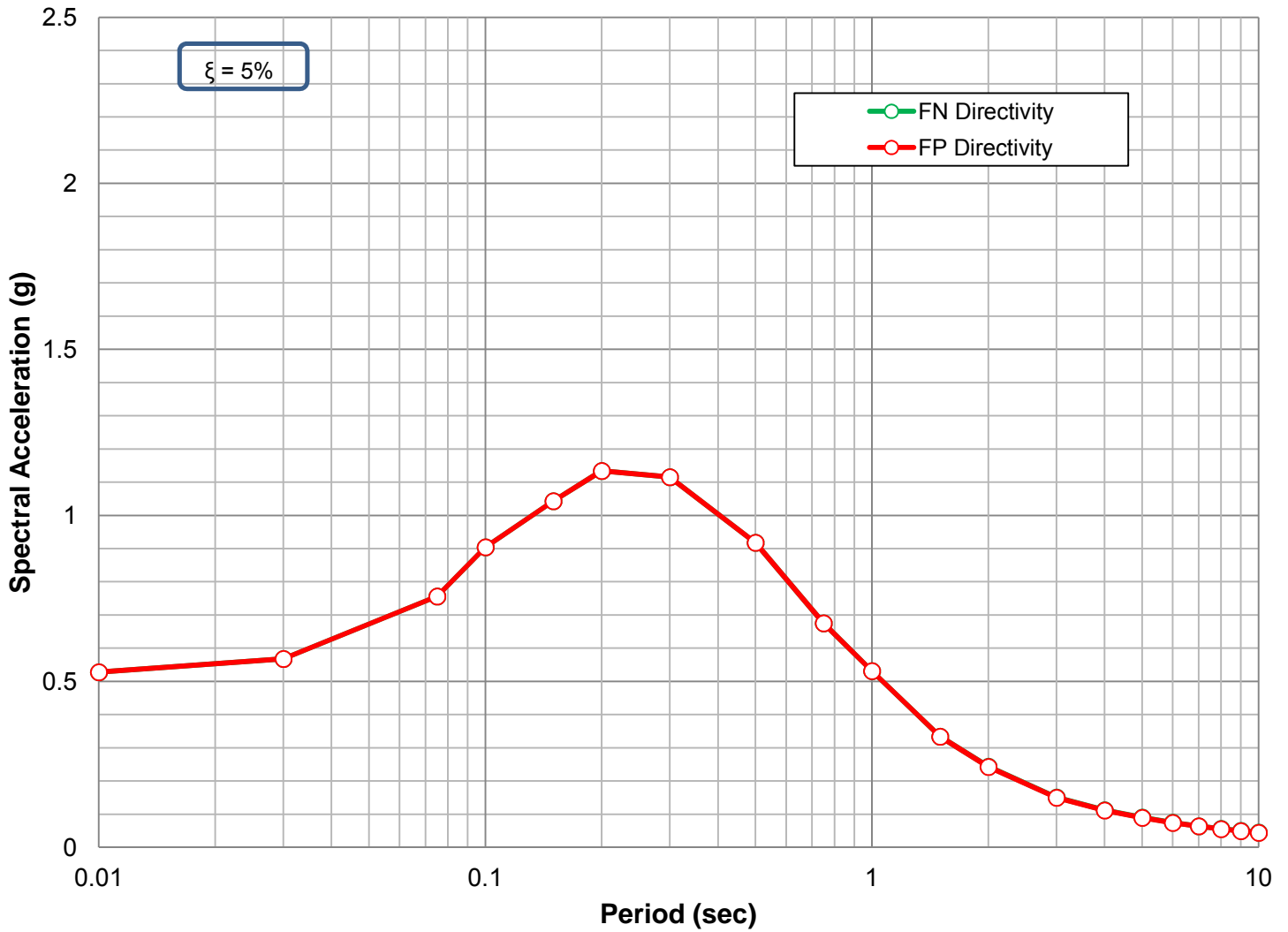
975 years



**UNIFORM HAZARD SPECTRA, COMPARISON OF THE ONSHORE LOCATION WITH USGS STUDIES
(USGS UHS FOR VS30=760 M/S (2493 FT/S) AMPLIFIED USING ASCE AMPLIFICATION FACTORS)**

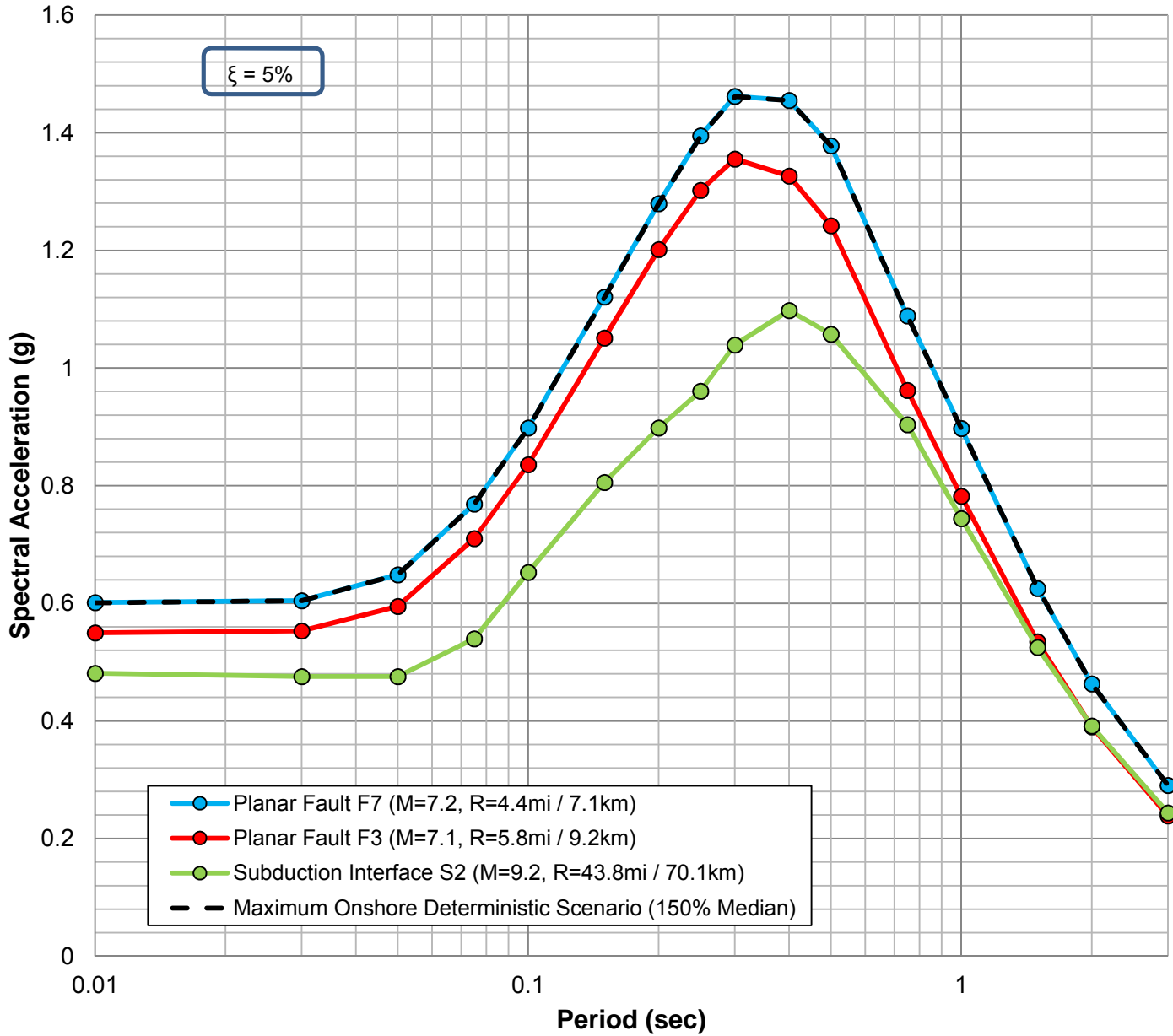
LNG FACILITIES
ALASKA LNG PROJECT
NIKISKI, ALASKA

OBE



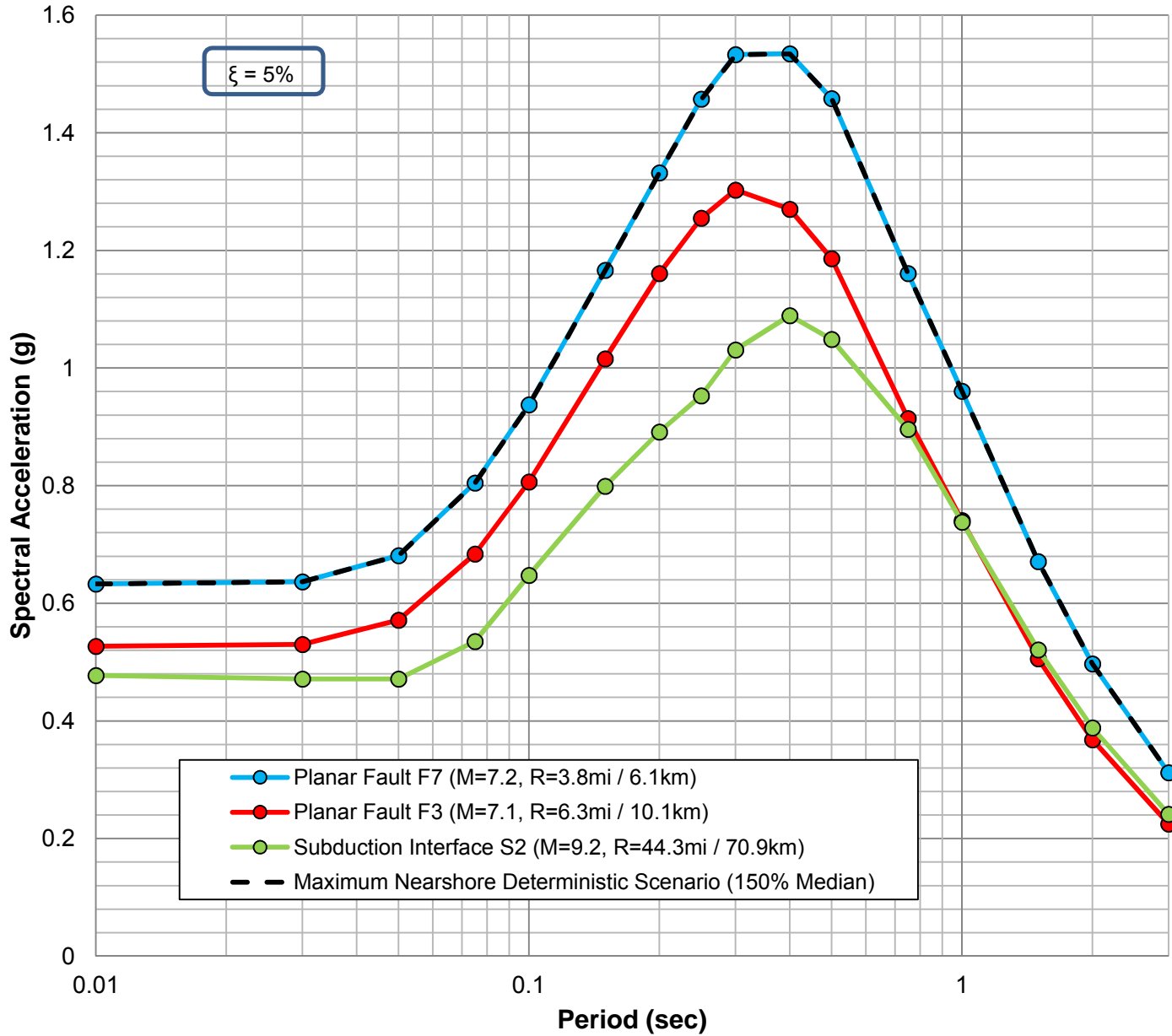
5-PERCENT DAMPED HORIZONTAL ACCELERATION RESPONSE SPECTRUM AT GROUND SURFACE (VS30=885FT/S) FOR OBE PER NFPA-59A (2006) - FAULT NORMAL (FN) AND FAULT PARALLEL (FP)

LNG FACILITIES
ALASKA LNG PROJECT
NIKISKI, ALASKA



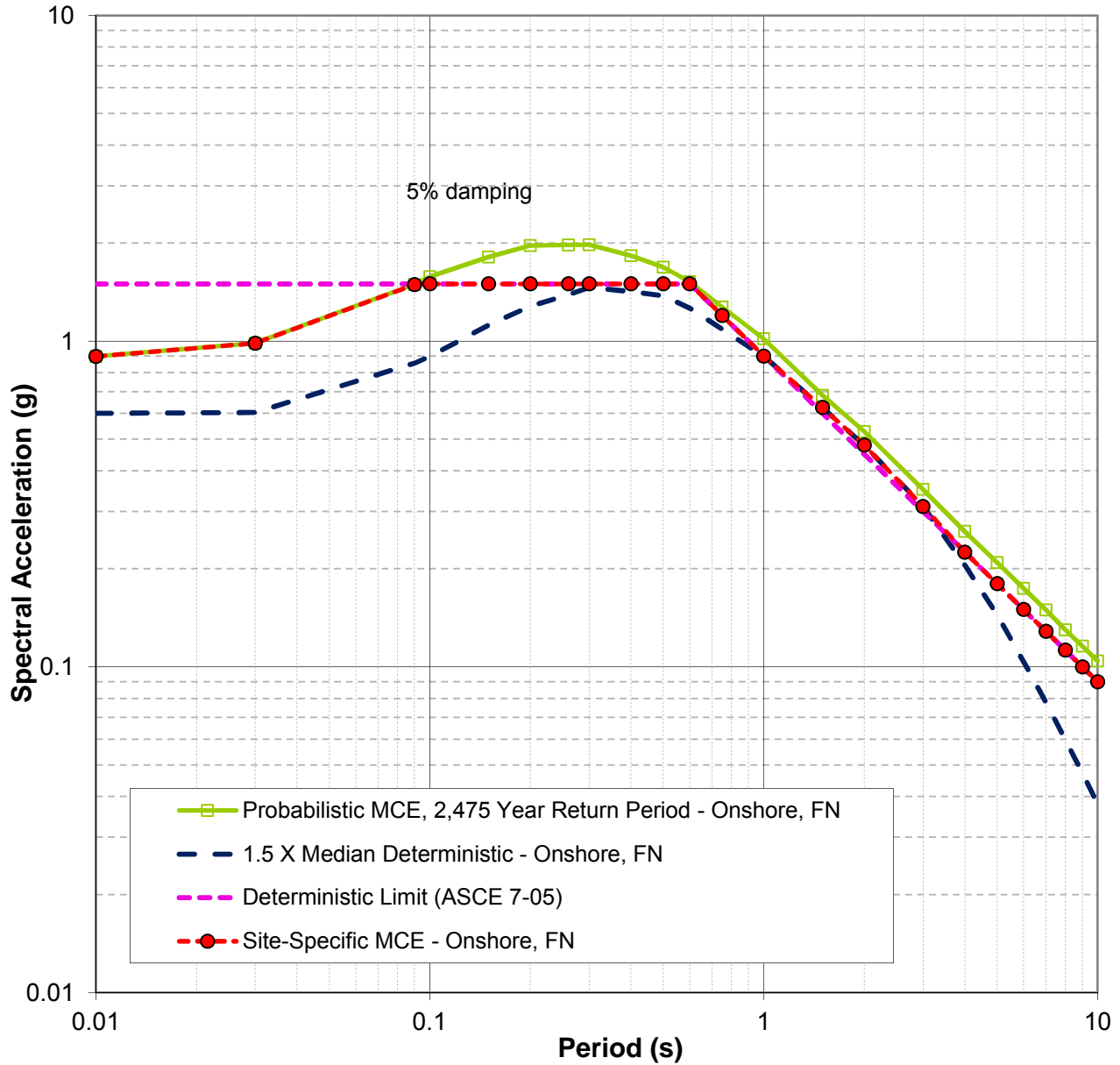
DEVELOPMENT OF THE 150% MEDIAN ONSHORE DETERMINISTIC RESPONSE SPECTRUM - NO DIRECTIVITY (VS30 = 885 FT/S)

LNG FACILITIES
 ALASKA LNG PROJECT
 NIKISKI, ALASKA



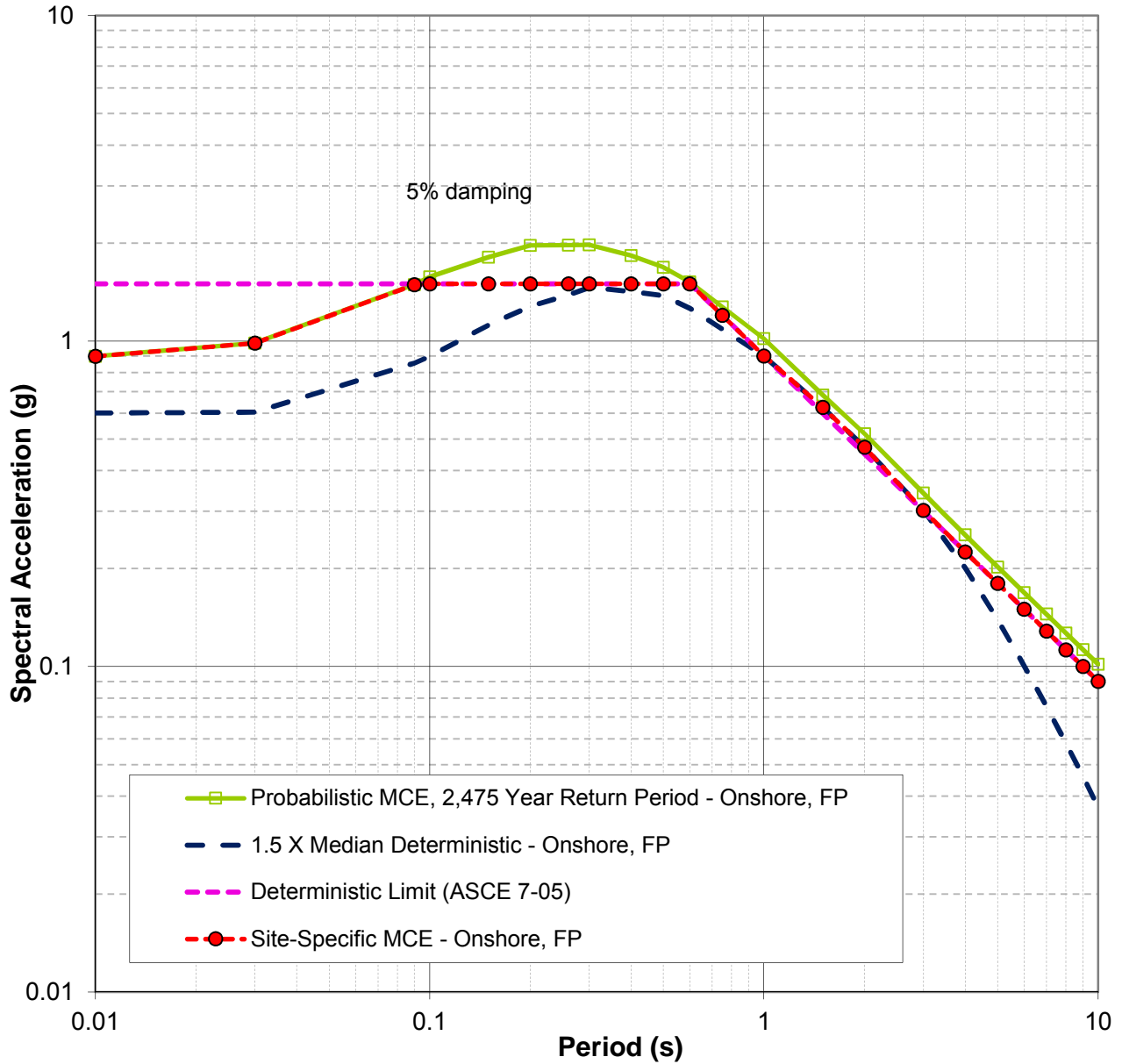
DEVELOPMENT OF THE 150% MEDIAN NEARSHORE DETERMINISTIC RESPONSE SPECTRUM - NO DIRECTIVITY (VS30 = 885 FT/S)

LNG FACILITIES
 ALASKA LNG PROJECT
 NIKISKI, ALASKA



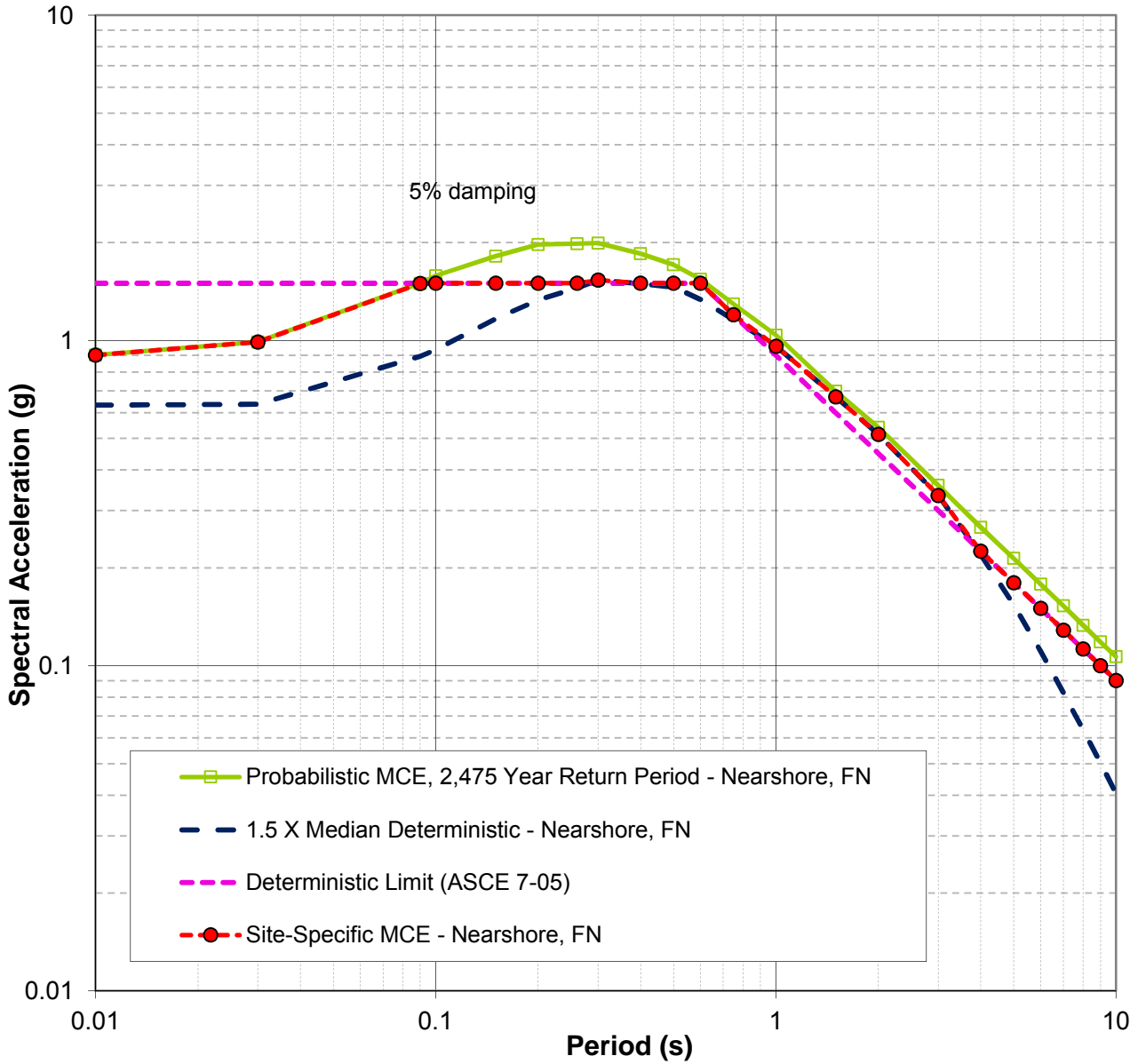
DEVELOPMENT OF MAXIMUM CONSIDERED EARTHQUAKE (MCE) SPECTRUM AT GROUND SURFACE (VS30=885 FT/S) PER ASCE 7-05 - ONSHORE LOCATION, FAULT NORMAL

LNG FACILITIES
 ALASKA LNG PROJECT
 NIKISKI, ALASKA



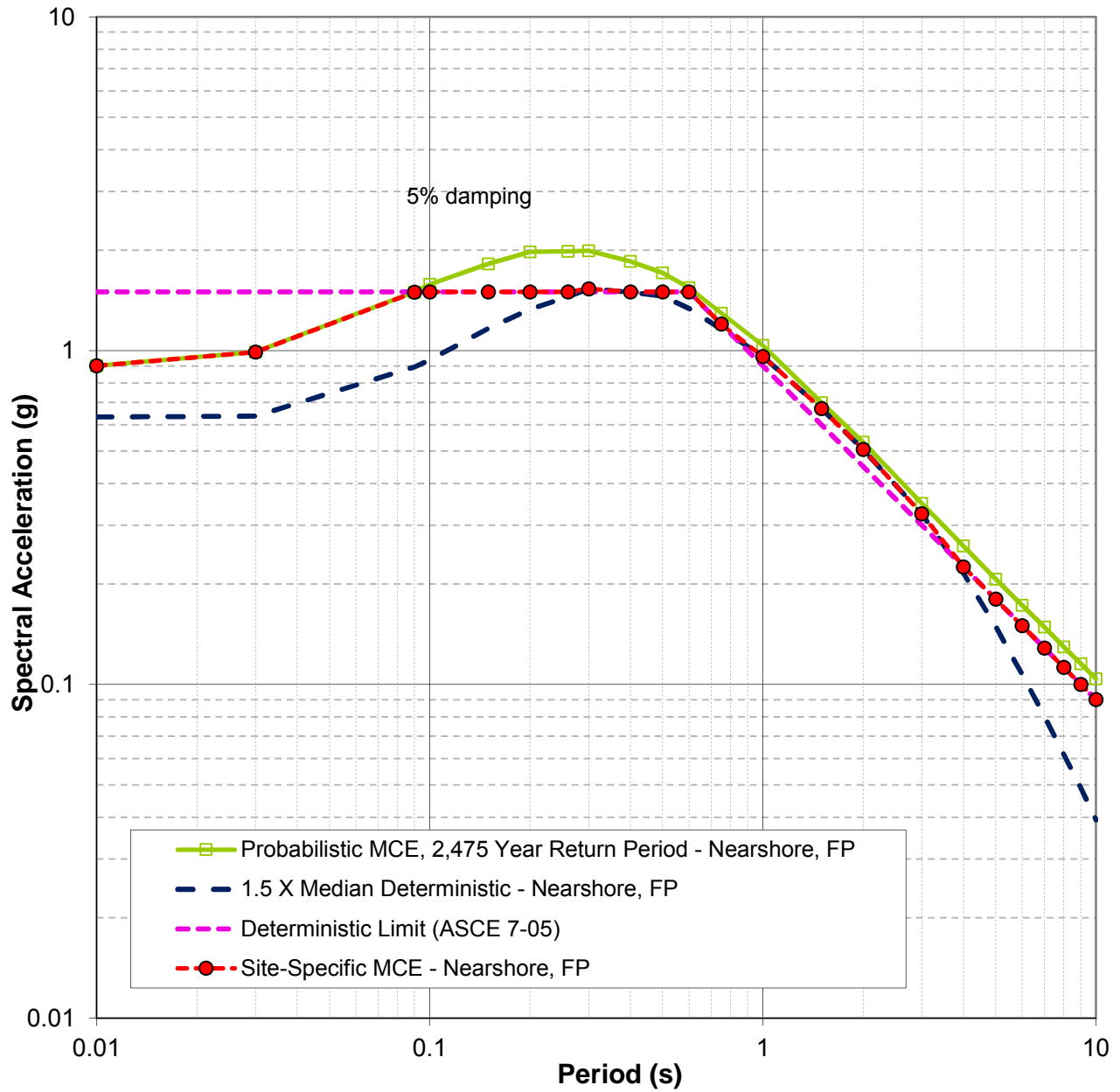
DEVELOPMENT OF MAXIMUM CONSIDERED EARTHQUAKE (MCE) SPECTRUM AT GROUND SURFACE (VS30=885 FT/S) PER ASCE 7-05 - ONSHORE LOCATION, FAULT PARALLEL

LNG FACILITIES
 ALASKA LNG PROJECT
 NIKISKI, ALASKA



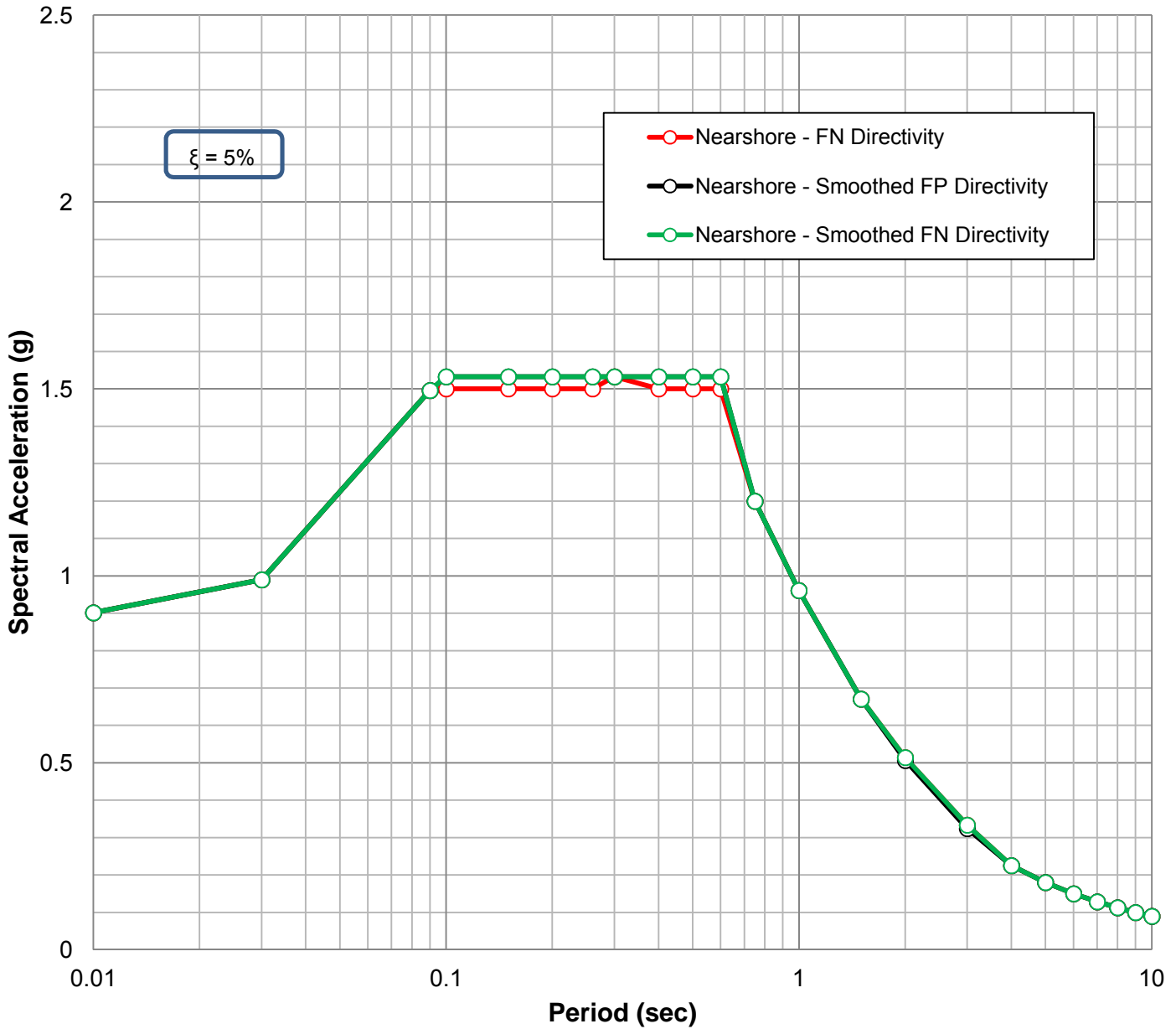
DEVELOPMENT OF MAXIMUM CONSIDERED EARTHQUAKE (MCE) SPECTRUM AT GROUND SURFACE (VS30=885 FT/S) PER ASCE 7-05 - NEARSHORE LOCATION, FAULT NORMAL

LNG FACILITIES
 ALASKA LNG PROJECT
 NIKISKI, ALASKA



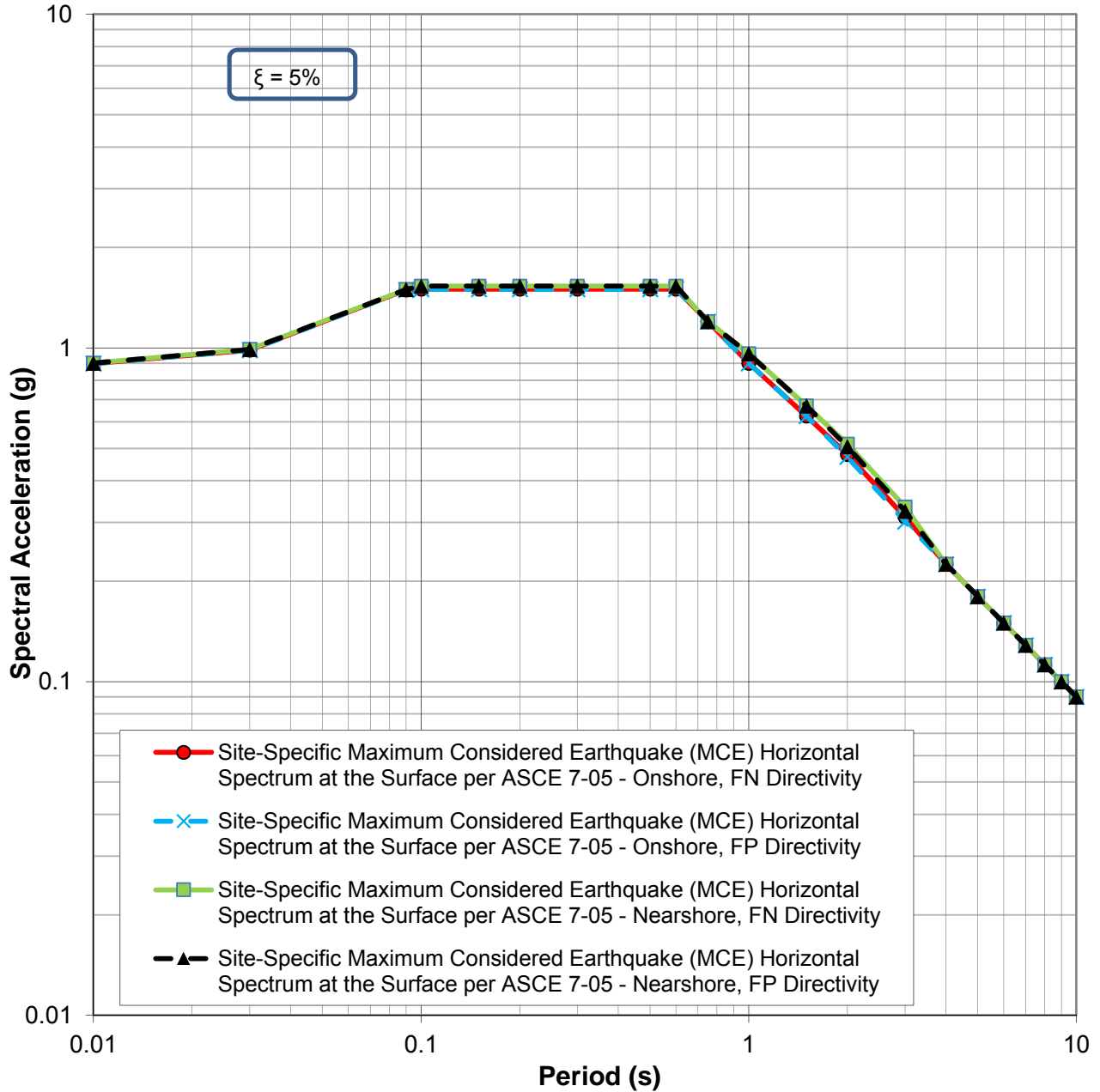
DEVELOPMENT OF MAXIMUM CONSIDERED EARTHQUAKE (MCE) SPECTRUM AT GROUND SURFACE (VS30=885 FT/S) PER ASCE 7-05 - NEARSHORE LOCATION, FAULT PARALLEL

LNG FACILITIES
 ALASKA LNG PROJECT
 NIKISKI, ALASKA



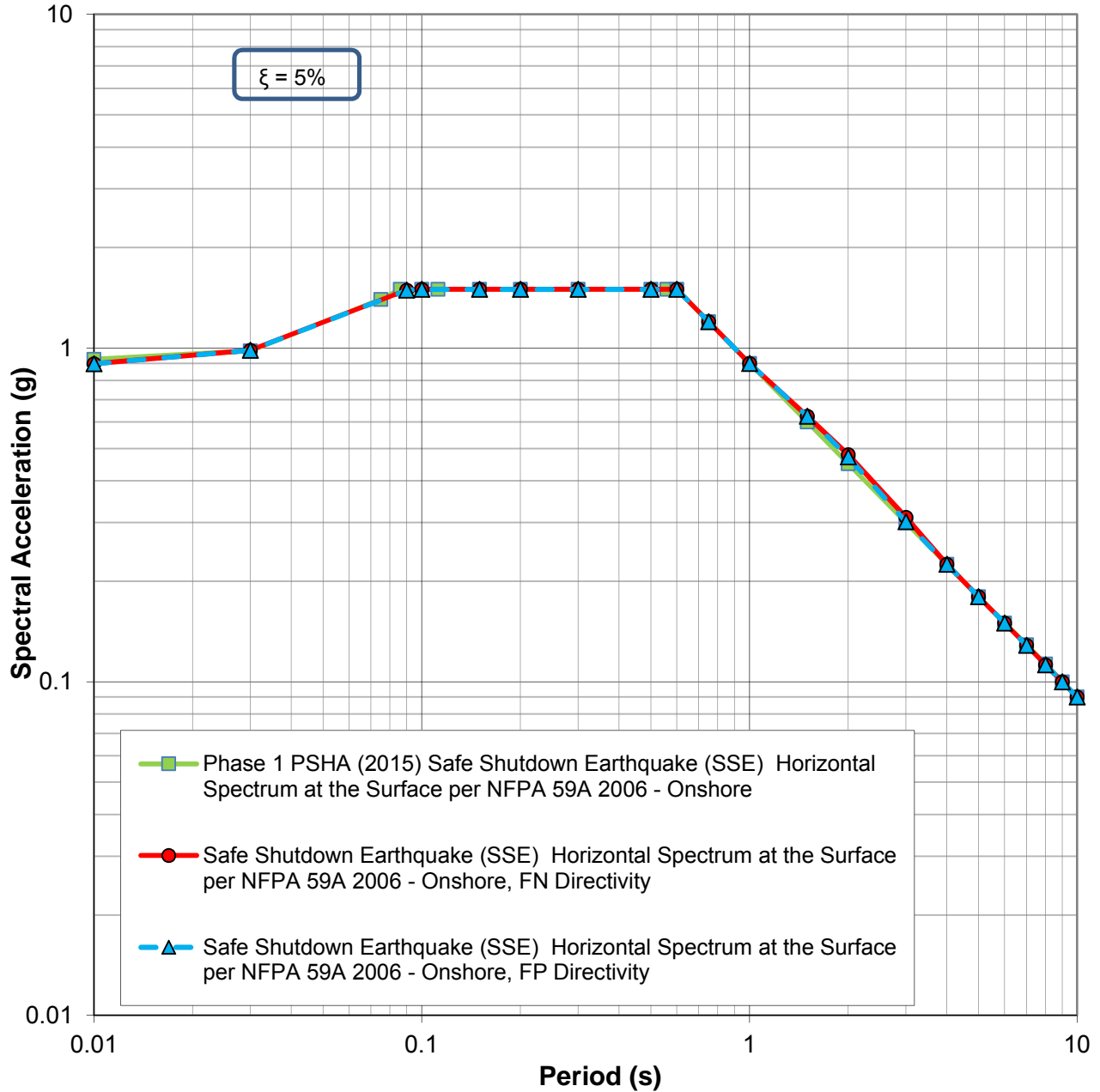
5-PERCENT DAMPED SMOOTHED HORIZONTAL ACCELERATION RESPONSE SPECTRA AT GROUND SURFACE (VS30=885 FT/S) PER ASCE 7-05 GUIDELINES - NEARSHORE LOCATION, FAULT NORMAL AND FAULT PARALLEL

LNG FACILITIES
ALASKA LNG PROJECT
NIKISKI, ALASKA



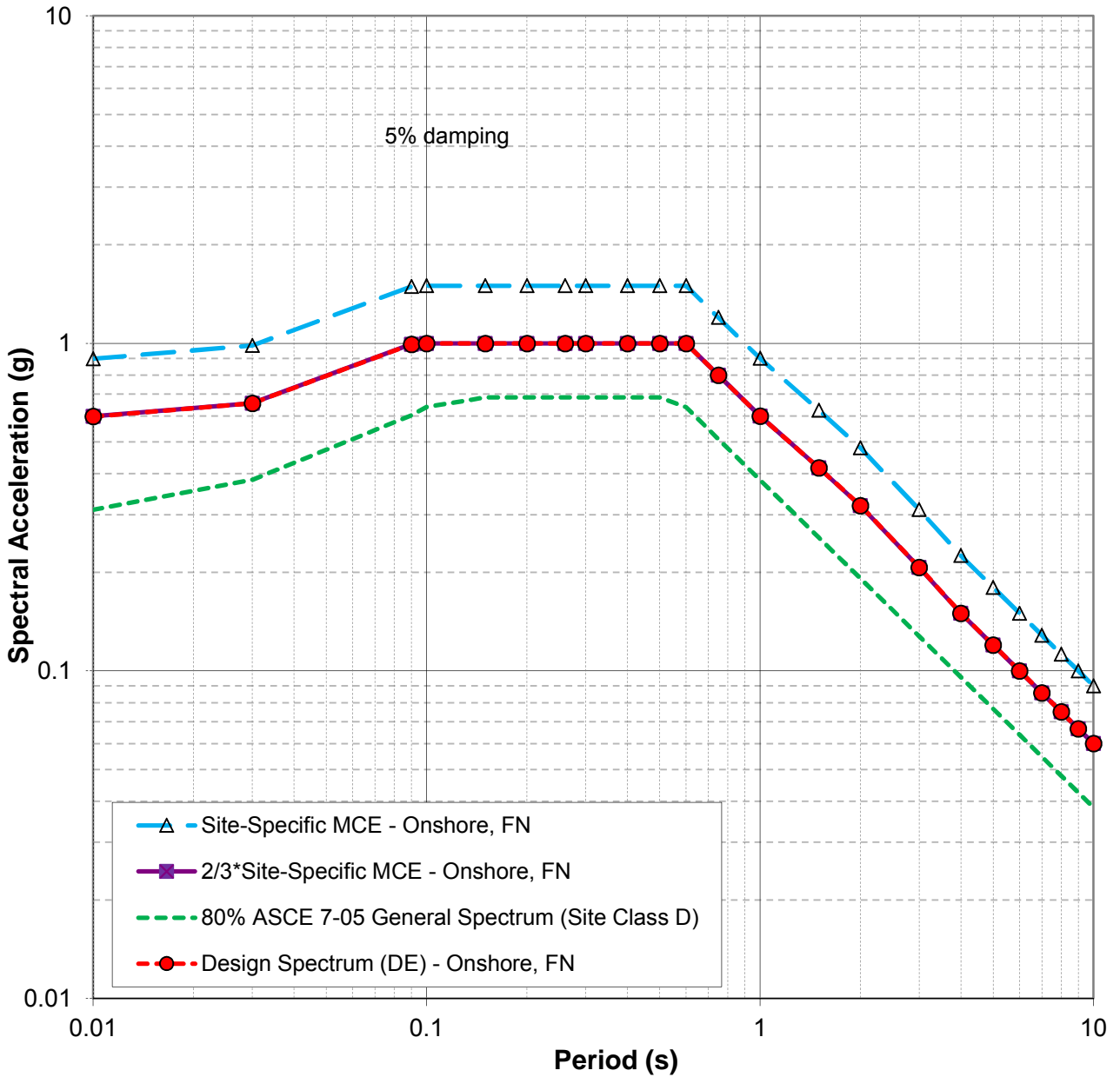
COMPARISON OF MAXIMUM CONSIDERED EARTHQUAKE (MCE) SPECTRA AT GROUND SURFACE (VS30 = 885 FT/S) PER ASCE 7-05 ESTIMATED FOR THE REPRESENTATIVE ONSHORE AND NEARSHORE LOCATIONS (VS30 = 885 FT/S)

LNG FACILITIES
ALASKA LNG PROJECT
NIKISKI, ALASKA



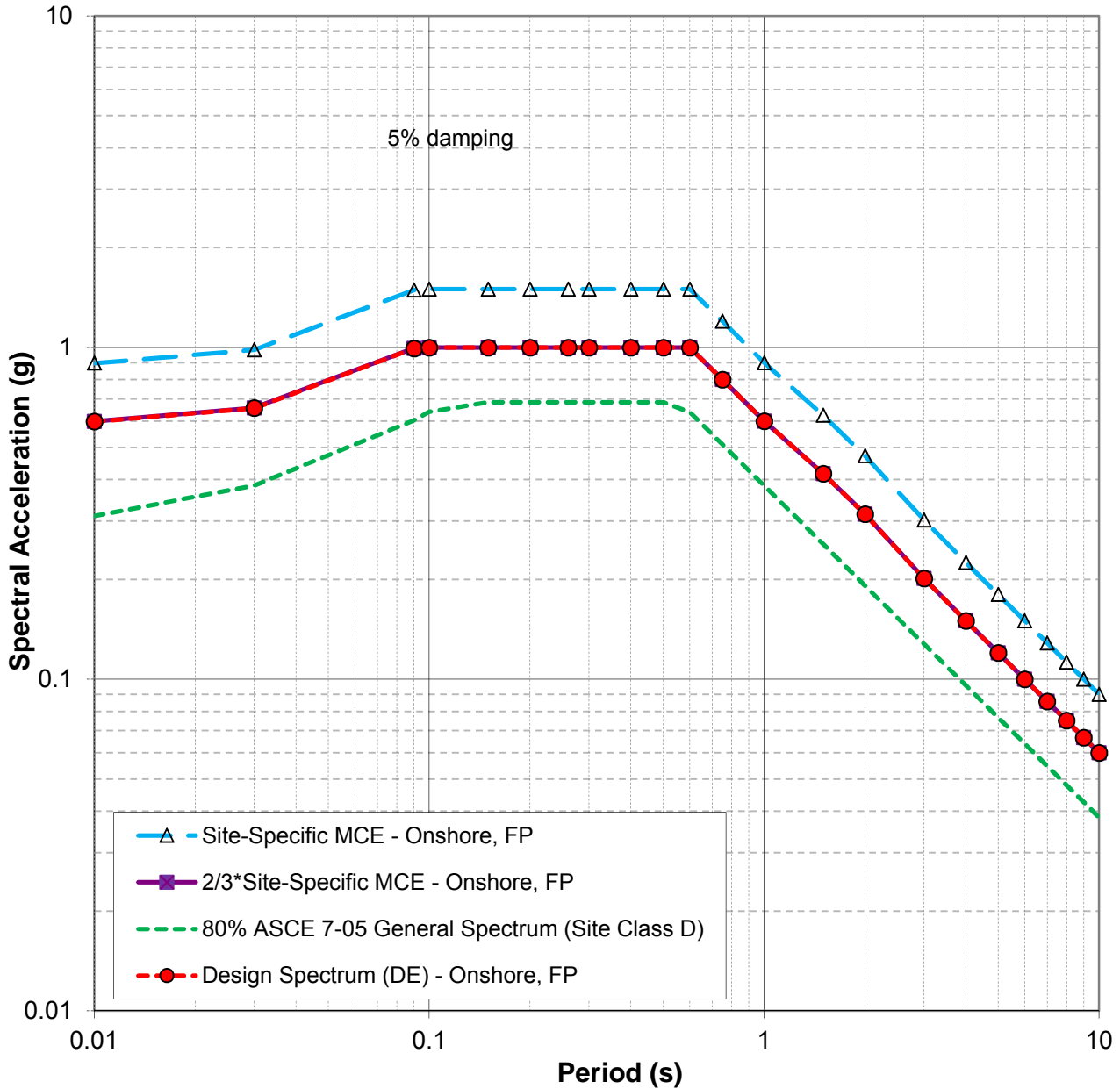
COMPARISON OF MAXIMUM CONSIDERED EARTHQUAKE (MCE) SPECTRA (FN AND FP) AT GROUND SURFACE (VS30=885 FT/S) PER ASCE 7-05 ESTIMATED FOR THE REPRESENTATIVE ONSHORE LOCATION TO THE PHASE 1 PSHA RESULTS (VS30 = 900 FT/S)

LNG FACILITIES
ALASKA LNG PROJECT
NIKISKI, ALASKA



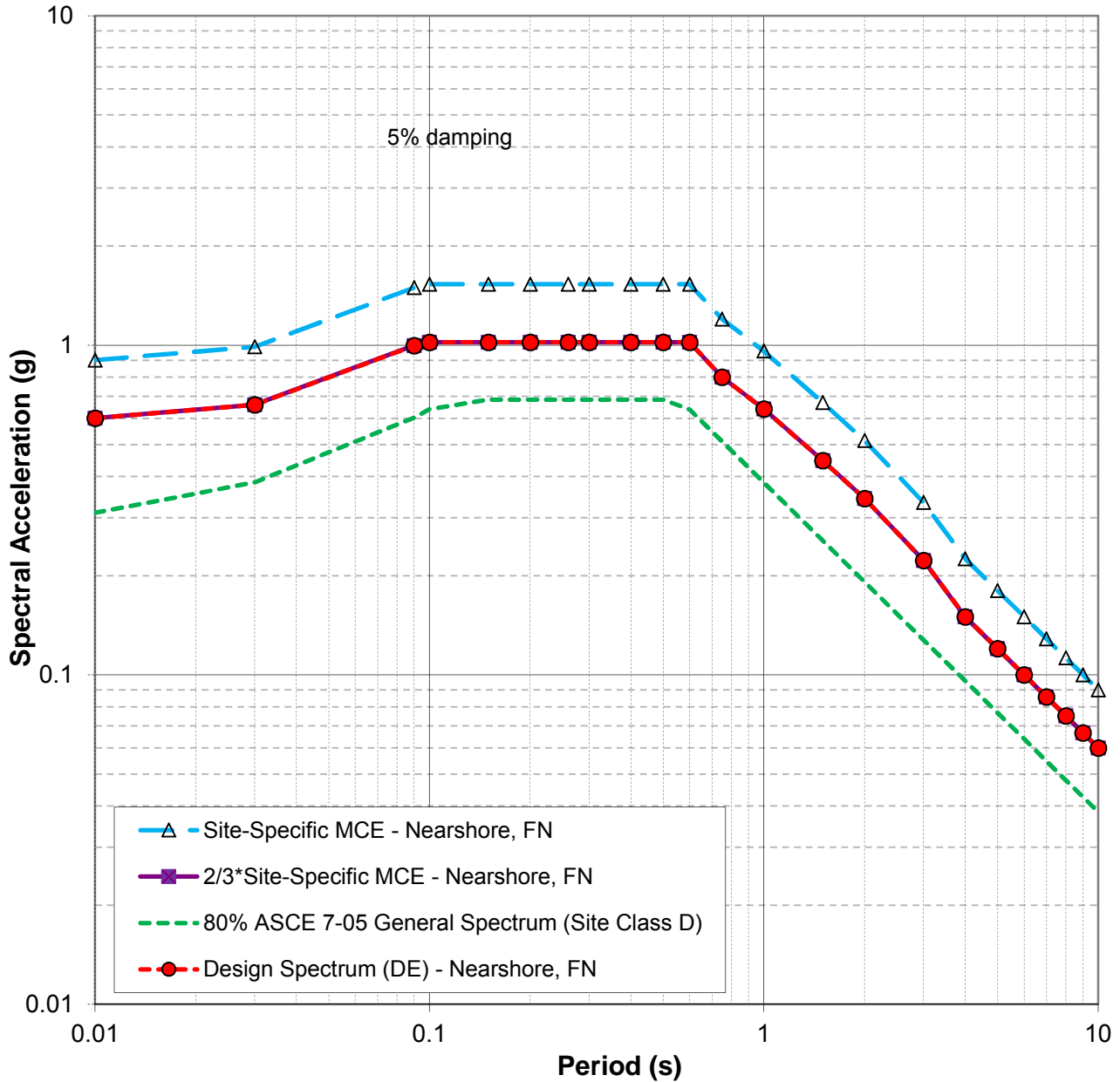
**DEVELOPMENT OF DESIGN EARTHQUAKE (DE) SPECTRUM AT GROUND SURFACE (VS30=885 FT/S)
 PER ASCE 7-05 - ONSHORE LOCATION, FAULT NORMAL**

LNG FACILITIES
 ALASKA LNG PROJECT
 NIKISKI, ALASKA



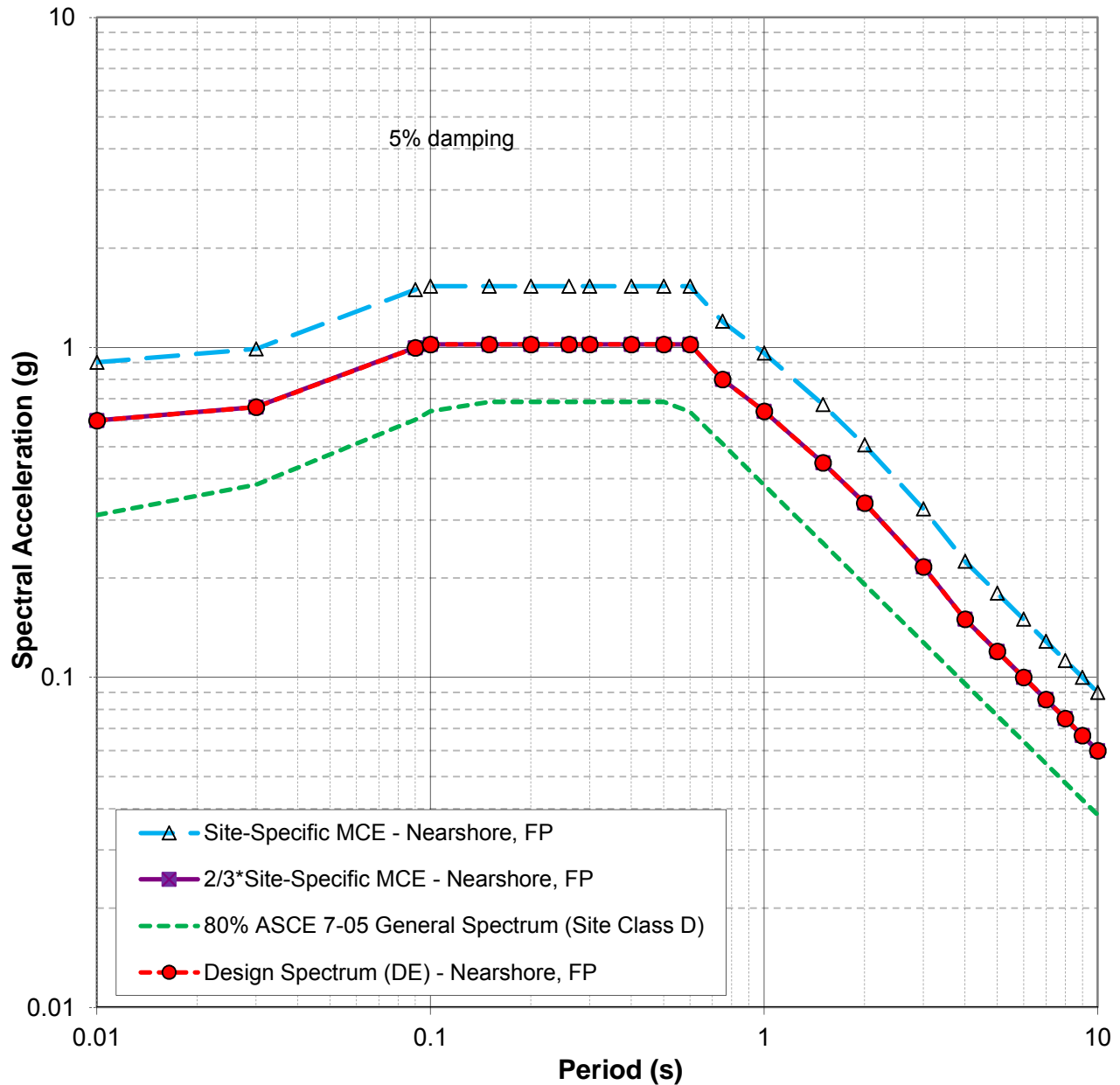
**DEVELOPMENT OF DESIGN EARTHQUAKE (DE) SPECTRUM AT GROUND SURFACE (VS30=885 FT/S)
 PER ASCE 7-05 - ONSHORE LOCATION, FAULT PARALLEL**

LNG FACILITIES
 ALASKA LNG PROJECT
 NIKISKI, ALASKA



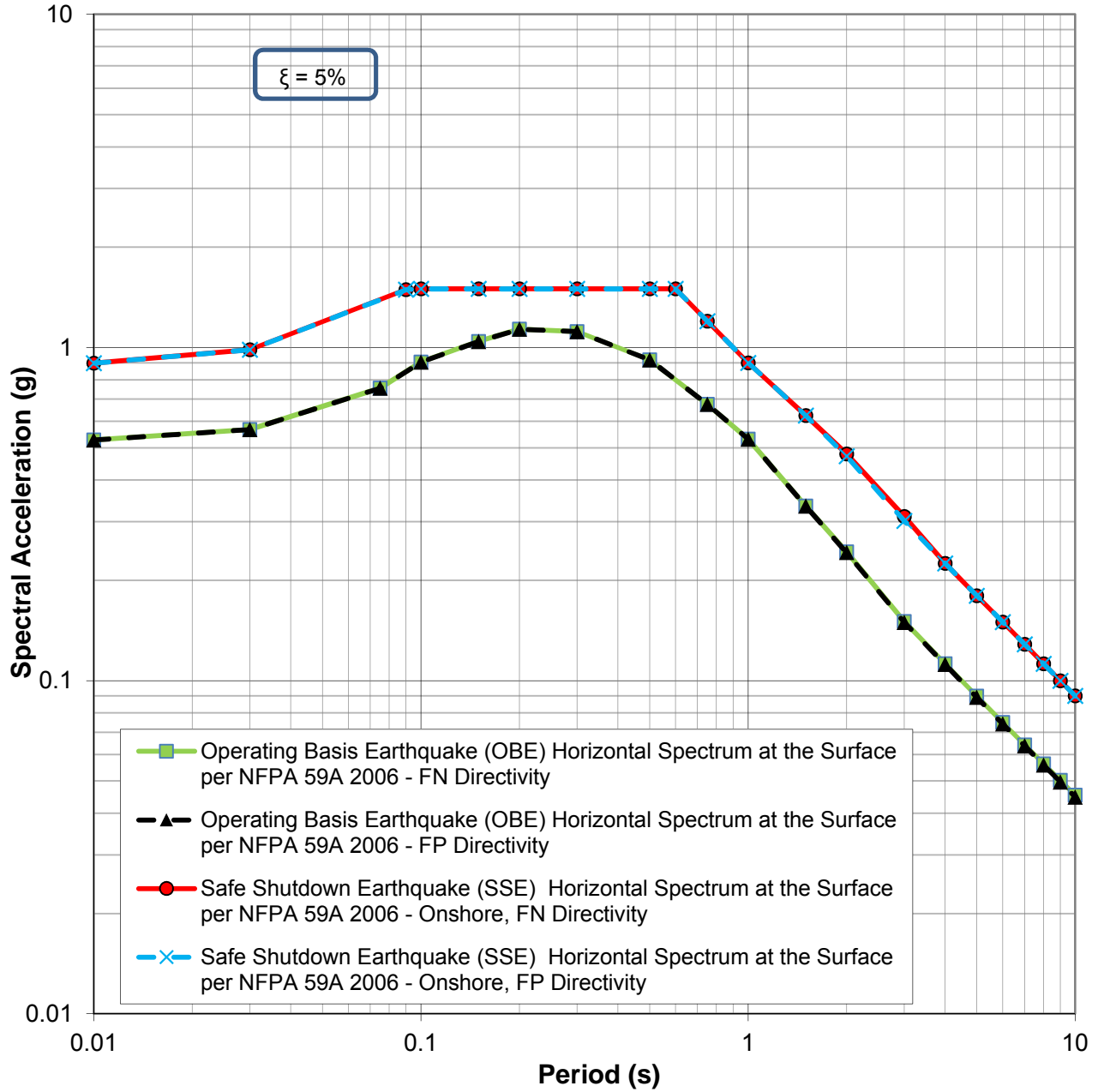
**DEVELOPMENT OF DESIGN EARTHQUAKE (DE) SPECTRUM AT GROUND SURFACE (VS30=885 FT/S)
 PER ASCE 7-05 - NEARSHORE LOCATION, FAULT NORMAL**

LNG FACILITIES
 ALASKA LNG PROJECT
 NIKISKI, ALASKA



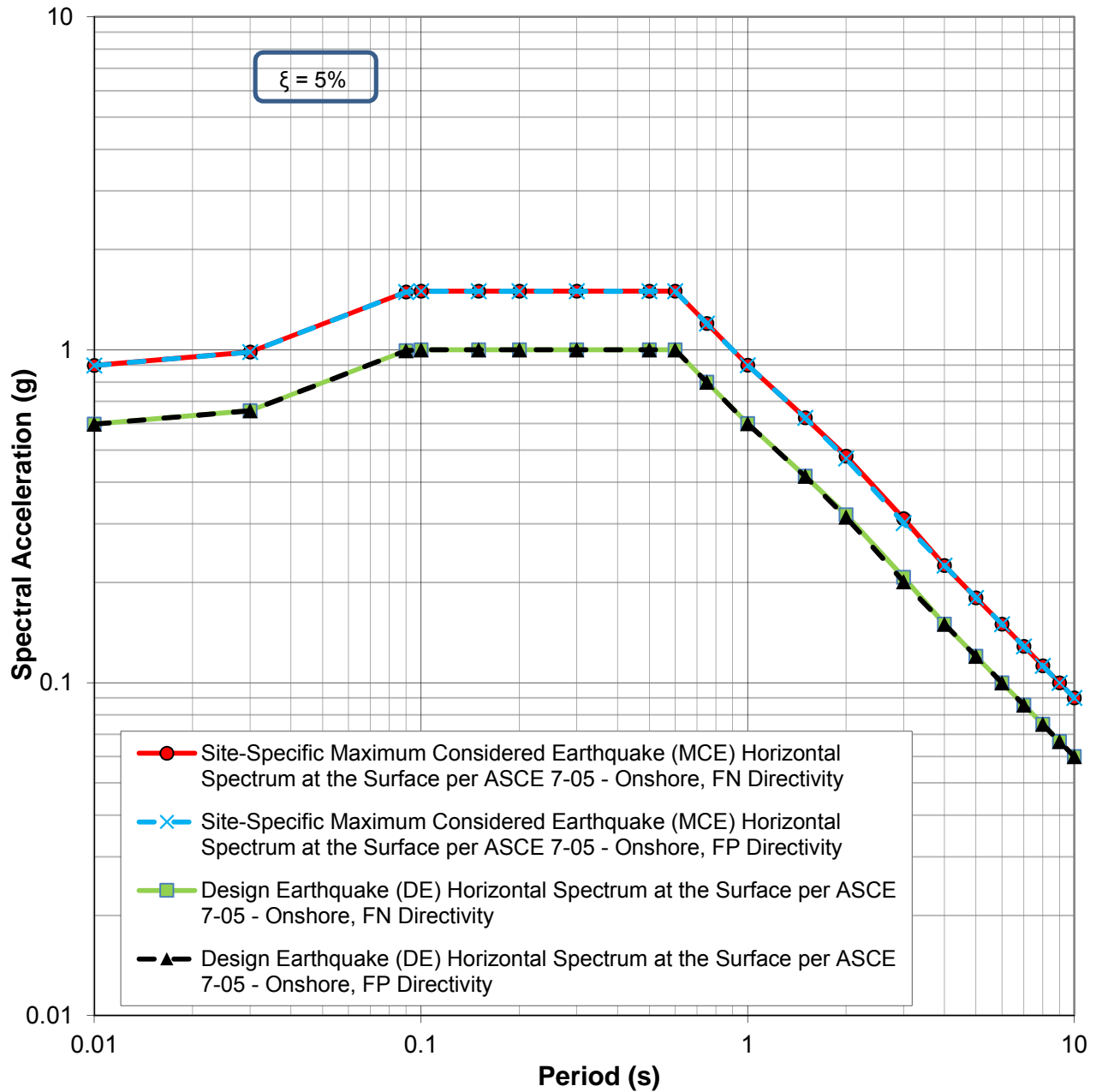
**DEVELOPMENT OF DESIGN EARTHQUAKE (DE) SPECTRUM AT GROUND SURFACE (VS30=885 FT/S)
PER ASCE 7-05 - ONSHORE LOCATION, FAULT PARALLEL**

LNG FACILITIES
ALASKA LNG PROJECT
NIKISKI, ALASKA



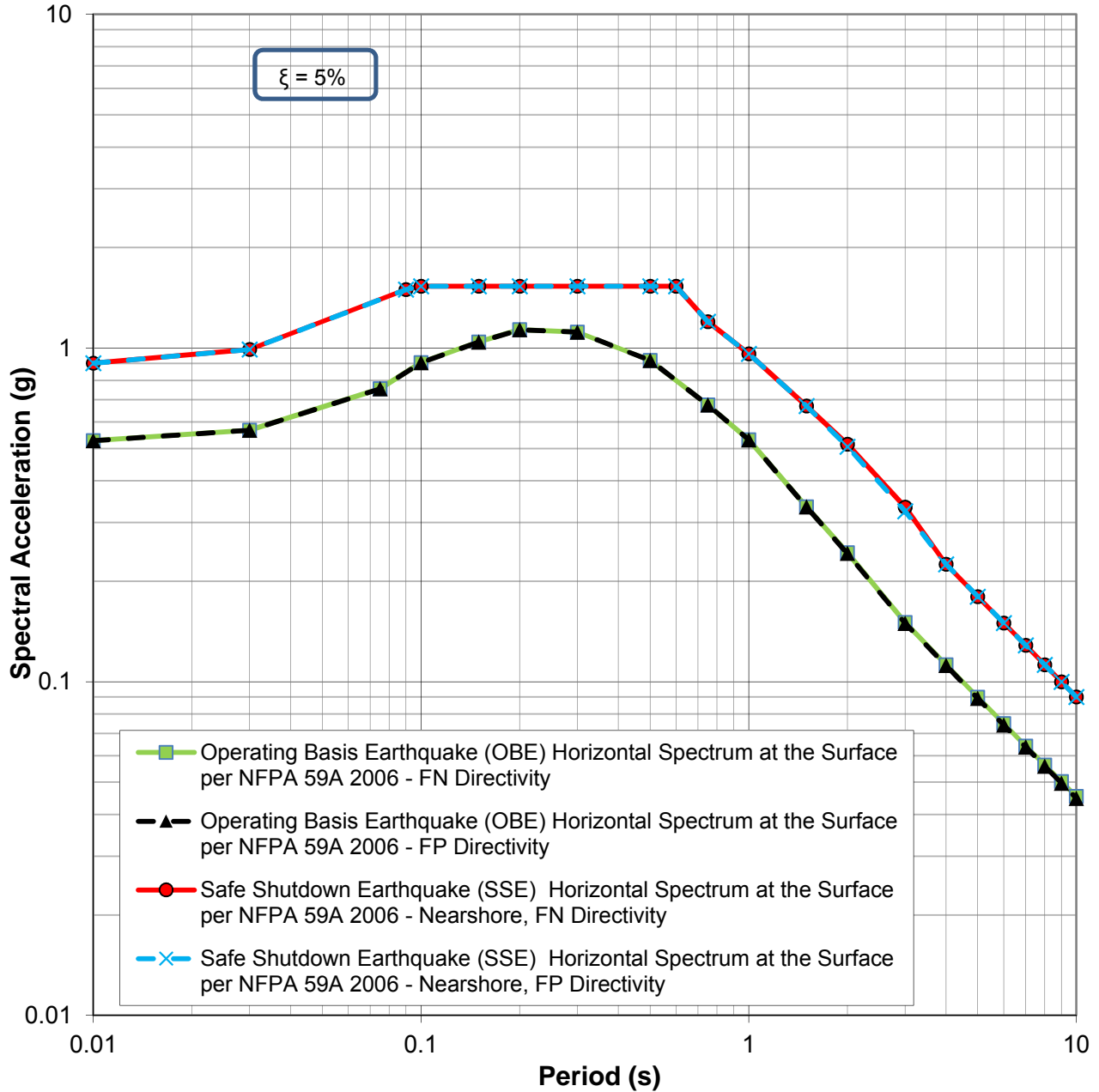
**5-PERCENT DAMPED HORIZONTAL ACCELERATION RESPONSE SPECTRA AT GROUND SURFACE
(VS30=885 FT/S) PER NFPA-59A 2006 GUIDELINES - ONSHORE LOCATION**

LNG FACILITIES
ALASKA LNG PROJECT
NIKISKI, ALASKA



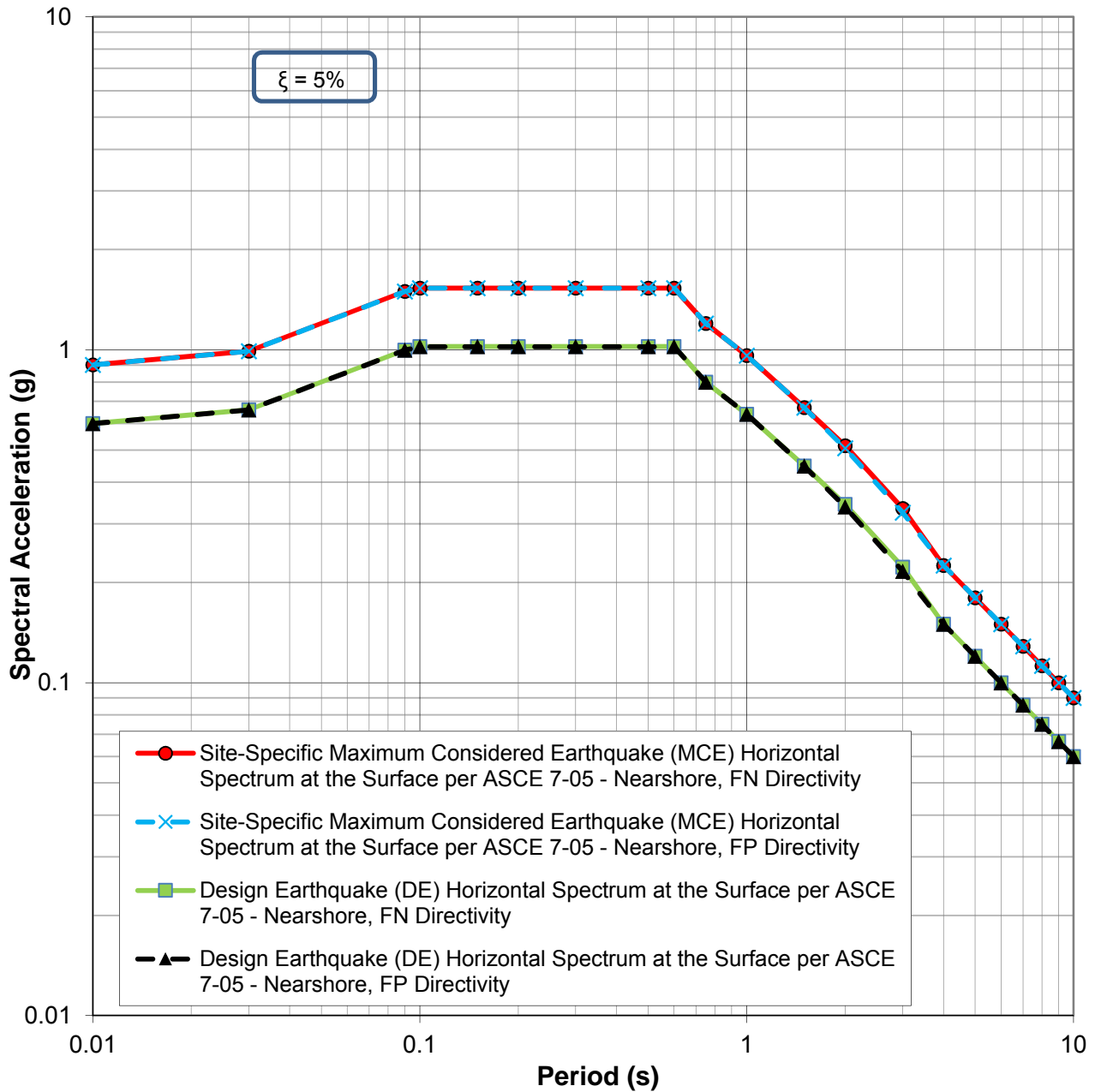
**5-PERCENT DAMPED HORIZONTAL ACCELERATION RESPONSE SPECTRA AT GROUND SURFACE
(VS30=885 FT/S) PER ASCE 7-05 GUIDELINES - ONSHORE LOCATION**

LNG FACILITIES
ALASKA LNG PROJECT
NIKISKI, ALASKA



**5-PERCENT DAMPED HORIZONTAL ACCELERATION RESPONSE SPECTRA AT GROUND SURFACE
(VS30=885 FT/S) PER NFPA-59A 2006 GUIDELINES - NEARSHORE LOCATION**

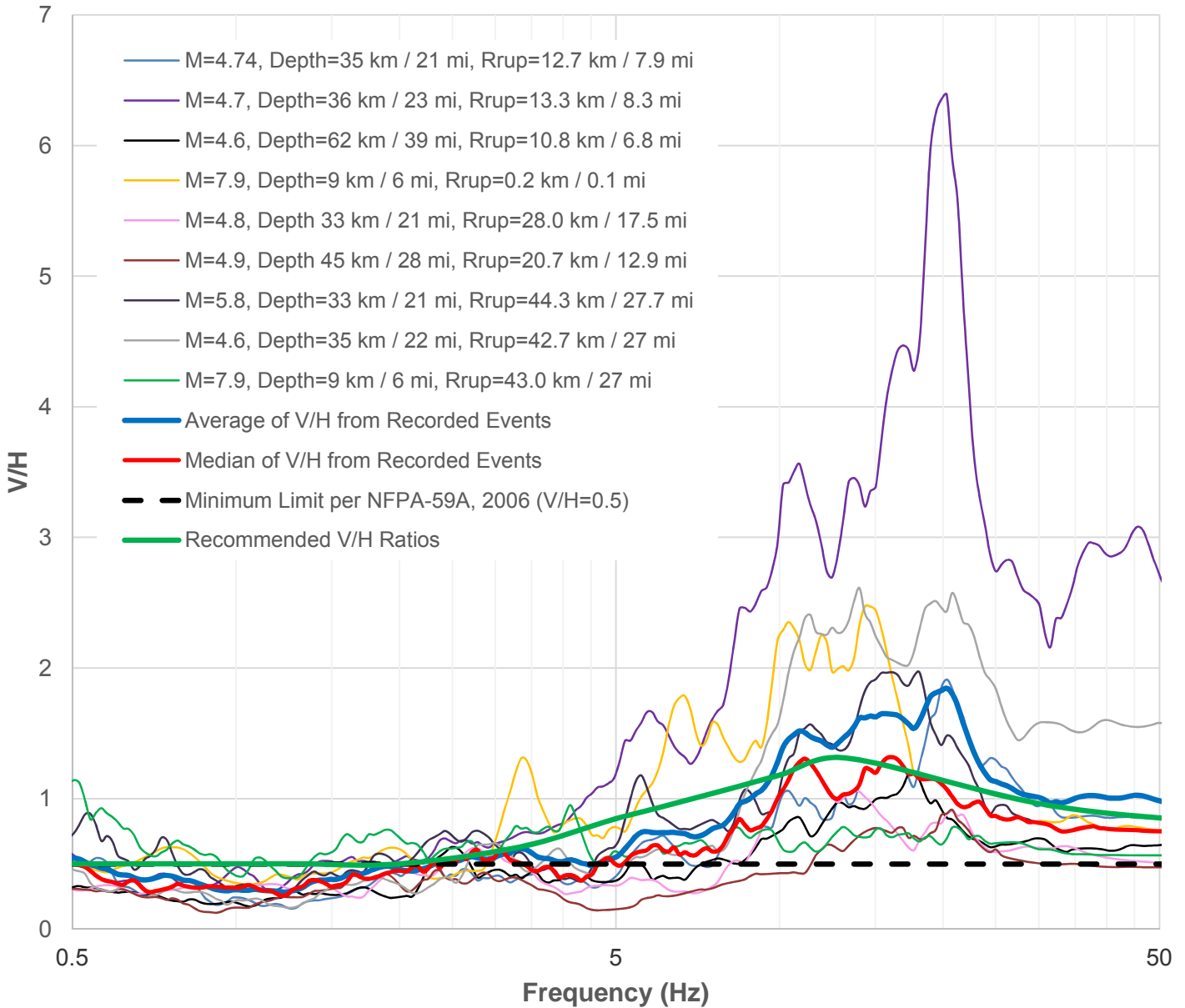
LNG FACILITIES
ALASKA LNG PROJECT
NIKISKI, ALASKA



**5-PERCENT DAMPED HORIZONTAL ACCELERATION RESPONSE SPECTRA AT GROUND SURFACE
(VS30=885 FT/S) PER ASCE 7-05 GUIDELINES - NEARSHORE LOCATION**

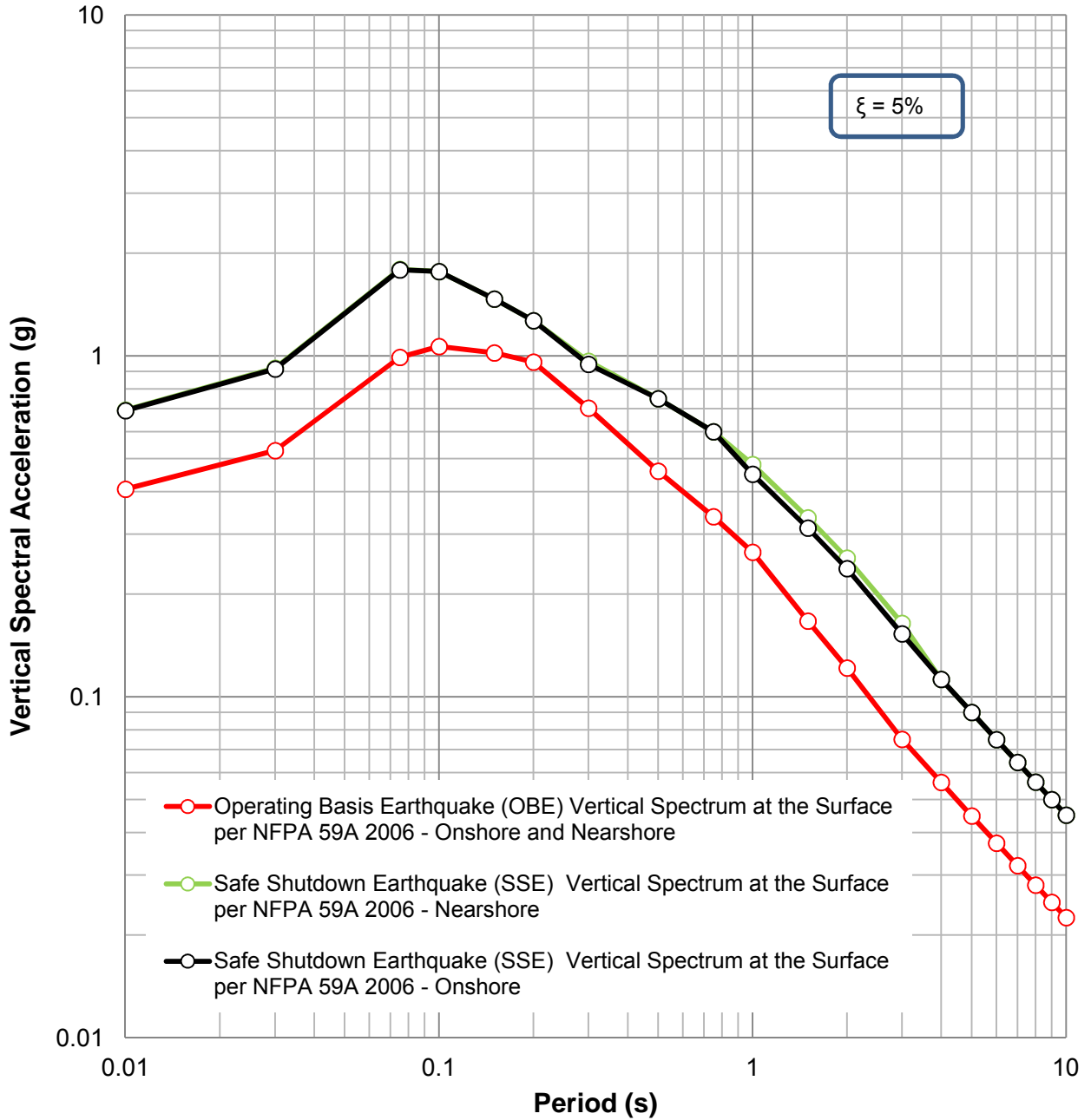
LNG FACILITIES
ALASKA LNG PROJECT
NIKISKI, ALASKA

Combined Alaska EQs, R = 0 - 50 km / 0 - 31 mi



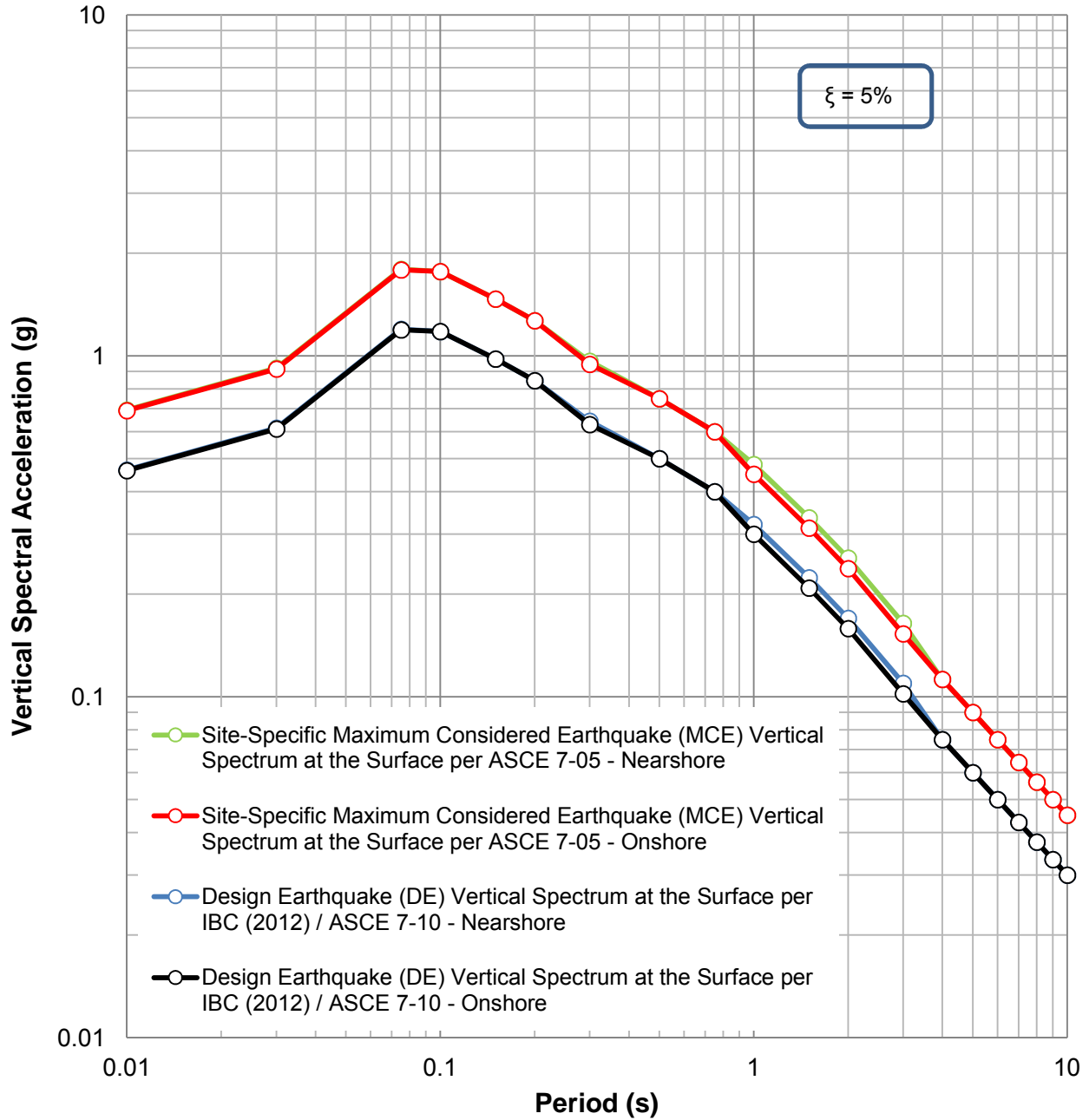
VERTICAL TO HORIZONTAL SPECTRAL ACCELERATION RATIOS (V/H) OF ALASKA RECORDS FOR SITE CLASS D AND R = 0 - 31 MI (0 - 50 KM)

LNG FACILITIES
 ALASKA LNG PROJECT
 NIKISKI, ALASKA



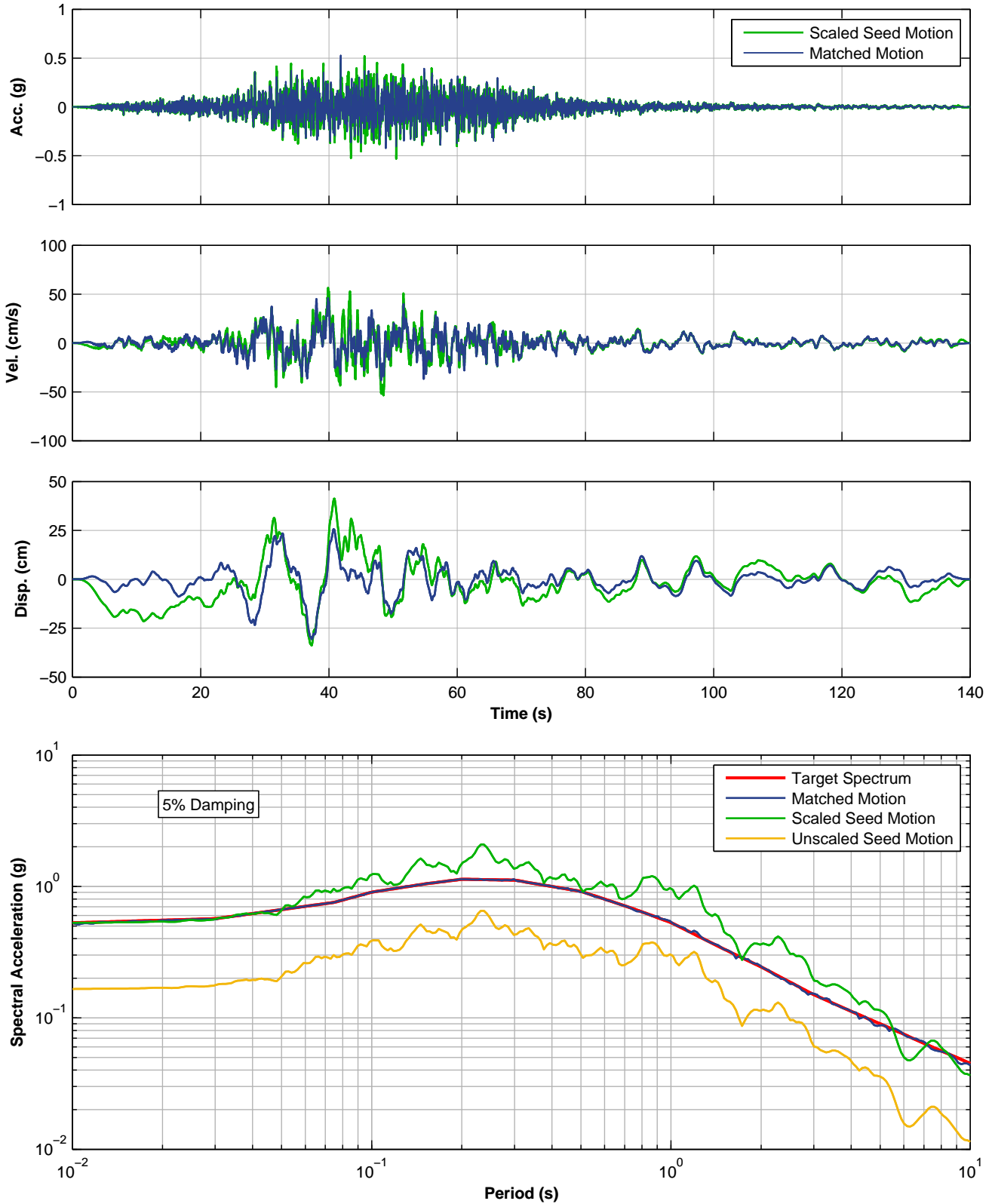
**5-PERCENT DAMPED VERTICAL ACCELERATION RESPONSE SPECTRA AT GROUND SURFACE
 (VS30=885 FT/S) PER NFPA-59A 2006 GUIDELINES**

LNG FACILITIES
 ALASKA LNG PROJECT
 NIKISKI, ALASKA

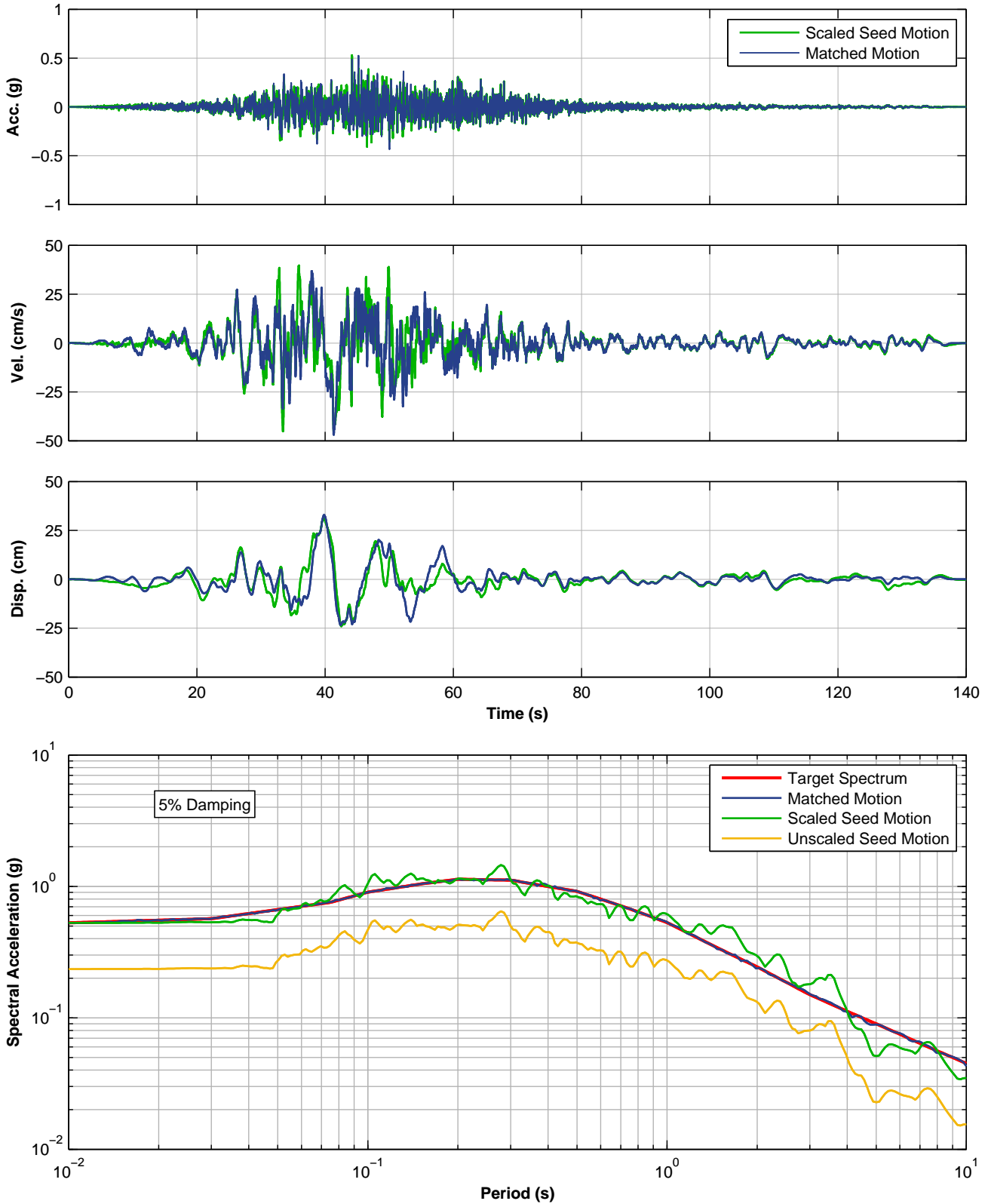


**5-PERCENT DAMPED VERTICAL ACCELERATION RESPONSE SPECTRA AT GROUND SURFACE
(VS30=885 FT/S) PER ASCE 7-05 GUIDELINES**

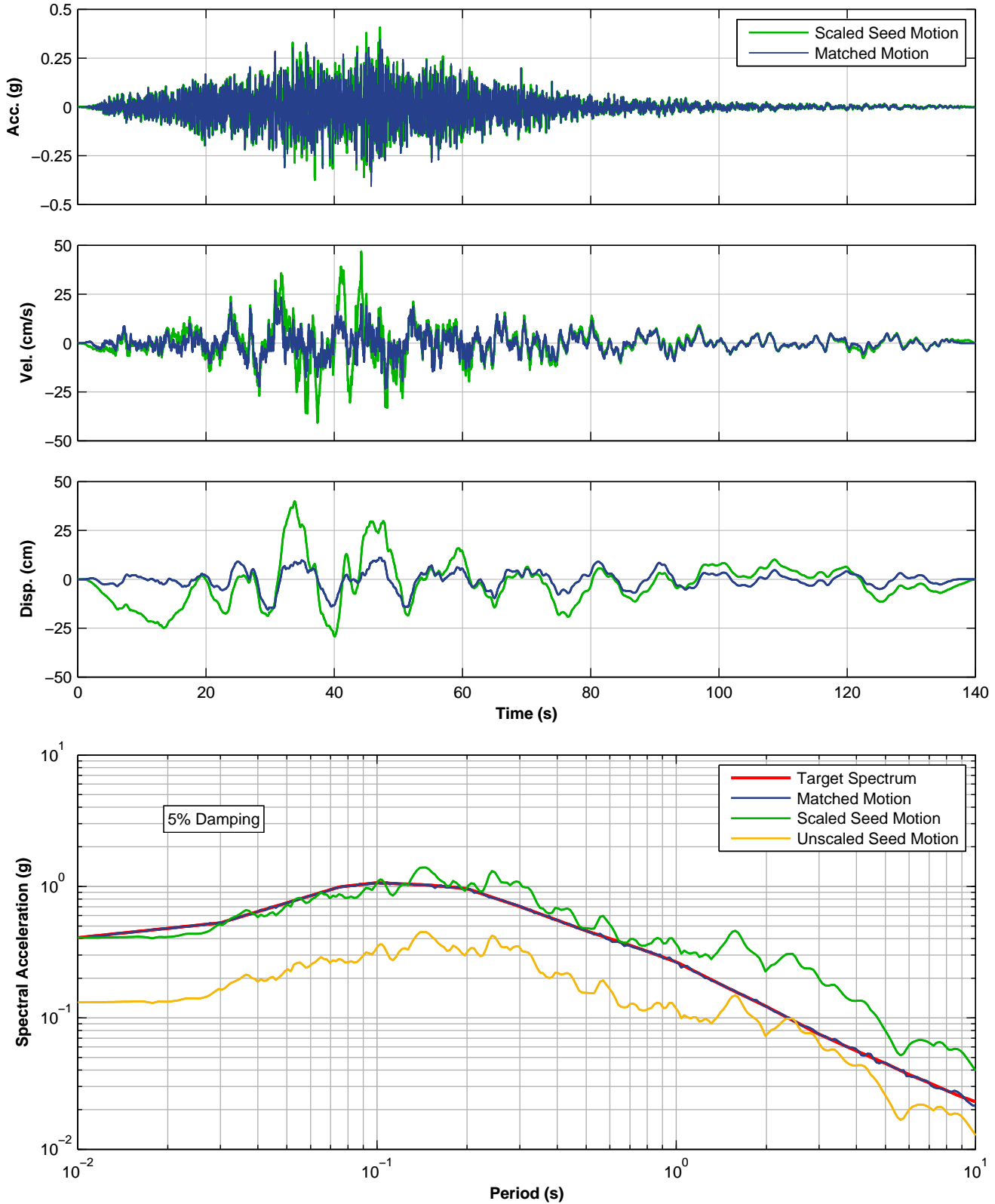
ONSHORE LNG FACILITIES
ALASKA LNG PROJECT
NIKISKI, ALASKA



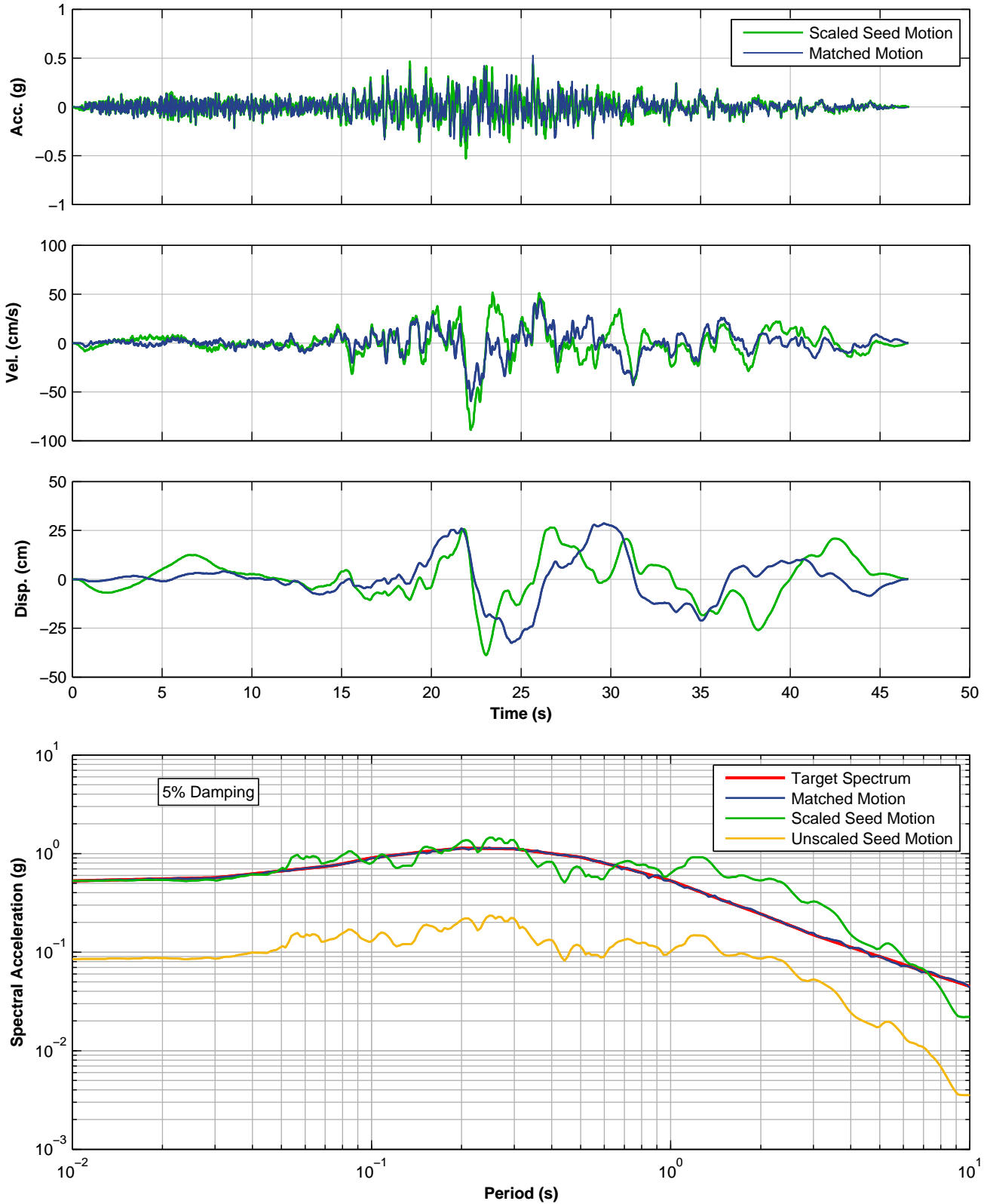
**SPECTRALLY MATCHED MEP MOTION, EW COMPONENT, 2010 CHILE EQ
OBE LEVEL PER NFPA 59A 2006 – ONSHORE AND NEARSHORE, FAULT NORMAL
LNG FACILITIES
ALASKA LNG PROJECT
NIKISKI, ALASKA**



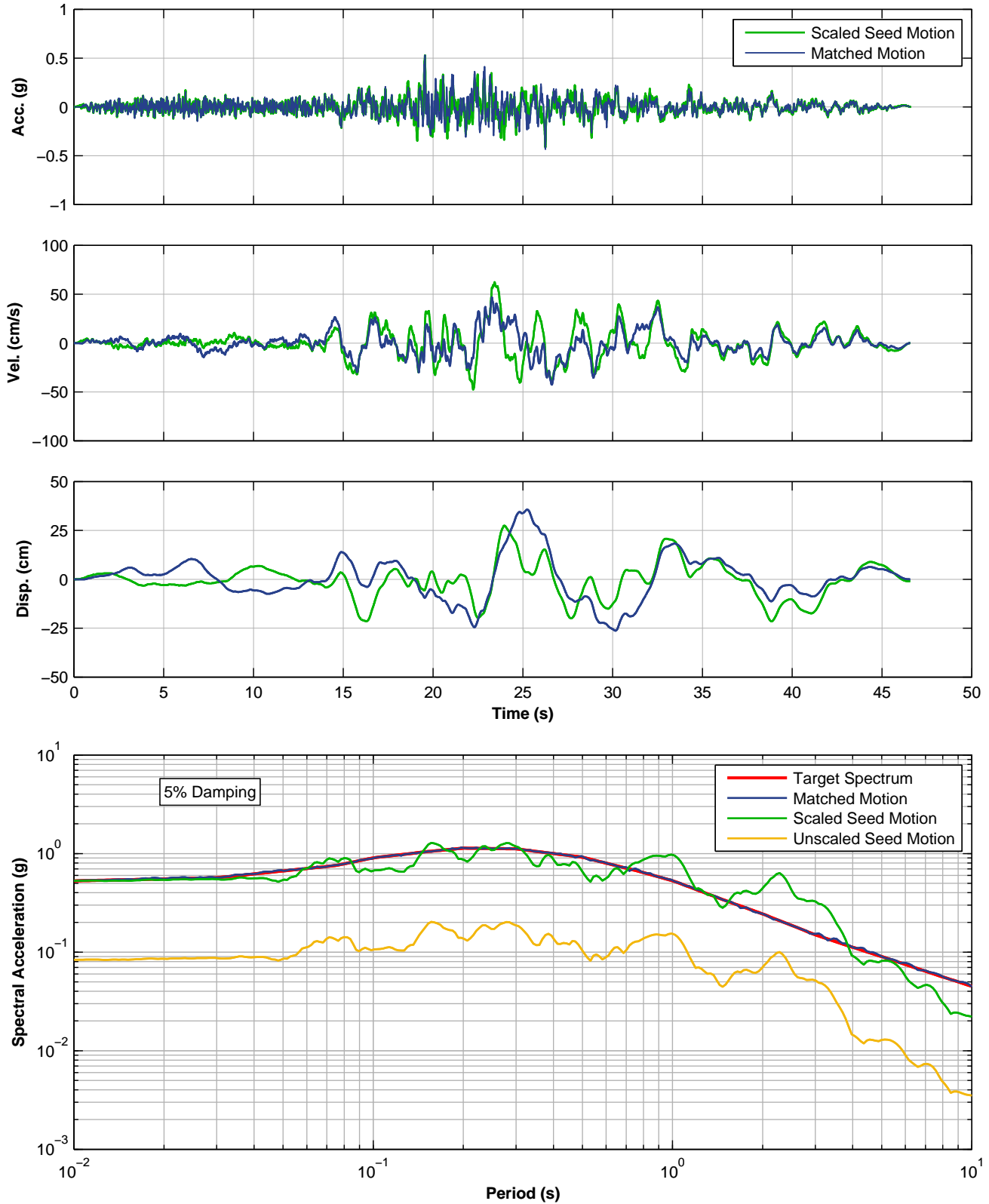
**SPECTRALLY MATCHED MEP MOTION, NS COMPONENT, 2010 CHILE EQ
OBE LEVEL PER NFPA 59A 2006 – ONSHORE AND NEARSHORE, FAULT PARALLEL
LNG FACILITIES
ALASKA LNG PROJECT
NIKISKI, ALASKA**



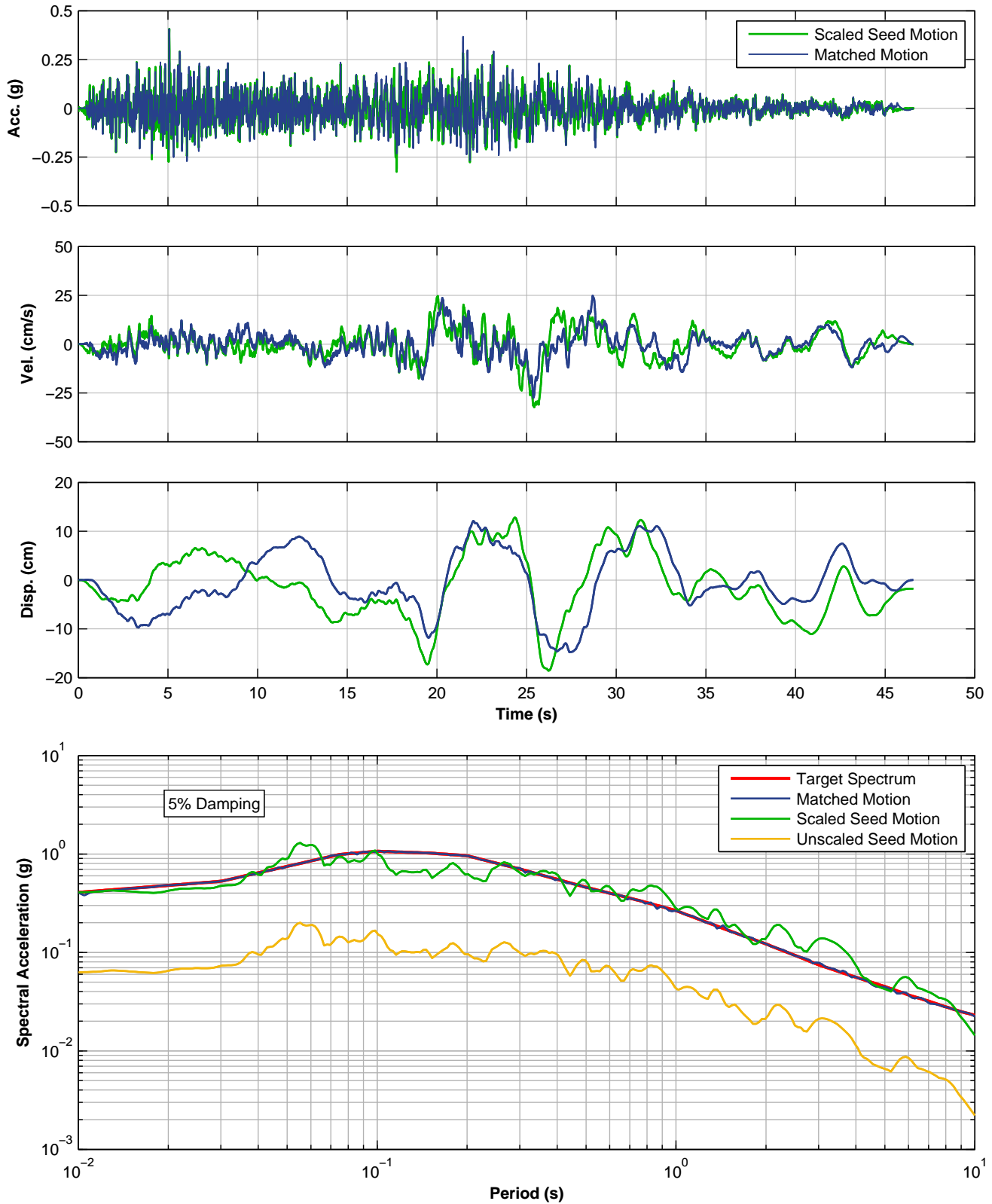
**SPECTRALLY MATCHED MEP MOTION, V COMPONENT, 2010 CHILE EQ
 OBE LEVEL PER NFPA 59A 2006 – ONSHORE AND NEARSHORE
 LNG FACILITIES
 ALASKA LNG PROJECT
 NIKISKI, ALASKA**



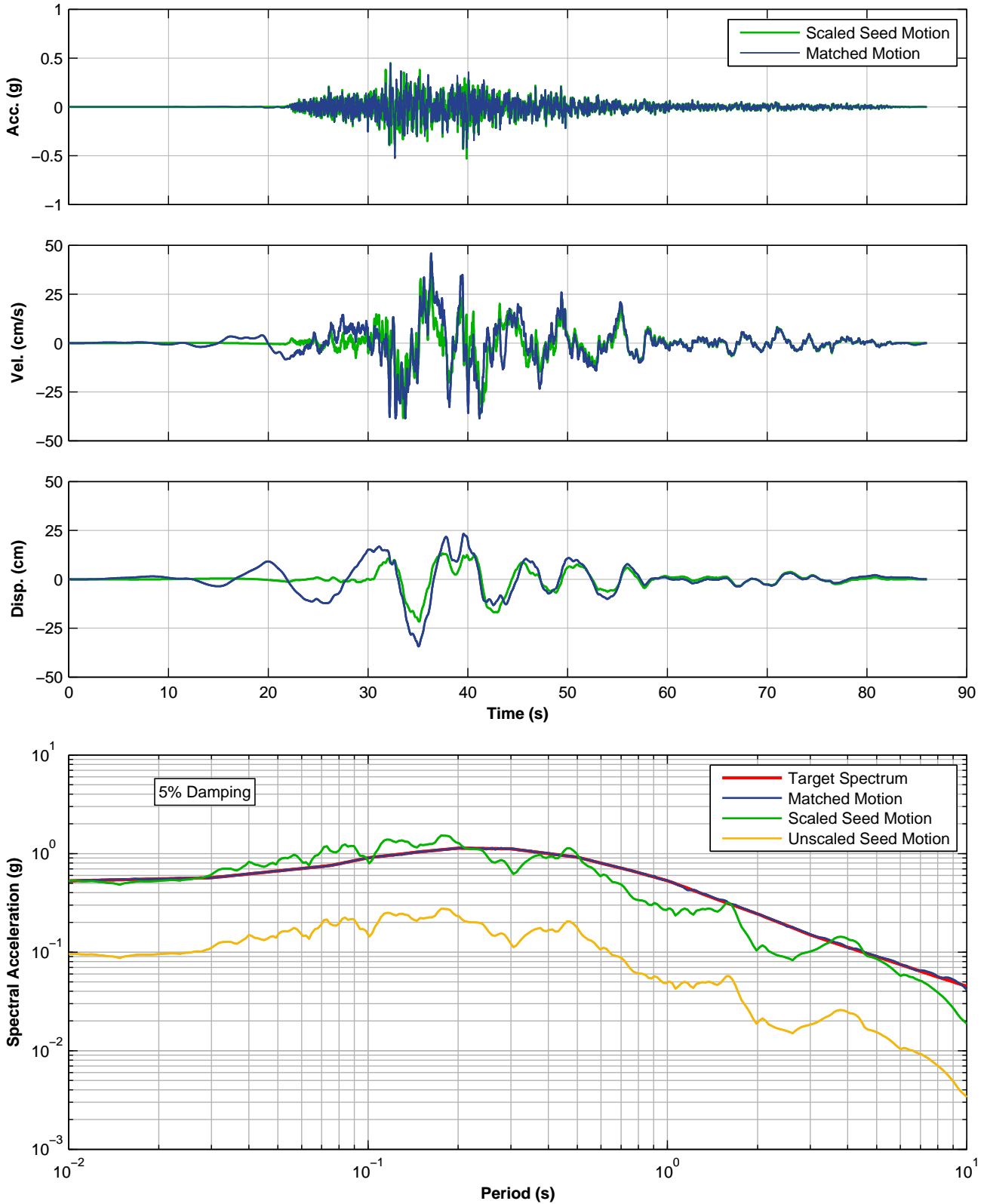
**SPECTRALLY MATCHED CTO MOTION, 180 COMPONENT, 2001 EL SALVADOR EQ
OBE LEVEL PER NFPA 59A 2006 – ONSHORE AND NEARSHORE, FAULT NORMAL
LNG FACILITIES
ALASKA LNG PROJECT
NIKISKI, ALASKA**



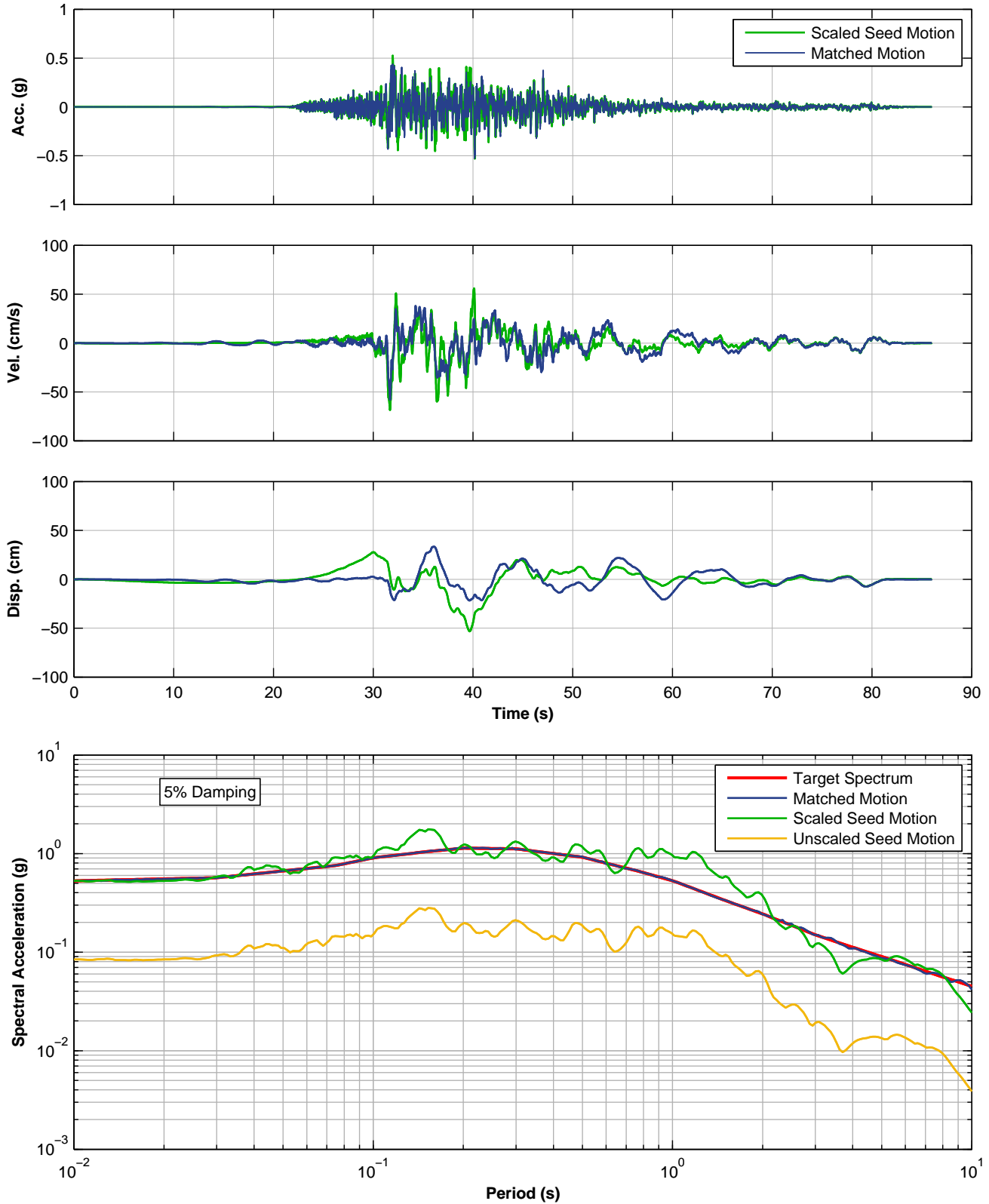
**SPECTRALLY MATCHED CTO MOTION, 270 COMPONENT, 2001 EL SALVADOR EQ
OBE LEVEL PER NFPA 59A 2006 – ONSHORE AND NEARSHORE, FAULT PARALLEL
LNG FACILITIES
ALASKA LNG PROJECT
NIKISKI, ALASKA**



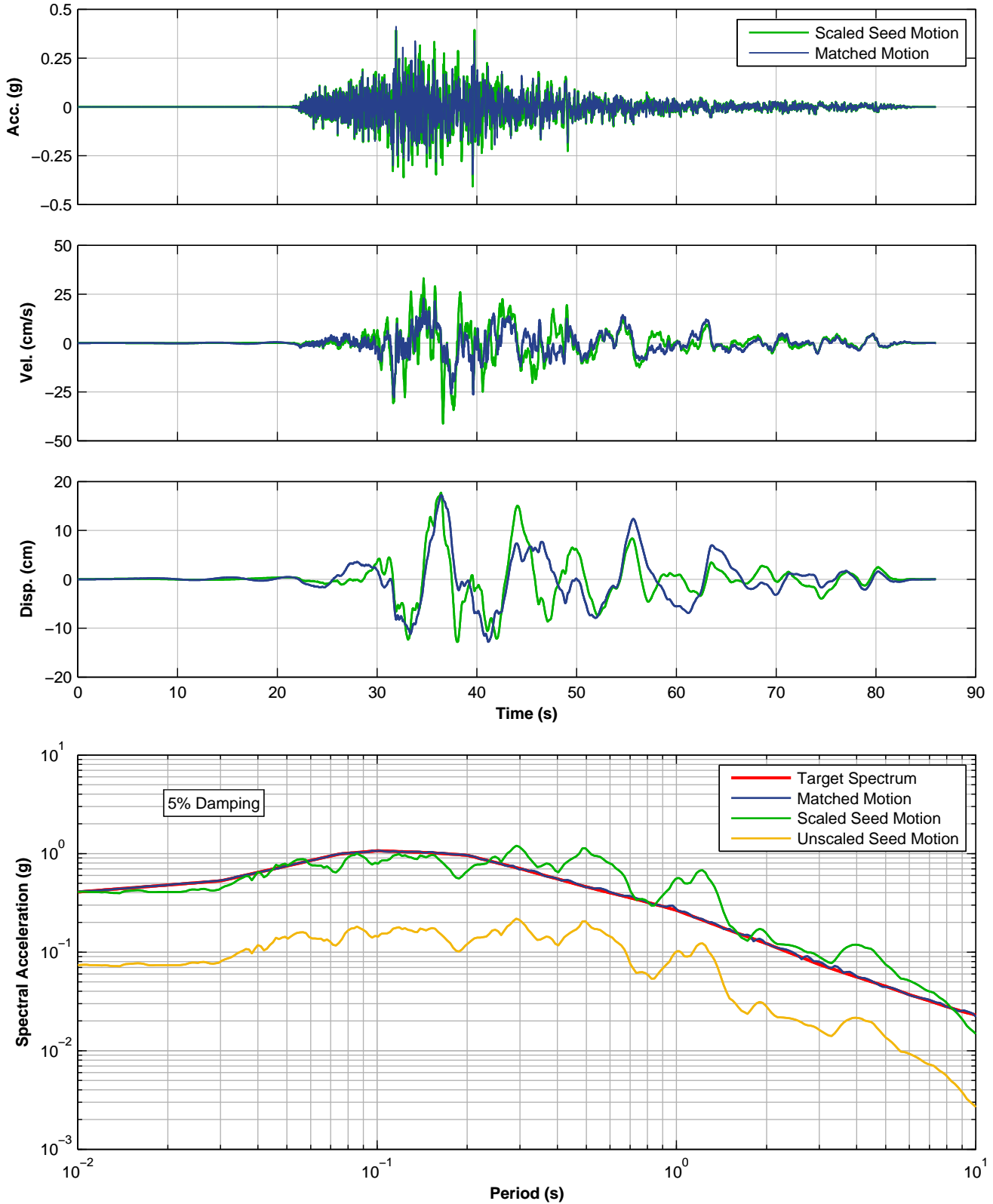
**SPECTRALLY MATCHED CTO MOTION, UP COMPONENT, 2001 EL SALVADOR EQ
OBE LEVEL PER NFPA 59A 2006 – ONSHORE AND NEARSHORE
LNG FACILITIES
ALASKA LNG PROJECT
NIKISKI, ALASKA**



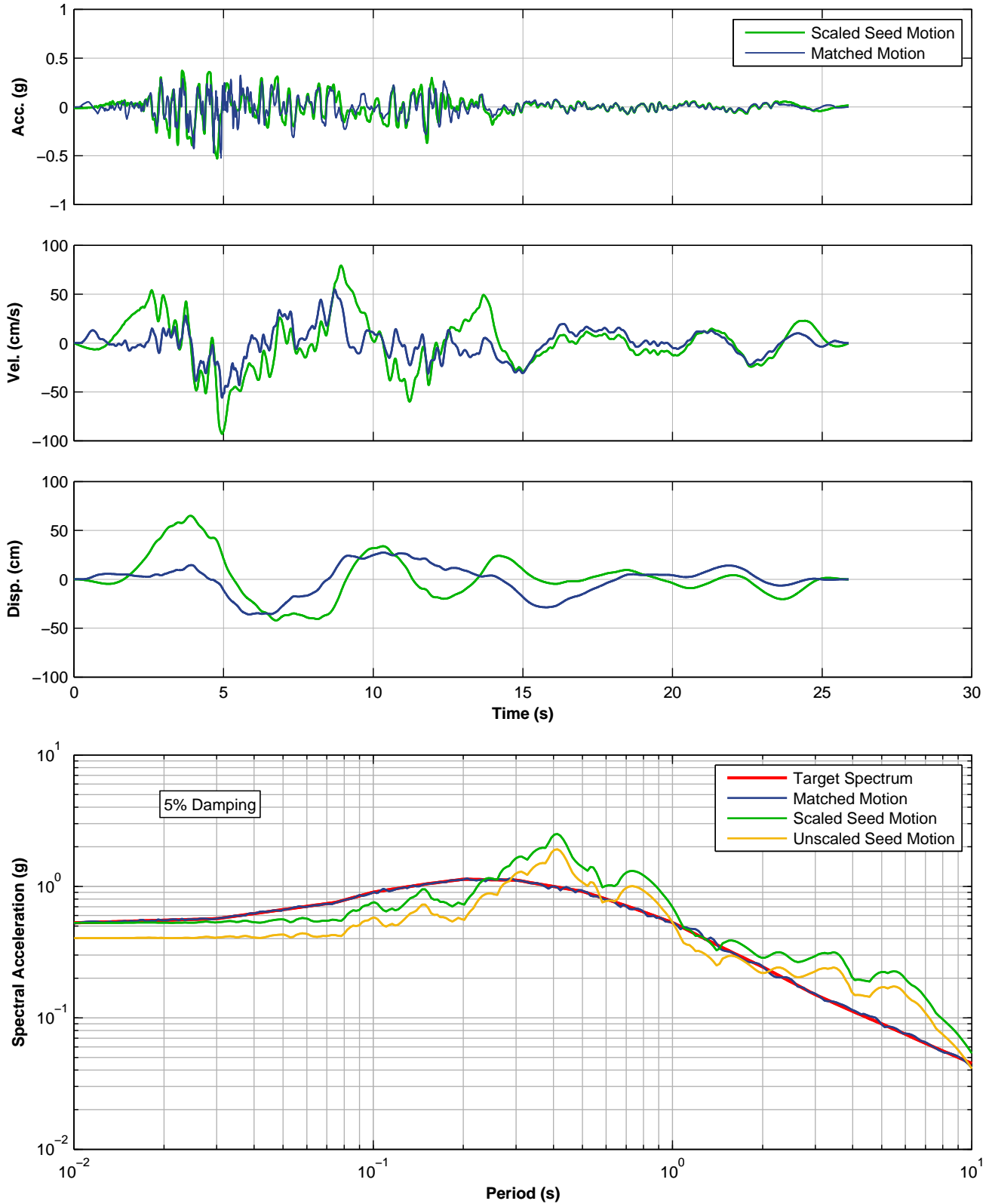
**SPECTRALLY MATCHED CARLO MOTION, 090 COMPONENT, 2002 DENALI EQ, ALASKA
OBE LEVEL PER NFPA 59A 2006 – ONSHORE AND NEARSHORE, FAULT NORMAL
LNG FACILITIES
ALASKA LNG PROJECT
NIKISKI, ALASKA**



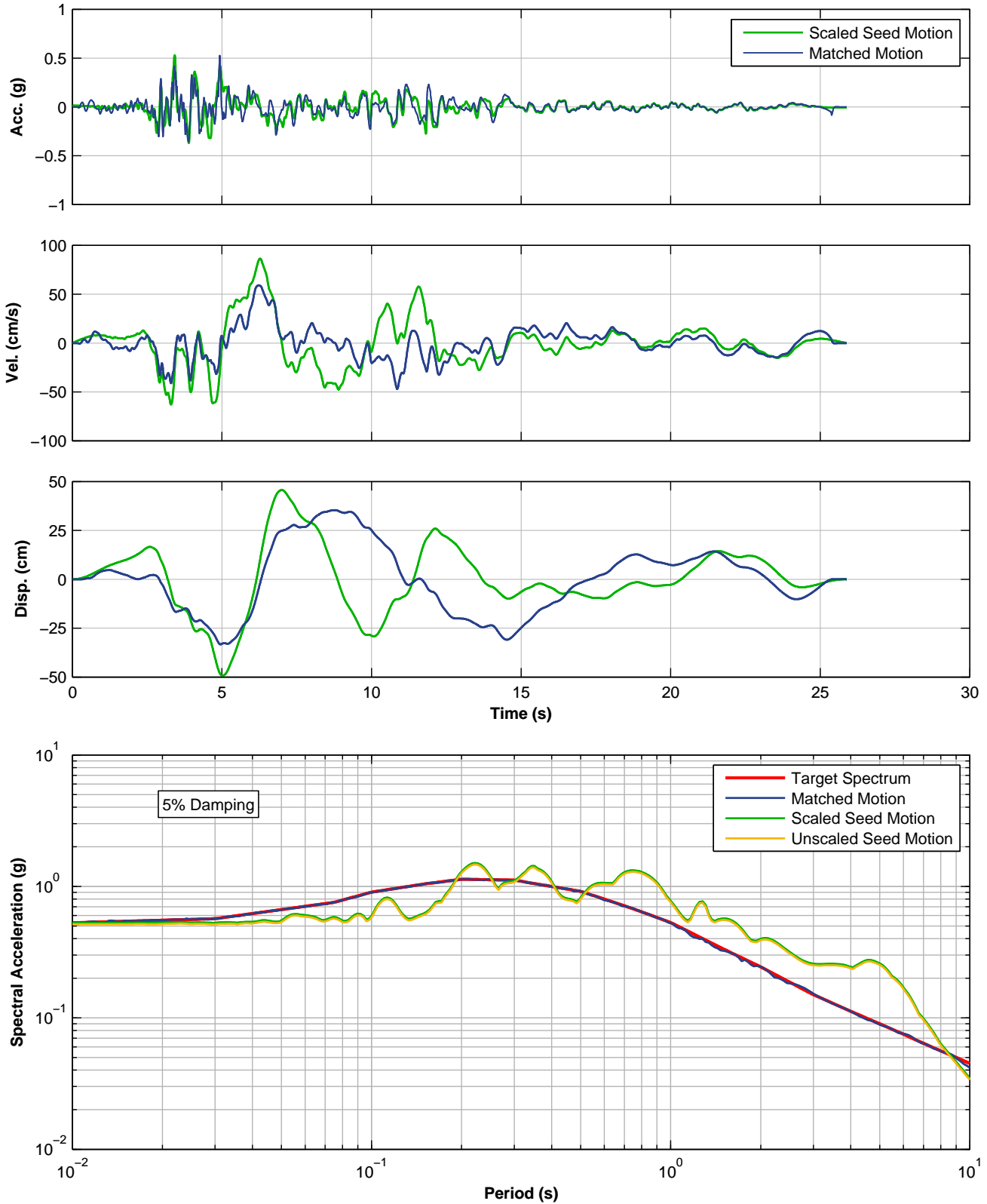
**SPECTRALLY MATCHED CARLO MOTION, 360 COMPONENT, 2002 DENALI EQ, ALASKA
OBE LEVEL PER NFPA 59A 2006 – ONSHORE AND NEARSHORE, FAULT PARALLEL
LNG FACILITIES
ALASKA LNG PROJECT
NIKISKI, ALASKA**



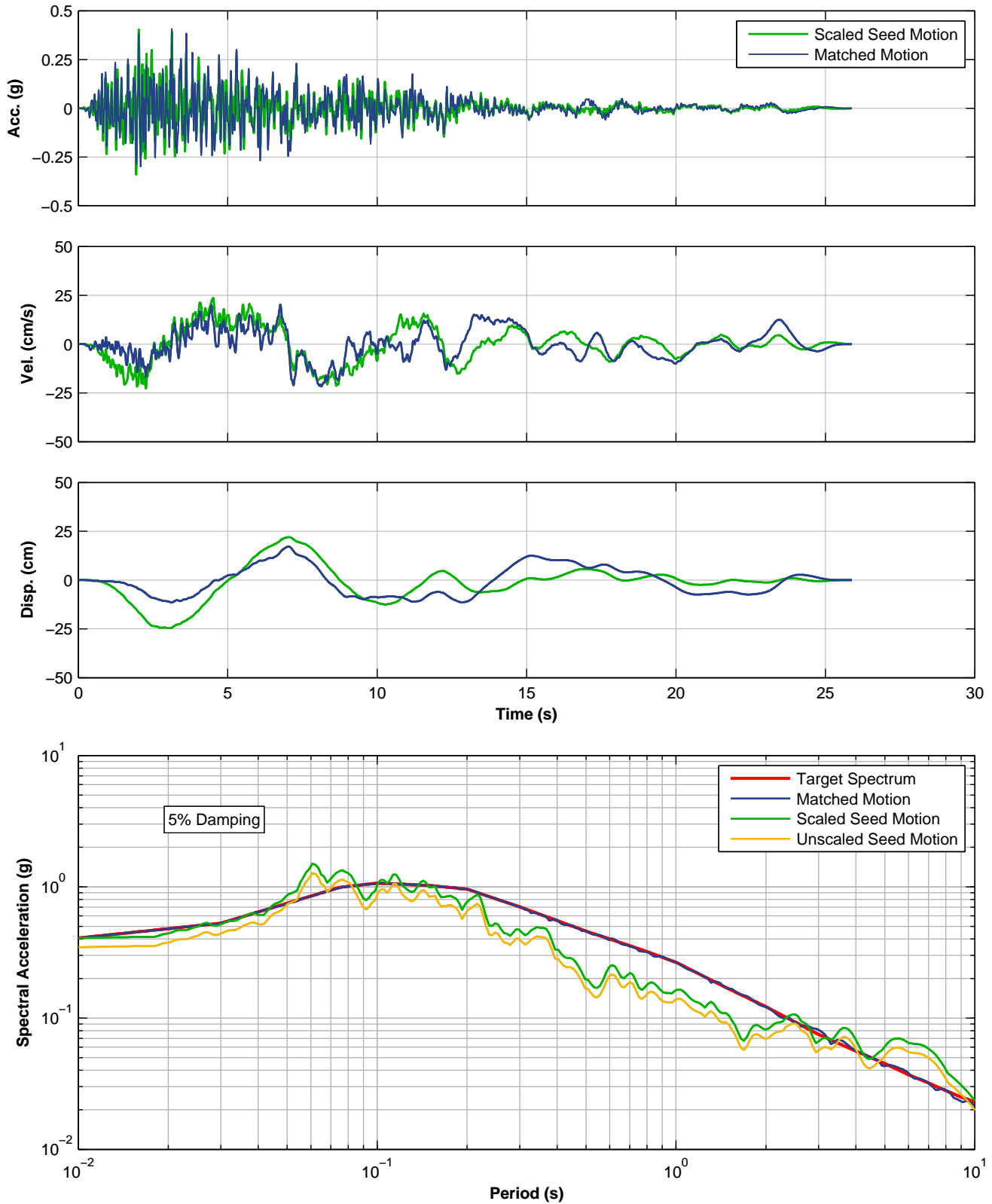
**SPECTRALLY MATCHED CARLO MOTION, UP COMPONENT, 2002 DENALI EQ, ALASKA
OBE LEVEL PER NFPA 59A 2006 – ONSHORE AND NEARSHORE
LNG FACILITIES
ALASKA LNG PROJECT
NIKISKI, ALASKA**



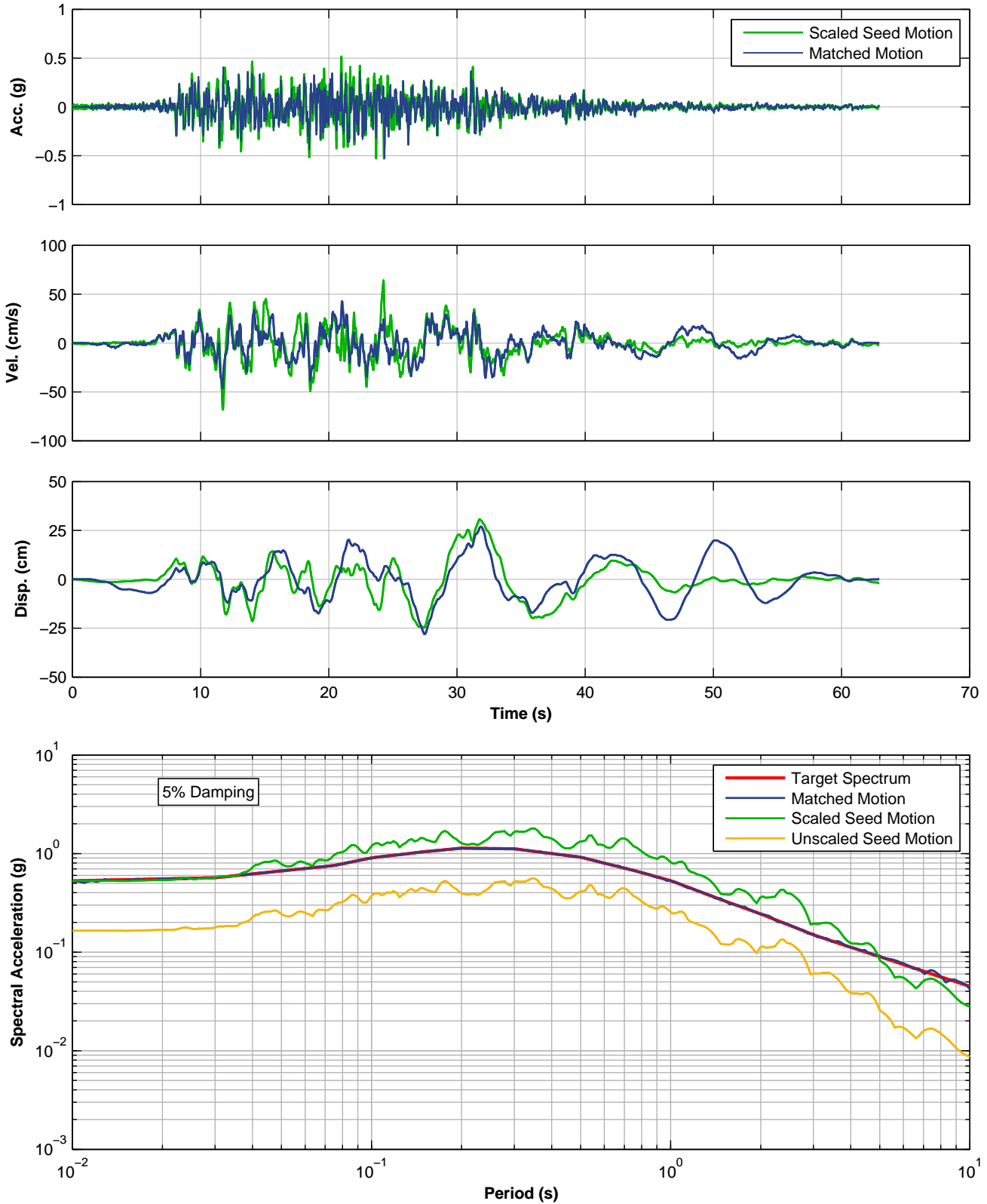
**SPECTRALLY MATCHED DZC MOTION, 180 COMPONENT, 1999 DUZCE EQ, TURKEY
OBE LEVEL PER NFPA 59A 2006 – ONSHORE AND NEARSHORE, FAULT NORMAL
LNG FACILITIES
ALASKA LNG PROJECT
NIKISKI, ALASKA**



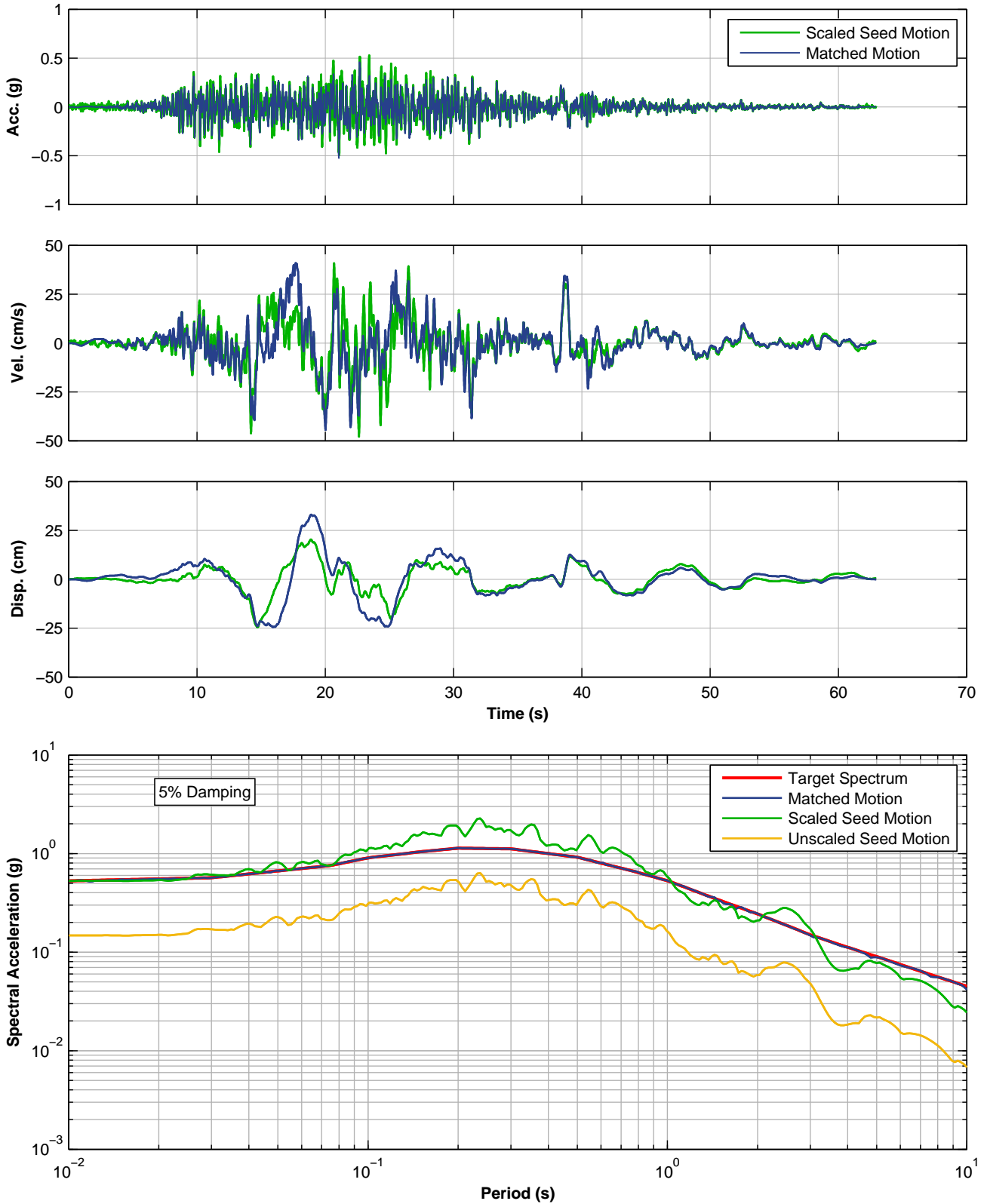
**SPECTRALLY MATCHED DZC MOTION, 270 COMPONENT, 1999 DUZCE EQ, TURKEY
OBE LEVEL PER NFPA 59A 2006 – ONSHORE AND NEARSHORE, FAULT PARALLEL
LNG FACILITIES
ALASKA LNG PROJECT
NIKISKI, ALASKA**



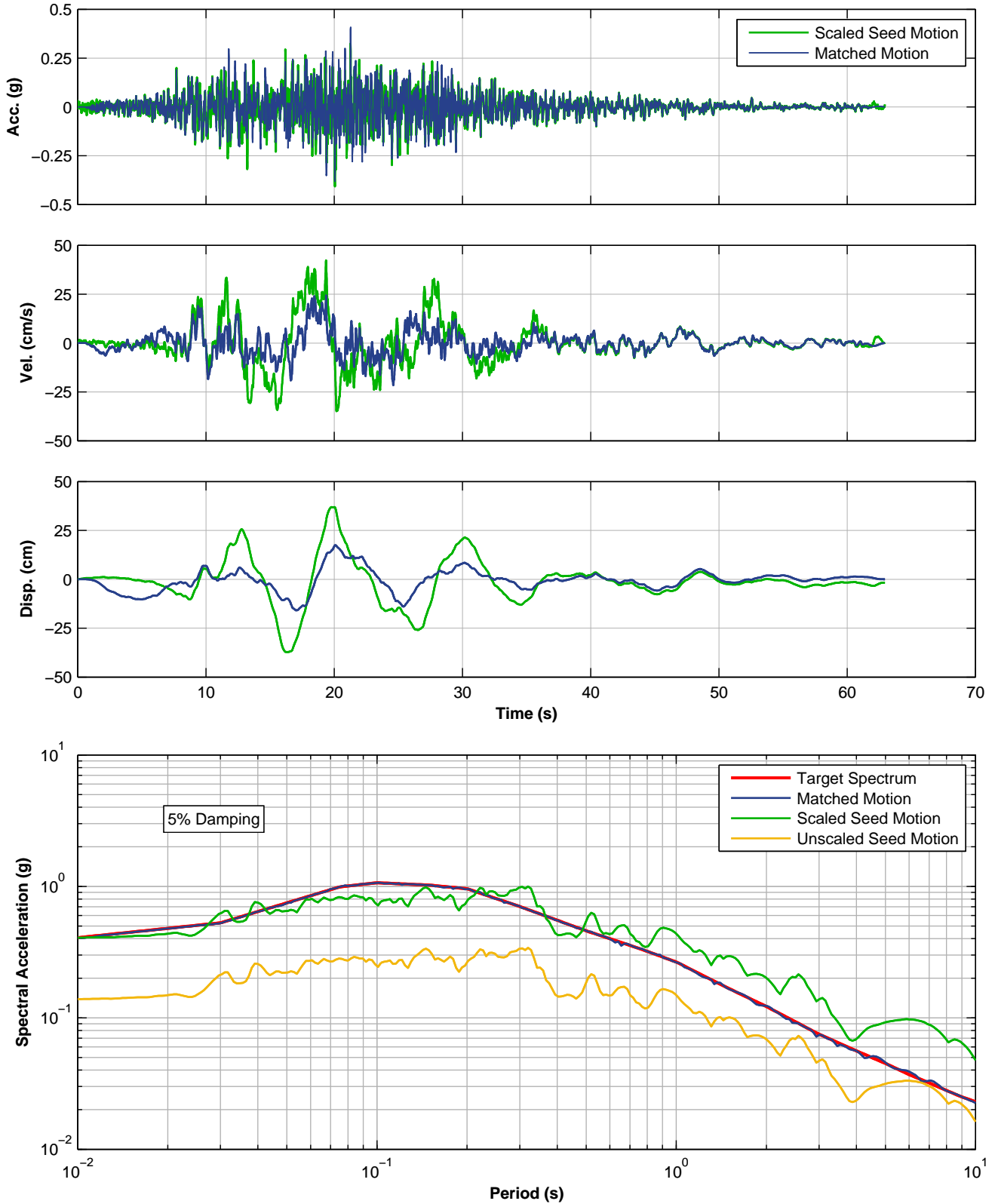
**SPECTRALLY MATCHED DZC MOTION, UP COMPONENT, 1999 DUZCE EQ, TURKEY
OBE LEVEL PER NFPA 59A 2006 – ONSHORE AND NEARSHORE
LNG FACILITIES
ALASKA LNG PROJECT
NIKISKI, ALASKA**



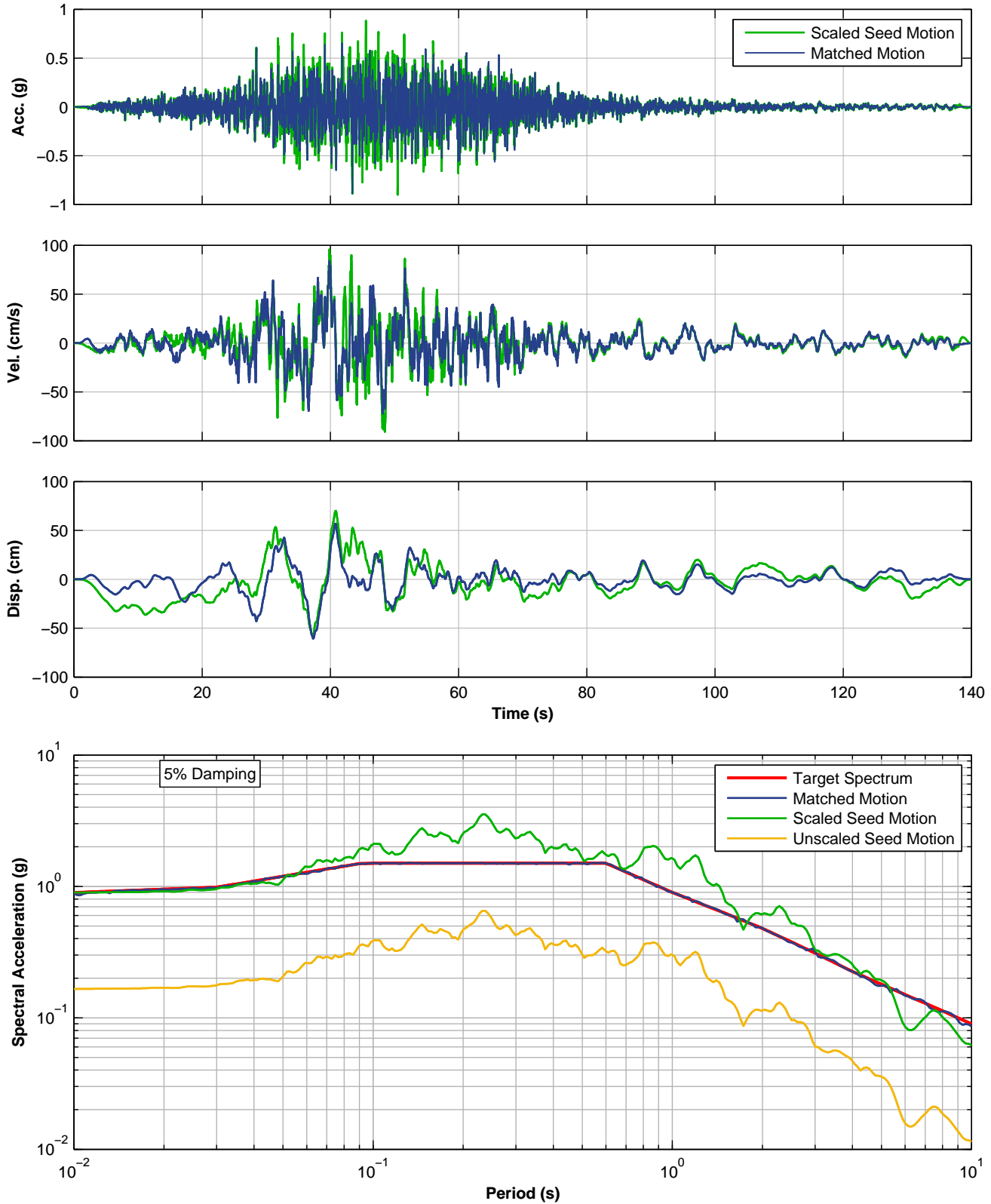
**SPECTRALLY MATCHED UNIO MOTION, N00W COMPONENT, 1985 MEXICO EQ
OBE LEVEL PER NFPA 59A 2006 – ONSHORE AND NEARSHORE, FAULT NORMAL
LNG FACILITIES
ALASKA LNG PROJECT
NIKISKI, ALASKA**



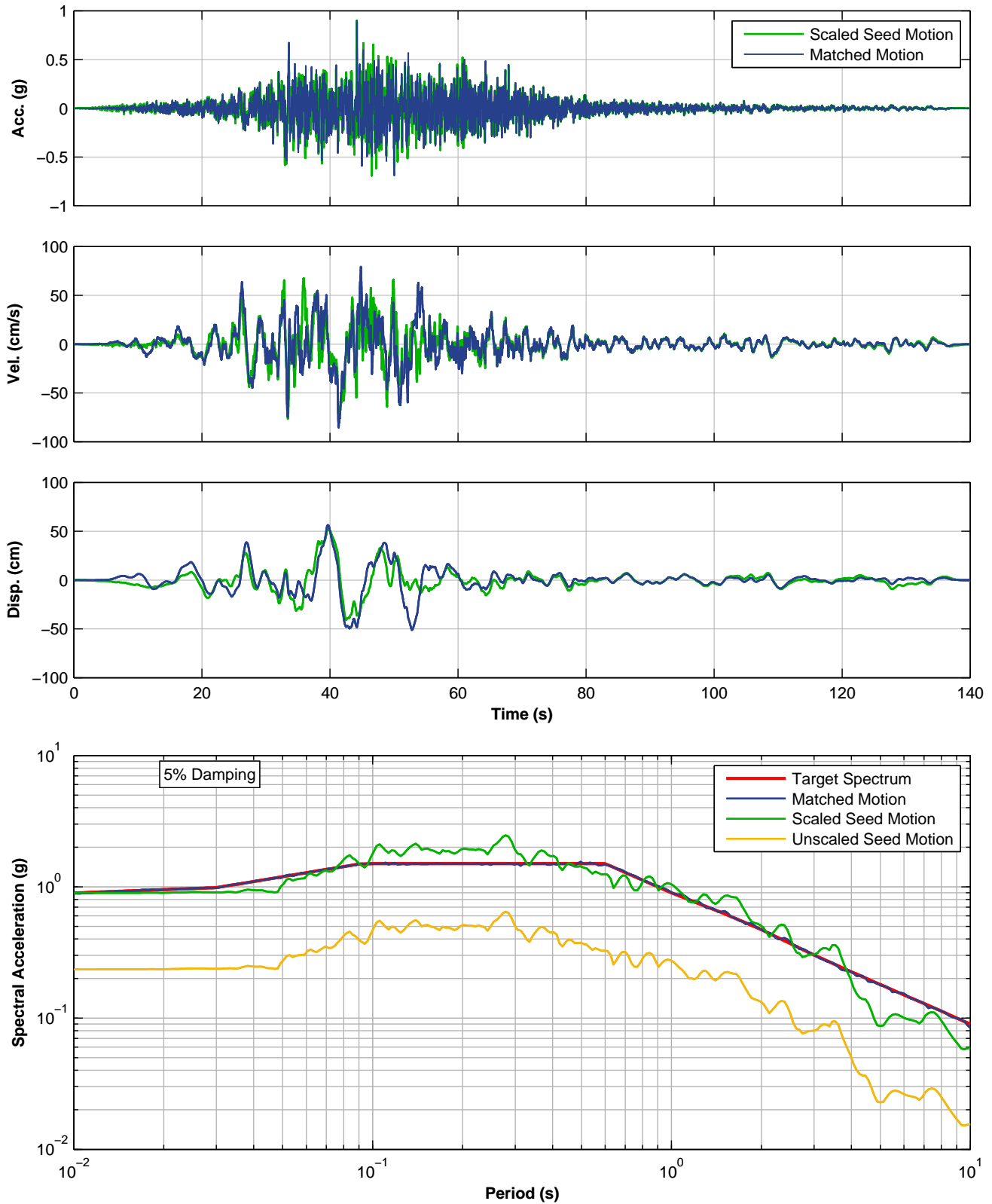
**SPECTRALLY MATCHED UNIO MOTION, N90W COMPONENT, 1985 MEXICO EQ
OBE LEVEL PER NFPA 59A 2006 – ONSHORE AND NEARSHORE, FAULT PARALLEL
LNG FACILITIES
ALASKA LNG PROJECT
NIKISKI, ALASKA**



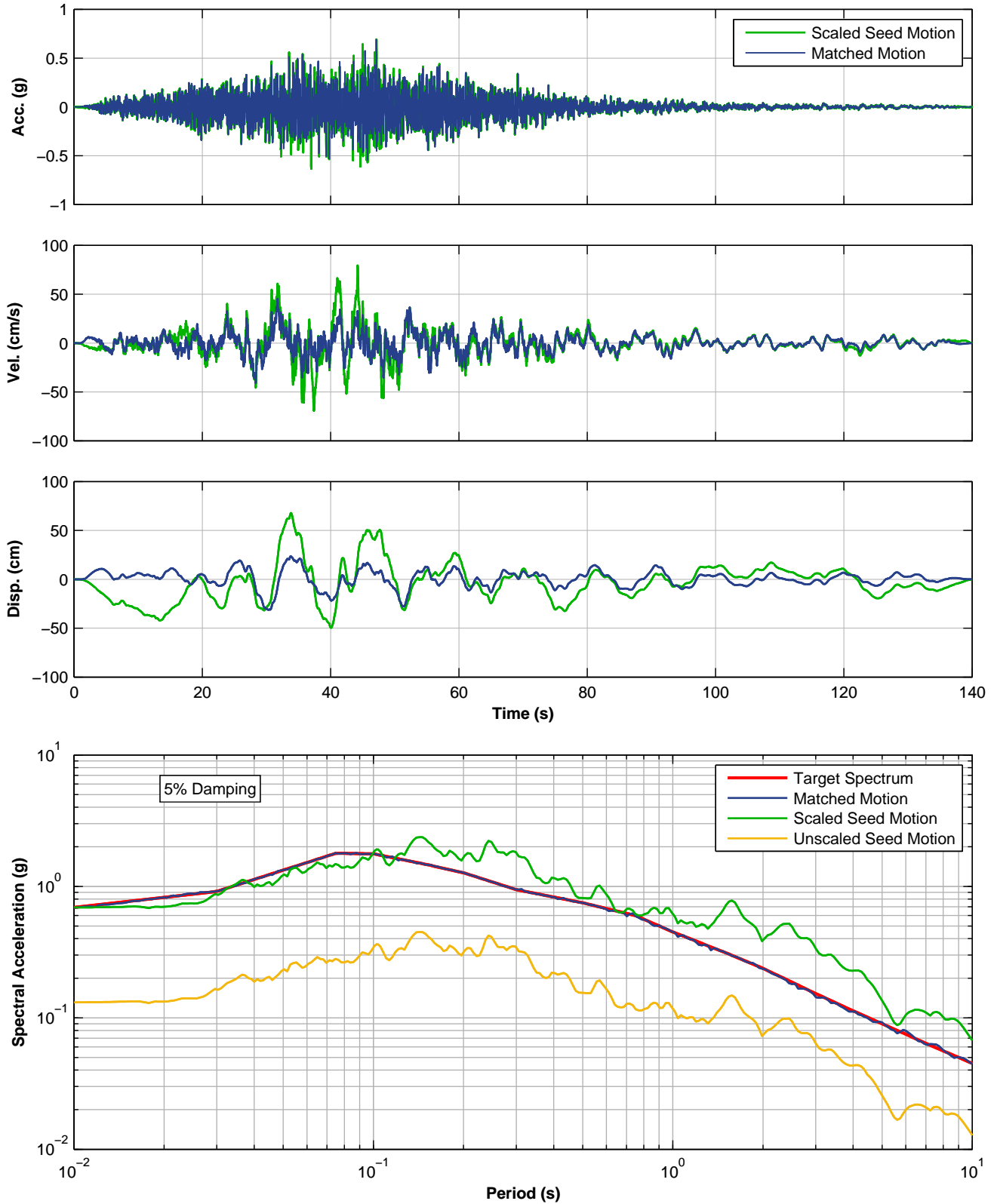
**SPECTRALLY MATCHED UNIO MOTION, UP COMPONENT, 1985 MEXICO EQ
 OBE LEVEL PER NFPA 59A 2006 – ONSHORE AND NEARSHORE
 LNG FACILITIES
 ALASKA LNG PROJECT
 NIKISKI, ALASKA**



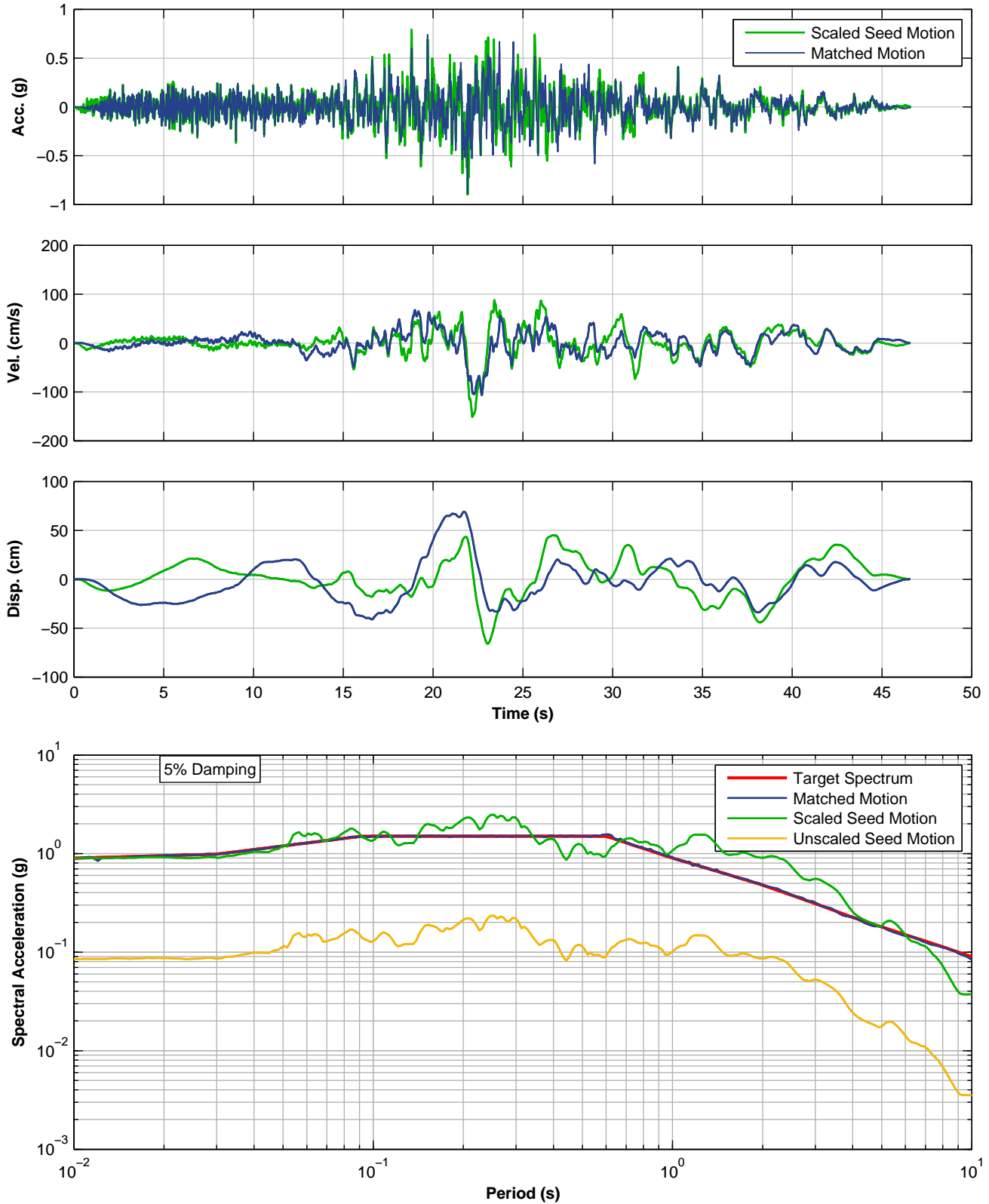
**SPECTRALLY MATCHED MEP MOTION, EW COMPONENT, 2010 CHILE EQ
 SSE LEVEL PER NFPA 59A 2006 – ONSHORE, FAULT NORMAL
 LNG FACILITIES
 ALASKA LNG PROJECT
 NIKISKI, ALASKA**



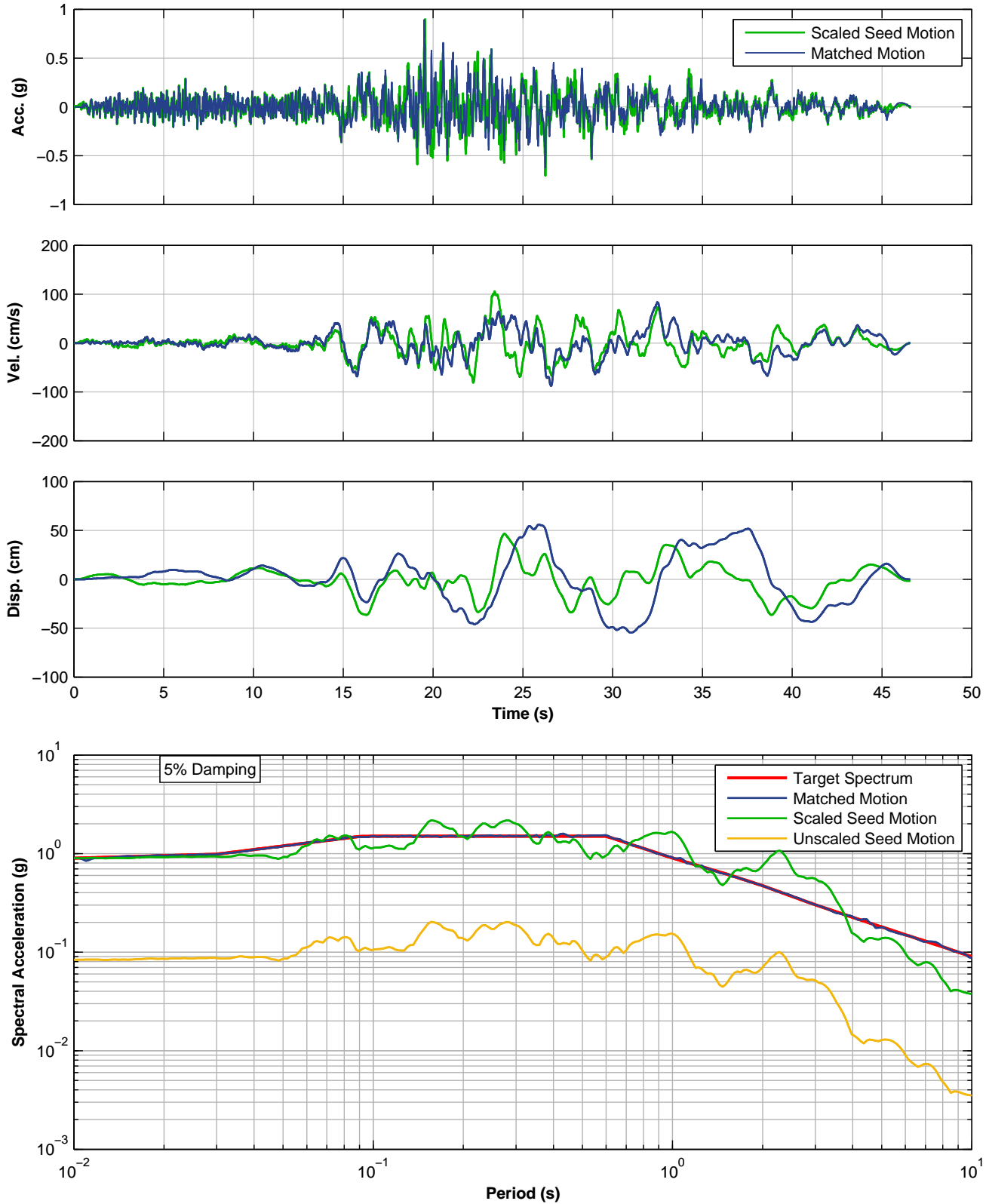
**SPECTRALLY MATCHED MEP MOTION, NS COMPONENT, 2010 CHILE EQ
SSE LEVEL PER NFPA 59A 2006 – ONSHORE, FAULT PARALLEL
LNG FACILITIES
ALASKA LNG PROJECT
NIKISKI, ALASKA**



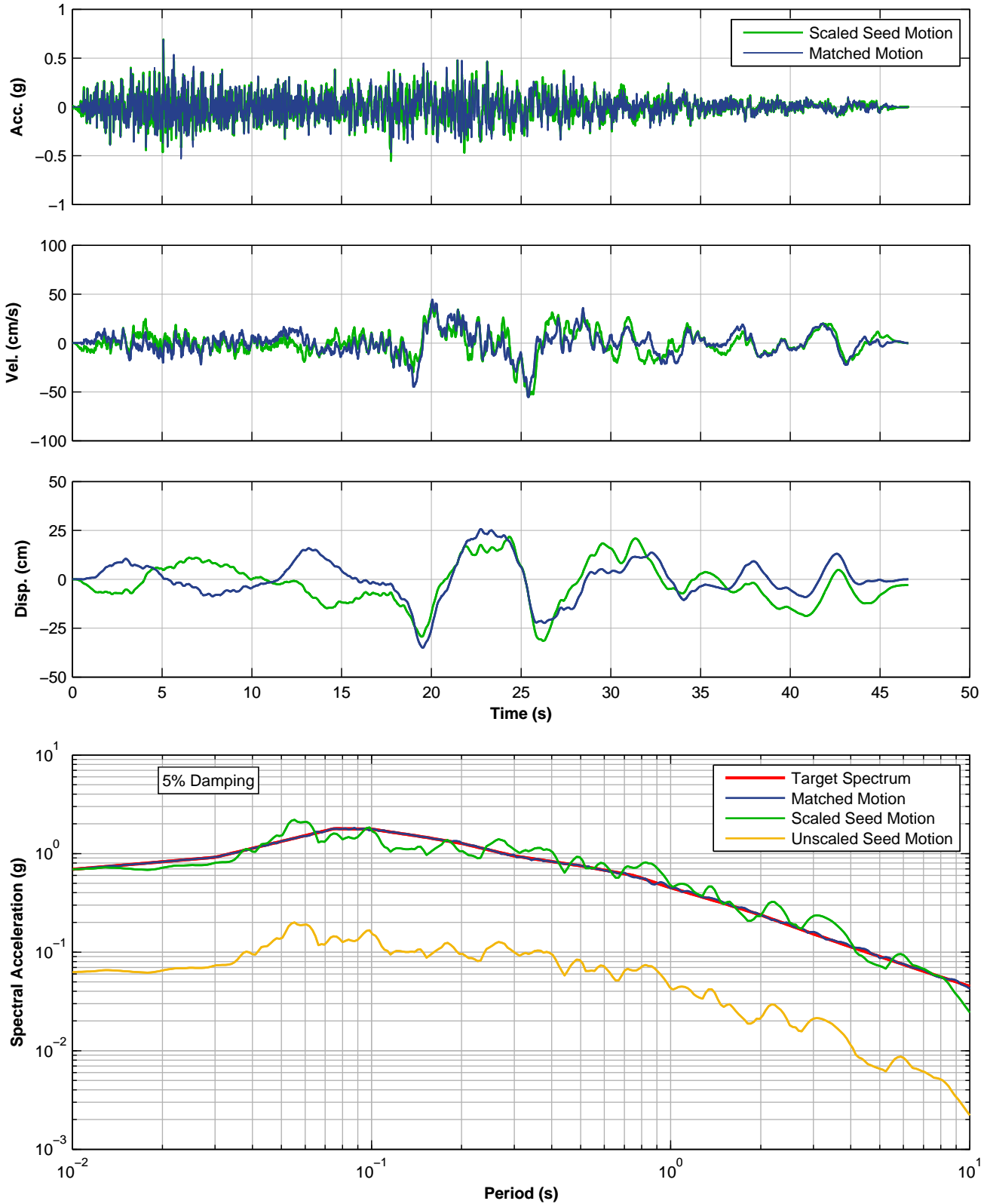
SPECTRALLY MATCHED MEP MOTION, V COMPONENT, 2010 CHILE EQ
SSE LEVEL PER NFPA 59A 2006 – ONSHORE
LNG FACILITIES
ALASKA LNG PROJECT
NIKISKI, ALASKA



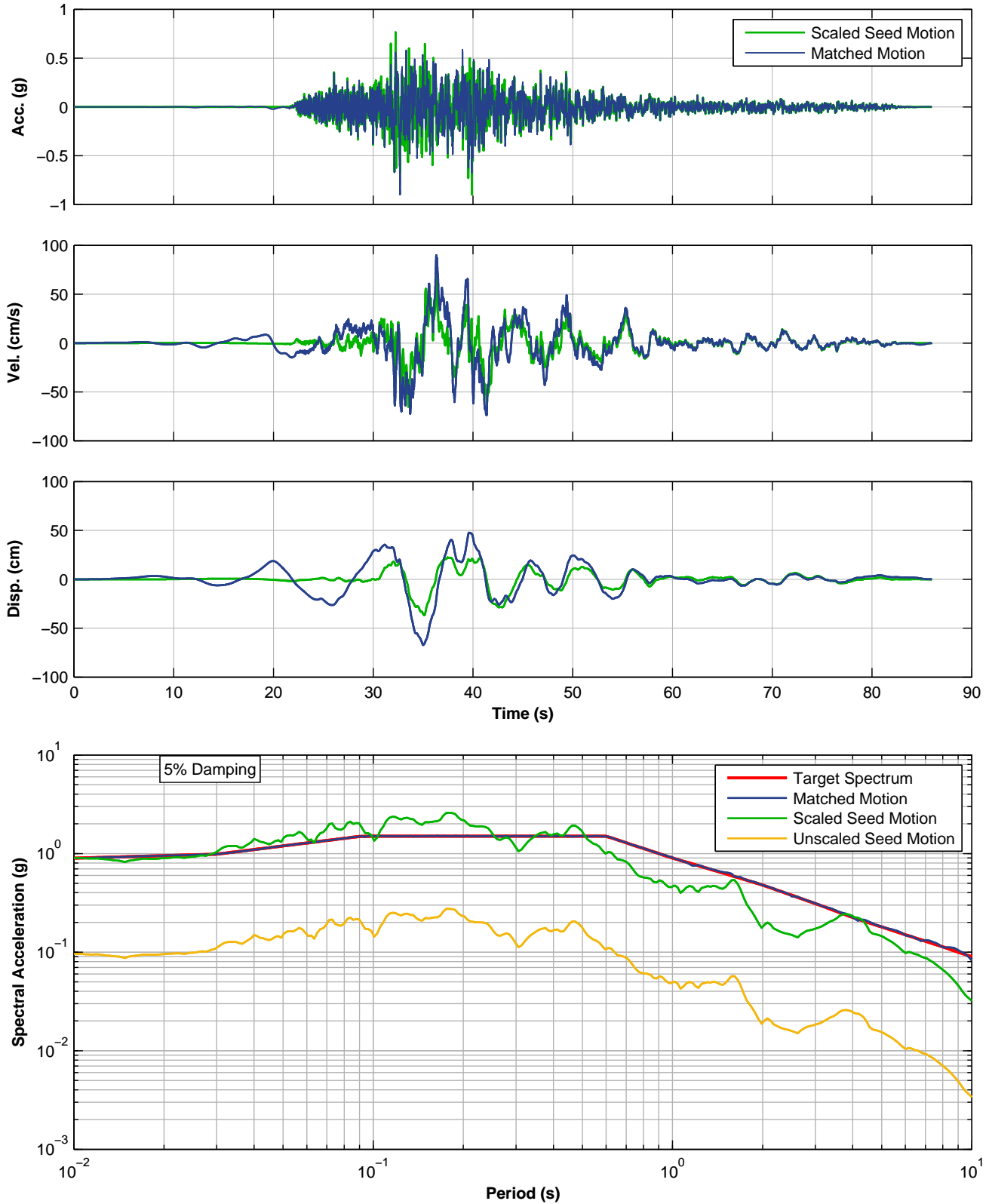
**SPECTRALLY MATCHED CTO MOTION, 180 COMPONENT, 2001 EL SALVADOR EQ
SSE LEVEL PER NFPA 59A 2006 – ONSHORE, FAULT NORMAL
LNG FACILITIES
ALASKA LNG PROJECT
NIKISKI, ALASKA**



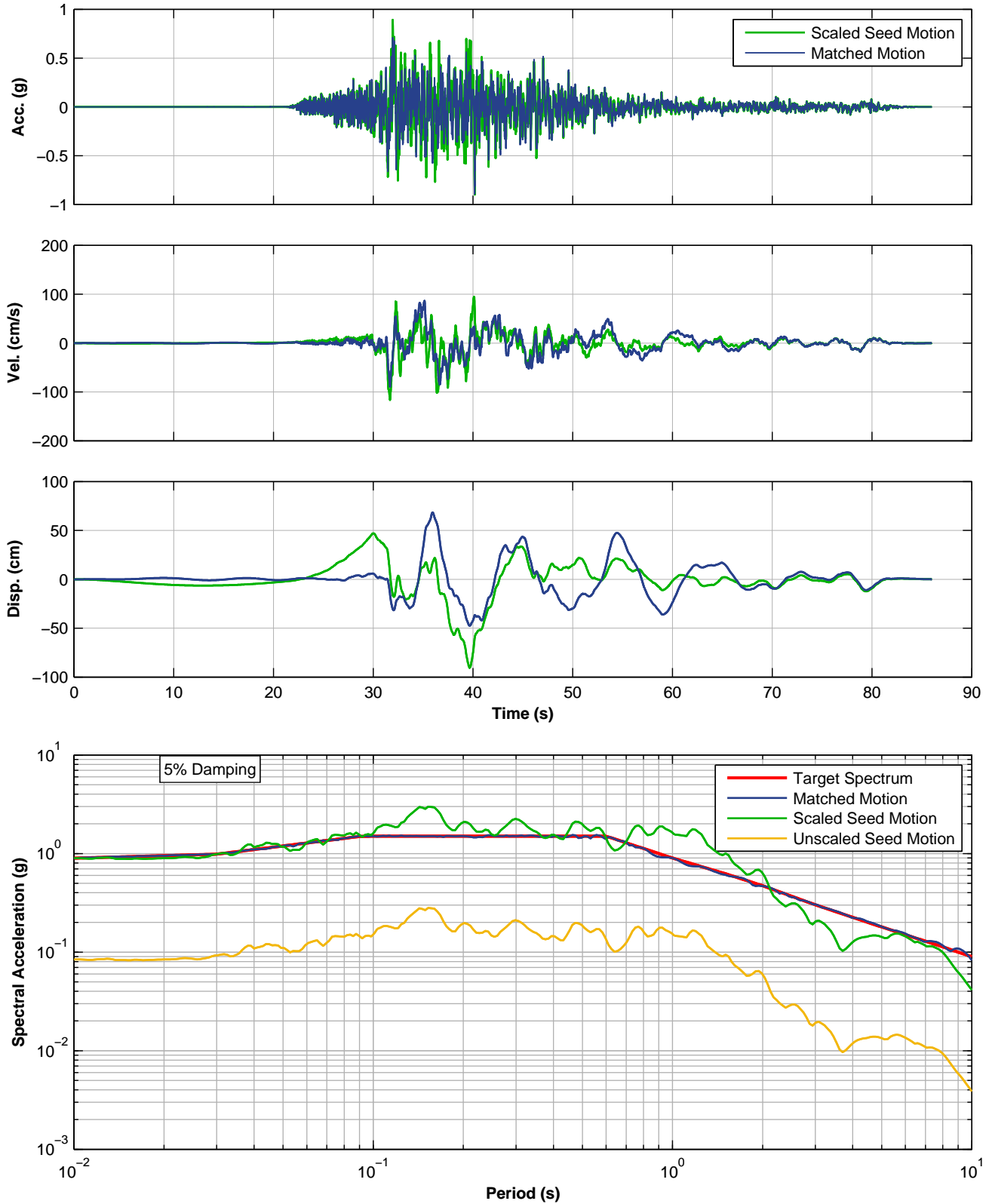
**SPECTRALLY MATCHED CTO MOTION, 270 COMPONENT, 2001 EL SALVADOR EQ
SSE LEVEL PER NFPA 59A 2006 – ONSHORE, FAULT PARALLEL
LNG FACILITIES
ALASKA LNG PROJECT
NIKISKI, ALASKA**



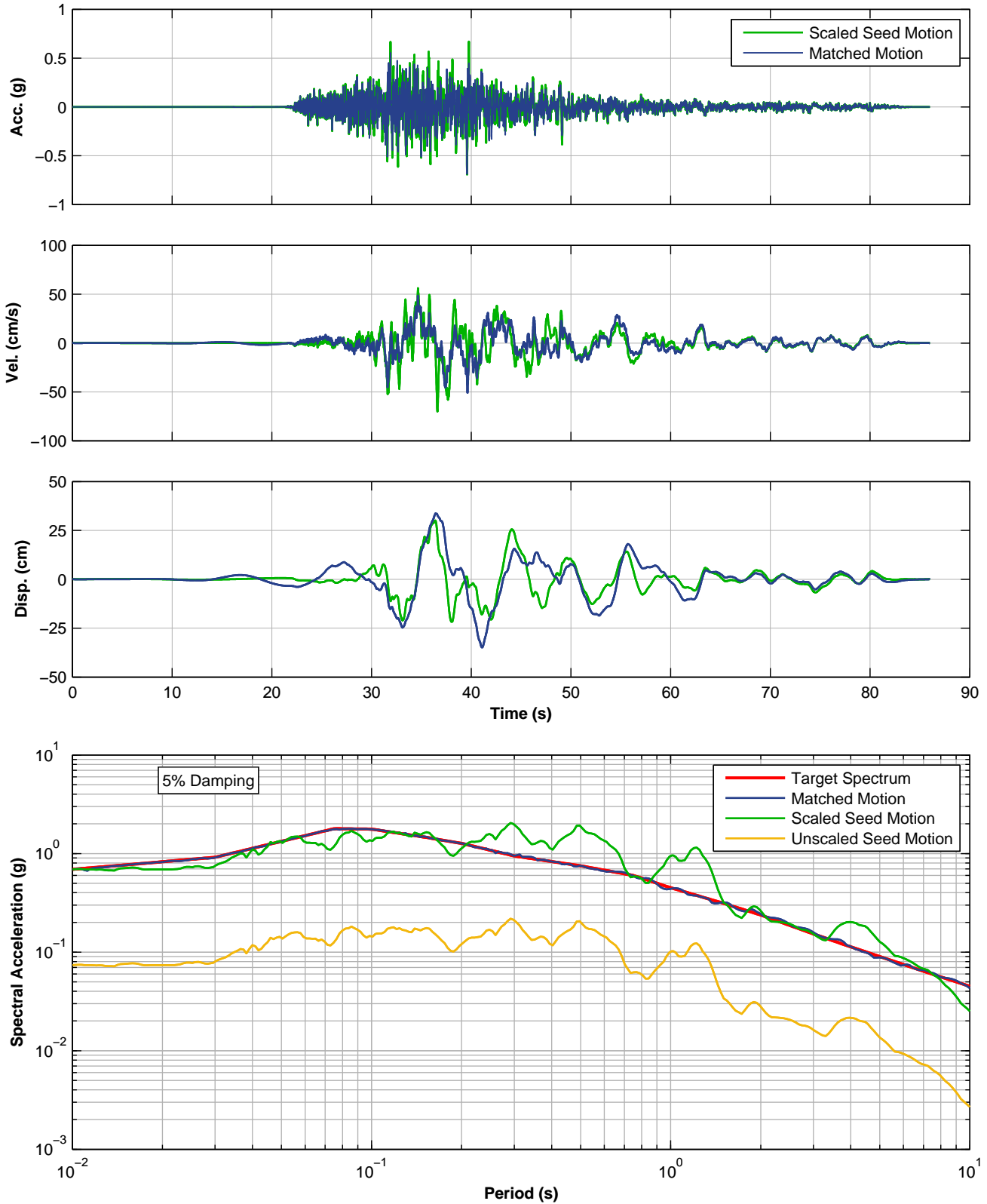
**SPECTRALLY MATCHED CTO MOTION, UP COMPONENT, 2001 EL SALVADOR EQ
SSE LEVEL PER NFPA 59A 2006 – ONSHORE
LNG FACILITIES
ALASKA LNG PROJECT
NIKISKI, ALASKA**



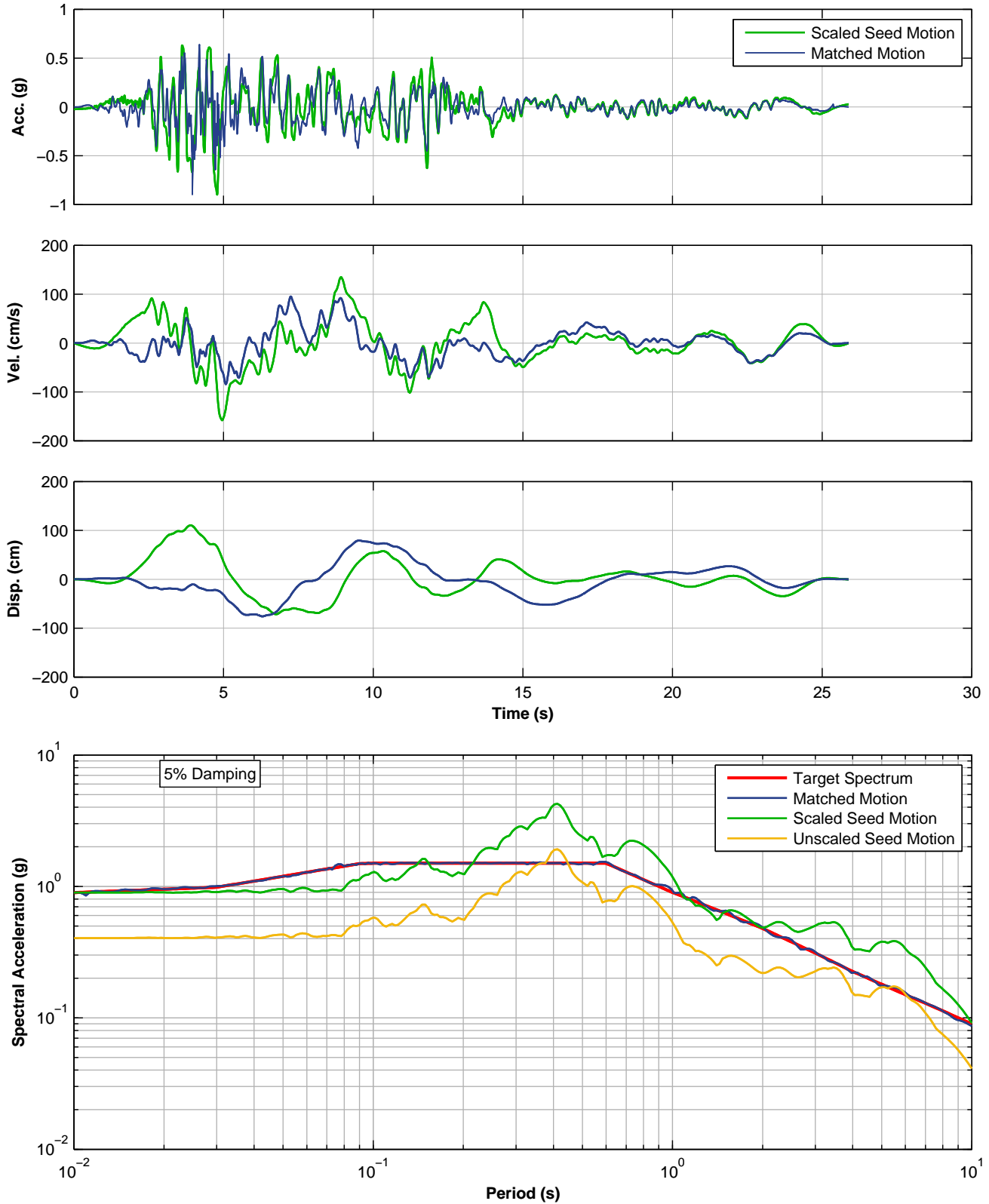
**SPECTRALLY MATCHED CARLO MOTION, 090 COMPONENT, 2002 DENALI EQ, ALASKA
SSE LEVEL PER NFPA 59A 2006 – ONSHORE, FAULT NORMAL
LNG FACILITIES
ALASKA LNG PROJECT
NIKISKI, ALASKA**



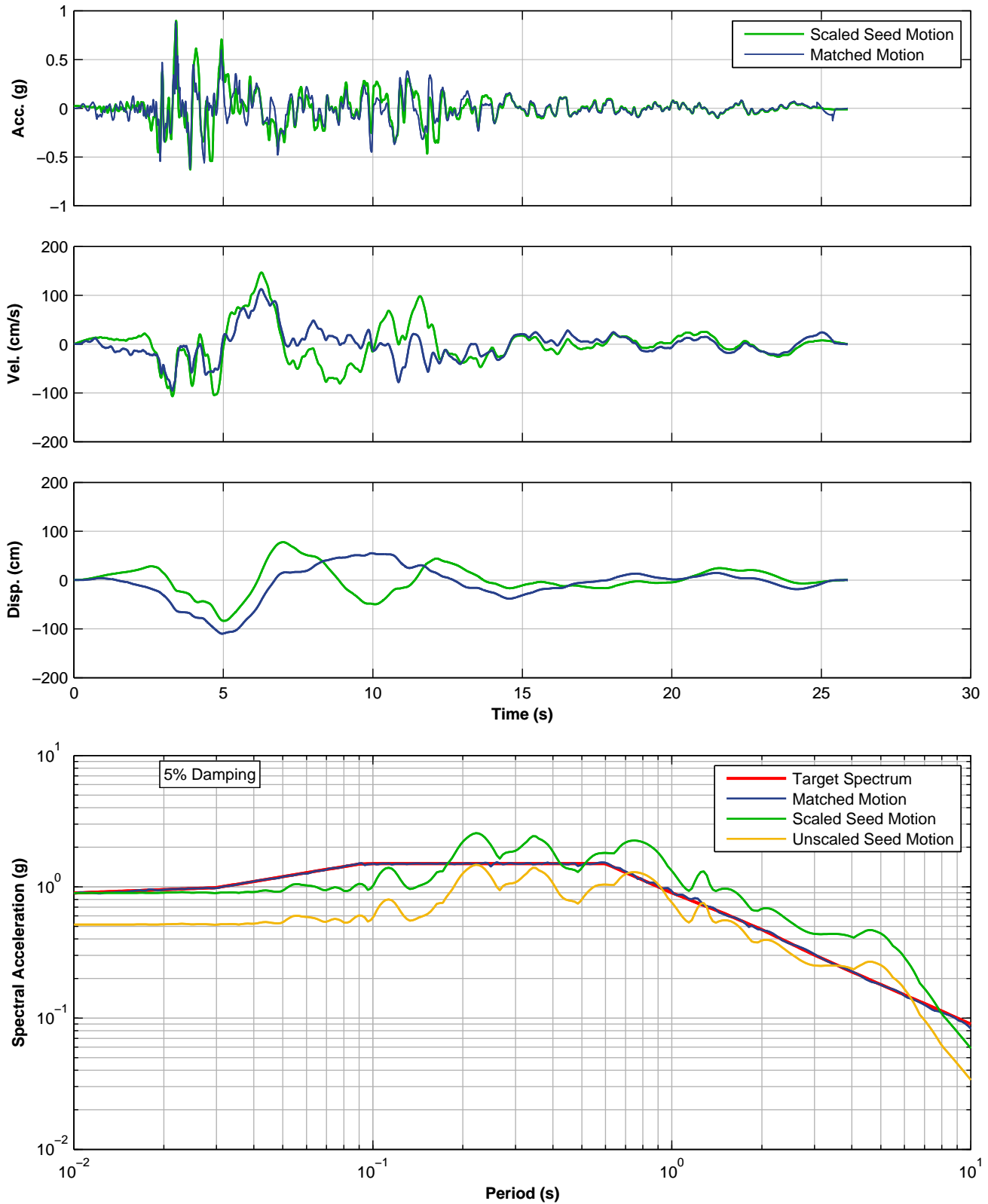
**SPECTRALLY MATCHED CARLO MOTION, 360 COMPONENT, 2002 DENALI EQ, ALASKA
SSE LEVEL PER NFPA 59A 2006 – ONSHORE, FAULT PARALLEL
LNG FACILITIES
ALASKA LNG PROJECT
NIKISKI, ALASKA**



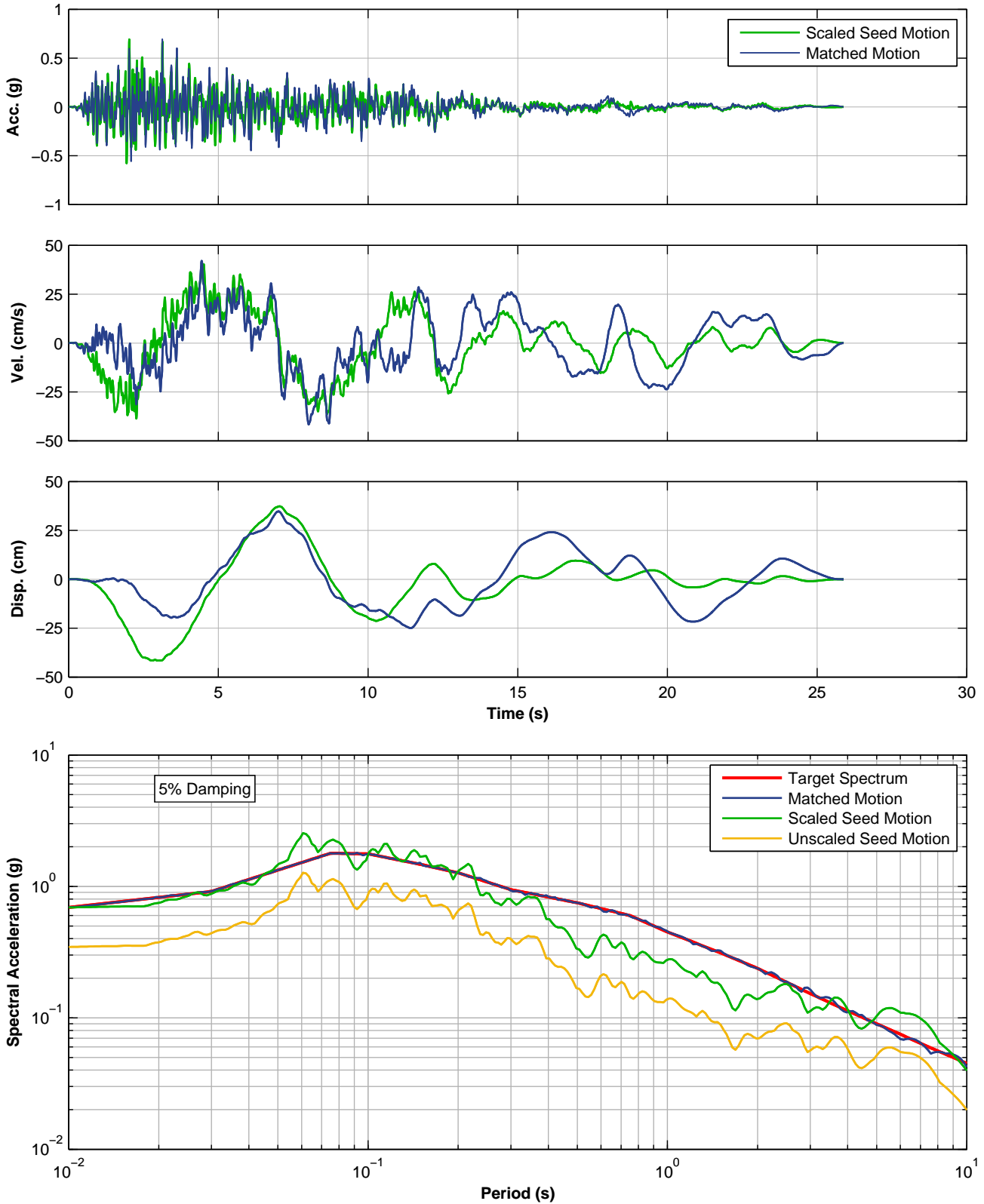
**SPECTRALLY MATCHED CARLO MOTION, UP COMPONENT, 2002 DENALI EQ, ALASKA
SSE LEVEL PER NFPA 59A 2006 – ONSHORE
LNG FACILITIES
ALASKA LNG PROJECT
NIKISKI, ALASKA**



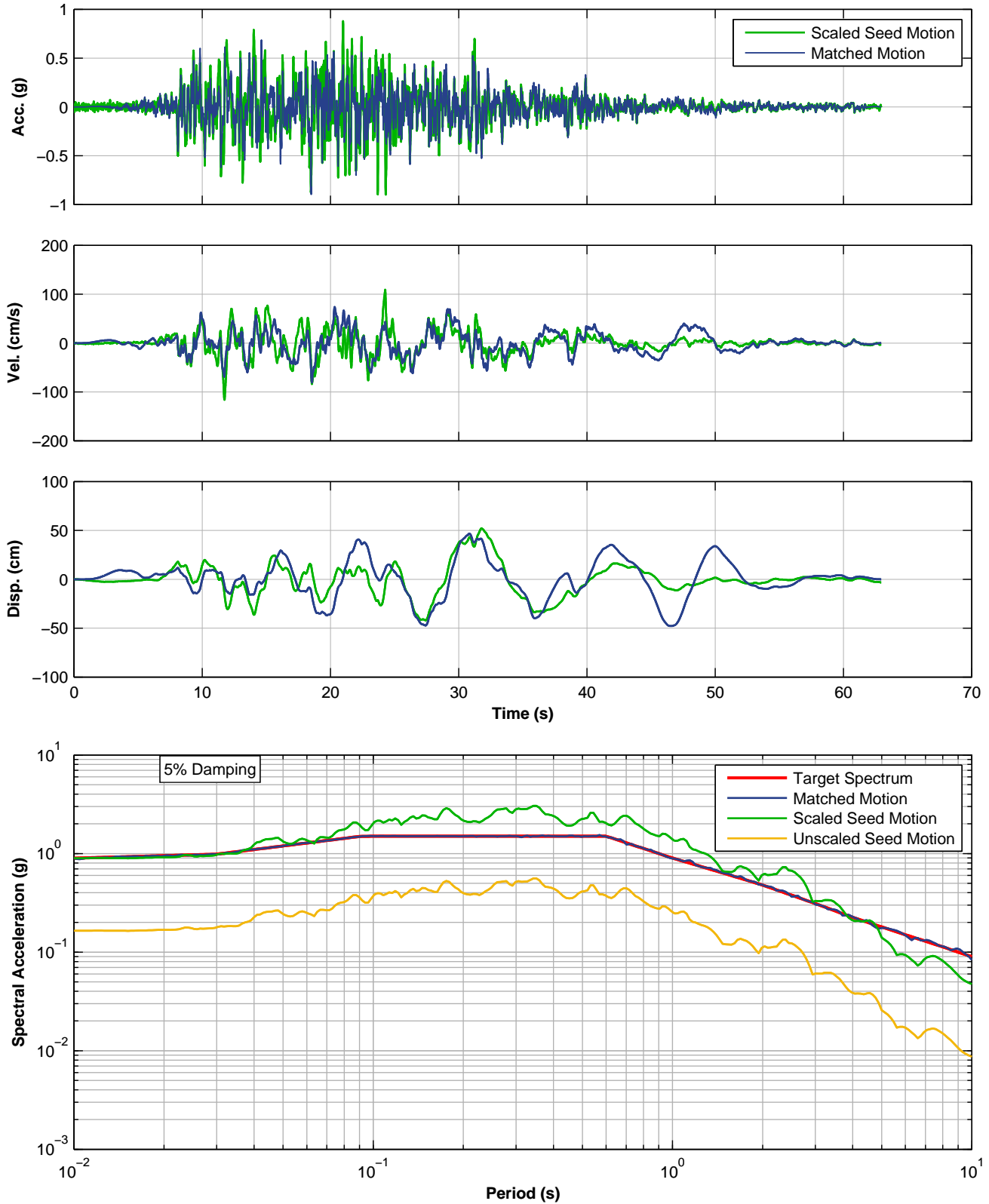
**SPECTRALLY MATCHED DZC MOTION, 180 COMPONENT, 1999 DUZCE EQ, TURKEY
SSE LEVEL PER NFPA 59A 2006 – ONSHORE, FAULT NORMAL
LNG FACILITIES
ALASKA LNG PROJECT
NIKISKI, ALASKA**



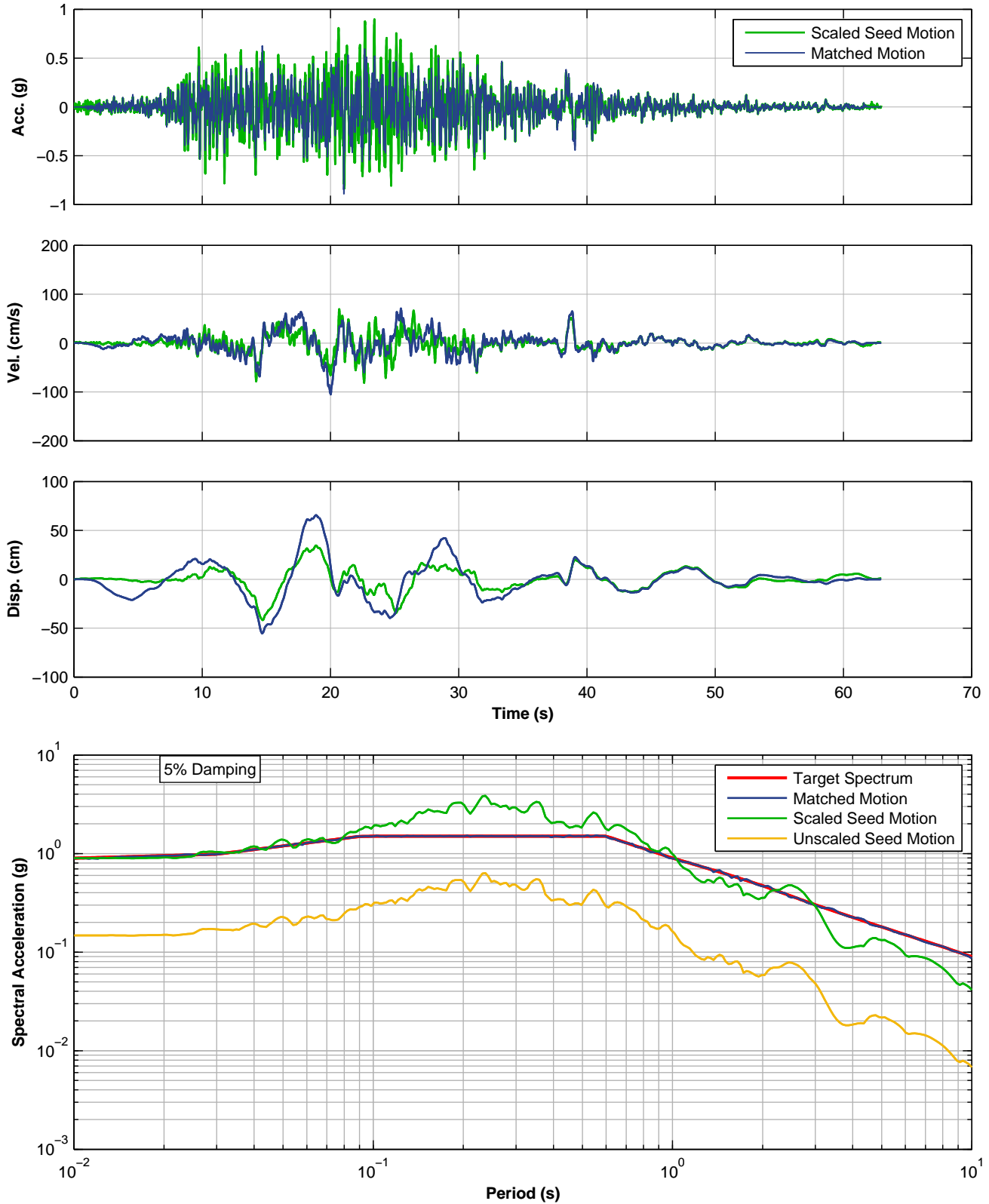
**SPECTRALLY MATCHED DZC MOTION, 270 COMPONENT, 1999 DUZCE EQ, TURKEY
SSE LEVEL PER NFPA 59A 2006 – ONSHORE, FAULT PARALLEL
LNG FACILITIES
ALASKA LNG PROJECT
NIKISKI, ALASKA**



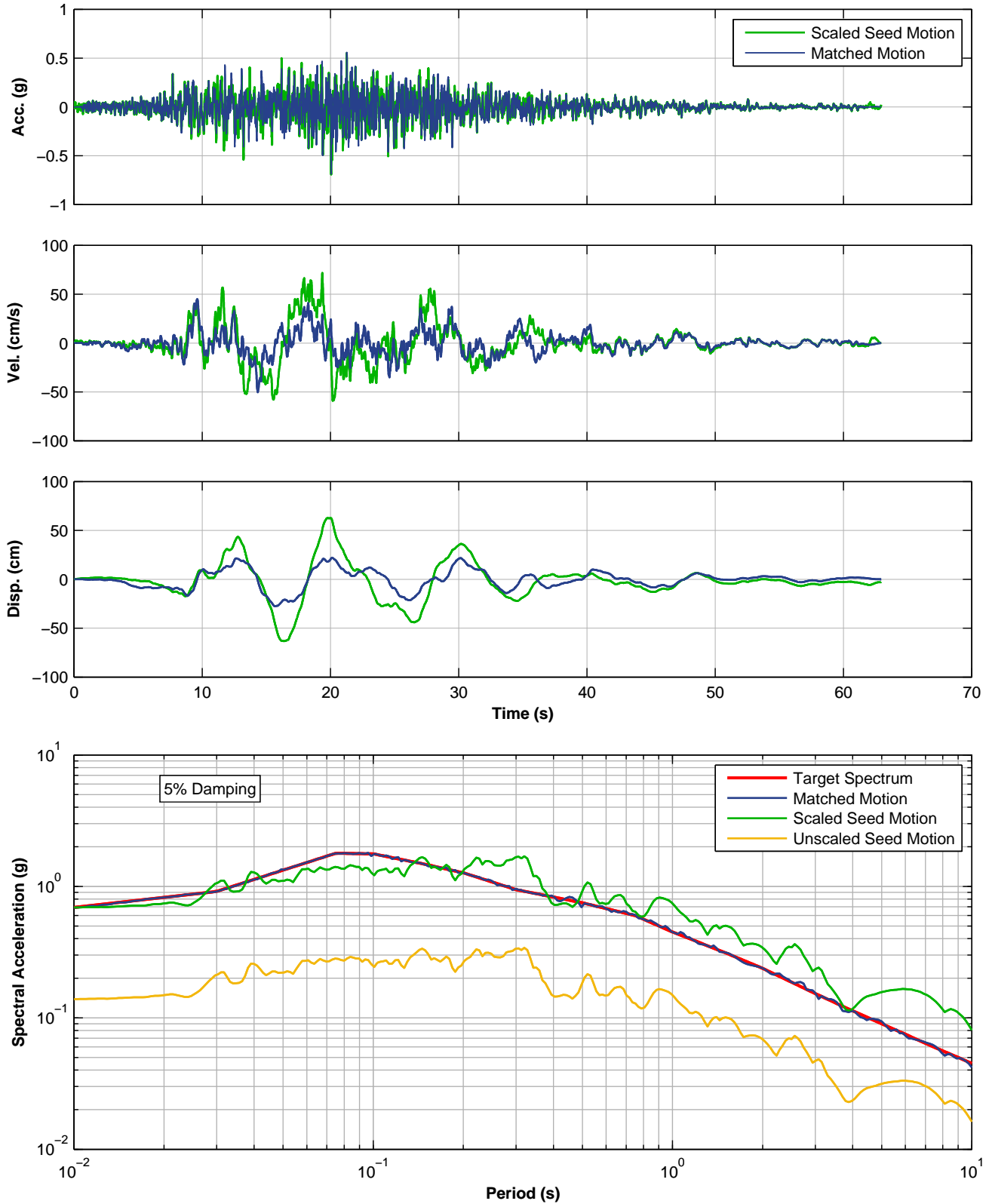
SPECTRALLY MATCHED DZC MOTION, UP COMPONENT, 1999 DUZCE EQ, TURKEY
SSE LEVEL PER NFPA 59A 2006 – ONSHORE
LNG FACILITIES
ALASKA LNG PROJECT
NIKISKI, ALASKA



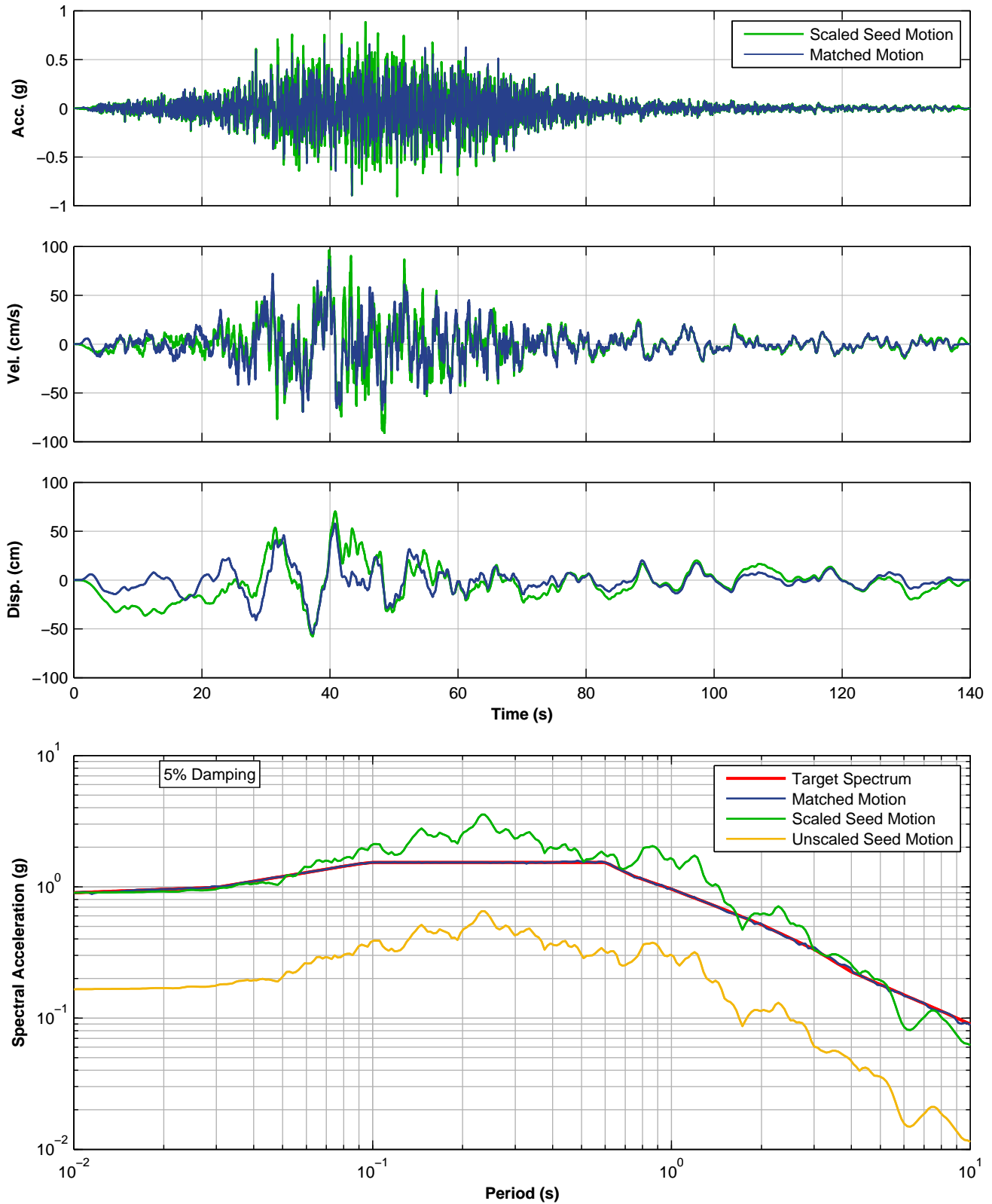
**SPECTRALLY MATCHED UNIO MOTION, N00W COMPONENT, 1985 MEXICO EQ
SSE LEVEL PER NFPA 59A 2006 – ONSHORE, FAULT NORMAL
LNG FACILITIES
ALASKA LNG PROJECT
NIKISKI, ALASKA**



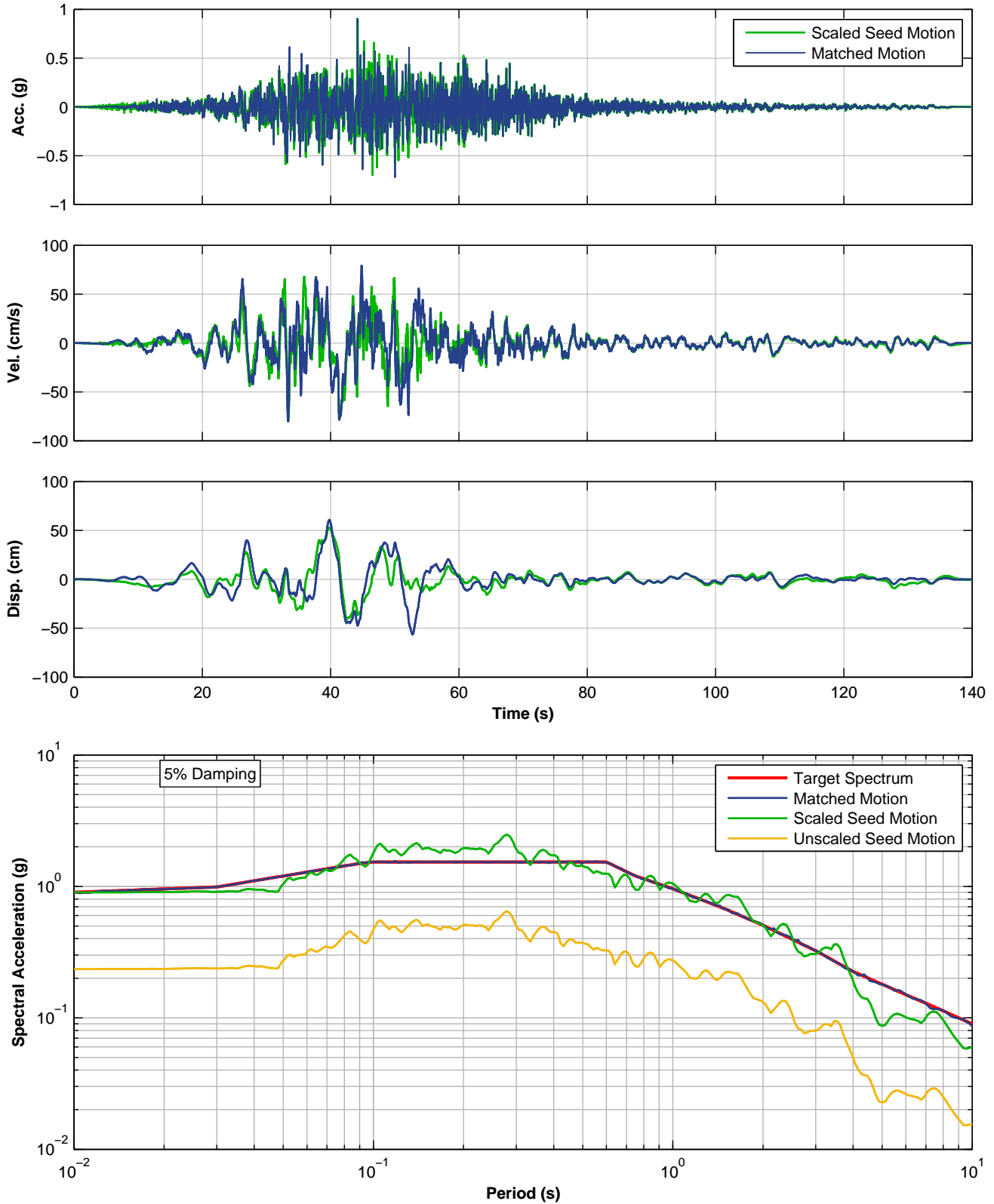
**SPECTRALLY MATCHED UNIO MOTION, N90W COMPONENT, 1985 MEXICO EQ
SSE LEVEL PER NFPA 59A 2006 – ONSHORE, FAULT PARALLEL
LNG FACILITIES
ALASKA LNG PROJECT
NIKISKI, ALASKA**



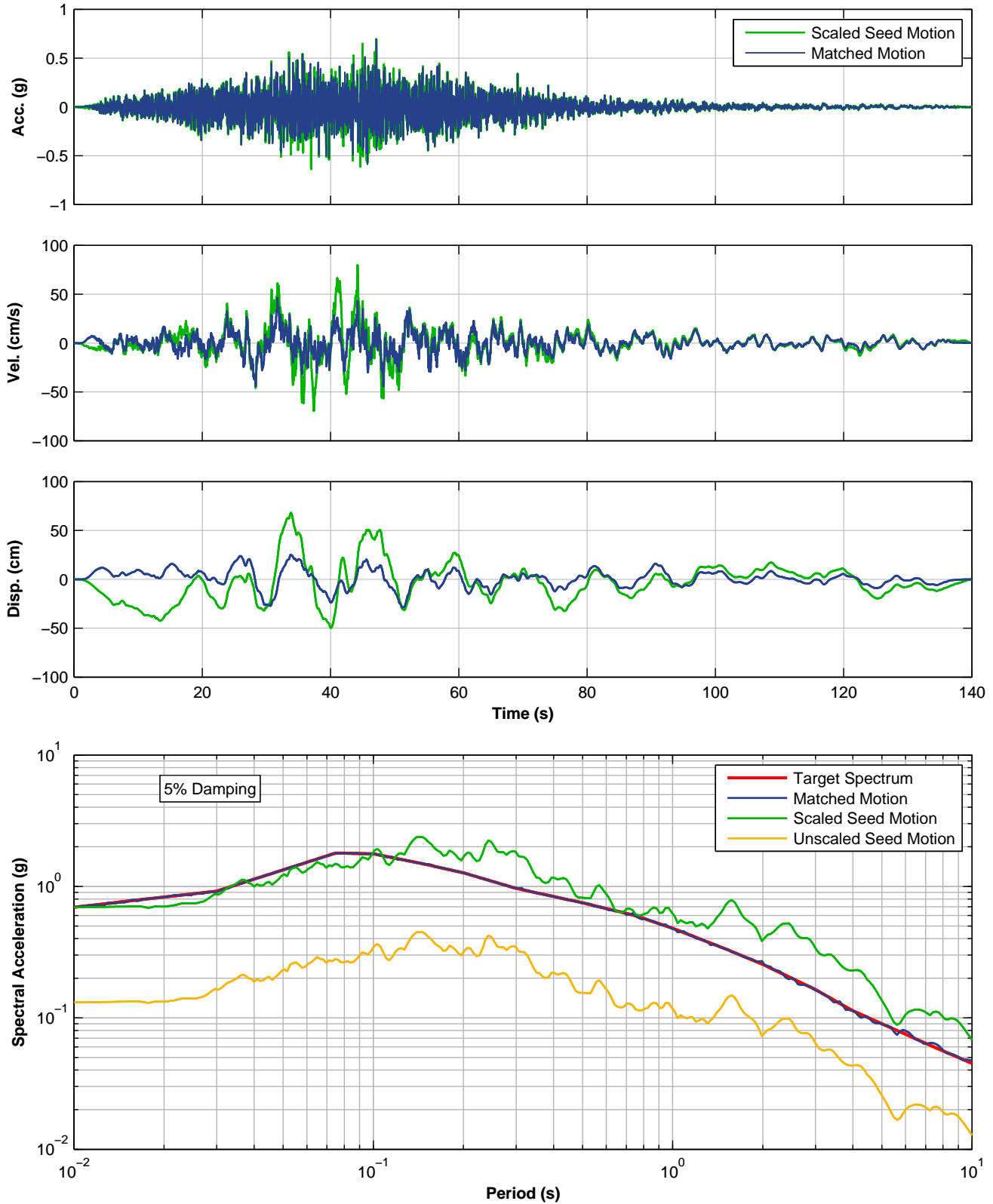
**SPECTRALLY MATCHED UNIO MOTION, UP COMPONENT, 1985 MEXICO EQ
SSE LEVEL PER NFPA 59A 2006 – ONSHORE
LNG FACILITIES
ALASKA LNG PROJECT
NIKISKI, ALASKA**



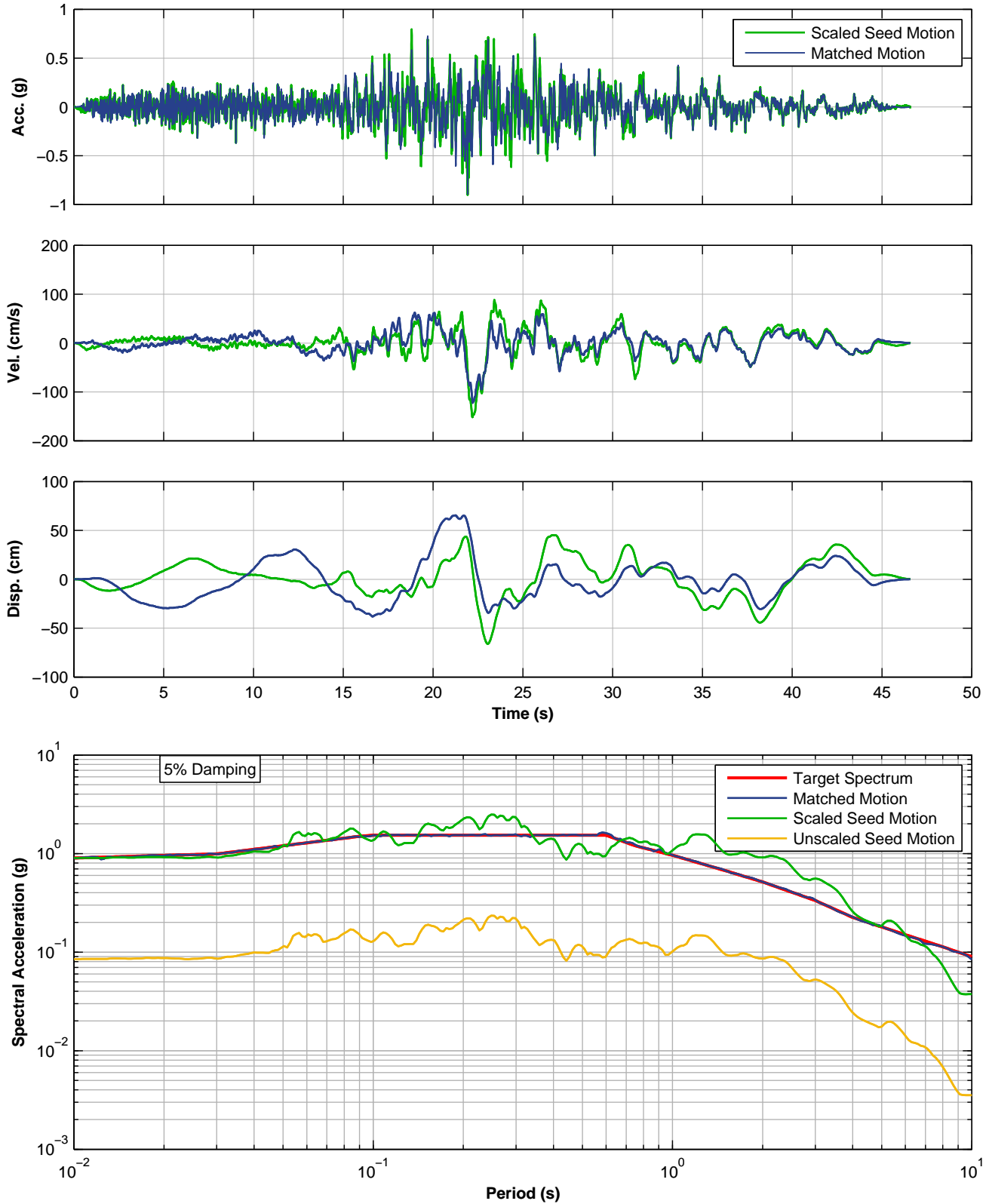
**SPECTRALLY MATCHED MEP MOTION, EW COMPONENT, 2010 CHILE EQ
SSE LEVEL PER NFPA 59A 2006 – NEARSHORE, FAULT NORMAL
LNG FACILITIES
ALASKA LNG PROJECT
NIKISKI, ALASKA**



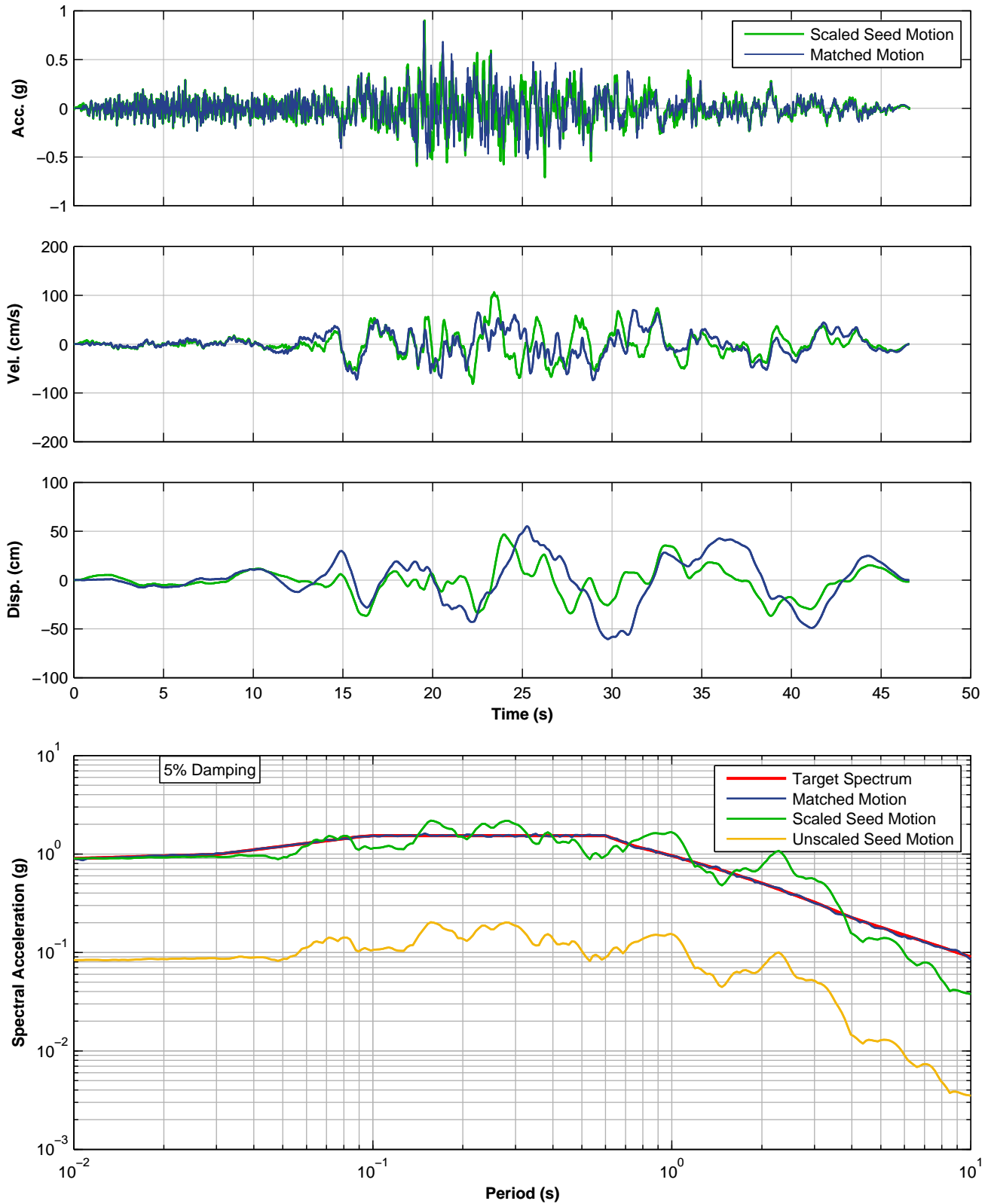
**SPECTRALLY MATCHED MEP MOTION, NS COMPONENT, 2010 CHILE EQ
SSE LEVEL PER NFPA 59A 2006 – NEARSHORE, FAULT PARALLEL
LNG FACILITIES
ALASKA LNG PROJECT
NIKISKI, ALASKA**



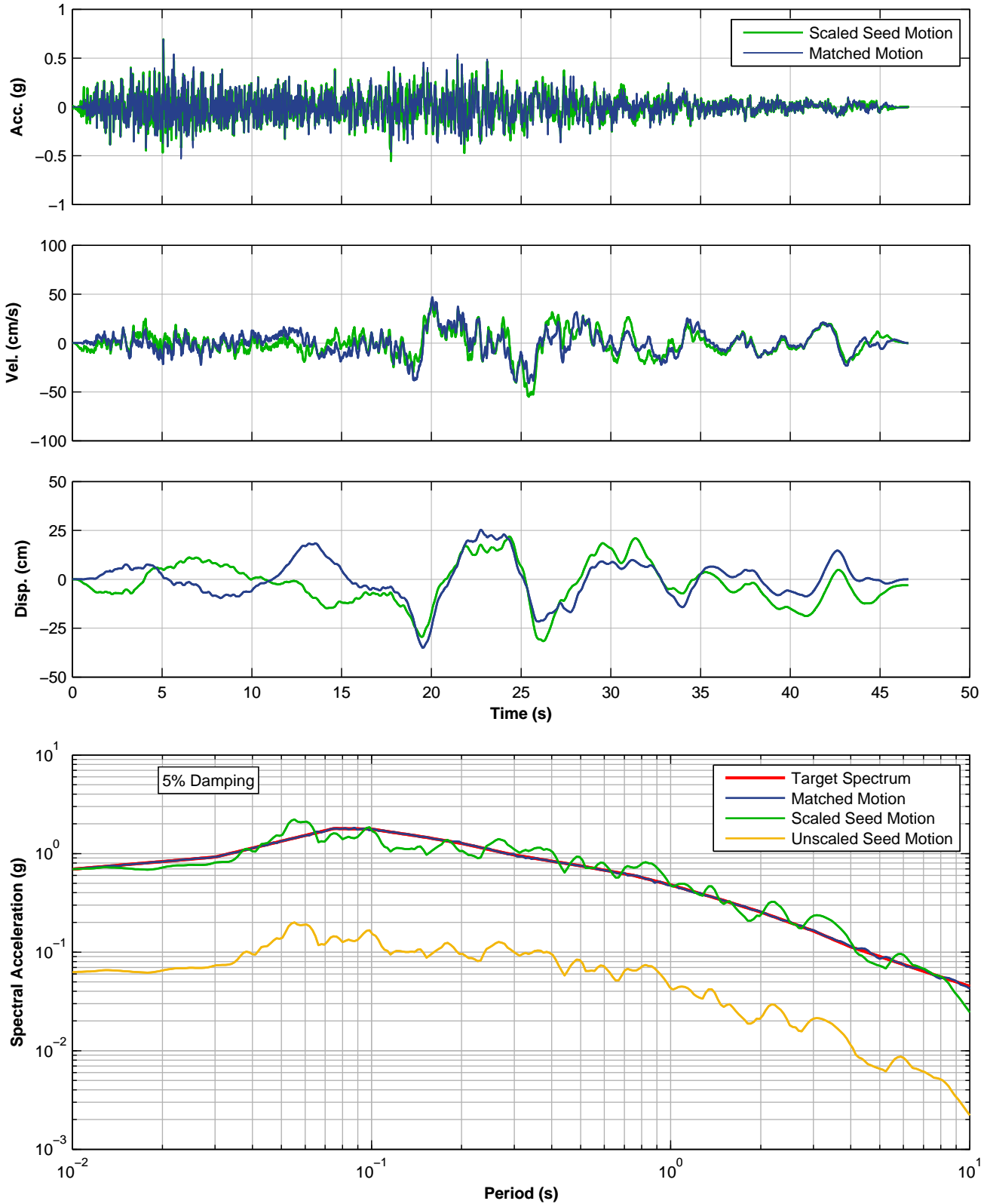
SPECTRALLY MATCHED MEP MOTION, V COMPONENT, 2010 CHILE EQ
SSE LEVEL PER NFPA 59A 2006 – NEARSHORE
LNG FACILITIES
ALASKA LNG PROJECT
NIKISKI, ALASKA



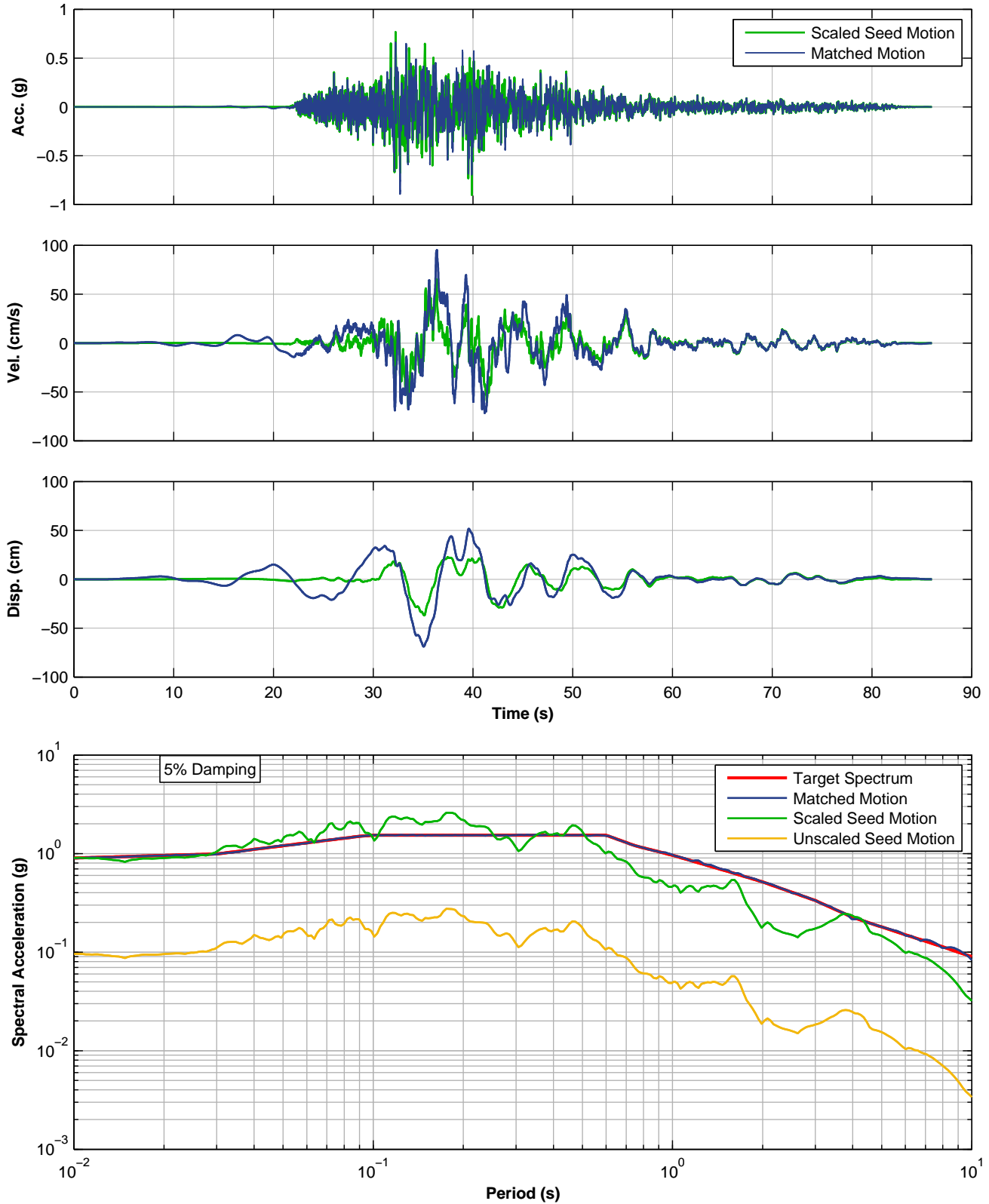
**SPECTRALLY MATCHED CTO MOTION, 180 COMPONENT, 2001 EL SALVADOR EQ
SSE LEVEL PER NFPA 59A 2006 – NEARSHORE, FAULT NORMAL
LNG FACILITIES
ALASKA LNG PROJECT
NIKISKI, ALASKA**



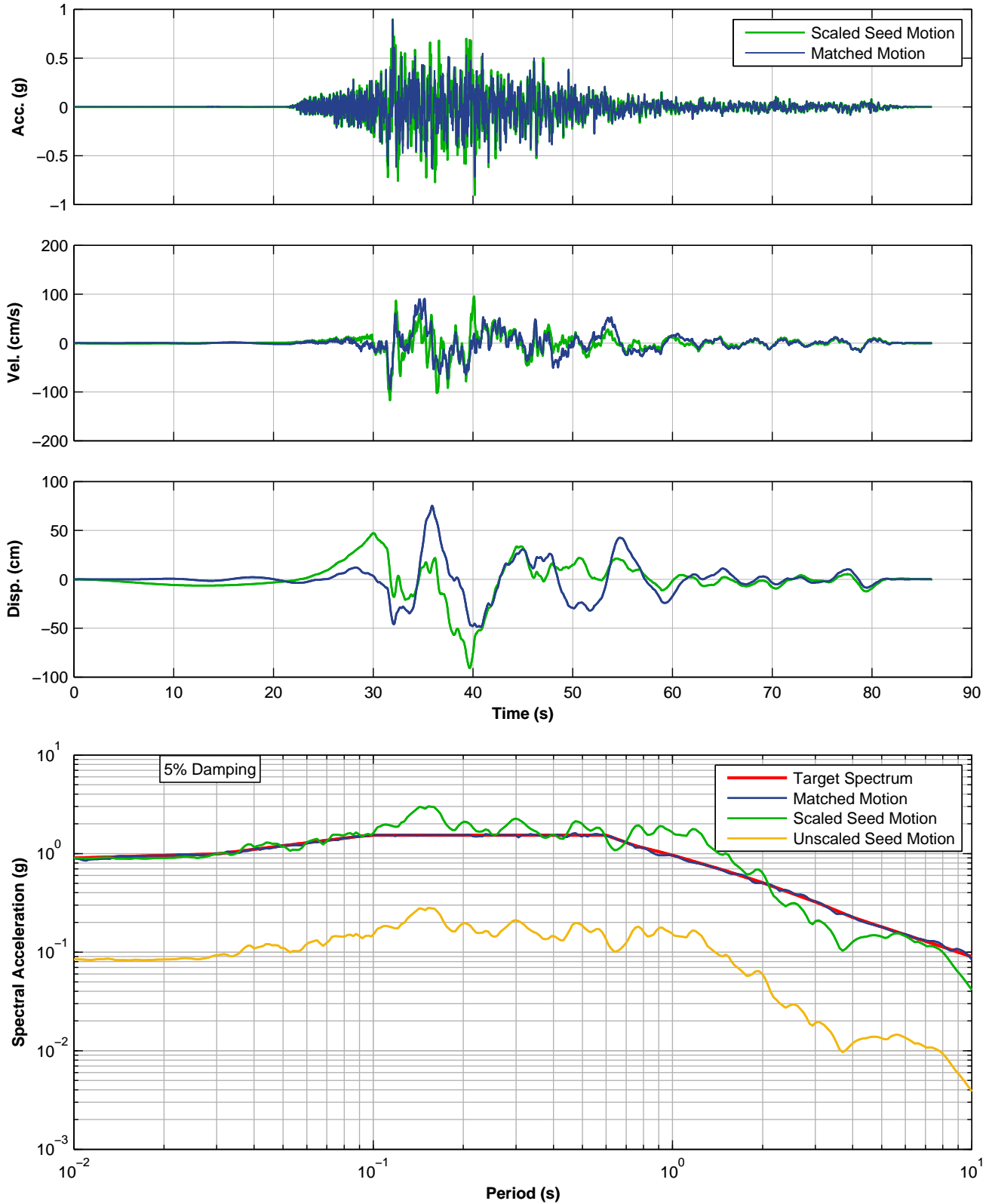
**SPECTRALLY MATCHED CTO MOTION, 270 COMPONENT, 2001 EL SALVADOR EQ
SSE LEVEL PER NFPA 59A 2006 – NEARSHORE, FAULT PARALLEL
LNG FACILITIES
ALASKA LNG PROJECT
NIKISKI, ALASKA**



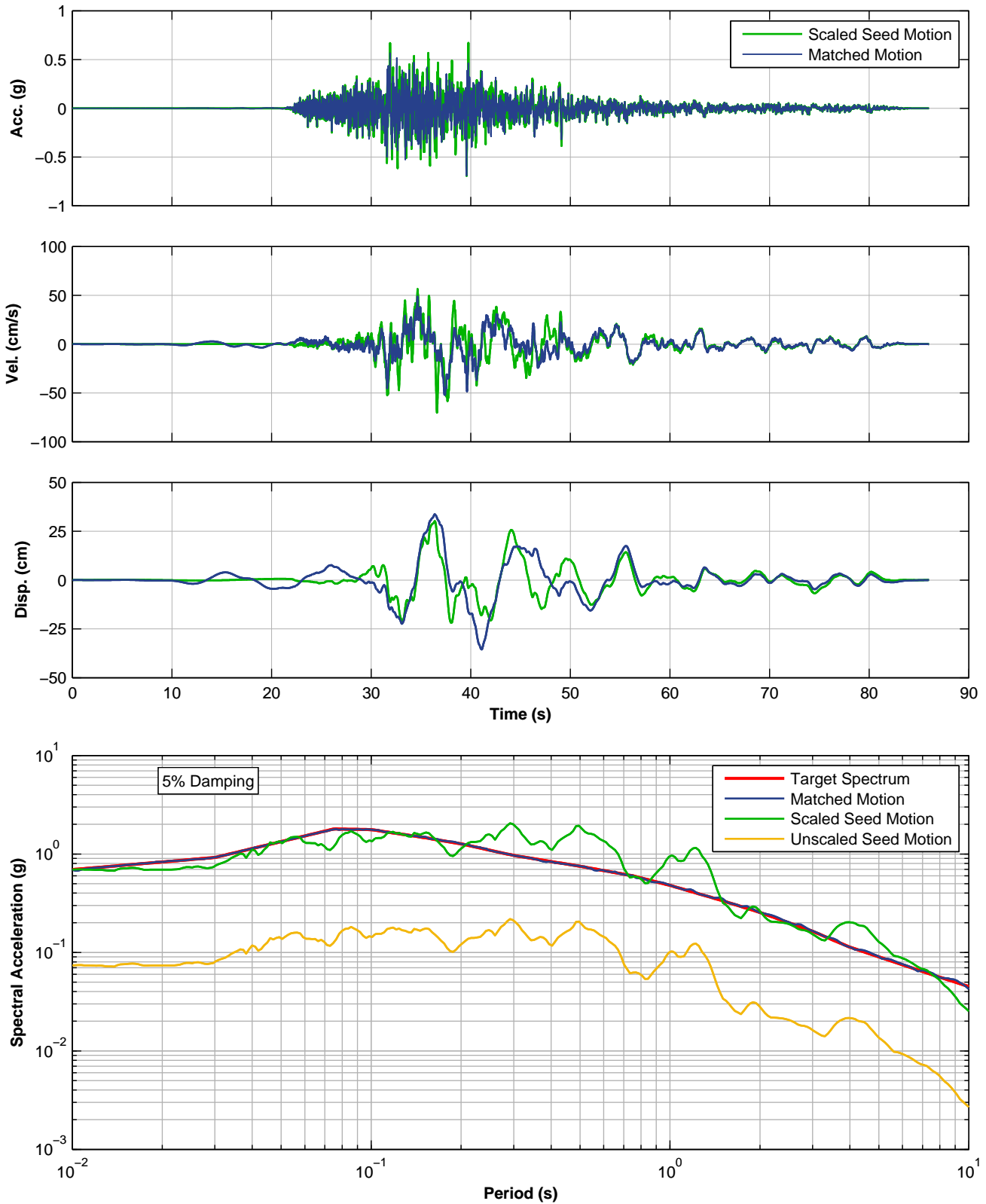
**SPECTRALLY MATCHED CTO MOTION, UP COMPONENT, 2001 EL SALVADOR EQ
SSE LEVEL PER NFPA 59A 2006 – NEARSHORE
LNG FACILITIES
ALASKA LNG PROJECT
NIKISKI, ALASKA**



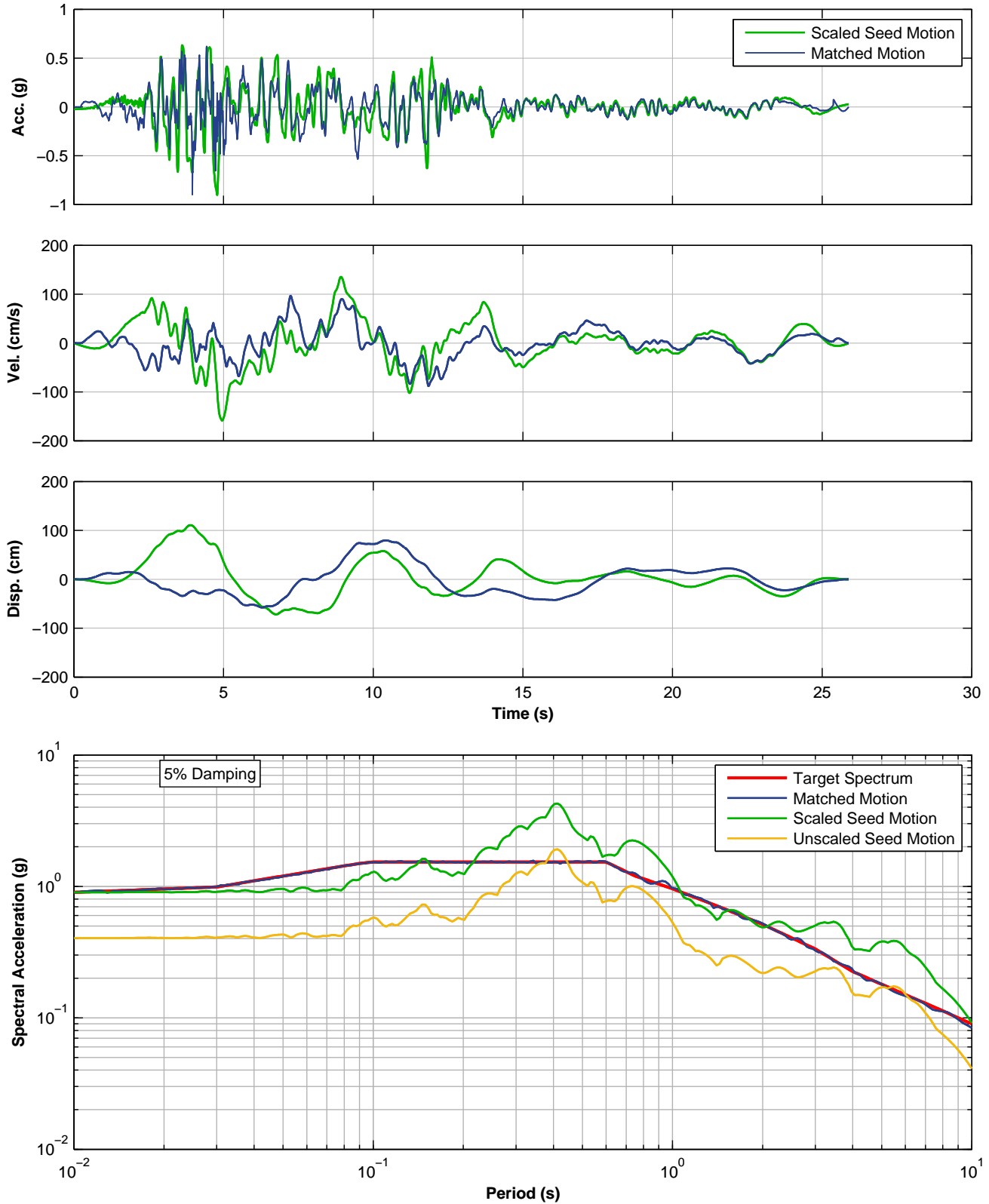
**SPECTRALLY MATCHED CARLO MOTION, 090 COMPONENT, 2002 DENALI EQ, ALASKA
SSE LEVEL PER NFPA 59A 2006 – NEARSHORE, FAULT NORMAL
LNG FACILITIES
ALASKA LNG PROJECT
NIKISKI, ALASKA**



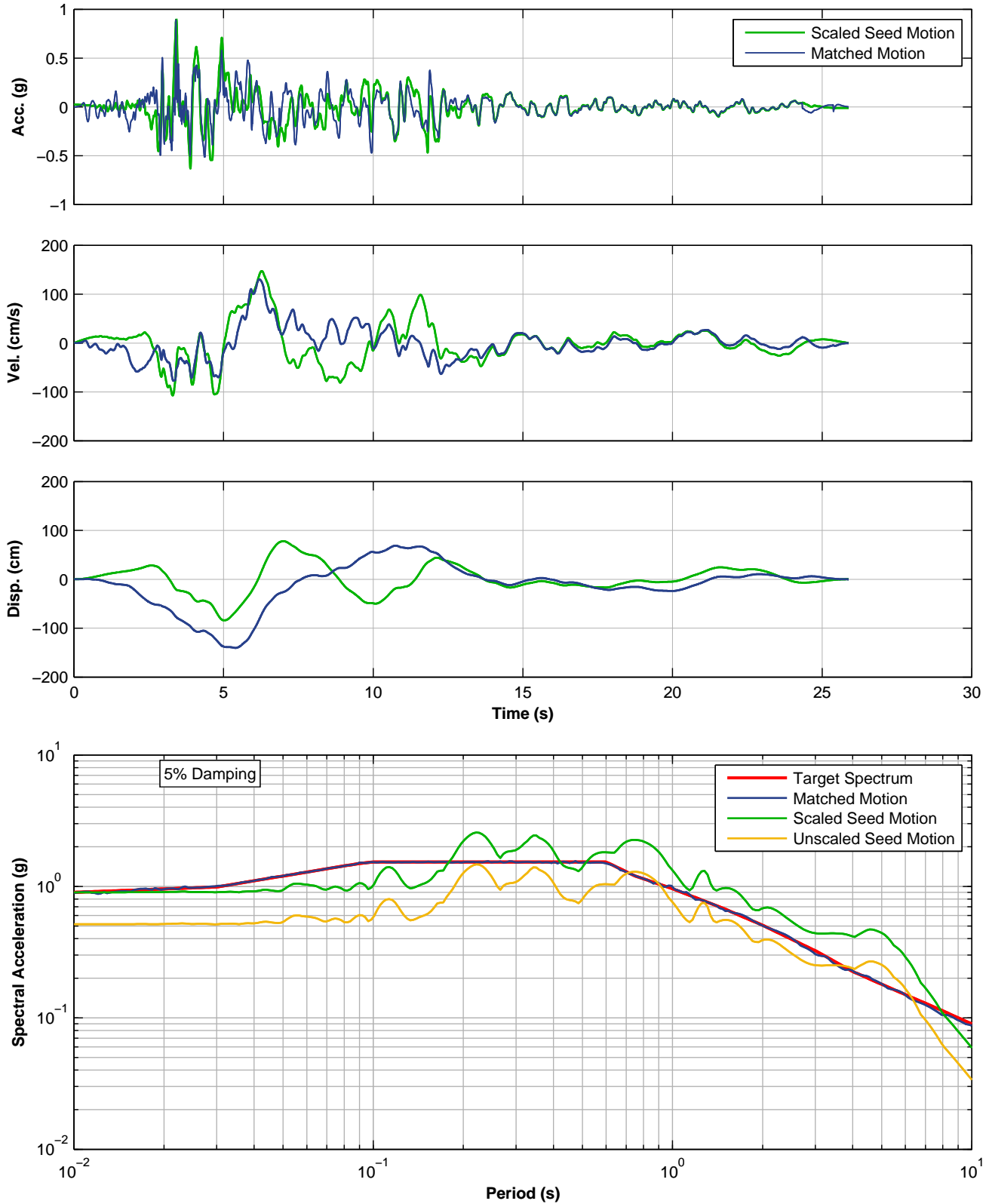
**SPECTRALLY MATCHED CARLO MOTION, 360 COMPONENT, 2002 DENALI EQ, ALASKA
SSE LEVEL PER NFPA 59A 2006 – NEARSHORE, FAULT PARALLEL
LNG FACILITIES
ALASKA LNG PROJECT
NIKISKI, ALASKA**



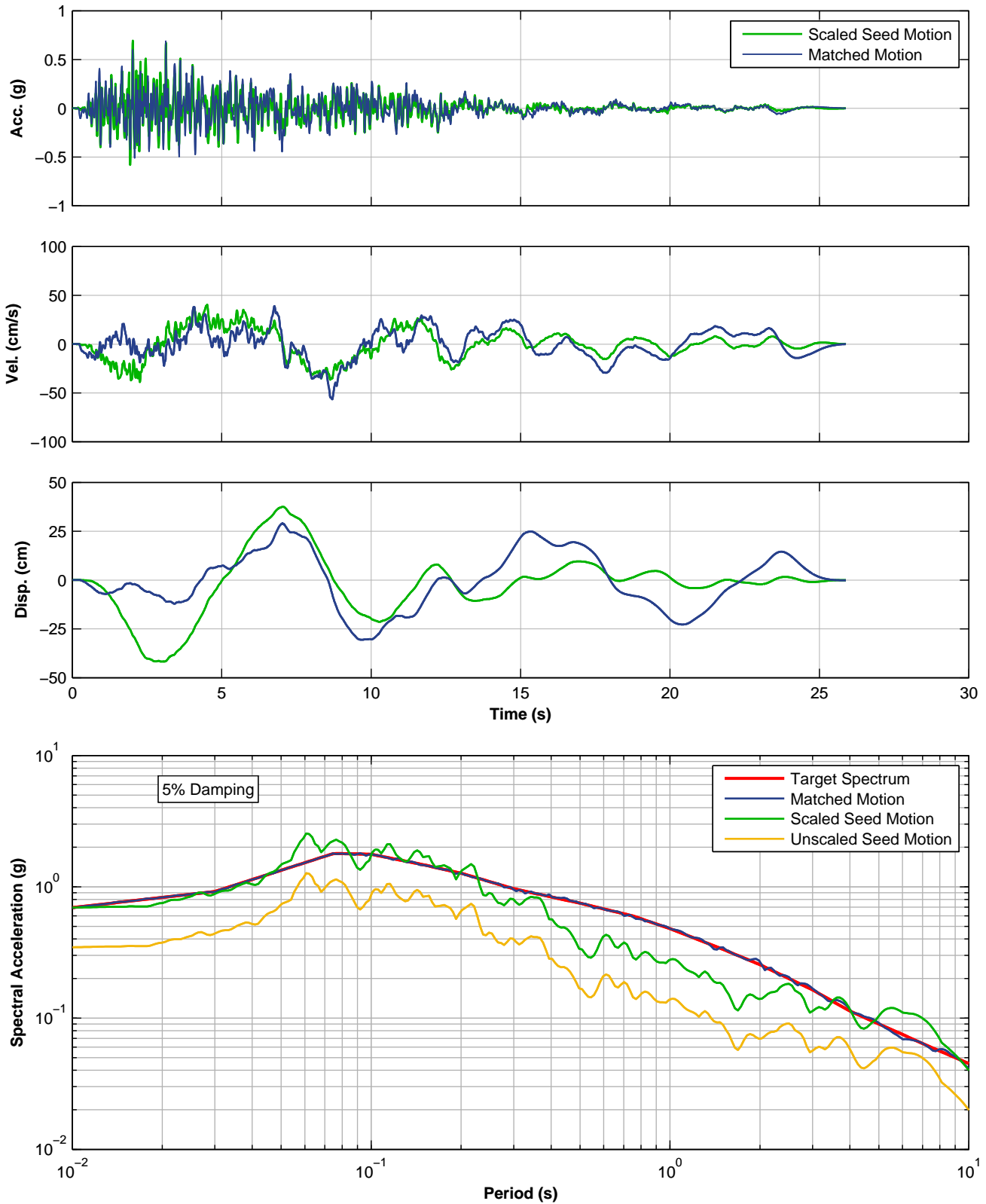
**SPECTRALLY MATCHED CARLO MOTION, UP COMPONENT, 2002 DENALI EQ, ALASKA
SSE LEVEL PER NFPA 59A 2006 – NEARSHORE
LNG FACILITIES
ALASKA LNG PROJECT
NIKISKI, ALASKA**



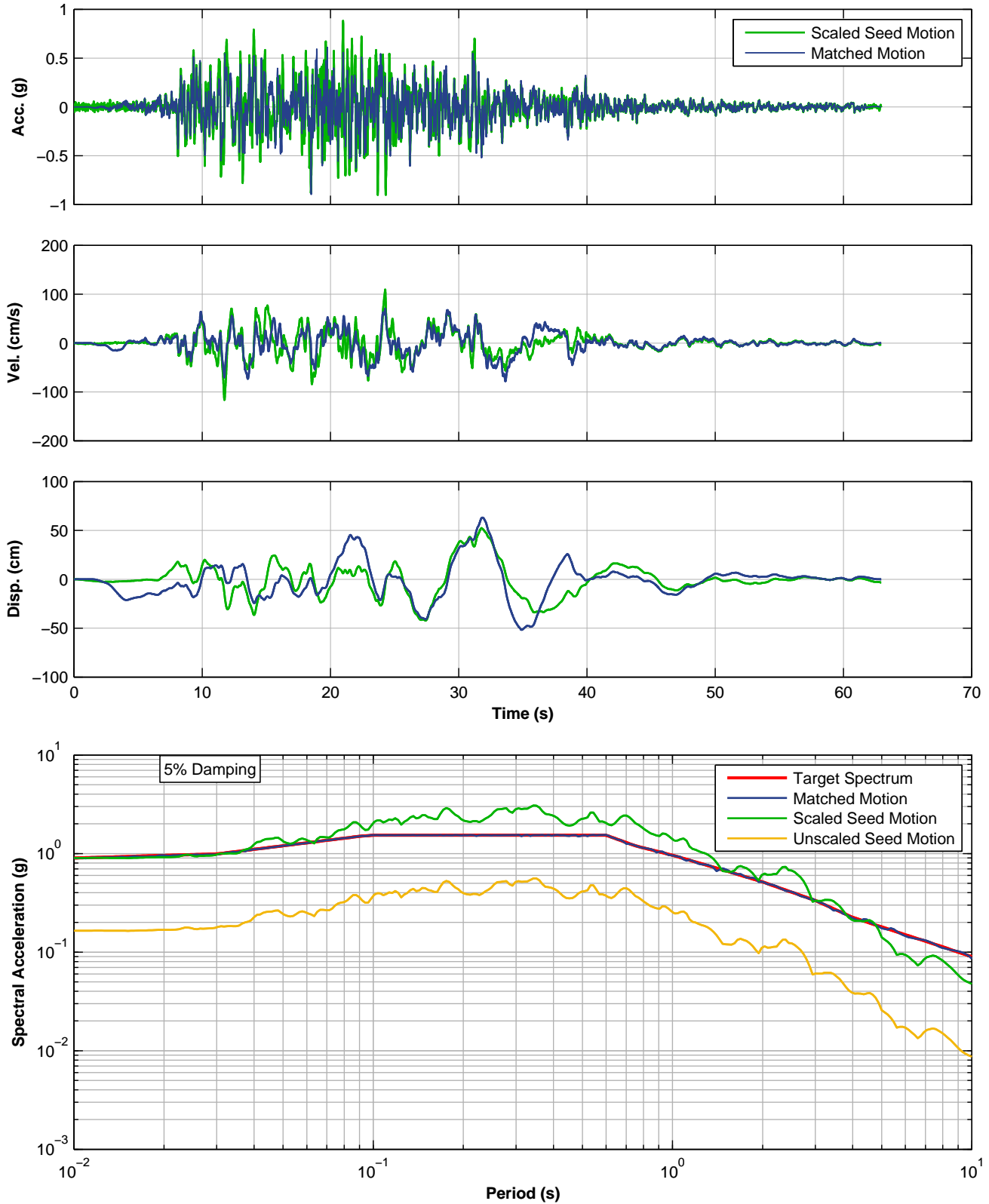
**SPECTRALLY MATCHED DZC MOTION, 180 COMPONENT, 1999 DUZCE EQ, TURKEY
SSE LEVEL PER NFPA 59A 2006 – NEARSHORE, FAULT NORMAL
LNG FACILITIES
ALASKA LNG PROJECT
NIKISKI, ALASKA**



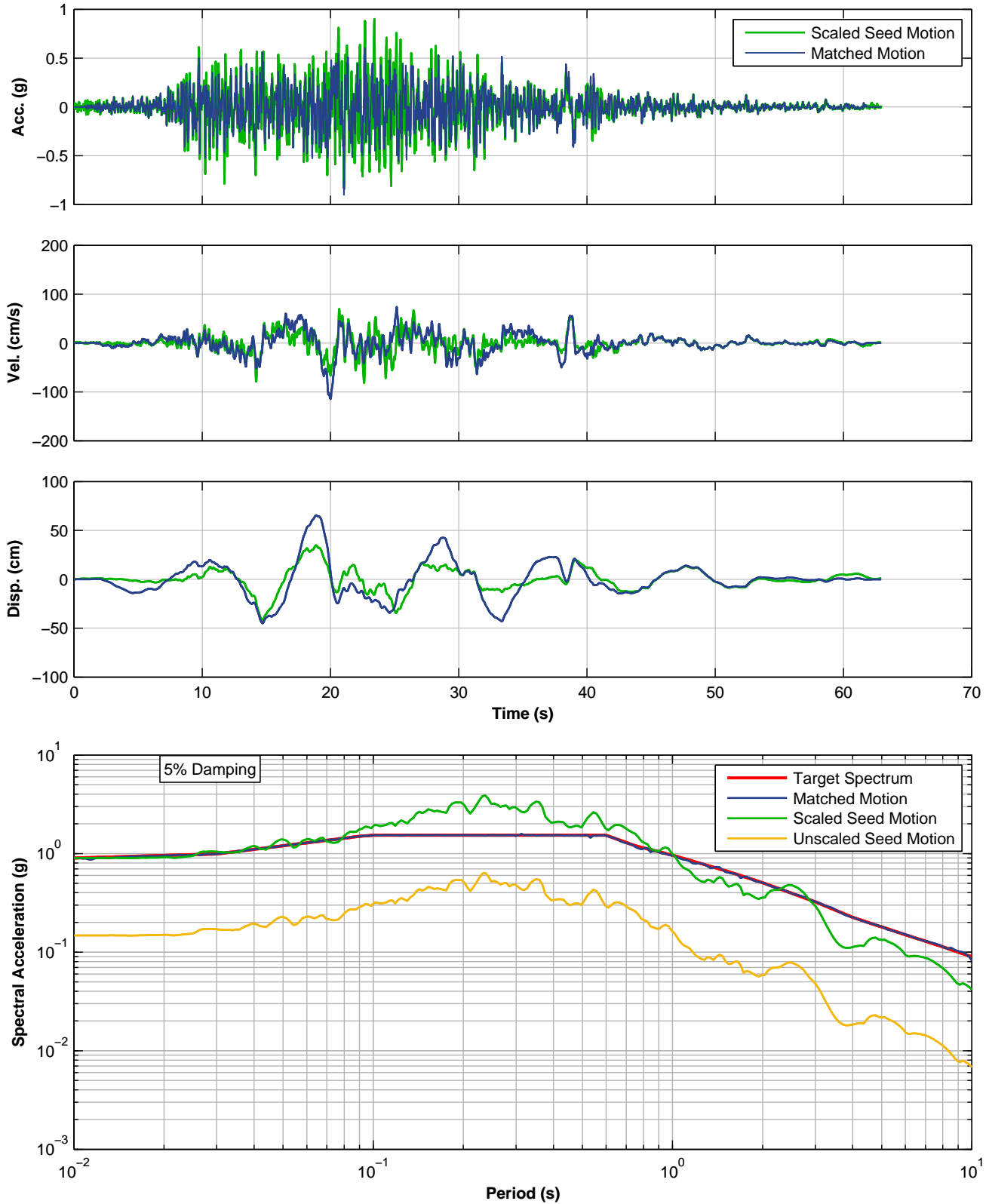
**SPECTRALLY MATCHED DZC MOTION, 270 COMPONENT, 1999 DUZCE EQ, TURKEY
SSE LEVEL PER NFPA 59A 2006 – NEARSHORE, FAULT PARALLEL
LNG FACILITIES
ALASKA LNG PROJECT
NIKISKI, ALASKA**



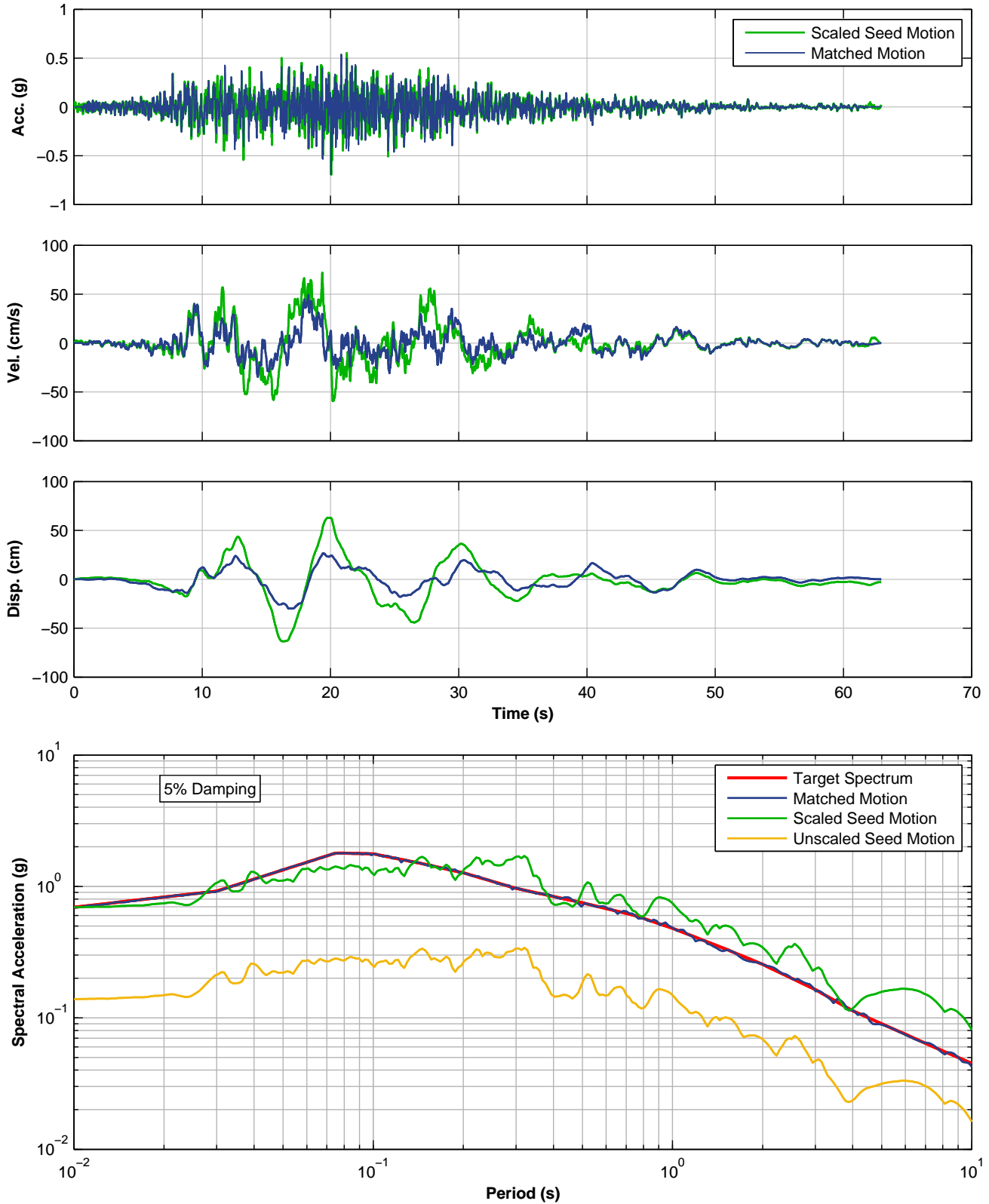
SPECTRALLY MATCHED DZC MOTION, UP COMPONENT, 1999 DUZCE EQ, TURKEY
SSE LEVEL PER NFPA 59A 2006 – NEARSHORE
LNG FACILITIES
ALASKA LNG PROJECT
NIKISKI, ALASKA



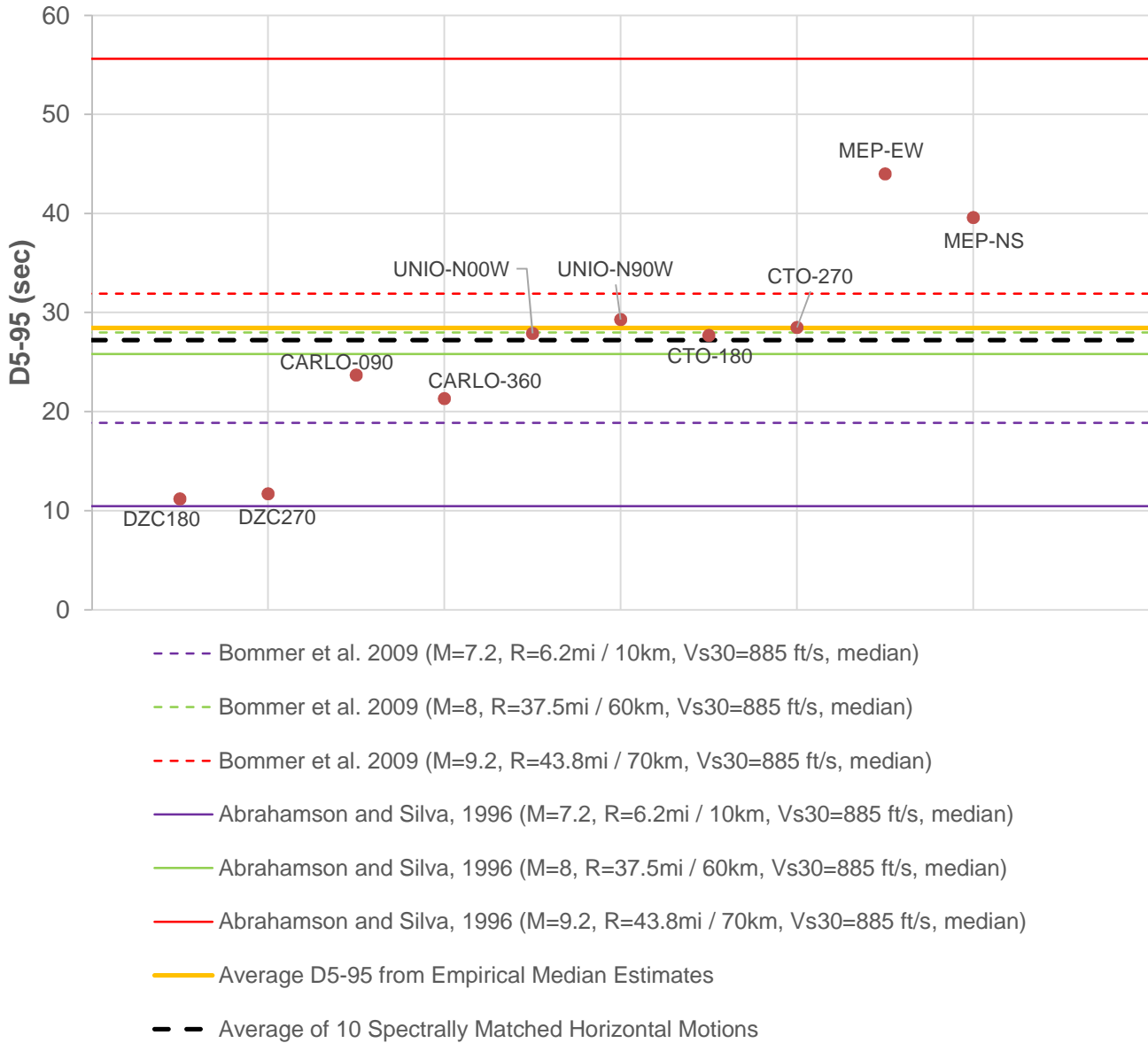
**SPECTRALLY MATCHED UNIO MOTION, N00W COMPONENT, 1985 MEXICO EQ
SSE LEVEL PER NFPA 59A 2006 – NEARSHORE, FAULT NORMAL
LNG FACILITIES
ALASKA LNG PROJECT
NIKISKI, ALASKA**



**SPECTRALLY MATCHED UNIO MOTION, N90W COMPONENT, 1985 MEXICO EQ
SSE LEVEL PER NFPA 59A 2006 – NEARSHORE, FAULT PARALLEL
LNG FACILITIES
ALASKA LNG PROJECT
NIKISKI, ALASKA**

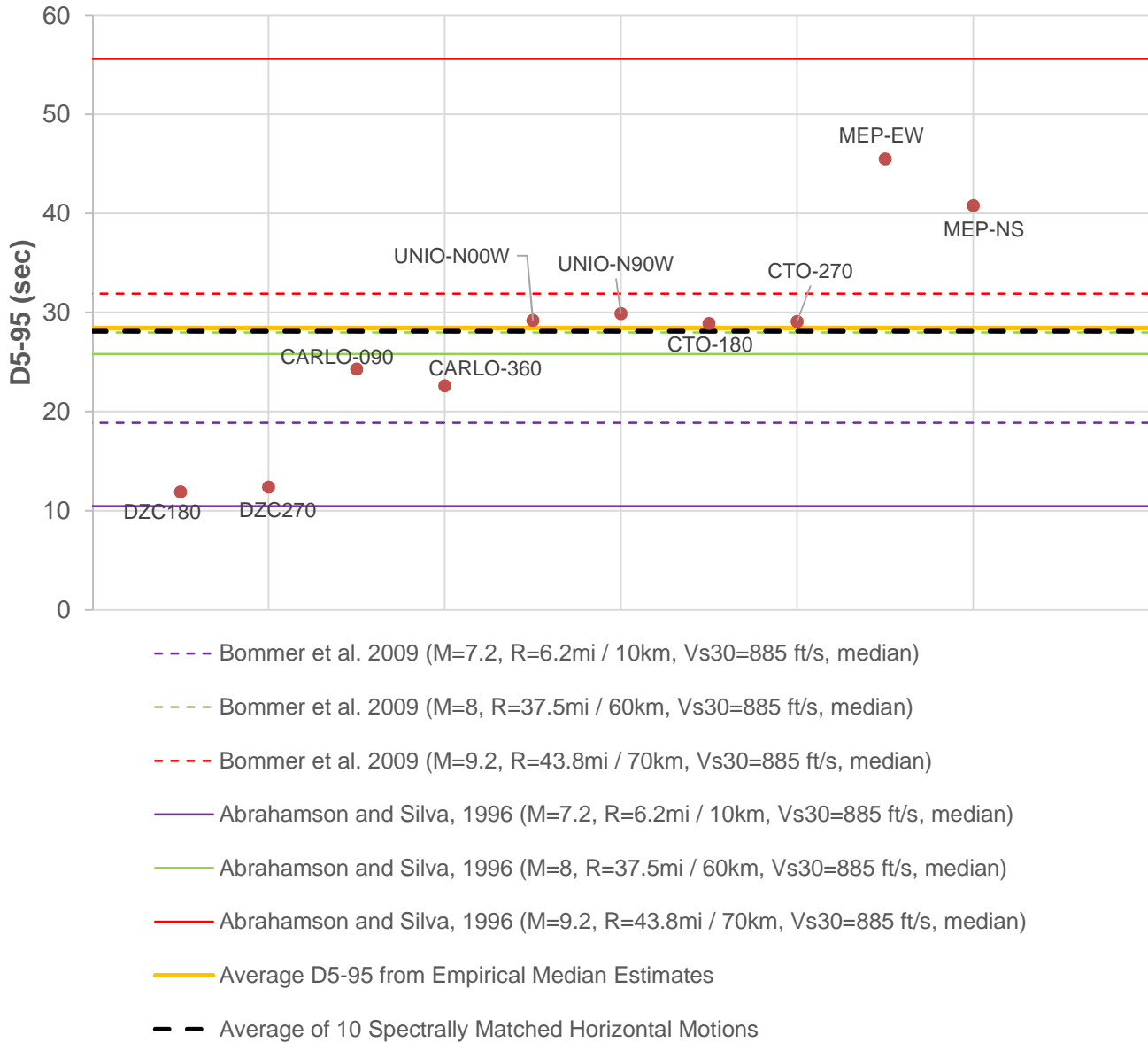


**SPECTRALLY MATCHED UNIO MOTION, UP COMPONENT, 1985 MEXICO EQ
SSE LEVEL PER NFPA 59A 2006 – NEARSHORE
LNG FACILITIES
ALASKA LNG PROJECT
NIKISKI, ALASKA**



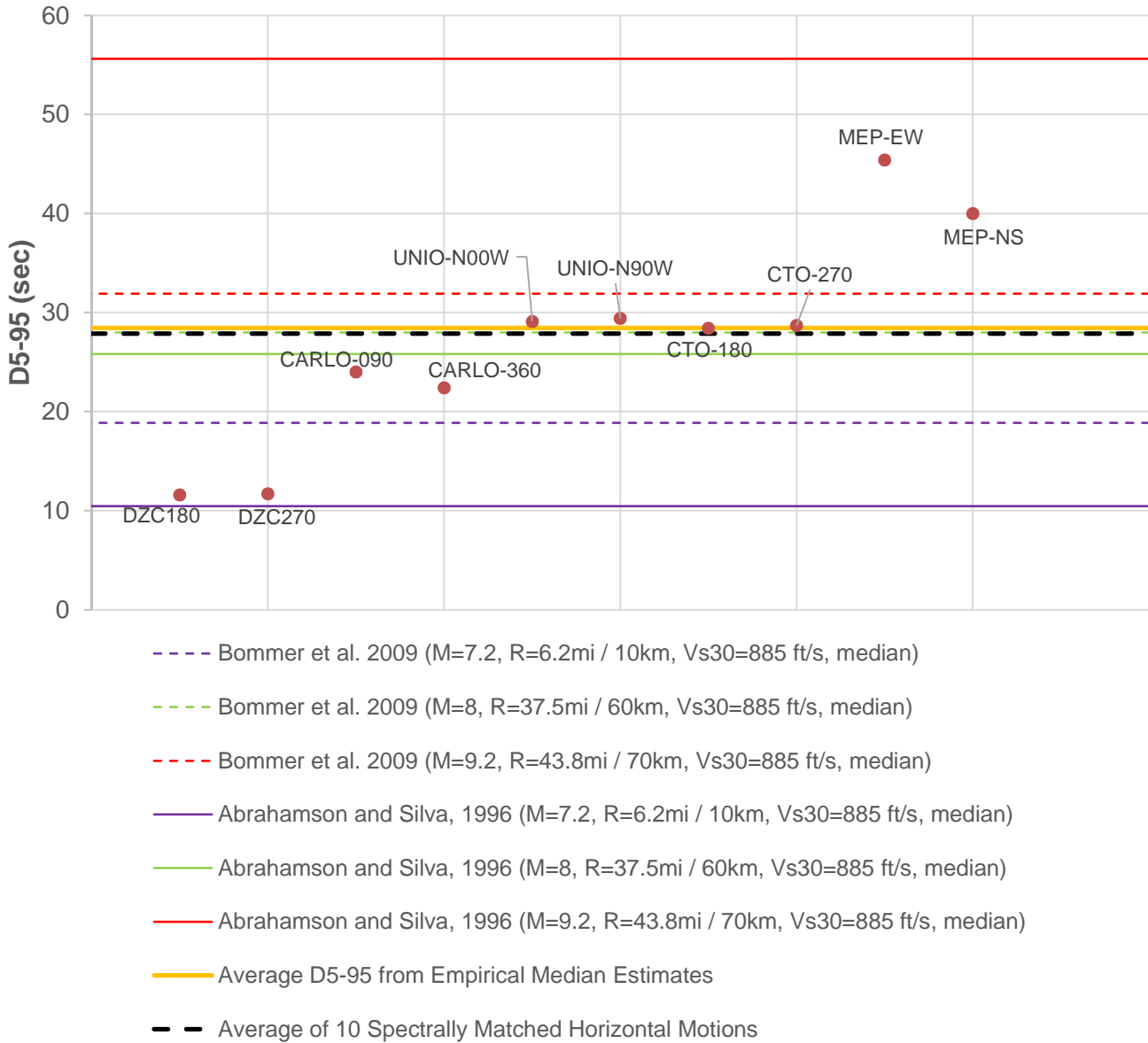
COMPARISON OF SIGNIFICANT DURATION D(5-95) OF SPECTRALLY MATCHED HORIZONTAL GROUND MOTIONS FOR OBE LEVEL PER NFPA 59A 2006 WITH THE DETERMINISTIC ESTIMATES USING EMPIRICAL RELATIONSHIPS

LNG FACILITIES
 ALASKA LNG PROJECT
 NIKISKI, ALASKA



COMPARISON OF SIGNIFICANT DURATION D(5-95) OF SPECTRALLY MATCHED HORIZONTAL GROUND MOTIONS FOR SSE LEVEL FOR ONSHORE LOCATION PER NFPA 59A 2006 WITH THE DETERMINISTIC ESTIMATES USING EMPIRICAL RELATIONSHIPS

LNG FACILITIES
 ALASKA LNG PROJECT
 NIKISKI, ALASKA



COMPARISON OF SIGNIFICANT DURATION D(5-95) OF SPECTRALLY MATCHED HORIZONTAL GROUND MOTIONS FOR SSE LEVEL FOR NEARSHORE LOCATION PER NFPA 59A 2006 WITH THE DETERMINISTIC ESTIMATES USING EMPIRICAL RELATIONSHIPS

LNG FACILITIES
 ALASKA LNG PROJECT
 NIKISKI, ALASKA